DOKUZ EYLÜL UNIVERSITY

GRADUATE SCHOOL OF NATURAL AND APPLIED SCIENCES

THERMAL PROPERTIES AND MECHANICAL ANISOTROPY IN POLYMER COMPOSITES

by

Volkan ÇEÇEN

September, 2006

İZMİR

THERMAL PROPERTIES AND MECHANICAL ANISOTROPY IN POLYMER COMPOSITES

A Thesis Submitted to the

Graduate School of Natural and Applied Sciences of Dokuz Eylül University

In Partial Fulfillment of the Requirements for the Degree of Doctor of Philosophy in

Mechanical Engineering, Energy Program

by

Volkan ÇEÇEN

September, 2006

İZMİR

Ph.D. THESIS EXAMINATION RESULT FORM

We have read the thesis entitled **"THERMAL PROPERTIES AND MECHANICAL ANISOTROPY IN POLYMER COMPOSITES"** completed by **Volkan ÇEÇEN** under supervision of **Prof. Dr. İsmail Hakkı TAVMAN** and we certify that in our opinion it is fully adequate, in scope and in quality, as a thesis for the degree of Doctor of Philosophy.

Prof. Dr. İsmail Hakkı TAVMAN

Supervisor

Prof. Dr. Tevfik AKSOY

Committee Member

Asst. Prof. Dr. Dilek KUMLUTAŞ

Committee Member

Prof. Dr. Yıldırım AYDOĞDU

Jury Member

Assoc. Prof. Dr. Hasan YILDIZ

Jury Member

Prof.Dr. Cahit HELVACI
Director
Graduate School of Natural and Applied Sciences

THERMAL PROPERTIES AND MECHANICAL ANISOTROPY IN POLYMER COMPOSITES

ABSTRACT

The primary purpose of the study is to investigate the anisotropic behavior of different non-crimp stitched fabric (NCF) reinforced polyester and epoxy composites. Composite laminates were manufactured by vacuum infusion of resin into the fabric. Tensile and three-point bending flexural tests were conducted up to failure on specimens strengthened with different layouts of fibrous plies in NCF. In this study an important practical problem in fibrous composites, interlaminar shear strength as measured in short beam shear tests was discussed. The fabric composites were tested in three directions: 0°, 45° and 90°. Extensive photographs of multilayered composites resulting from a variety of uniaxial loading conditions were presented.

Another aim of the present work is to investigate the interaction between fiber and matrix material. The experiments, in conjunction with scanning electron photomicrographs of fractured surfaces of composites, were interpreted in an attempt to explain the stability and/or the instability of matrix-fiber interfaces. Infrared spectrum of composites were obtained by Fourier transform infrared spectroscopy (FT-IR).

Thermal investigations on six selected type composites have been made. They differ with regard to the type of the resin matrix that have been reinforced with the different type of fiber. The resin types used for this study range from polyester and epoxy, while fiber reinforcements include non-crimp stitched glass, carbon and aramid fabric. Thin composite samples for heat capacity and thermal conductivity measurements were fabricated by hand lay-up method. Changes in the specific heat capacity of composites have been determined by differential scanning calorimetry over a temperature range from 20 up to 250 °C. Thermal conductivity measurements in through the thickness direction of composites were performed using a differential

scanning calorimeter (DSC). Measurements were carried out over a wide range of temperatures from about 45 to 235 °C. The thermal stability of composites in air atmosphere has been followed over a temperature range of approximately 30-550 °C using thermogravimetric (TGA) and differential thermal analysis (DTA).

POLİMER KOMPOZİTLERİN TERMAL ÖZELLİKLERİ VE MEKANİK ANİZOTROPİSİ

ÖZ

Bu çalışmanın başlıca amacı, kıvrımsız dikişli elyaf kumaş tipleriyle takviye edilmiş polyester ve epoksi bazlı kompozitlerin anizotropik davranışlarını araştırmaktır. Kompozit tabakalar, elyaf kumaş içerisine vakum basıncı altında reçine sevkiyle üretilmiştir. Değişik düzenlerde yerleştirilmiş fiber katlarını ihtiva eden kıvrımsız elyaf kumaşlarla takviye edilmiş kompozit numuneler üzerine, hasar görene dek, çekme ve üç-nokta eğilme deneyleri tatbik edilmiştir. Bu çalışmada, fiber takviyeli kompozitlerde pratik bir öneme sahip, kısa kirişli kayma deneyi ile ölçülebilen, tabakalar arası kayma gerilmeleri ele alınmıştır. Elyaf kumaş takviyeli kompozitler üç ayrı yönde test edilmiştir: 0°, 45° ve 90°. Tabakalı kompozitlerde eksenel yükleme şartlarındaki farklılığın neticesini gösteren fotoğraflar kapsamlı bir biçimde sunulmuştur.

Takdim edilen çalışmanın bir diğer amacı, fiber ve matris malzeme arasındaki etkileşimi incelemektir. Matris-fiber arayüzeyinin kararlılığı ve/veya kararsızlığını izah edebilmek gayesiyle, kompozitlerin kırılma yüzeylerinin elektron mikroskobuyla büyültülmüş fotoğrafları yorumlanmıştır. Kompozitlerin kızılötesi tayfı, Fourier dönüşüm kızılötesi spektroskopisi ile elde edilmiştir (FT-IR).

Termal araştırmalar seçilen altı tip kompozit üzerinde gerçekleştirilmiştir. Kompozitlerin farklılığı, değişik matris tiplerinin değişik tipte fiber malzemeyle takviye edilmesinden kaynaklanmaktadır. Bu çalışmada kullanılan matris malzeme tipleri polyester reçine ve epoksi reçineyi, fiber tipleri ise kıvrımsız dikişli cam, karbon ve aramid elyaf kumaşlarını içermektedir. Isıl kapasite ve ısı iletim katsayısı ölçümlerinde kullanılan ince kompozit numuneler elle yatırma yöntemiyle üretilmiştir. Kompozitlerin ısıl kapasite değişimleri 20°C'den 250°C'ye varan sıcaklık aralığında diferansiyel taramalı kalorimetre ile belirlenmiştir. Kompozitlerin, kalınlıkları boyunca, ısı iletim katsayısı ölçümleri yine diferansiyel taramalı

kalorimetre kullanılarak yapılmıştır (DSC). Ölçümler 45°C'den 235°C'ye varan geniş bir sıcaklık aralığında gerçekleştirilmiştir. Kompozitlerin termal kararlılığı hava atmosferinde ve yaklaşık olarak 30-550°C sıcaklık aralığında termogravimetrik analiz (TGA) cihazı ve diferansiyel termal analiz (DTA) cihazı kullanılarak incelenmiştir.

Anahtar kelimeler: Polimer kompozitler; Mekanik anizotropi; Isıl kapasite; Isı iletim katsayısı; Termal kararlılık

CONTENTS

CHAPTER ONE
INTRODUCTION

1.1 Motivation

Until the beginning of the nineteenth century, the materials developed, manufactured and used, whether homogeneous or composite, were basically inorganic in nature. Complex organic substances such as coal and oil were subjected to destructive processes to produce simpler chemicals such as coal gas and gasoline. However, during the twentieth century, organic chemists have developed the means of reversing this destructive process and of creating from the by-products materials that do not occur naturally. Most important among these new substances are the 'super-polymers', commonly called 'plastics', a term which in many cases is misleading, and the production of these materials has increased dramatically since the Second World War.

The possibilities of using these plastic materials in engineering situations are now being extensively examined, and in the field of structural engineering such development is taking place mainly in their use as glass fibre-reinforced plastics, the plastic material most widely used being polyester resin. A large number of materials, e.g. jute, asbestos, carbon and boron, have been used for the fiber reinforcement of the plastic matrix, the main function of the fibers being to carry the majority of the load applied to the composite and to improve the stiffness characteristics of the polymer matrix. The most widely used material for the reinforcement of polymer is glass fiber in all its various forms, partly because of its high strength and its low specific gravity, partly because of its chemical inertness, and partly because of its being relatively inexpensive to produce. Notwithstanding these, development of new higher modulus fibers such as boron, graphite, silicon carbide, and beryllium gives us reinforcements having several times the modulus of elasticity of glass fibers with densities as low as or lower than glass and strengths close to that of glass fibers. In addition to having available new chemical types of fibers, there are also a number of options with regard to fiber diameter, fiber length, and grouping of filaments into

strands, roving, and yarn. These types and forms of fibers give us a new degree of freedom in terms of being able to select the most appropriate type fiber for a given application. Newly developed, high modulus resins, such as the cycloaliphatic epoxies, and new high temperature resistant resins, such as polybenzimidazole and polyimide resins offer another degree of freedom in terms of material selection.

1.1.1 Mechanical Anisotropy in Polymer Composites

Many of the new advanced fibers and resins are being combined together in unidirectional preimpregnated form, such as yarn, tape, and sheet material. The availability of such unidirectional "prepreg" material permits precise orientation of each ply in a composite at any desired angle. This allows the designer to specify the appropriate orientation of each ply in a composite which will give maximum structural efficiency for a given application.

Designs of reinforced plastics parts were generally on a substitution basis for previously made metal parts. Most parts were made either of parallel or cross-laminated fabrics, which in some cases resulted in superfluous reinforcement in certain directions. The number of combinations of fabrics and resins popular with designers, although significant, was still small enough so that most of the design data needed could be obtained experimentally. The limited number of variables, especially in types of reinforcements and physical form of the reinforcements was conductive to the development of reinforced plastics technology primarily through empiricism.

1.1.2 Thermal Properties of Polymer Composites

Fiber-reinforced-plastic materials are considered as replacements for metals in situations where we need excellent specific strength properties, e.g. strength/weight and or stiffness/weight ratios. While such composites have other advantageous properties over metals, e.g. corrosion resistance, they also have characteristics which may not be so beneficial in some applications. Among the latter is the thermal

conductivity, where the magnitude of conductivity of composites, on average, is much lower than that of metals and is also anisotropic. Hence, in general, it is much more difficult to dissipate heat in a fiber-reinforced-plastic than in a metal, and in some situations this may be an important consideration, particularly if electronic components are situated very near to the material.

The design of electronically and thermally conductive polymer composites require high electrical conductivity for signal transmission, high thermal conductivity for dissipating heat from a powered device, and high flexibility to avoid a failure due to thermal stresses generated during thermal cycling. For example, new applications, like heat sinks in electronic packaging, require new composites with higher thermal conductivity. However, commonly used plastics are electrical insulators with a low thermal conductivity. By the addition of reinforcements to plastics the thermal behavior of polymers can be increased significantly. Such reinforced polymers with higher thermal conductivities than unreinforced ones become more and more an important area of study because of the wide range of applications, e.g. in electronic packaging in applications with decreasing geometric dimensions and increasing output of power, like in computer chips or in electronic packaging. The higher thermal conductivity can be achieved by the use of a suitable reinforcement such as carbon fiber or magnetite particles.

The specific heat (heat capacity per unit mass) is also a critical property in many applications. It is a thermodynamic quantity that is relatively easily determined for small and homogeneous samples. However, for composite materials having different phases, where the quantity to be measured is the specific heat of the bulk of the body, including all present phases, it is almost impossible to prepare a small and representative sample, so that the measurement of this property must become particularly troublesome.

Therefore, it is important to tailor the thermal conductivity and heat capacity of composites but the basic properties must first be known.

1.2 Relevance of the Present Study

A key feature of fiber composites that makes them so promising as engineering materials is the opportunity to tailor the materials through the control of fiber and matrix combinations and the selection of processing techniques. Matrix materials and fabrication processes are available that do not significantly degrade the intrinsic properties of the fiber. In principle, an infinite range of composite types exists, from randomly oriented chopped fiber based materials at the low property end to continuous, unidirectional fiber composites at the high-performance end. Composites can differ in the amount of fiber, fiber type, fiber length, fiber orientation, and possibly fiber hybridization. In general, short-fiber composites are used in lightly loaded or secondary structural applications, while continuous fiber-reinforced composites are utilized in primary applications and are considered high-performance structural materials.

By nature, continuous-fiber composites are highly anisotropic. Maximum properties can be achieved if all the fibers are aligned in the fiber-axis direction. The properties, such as modulus and strength, decrease rapidly in directions away from the fiber direction. To obtain more orthotropic properties, alternate layers of fibers may vary between 0 and 90°, resulting in less directionality, but at the expense of absolute properties in the fiber direction. A laminate is fabricated by stacking a number of thin layers of fibers and matrix, consolidating them into the desired thickness. A laminate is the most common form of composites for structural applications. The fiber orientation in each layer as well as the stacking sequence of various layers can be manipulated to produce a wide scope of physical and mechanical properties.

One of the outstanding characteristics of the rapidly increasing technology of composite materials is the almost unlimited freedom of choice that presents itself to the designer. Since not only the number of constituent in a composite materials but also their distribution and orientation within a given structural shape are subject to choice and can possibly lead to identical performance characteristics, it is one of the

foremost requirements for developing the technology to also provide avenues for making this choice an intelligent one.

The textile industry has developed the ability to produce net-shape/near-net-shape fabrics using highly automated techniques such as stitching, weaving, braiding and knitting. Multiaxial multiply fabrics (MMF), also called 'non-crimp fabrics' (NCF) are a promising class of composite preforms that consists of unidirectional plies arranged in a number of possible orientations relative to the fabric warp direction; the individual plies are stitched together by warp knitting process by stitching yarns piercing through the fibrous plies.

During NCF based composites manufacturing, preforms are laid up with desired stacking sequence on the mould tool and infiltrated by a thermoset resin to form the composite. Compared to the time consuming and expensive unidirectional (UD) tape layout, the MMFs are produced in one step, so the lay up time is drastically reduced. In such instances, the MMFs with a high amount of formability/drapability should be used to form over a relatively complex shaped tool for subsequent consolidation to produce the required composite component. The use of this preforms overcomes the disadvantages of the wrinkling that is normally experienced with standard woven fabric and prepreg tape. For this reason, the use of composites reinforced with NCF is growing rapidly in aircraft, automobiles, yachts, wind turbine blades and other complex structural components.

The major goal of the research described in this paper has been to study the anisotropy of the non-crimp fabric reinforced polyester composites. This anisotropic study was carried out to investigate the effects of geometric variables, such as geometry of fiber orientation, on structural integrity and strength of the multiaxial multiply fabric (MMF) or non-crimp stitched fabric (NCF) reinforced composites. Hence, tensile, three-point bending and short beam shear tests were conducted at different off-axial angles (0°, 45° and 90°) with respect to the longitudinal direction. Another aim of this study is to identify the dependence of fracture surface on this off-axial variation. In addition to the extensive efforts in elucidating the variation in the

mechanical properties of different NCF based laminates, the work presented here focuses, also, on the type of interactions that are established between polymer matrix and fiber. Fourier transform infrared (FT-IR) spectroscopic studies were performed to investigate the interaction between fiber and polymer matrix. Scanning electron microscope (SEM) was also helpful and additionally used to describe the morphological features of fractured surfaces of polymer composites.

In this study, the heat capacity and the thermal conductivity of polyester and epoxy composites reinforced with non-crimp stitched glass, carbon and aramid fabrics were measured using heat-flux differential scanning calorimetry (DSC). For the heat capacity measurements the sample and a standard material (with a given specific heat) are separately subjected to the same linear temperature variation. In order to reduce uncertainty of the rate of the energy added to the material, a 10 °C/min scan was applied for all measurements within the temperature range from 20 to 250 °C. Continuous isothermal scans are conducted before and after the dynamic scan. The differential scanning calorimeter was adapted to perform the measurement of thermal conductivity of polymeric composite materials. This method requires many samples with different heights which are heated in such a way that a sensor material put on their top undergoes a first-order phase transition. The analysis of heat transfer of such experiment predicts that the slope of the differential power during the first-order transition of sensor material is proportional to the heating rate and inversely proportional to the sum of the thermal resistances. The technique was applied to polyester and epoxy based composites of varied thickness over the temperature range 45-235 °C.

1.3 Examples of Past Research

1.3.1 Research on Thermal Properties of Polymer Composites

Although there exists in the literature a large knowledge base for the mechanical properties of composite materials, only limited information is available on the thermal properties. The limited works include those by Springer & Tsai (1967),

Demain & Issi (1993), Grove (1990), Pilling, Yates, Black & Tattersall (1979), and Hasselman, Donaldson & Thomas (1993). Springer et al. (1967) considered composite thermal conductivities of unidirectional composites and obtained expressions for predicting conductivities in the principal directions, along and normal to the fibers. The parallel conductivity is obtained by using the mixture rule, while the normal conductivity is obtained by means of an analogy between thermal lead-ins and the constitudinal shear loading of a unidirectional composite.

Demain et al. (1993) reported the measurements of thermal and electrical conductivities of polycarbonate specimens as a function of chopped pitch-based carbon fiber concentration. Grove (1990) modeled the transverse thermal conductivity in continuous unidirectional fiber composite materials by combining finite element analysis and spatial statistical techniques. Pilling et al. (1979) reported measurements of thermal conductivity between 80 and 270 K of epoxy resin specimens reinforced with carbon fibers. They measured both in-plane and out-of-plane thermal conductivity. Lastly, Hasselman et al. (1993) modeled the effective thermal conductivity of a uniaxial composite with cylindrically orthotropic carbon fibers and interfacial thermal barrier.

Ott (1979) determined the thermal conductivity of various composite materials consisting of epoxy and unsaturated polyester resin reinforced with glass fibers, asbestos fibers, quartz, fused silica and zircon. Measurements were carried out in the temperature range from -180 to 140 °C. Thermal conductivity measurements were performed using a two-plates-apparatus. With the help of the data obtained, the applicability of different mixing rules and models for calculating the thermal conductivity of composite materials was examined. It was found that the mixing rules normally employed have but limited use in this case.

Several researchers have reported on the improvement of thermal conductivities of polymers by fillers (Agari & Uno, 1986; de Aranjo & Rozenberg, 1976) thermal conduction mechanisms and various models (Agari, Ueda & Nagai, 1993; Fricke, 1924; Katz & Milewak, 1978). Progelhof, Throne & Reutsch (1976) have reviewed

the prediction of thermal conductivity of composite systems and presented various theoretical and empirical models with a brief description focusing the relative merits. Maewal, Gurtman & Hegemier (1978) have analysed the heat transfer in unidirectional fibrous composites with a periodic hexagonal microstructure primarily in the fiber direction using a binary mixture theory. Expressions for the longitudinal and transverse thermal conductivity of transversely isotropic fiber composites have been summarized by Chamis (1984).

Although several traditional methods, steady-state and transient, have been used for a long time to measure the thermal conductivity of polymer composites (Mark, 1989; Brown, 1999), most of them are not adequate for composite materials and present disadvantages such as requiring large samples and long experimental time for each determination. In this panorama, a relatively new application of differential scanning calorimetry (DSC) has become a good alternative for such measurements, especially due to its sensitivity and versatility.

Kalogiannakis, Hemelrijck & Assche (2003) have studied the heat capacity and the thermal conductivity of carbon/epoxy and glass/epoxy cross-ply laminates were determined in a temperature range of interest for the aircraft industry using an ASTM method based on Modulated Temperature Differential Scanning Calorimetry. They found that the heat capacity is more strongly dependent on the temperature than the thermal conductivity. The former is clearly exhibiting an increasing value with temperature. Comparing the two materials, it can be concluded again that carbon/epoxy is more conductive as well as more dependent on the temperature.

The work performed by Kuriger & Alam (2002) investigated experimentally the thermal properties of polypropylene composites reinforced with aligned carbon fiber. The specific heat capacity was experimentally determined using a DSC. The results for the density, specific heat, and thermal diffusivity were then used to determine the longitudinal and transverse thermal conductivity values. Their results indicate that the thermal conductivity increased with fiber volume fraction and was much greater in the longitudinal direction of the composite as opposed to the transverse direction.

Most specific heat capacity values of composites at different filler contents are normally obtained by using the rule of mixture when the heat capacities of the filler and the matrix are known (Bujard, Kuhnlein, Ino & Shiobata, 1994; Johansson, Joelsson & Bastos, 1992; Krielaart, Brakman & Vanderzwaag, 1996). However, by utilizing the new temperature-modulated differential scanning calorimetry technique, the determination of the absolute value of heat capacity of the material is much quicker, easier, and more accurate (Gill, Sauerbrunn & Reading, 1993; Boller, Jin & Wunderlich, 1994).

The work of Ishida & Rimdusit (1999) attempt to investigate the effect of boron nitride filler on the specific heat capacity of filled polybenzoxazine as these composite systems exhibited extraordinarily high values of thermal conductivity (Ishida & Rimdusit, 1998). The effect of particle size, shape, surface area, and filler loading on composite specific heat capacities as a function of temperature is studied to verify its structure-insensitive property characteristic.

1.3.2 Researches on Mechanical Characterization of Polymer Composites

The resin matrix, the type of reinforcement, lay-up configuration and the distribution and orientation of the reinforcement are all of critical importance in the performance of the resulting composites. In addition, the service temperature requirements and the necessary fabrication techniques have an important bearing on the selection of a particular system and maximum strength obtainable.

All of the variables have been the subject of numerous investigations (Wang, Li & Do, 1995; Drapier & Wisnom, 1999; Drapier & Wisnom, 1999; Crookston, Long & Jones, 2005; Roth & Himmel, 2002; Sjogren, Edgren & Aps, 2004; Mikael & Peter, 2000; Huang & Young, 1995). The success of these studies is indicated by the constantly increasing strength levels obtained in reinforced plastic systems.

The mechanical properties of NCF composites from the resin transfer molding process were evaluated (Wang et al., 1995). Due to their close fiber packing and

dense structures, reasonably high fiber volume fraction (about 50%) in the final composite part can be obtained even from the wet manual lay-up process. This can result in good mechanical properties as well as significant savings in resin consumption.

The relationship between the mechanical properties and the process in which the MMF and composite are manufactured has received considerable attention in recent years. Many of these studies, both theoretical and experimental, the individual properties of multiaxial multilayer warp knit (non-crimp) fabric reinforced polymer composites, and some of the predictive models available for determining them have been extensively reviewed elsewhere (Leong, Ramakrishna, Huang & Bibo, 2000) and will be discussed further only where directly applicable to this study.

The effect of through-the-thickness stitching on the in-plane mechanical properties of fiber-reinforced polymer composites has been studied from many viewpoints using both empirical and theoretical methods. In spite of the difficulties of correlation and the differences of test conditions between the classical models and reinforced composites, many of the controlling parameters should be common to both systems. Mouritz, Leong & Herszberg (1997) gave an excellent review of the stitching problems encountered in the fiber reinforced polymer (FRP) composites.

It is unfortunate that very few significant work efforts are based upon experiments carried out with damage development in MMF composites (Sjogren et al., 2004; Edgren, Matsson, Asp & Varna, 2004). Bibo, Hogg & Kemp (1997) has shown how crimp in the tows has a pronounced effect on the mechanisms of failure in the non-crimp fabrics, but with subtle differences driving failure in tension and compression.

The work of Truong, Vettori, Lomov & Verpoest (2005), where the mechanical properties of the composites were measured in a number of orientations relative to the stitching direction for different NCF based laminates, had shown that the stitching has limitations on stiffness of multiaxial multiply carbon fabrics (MMCF). On the other hand, when the damage development is investigated by C-scan and X-

ray imaging, the relation between stitching and damage (as a result of crack initiating resin rich pockets created by stitching) patterns is observed.

Wang (2002) has studied the mechanical properties of composite laminates reinforced with stitched multi-layer, multi-axial non-crimp fabrics (NCFs). Composite panels have been fabricated using the manual lay-up process. The composite panels are tested in tension, flexure, and compression along three directions: 0, 90, and 45 degrees. The experimental results indicate that, generally, the highest strength is observed in flexure, followed by compression and tension.

With regard to new improved constituent materials for composites can, however, some potential pitfalls which must be recognized and investigated at an early stage. Relatively little research has been reported on the mechanical performance of carbon fiber/unsaturated polyester composites despite its importance in many dynamically loaded structures (Xu, Liu, Gao, Fang & Yao, 1996; Yu, Liu & Jang, 1994). The number of combinations of carbon fabrics and unsaturated polyester resin popular with designers, although significant, was still small enough so that most of the design data needed.

CHAPTER TWO
BACKGROUND

2.1 Polymer Matrix Composites

The most significant advantage of polymer matrix composites (PMCs) derives from the fact that they are lightweight materials with high strength and modulus values. The light weight of PMCs is due to the low specific gravities of their constituents. Polymers used in PMCs have specific gravities between 0.9 and 1.5, and the reinforcing fibers have specific gravities between 1.4 and 2.6 (Mallick, 1993). Depending on the types of fiber and polymer used and their relative volume fractions, the specific gravity of a PMC is between 1.2 and 2, compared to 7.87 for steel and 2.7 for aluminum alloys. Because of their low specific gravities, the strength-to-weight ratios of PMCs are comparatively much higher than those of metals and their composites (Table 2.1). Although the cost of PMCs can be higher than that of many metals, especially carbon or boron fibers are used as reinforcements, their cost on a unit volume basis can be competitive with that of the high performance metallic alloys used in the aerospace industry.

A second advantage of PMCs is the design flexibility and the variety of design options that can be exercised with them. Fibers in PMC can be selectively placed or oriented to resist load in any direction, thus producing directional strengths or moduli instead of equal strength or modulus in all directions as in isotropic materials such as metals and unreinforced polymers. Similarly, fiber type and orientation in a PMC can be controlled to produce a variety of thermal properties such as the coefficient of thermal expansion (Table 2.2). PMCs can be combined with aluminum honeycomb, structural plastic foam, or balsa wood to produce sandwich structures that are stiff and at the same time lightweight. Two or more different types of fibers can be used to produce a hybrid construction with high flexural stiffness and impact resistance (Mallick, 1997).

There are several other advantages of PMCs that make them desirable in many applications. They have damping factors that are higher than those of metals (Table 2.3), which means that noise and vibrations are damped in PMC structures more effectively than in metal structures. They also do not corrode. However, depending on the nature of the matrix and fibers, their properties may be affected by environmental factors such as elevated temperatures, moisture, chemicals, and ultraviolet light.

Table 2.1 Comparative properties of metals and polymeric matrix composites[a] (Mallick, 1993, p. 13)

Material	Density (g/cm^3)	Modulus (GPa)	Tensile strength (MPa)	Yield strength (MPa)	Modulus-to-weight ratio (10^6 m)	Tensile strength-to-weight ratio (10^3 m)	Elongation (%)
SAE 1010 steel (cold drawn)	7.87	207	365	303	2.68	4.72	20
AISI 4340 steel (quenched and tempered)	7.87	207	1722	1515	2.68	22.3	–
6061-T6 aluminum alloy	2.70	68.9	310	275	2.60	11.7	15
7075-T6 aluminum alloy	2.70	68.9	572	503	2.60	21.6	11
AZ80A-T5 magnesium alloy	1.74.	44.8	379	276	2.62	22.2	7
Ti-6Al-4V titanium alloy (aged)	4.43.	110	1171	1068	2.53	26.9	8
High strength carbon fiber/epoxy (unidirectional)	1.55	138	1550	–	9.07	101.9	1.1
High modulus carbon fiber/epoxy (unidirectional)	1.63	215	1240	–	13.44	77.5	0.6
E glass fiber/epoxy (unidirectional)	1.85	39.3	965	–	2.16	53.2	2.5
Kevlar 49/epoxy (unidirectional)	1.38	75.8	1378	–	5.60	101.8	1.8
Carbon fiber/epoxy (quasi-isotropic)	1.55	45.5	579	–	2.99	38.1	–
E-glass fiber/epoxy (Random fiber SMC)	1.87	15.8	164	–	0.86	8.9	1.73

[a]For unidirectional composites, the modulus and strength values are in the fiber direction

Table 2.2 Coefficient of thermal expansion of polymeric matrix composites (Mallick, 1993, p. 14)

Material	CTE ($10^{-6}/°C$)		
	Unidirectional (0°)		Quasi-isotropic
	Longitudinal	Transverse	
E-glass/epoxy ($v_f = 0.6$)	7.13	32.63	12.6
Kevlar 49/epoxy ($v_f = 0.6$)	-3.6	54	-0.9 to 0.9
High modulus carbon/epoxy ($v_f = 0.6$)	-0.9	27	0 to 0.9
Random E-glass fiber composites			
SMC-R25 ($w_f = 0.25$)	23.2		
SMC-r50 ($w_f = 0.5$)	14.8		
Injection-molded Nylon 6,6 ($w_f = 0.5$)	18		
Steel	11-18		
Aluminum alloys	22-25		

Table 2.3 Damping coefficients of polymeric matrix composites

Material	Fiber orientation	Modulus (GPa)	Damping factor
E-glass/epoxy	0°	35.2	0.007
Carbon/epoxy	0°	188.9	0.0157
	22.5°	32.4	0.0164
	90°	6.9	0.0319
	[0/22.5/45/90]$_s$	69	0.0201
Low-carbon steel	-	207	0.0017
6061 aluminum alloy	-	70	0.0009

2.2 Reinforcements

The most common reinforcements are glass, carbon, aramid and boron fibers. Typical fiber diameters range from 5 μm to 20 μm. The diameter of a glass fiber is in the range of 5 to 25 μm, a carbon fiber is 5 to 8 μm, an aramid fiber is 12.5 μm. Because of this thin diameter, the fiber is flexible and easily conforms to various shapes. In general, fibers are made into strands for weaving or winding

operations. For delivery purposes, fibers are wound around a bobbin and collectively called a "roving". An untwisted bundle of carbon fibers is called "tow". In composites, the strength and stiffness are provided by the fibers. The matrix gives rigidity to the structure and transfers the load the fibers.

Fibers for composite materials can come in many forms, from continuous fibers to discontinuous fibers, long fibers to short fibers, organic fibers to inorganic fibers. The most widely used fiber materials in fiber-reinforced plastics (FRP) are glass, carbon, aramid, and boron. Glass is found in abundance and glass fibers are the cheapest among all other types of fibers. There are three major types of glass fibers: E-glass, S-glass, and S2-glass. The properties of these fibers are given in Table 2.4. The cost of E-glass is around $1.00/lb, S-glass is around $8.00/lb, and S2-glass is $5.00/lb. Carbon fibers range from low to high modulus and low to high strength. Cost of carbon fibers fall in a wide range from $8.00 to $60.00/lb. Aramid fibers cost approximately $15.00 to $20.00/lb. Some of the common types of reinforcements include:

- Continuous carbon tow, glass roving, aramid yarn
- Discontinuous chopped fibers
- Woven fabric
- Multidirectional fabric (stitched bonded for three dimensional properties)
- Stapled
- Woven or knitted three-dimensional preforms (Mazumdar, 2001, p. 42-45).

Table 2.4 Properties of fibers and conventional bulk materials (Mazumdar, 2001, p. 44)

Material	Diameter (μm)	Density (g/cm³)	Tensile Modulus (GPa)	Tensile Strength (GPa)	Specific Modulus	Specific Strength	Melting Point (°C)	Elongation at Break (%)	Relative Cost
Fibers									
E-glass	7	2.54	70	3.45	27	1.35	1540+	4.8	Low
S-glass	15	2.50	86	4.50	34.5	1.8	1540+	5.7	Moderate
Graphite, high modulus	7.5	1.9	400	1.8	200	0.9	>3500	1.5	High
Graphite, high strength	7.5	1.7	240	2.6	140	1.5	>3500	0.8	High
Boron	130	2.6	400	3.5	155	1.3	2300	-	High
Kevlar 29	12	1.45	80	2.8	55.5	1.9	500(D)	3.5	Moderate
Kevlar 49	12	1.45	130	2.8	89.5	1.9	500(D)	2.5	Moderate
Bulk materials									
Steel		7.8	208	0.34-2.1	27	0.04-0.27	1480	5-25	< Low
Aluminum alloys		2.7	69	0.14-0.62	26	0.05-0.23	600	8-16	Low

2.2.1 Fabrics

A fabric is defined as an integrated fibrous structure produced by fiber entanglement of yarn interlacing, interlooping, intertwining, or multiaxial placement. The textile industry has developed the ability to produce net-shape/near-net-shape fabrics using highly automated techniques such as stitching, weaving, braiding and knitting. Table 2.5 compares the four basic yarn-to-fabric formation techniques, and Figure 2.1 shows examples of fiber architecture created by these techniques (Ko, 1993).
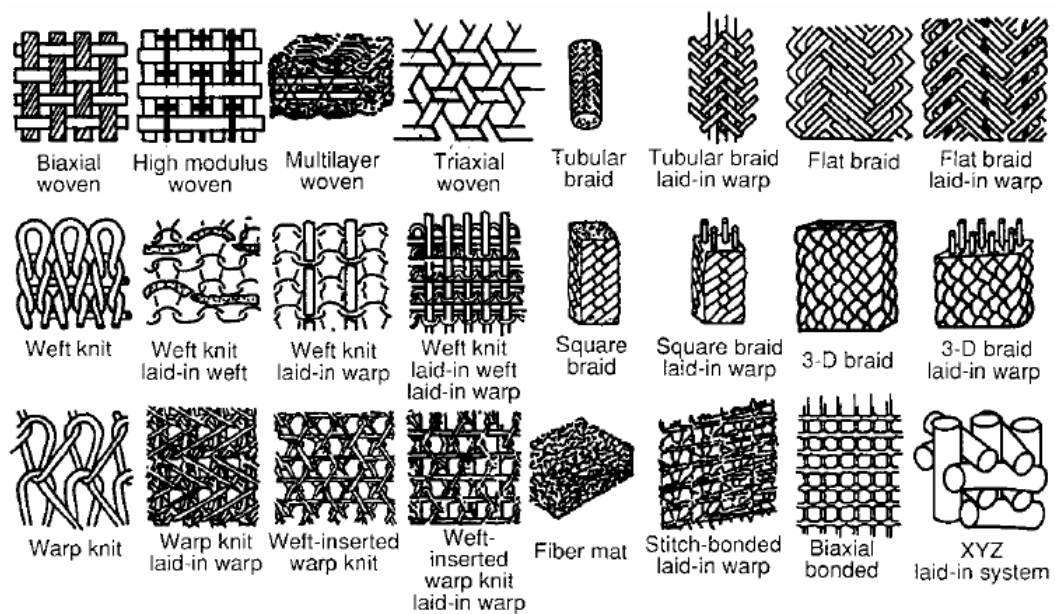
Figure 2.1 Linear, planar, and 3-D fibrous structures (Ko, 1993, p. 77).

In view of the potential for cost savings and enhanced mechanical performance, some of these traditional textile technologies have been adopted for manufacturing fabric reinforcement for advanced polymer composites. Knitting is particularly well suited to the rapid manufacture of components with complex shapes due to the low resistance to deformation of knitted fabrics. Furthermore, existing knitting machines have been successfully adapted to use various types of high-performance fibres, including glass, carbon, aramid and even ceramics, to produce both flat and net-shape/near-net-shape fabrics. The fabric preform is then shaped, as required, and consolidated into composite components using an

appropriate liquid moulding technique, e.g. resin transfer moulding (RTM) or resin film infusion (RFI) (Leong et al., 2000, p. 197).

Table 2.5 Comparison of yarn-to-fabric formation techniques (Ko, 1993, p. 77)

	Basic direction of yarn introduction	Basic fabric formation technique
Weaving	Two (0°/90°) (warp and fill)	Interlacing (by selective insertion of 90° yarns into 0° yarn system)
Braiding	One (machine direction)	Intertwining(position displacement)
Knitting	One (0° or 90°) (warp or fill)	Interlooping (by drawing loops of yarns over previous loops)
Nonwoven	Three or more (orthogonal)	Mutual fiber placement

2.2.1.1 Knitted Fabrics

Knitting refers to a technique for producing textile fabrics by intermeshing loops of yarns using knitting needles. A continuous series of knitting stitches or intermeshed loops is formed by the needle catching the yarn and drawing it through a previously formed loop to form a new loop. In a knit structure, rows, known in the textile industry as *courses*, run across the width of the fabric, and columns, known as *wales*, run along the length of the fabric. The loops in the courses and wales are supported by, and interconnected with, each other to form the final fabric (Figure 2.2) (Leong et al., 2000, p.198).

A wale of loops is produced by a single knitting needle during consecutive knitting cycles of the machine. The number of wales per unit width of fabric is dependent on inter alia the size and density of the needles used as well as the knit structure, yarn size, yarn type, and the applied yarn tension. A course of loops, on the other hand, is produced by a set of needles during one knitting cycle of the machine. The number of courses per unit length of fabric is controlled by manipulating the needle (knockover) motion and yarn feed (Leong et al., 2000, p.198).

Direction of knitting

(a)

Direction of knitting
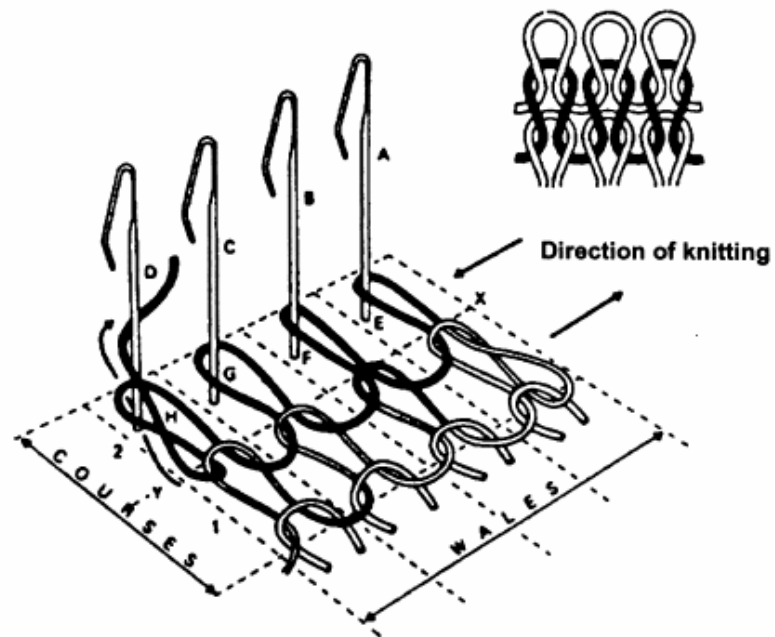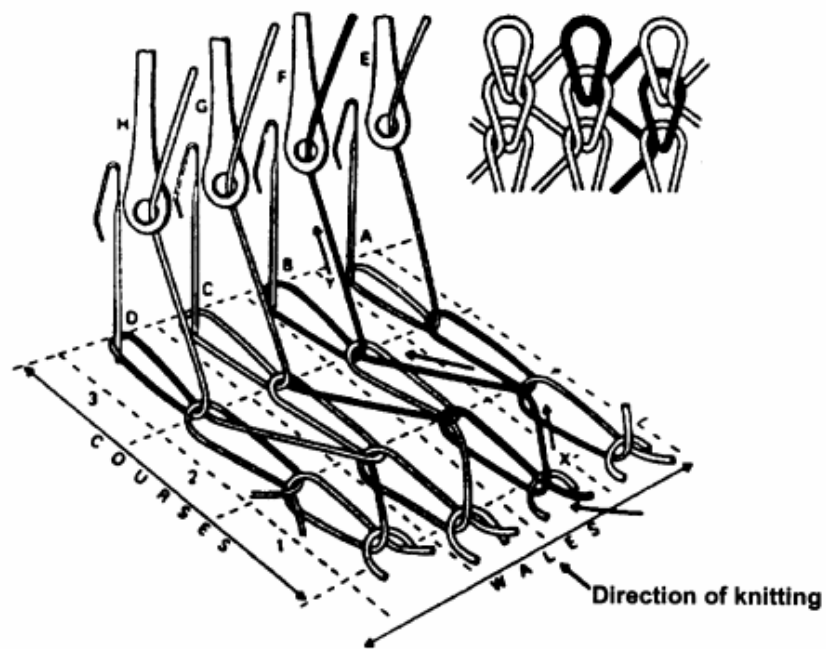
(b)

Figure 2.2 Schematic diagrams showing the wale and course components of a knitted fabric, and the principles of (a) weft and (b) warp knitting (Leong et al., 2000, p.198).

Depending on the direction in which the loops are formed, knitting can be broadly categorized into one of two types—*weft knitting* and *warp knitting* (Figure 2.2). Weft knitting is characterized by loops forming through the feeding of the weft yarn at right angles to the direction in which the fabric is produced (Figure 2.2a). Warp knitting, on the other hand, is characterized by loops forming through the feeding of the warp yarns, usually from warp beams, parallel to the direction in which the fabric is produced (Figure 2.2b) (Leong et al., 2000, p.199).

A principal set-up of the knitting elements in a warp knitting machine is shown in Figure 2.3. The yarn comes from a beam and runs through the guide bar (5), which makes a lapping movement through which the textile construction is determined. Each guide bar can act separately. The respective guide units place the yarn around the needle, which moves up and down and actually forms the loops. All needles are mounted on a needle bar (2) and act simultaneously in conjunction with tongue bar (4). The sinker units (3) hold the newly produced loops down on the trick plate (1) while a new row of loops is formed. A typical, simple warp knitted structure (tricot) is shown in Figure 5 on the right-hand side (Stumpf et al., 1998, p. 1513).

1: trick plate
2: needle bar
3: tongue bar
4: unit for weft insertion and holding down sinkers
5: guide bar
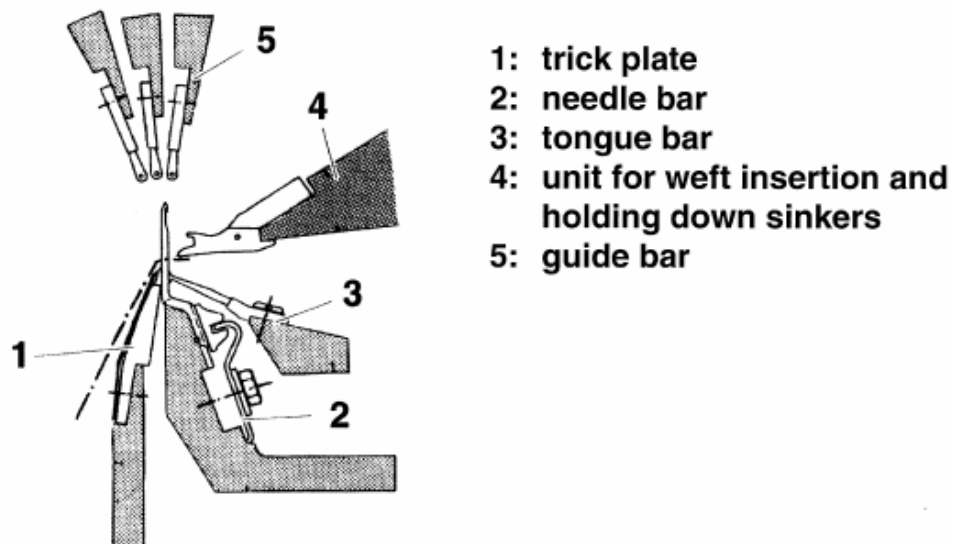
Figure 2.3 Warp knitting machine, principal set-up of knitting elements (Mayer RS3 MSU-V, with magazine weft insertion) (Stumpf et al., 1998, p. 1514).

In contrast to weft knitting, which in principle requires only one spool of yarn, warp knitting needs as many yarn ends as loops are to be formed in one step/one row. Therefore, the yarns are usually put on a so-called 'beam' before the actual knitting step. The result is a long drum that contains many parallel (say 1000, for instance) yarns spooled onto it, so that a family of parallel yarns can be obtained when pulling them off the drum. This makes warp knitting a technique particularly aimed at mass production (Stumpf et al., 1998, p. 1513).

Generally, weft-knit structures are less stable and, hence, stretch and distort more easily than warp-knit structures so that they are also more formable. It is noteworthy that an obvious advantage of warp over weft knitting is that the former tends to have a significantly higher production rate since many yarns are knitted at any one time. The ease with which weft-knitted fabrics unravel and the cost associated with warping beams are also important considerations in choosing between weft and warp knitting. Clearly, weft knitting is preferred for developmental work whereas warp knitting would be more favourable in large-scale production (Leong et al., 2000, p. 199-200).

As shown in Figure 2.4 and Figure 2.5, knitting can produce a large number of stitch geometries. By controlling the stitch (loop) density, a wide range of pore geometry can be generated.
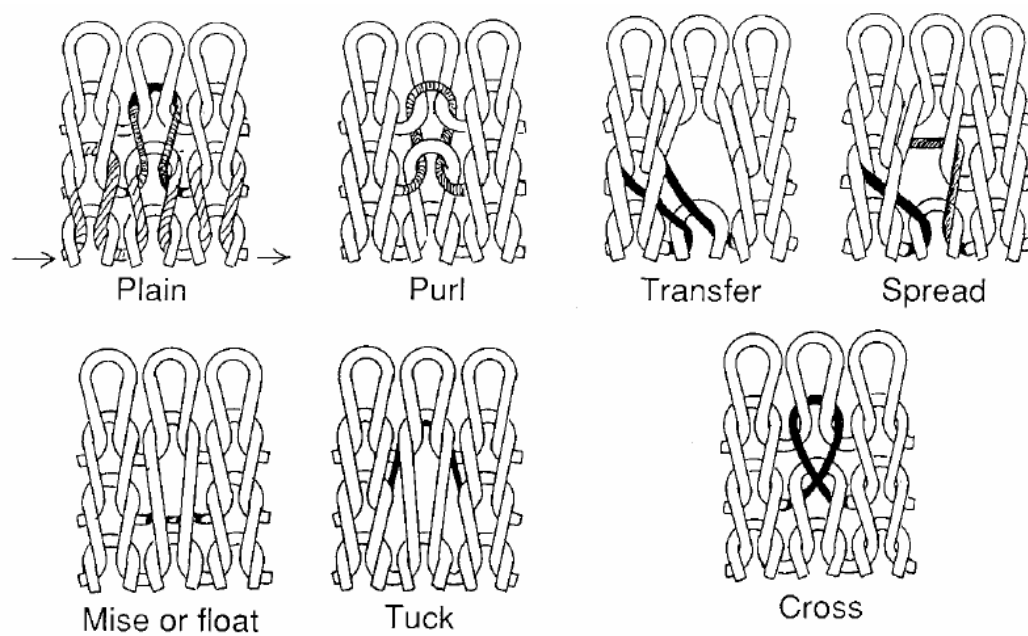
Figure 2.4 Weft-knit constructions (Ko, 1993, p. 81).
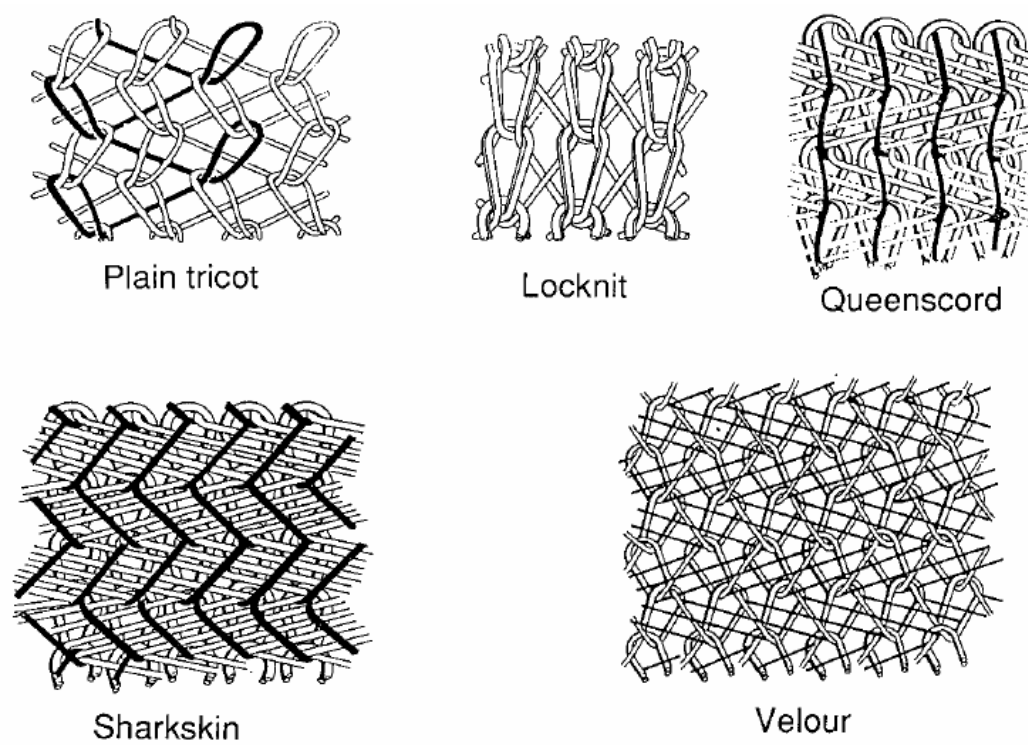
Figure 2.5 Warp-knit constructions (Ko, 1993, p. 81).

2.2.1.2 Multiaxial Multilayer Warp-Knit (Non-Crimp) Fabrics

With both weft and warp knitting, it is possible to insert straight (or almost straight) inlay yarns in course and wale directions (Ko, & Du, 1992). This changes the properties of the knitted fabric and the knitted fabric composite dramatically. The extensional deformability of the fabric in the direction of the inlay yarn is reduced to (almost) zero. At the same time, composite properties such as stiffness and strength increase strongly in the inlay direction. In these structures, the overall mechanical behaviour of both the fabric and the composite is mainly governed by the straight inlay yarns. Therefore, knitted fabrics with inlay yarns would better be classified under the category 'non-crimp fabrics' (also called 'multi-axial layers' or 'directionally oriented structures') rather than 'knitted fabrics'.
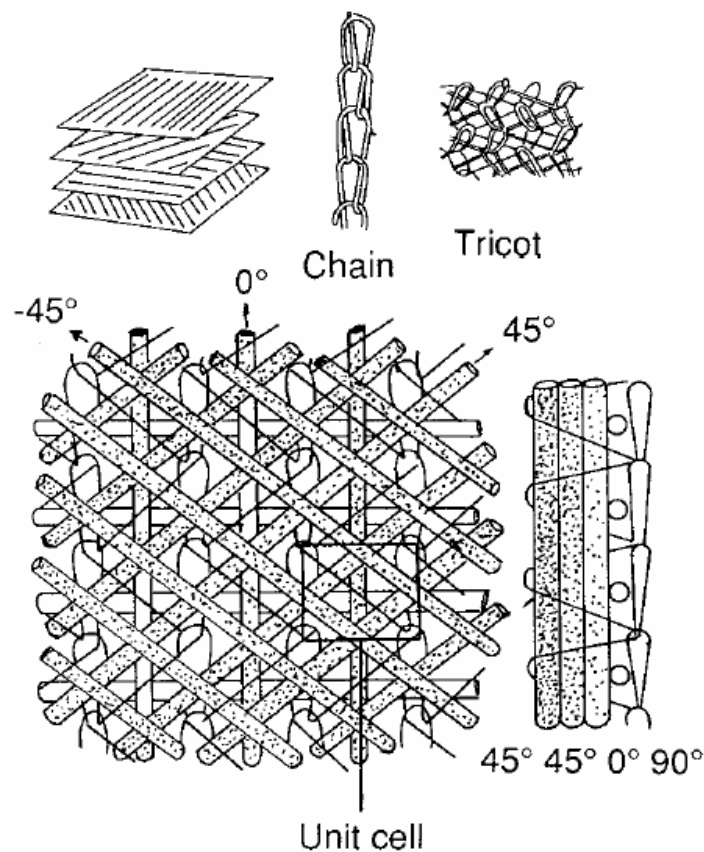
Figure 2.6 Multiaxial warp-knit fabric systems (Ko, 1989, p. 141).

Multiaxial non-crimp fabric (NCF) is a relatively new class of textile preform for polymer composites that consists of multiple layers of fibrous yarns stitched together by warp knitting (Figure 2.6). The most commonly used types of NCFs are biaxial, triaxial and quadriaxial fabrics in which straight, uncrimped yarns are aligned in the warp (0°), bias (30°< θ <90°) and/or weft (90°) directions to provide multidirectional in-plane properties. In addition, chopped fibre or fleece mat can be incorporated into the fabric, although their use is usually confined to the surface layer to provide a high quality finish to a composite product. The yarn layers and mats are bound together by warp knitting with a chain or tricot stitch pattern using polyester thread or (less often) aramid or glass yarn.

The combination of stacked fibre layers into a single, thick fabric overcomes the high cost and long production time often incurred with the manual hand laying of thick preforms using conventional single layer fabric and tape. A further advantage is that composites reinforced with NCF generally exhibit higher in-plane mechanical properties than conventional woven fabric composites because the yarns are not crimped. In addition, the interlaminar shear resistance, delamination toughness and impact damage tolerance of NCF composites is superior to conventional tape laminates because of the through-thickness reinforcement provided by the stitches.

A key advantage of NCFs is an ability to be deformed into relatively complex shapes without the wrinkling that is normally experienced with standard woven fabric and prepreg tape. For this reason, the use of composites reinforced with NCF is growing rapidly in aircraft, automobiles, yachts, wind turbine blades and other complex structural components (Kong, Mouritz, & Paton, 2004, p. 249).

According to a standard, multiaxial multiply fabrics (MMFs) consist of two components, the ply construction and the binding system. The ply construction is defined as 'a textile structure constructed out of one or more laid parallel non-crimped non-woven thread plies, which are differently oriented, with different thread densities of single thread plies and in which integration of fibre fleeces, films foams or other materials is possible'. The latest development available for producing

noncrimp fabrics is the so-called Liba (Copcentra) (Figure 2.7) systems. Figure 2.7 illustrates a four weft insertion system machine, but higher numbers are possible with larger machines which can also incorporate layers of fleeces or chopped strand mats (Bischoff et al., 1998; Franzke, Offermann, Bischoff & Wulfhorst, 1997; Hörsting et al., 1993). With the Liba system, reinforcing fibres are drawn from creels and then deposited in the required orientation via a weft insertion mechanism. The weft insertion mechanism comprises yarn carriers that oscillate between the width of the machine during which the fibre yarns are laid down and secured before they are all finally fixed together by means of a warp-knit structure (Dexter & Hasko, 1996)). Apart from 0° and 90°, the orientation of the fibre sheets can be laid down at off-axis angles of 30–60° (Bischoff et al., 1998; Hörsting et al., 1993). The warp knitting needles are inserted in the thickness direction of the fabric thus exposing the straight fibre yarns to impalement and consequently fibre damage and misalignment (Dexter et al., 1996).
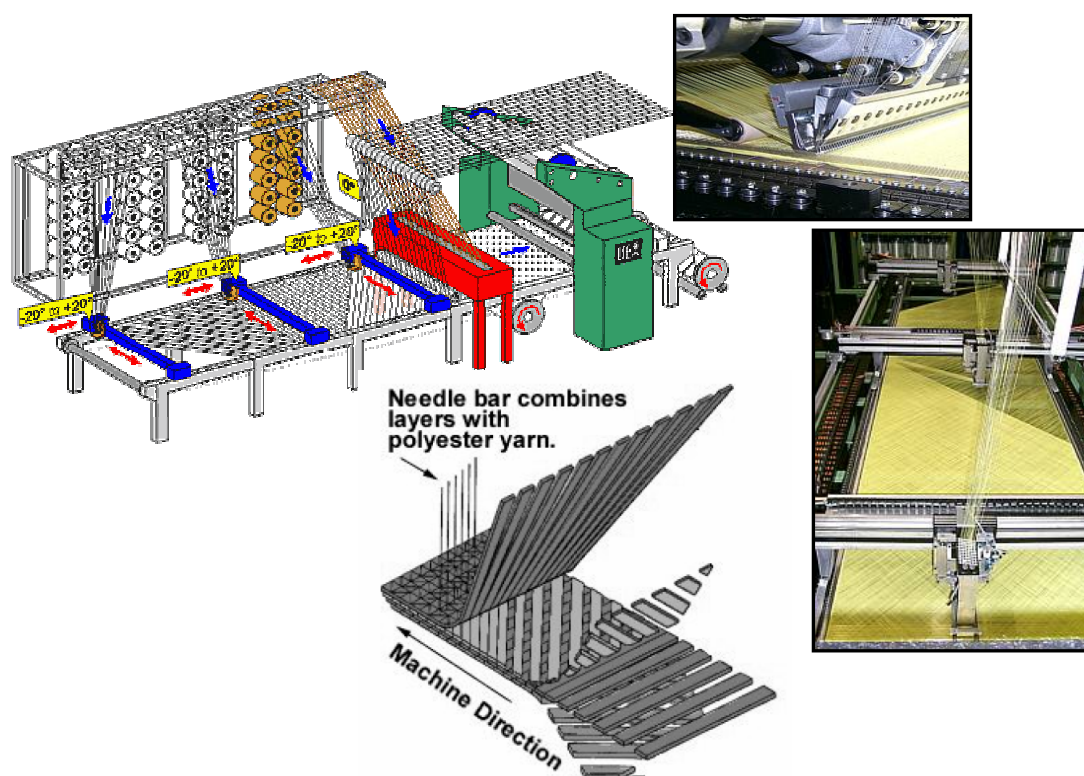
Figure 2.7 (a) Schematic of the Liba process for manufacturing non-crimp fabric; (b) knit loop formation; (c) examples of the fiber placement heads (from web cite of LIBA-Maschinenfabrik GmbH); (d) an example of the type of fabric that can be produced with this process (Mattsson, 2005).

2.3 Matrix Resins

2.3.1 Thermosets versus Thermoplastics

Nowadays both thermoplastic and thermosetting resins are used as matrices for composites. Each type exhibits particular advantages and disadvantages with respect to processability and service performance, as illustrated in Table 2.6. Although a wide range of different chemistries exists within each type, some general features can be distinguished, which have determined their area of application.

Table 2.6 Property/process characteristics for thermoplastic and thermosetting matrix systems

Property	Thermoset	Thermoplastic
Modulus	high	low
Service temp.	high	low
Toughness	low	high
Viscosity	low	high
Processing temp.	low	high
Relaxation time (at proc.)	long	short
Conversion costs	high	low
Recyclability	limited	good

Some of the basic properties of selected thermoset and thermoplastic resins are shown in Table 2.7 and Table 2.8, respectively.

Table 2.7 Typical unfilled thermosetting resin properties (Mazumdar, 2002, p. 48).

Resin Material	Density (g/cm^3)	Tensile Modulus (GPa)	Tensile Strength (MPa)
Epoxy	1.2-1.4	2.5-5.0	50-110
Phenolic	1.2-1.4	2.7-4.1	35-60
Polyester	1.1-1.4	1.6-4.1	35-95

In general the crosslinked structure of thermosetting polymers provides potential for higher stiffness and service temperatures than thermoplastics. The upper limit of service temperature for advanced composites is most often determined by the glass transition temperature.

On the other hand, toughness and elongation to break may be considerably for thermoplastic resins. This may be a particular advantage in applications where impact strength is a major requirement. Most high-performance thermoplastics offer outstanding interlaminar fracture toughness and acceptable post-impact compression response. This feature of thermoplastic materials has been the major reason for their increased use in composite structures.

Table 2.8 Typical unfilled thermoplastic resin properties (Mazumdar, 2002, p. 53).

Resin Material	Density (g/cm^3)	Tensile Modulus (GPa)	Tensile Strength (MPa)
Nylon	1.1	1.3-3.5	55-90
PEEK	1.3-1.35	3.5-4.4	100
PPS	1.3-1.4	3.4	80
Polyester	1.3-1.4	2.1-2.8	55-60
Polycarbonate	1.2	2.1-3.5	55-70
Acetal	1.4	3.5	70
Polyethylene	0.9-1.0	0.7-1.4	20-35
Teflon	2.1-2.3	–	10-35

From a processing viewpoint, the high melt viscosities of thermoplastics generally create considerable difficulties during fiber wet-out and impregnation. Thus, thermoplastic-based composites generally require higher processing temperatures and pressures to ensure sufficient flow during the final forming process.

The higher processing temperatures and pressures needed for the forming of thermoplastic-based composites generally impose stricter requirements on the processing equipment, and more advanced engineering is needed for tool construction. The higher processing temperatures may also induce considerable

difficulties in mismatch of thermal contraction between the matrix and fibers during the processing cycle.

The longer relaxation times for thermosetting materials may be a disadvantage, due to a reduced ability to relax process-induced internal stresses. In anisotropic composites in particular, the potential of the polymer to relax internal stress fields is important for the elimination of process-induced defects. Such defects, in the form of voids, microcracking, fiber buckling, warpage, and residual stresses may diminish the durability and long-term performance of the composite.

Thermoplastic-based composites offer potential for lower *conversion costs* from intermediate material forms into final end-use parts by process automation. Furthermore, thermoplastics also offer the advantage of having almost indefinite storage life, which facilitates the logistics of the manufacturing procedure.

Finally, thermoplastics may be post-formed and/or reprocessed by the reapplication of heat and pressure, which gives a potential for *recyclability*. The increased awareness, in these last years, about material Recyclability has brought about a heightened interest in thermoplastic matrix composites, especially in large volume areas such as the automobile industry.

2.4 Composite Processing

Processing is the science of transforming materials from one shape to the other. Because composite materials involve two or more different materials, the processing techniques used with composites are quite different than those for metals processing. Figure 2.8 classifies the frequently used composites processing techniques in the composite industry.
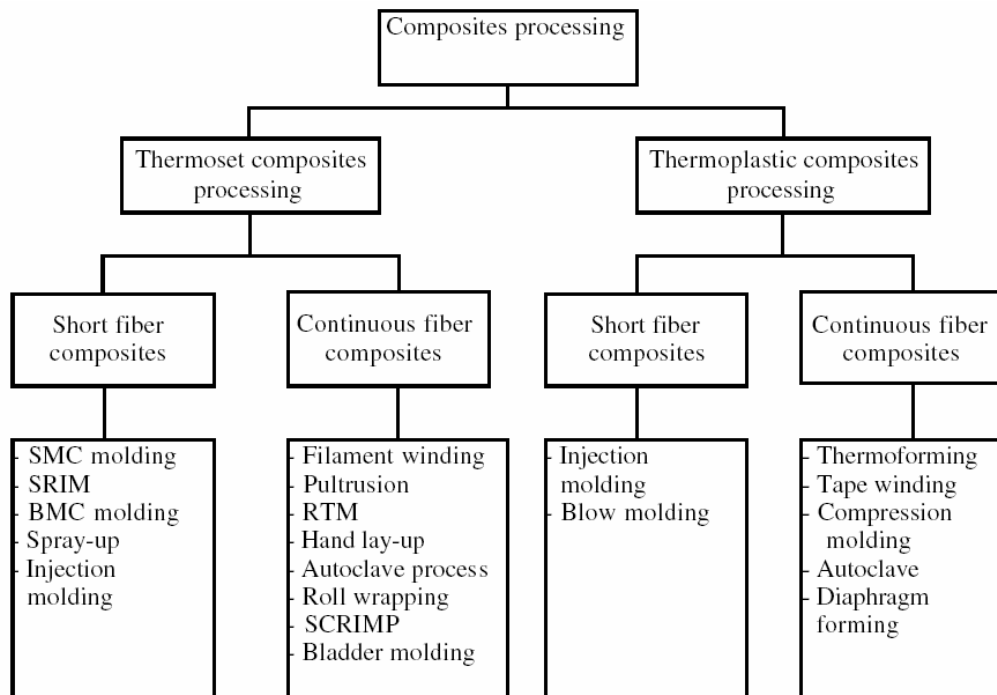
Figure 2.8 Classification of composites processing techniques (Mazumdar, 2002, p. 32).

Resin transfer molding (RTM) and resin film infusion (RFI) have become popular cost-effective processing techniques for the manufacture of primary composite structural components for the aerospace industry (Hasko, Dexter, Loos, & Kranbuehl, 1994). The resin infusion processes lend themselves to the use of near net shape textile preforms manufactured through a variety of automated textile processes such as knitting and braiding (Dexter, 1996). Often, these advanced fiber architecture preforms have through the-thickness stitching for improved damage tolerance and delamination resistance (Palmer, Dow, & Smith, 1991). The challenge facing the resin infusion techniques is to design a robust process that will consistently ensure complete infiltration and cure of a geometrically complex shape preform with the high fiber volume fraction needed for structural applications. One major disadvantage of the RTM and RFI processes is that they require expensive molds or tools that allow high-pressure resin infusion. In addition, long duration, high temperature cure cycles are required to fully cure the resin-saturated preforms. The vacuum assisted resin transfer molding (VARTM) or the patented SCRIMP (Seemann Composite Resin Infusion Molding Process) (Seemann, 1990; Seemann,

1994) processes have been developed as alternative low cost methods for the manufacture of composite structures.

VARTM has been used to successfully fabricate marine composites for both military and commercial applications (Lewis & Jakubowski, 1997; Nguyen, Juska, & Mayers, 1997; Lazarus, 1996) and structural laminates for ground combat vehicles (Pike, MacArthur, & Schade, 1996). The ability of the VARTM process to fabricate aircraft-quality stiffened composite structures, i.e., structures with a high fiber volume fraction and low void content, still needs to be established.

In the VARTM process, net shape, fiber performs are infiltrated with a liquid resin and then cured either at room temperature or at elevated temperature in an oven. Use of automated textile processes such as weaving and braiding to produce net shaped performs significantly reduces the lay-up and consolidation costs. Tooling costs are reduced because on one side of the part a flexible nylon or silicon rubber vacuum bag is used in place of a hard metal or composite tool. If the resin-infiltrated part can be cured under ambient conditions, the size of the structure that can be fabricated by VARTM is essentially unlimited.

2.4.1 Vacuum-Assisted Resin Transfer Molding (VARTM) Procedure

Both open mold approaches, where one surface is bagged with a flexible film, and closed-mold approaches to resin transfer molding are practiced. An example of open mold RTM, vacuum-assisted resin transfer molding (VARTM) is a common method employed as an alternative to autoclave use. In VARTM, atmospheric pressure is utilized to achieve consolidation and impregnation by vacuum bagging the laminate (Figure 2.9).
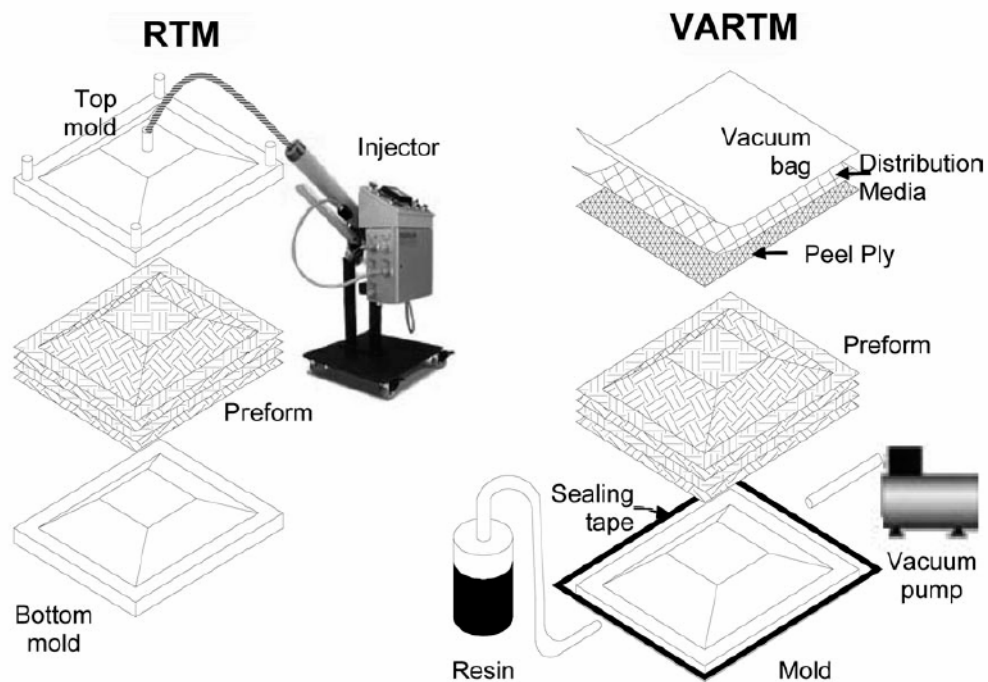
Figure. 2.9 The differences between Resin Transfer Molding and Vacuum Assisted Resin Transfer Molding (VARTM), (Šimáček & Advani, 2004, p. 356).

An inlet for the polymer is located at one or more points in the tool or bag, and vacuum outlets are located some distance away. The vacuum pump creates a pressure gradient of approximately 1 atm within the bag, which is sufficient for the impregnation of laminates large in size and complex geometry. For processes in which final cure occurs after the mold is filled, completion of the cure can be carried out in an oven while atmospheric pressure is maintained on the impregnated laminate.

The VARTM procedure for a representative flat panel (Figure 2.10) is described in the following steps:

1. Thoroughly clean the aluminum plate using sandpaper and acetone. On the cleaned surface, create a picture frame using masking tape. Then apply several coats of release agent to the metal surface inside of the masked frame. Remove the masking tape.

2. In place of the masking tape, apply a silicone bagging tape to the bare metal surface. The silicone tape should again form a picture frame. Add a strip of the tape to the outer edge of the length of the frame at either ends. These two strips will provide an added adhesive surface for attachment of the inlet and outlet tubing. Leave the paper backing on the silicone tape to protect it during the remainder of the lay-up procedure.

Figure 2.10 VARTM process (a) top view of VARTM setup; (b) side view of VARTM setup.

3. Place the fiber preform stack on the coated tool, inside the tape frame. A gap should exist between the silicone tape and both edges of the preform to allow for tubing. No gap should exist between the silicon tape and fiber preform along the panel width to avoid providing a flow pathway outside the preform to the vacuum port.

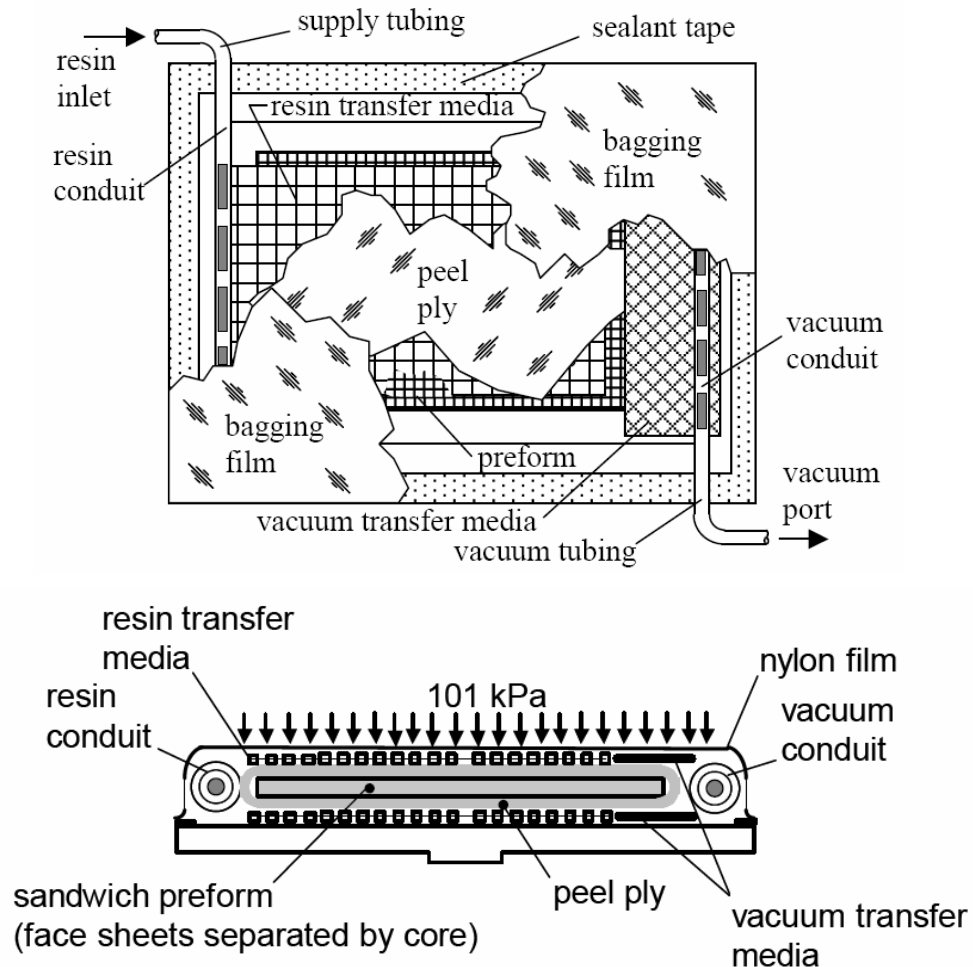4. Cut one layer of porous release film (with the same dimensions as the panel), and place it on top of the preform. The release film will allow the composite laminate to release from the distribution media.

5. Cut one layer of distribution medium (e.g., biplanar nylon 6 mesh with the same dimensions as the fiber preform) and stack it above the release cloth. A highly permeable distribution medium is incorporated into fiber preform as a surface layer. During infusion, resin flows preferentially across the surface and simultaneously through the preform thickness, which enables large parts to be fabricated.

6. Place distribution tubing across the width of the laminate. On the inlet side, place the tubing on top of the distribution media that overhangs the preform. Spiral wrap, 18-mm-diameter conduit is an ideal choice for the distribution tubing because it allows the resin to flow quickly into the distribution media and preform in a continuous line across the width.

7. Use flexible plastic tubing (vinyl or Teflon, depending on temperature requirements) to supply resin and draw vacuum on the laminate. It is critical to properly choose the location of the vacuum tubing to fully wet out the preform, reduce excessive resin bleeding (i.e. minimize waste), and avoid creating resin-starved regions near the vent locations after the inlet is closed. Connect the free end of the vacuum tubing to a resin trap, which catches any resin that might be pulled into the tube on its way to the vacuum pump.

8. With the laminate complete and the tubing in place, the part can be bagged using an appropriate film. Take care to eliminate creases in the bag and ensure an airtight seal with the tool surface and silicone bagging tape. Once bagging is complete, the laminate should be fully evacuated to 762 mmHg using the vacuum pump. Leaks can be detected by using either listening device or by clamping the vacuum line and using a vacuum gauge. Even a small leak in the system may result in voids and poor consolidation of the final composite part.

9. Before infiltration can occur, the resin must be degassed to remove any air bubbles that were introduced during mixing. Perform degassing separately in a vacuum chamber; degassing can typically require 1 to 4 h, depending on the resin viscosity. All air bubbles must be removed prior to infiltration.

10. With the bagged laminate under full vacuum, submerge the clamped end of the resin supply tubing in the degassed resin bucked. Remove the clamp while the tube end is submerged to prevent any air entering the tube and the part ahead of the resin. With the tube clamped removed, the resin flows through the supply tubing and into the distribution tubing. The spiral distribution tubing allows the resin to spread quickly across the width of the lay-up as it enters the distribution media. The distribution media provides the path for the resin to flow quickly down the length of the preform and then through the laminate thickness.

11. The flow-front of resin through the part can be viewed through the bagging film. Halt the flow of resin when the preform is fully infiltrated, as evidenced by resin beginning to enter the vacuum distribution tubing. Stop the resin flow by first clamping and severing the resin supply tubing and then clamping and severing the vacuum tubing. Again, these clamps must provide an airtight seal, because any leaks during cure will result in poor consolidation of the part. It is recommended that a second envelope bag be used to pull vacuum on the part during cure. Finally, place the vacuum sealed part in an oven, and heat it according to cure cycle prescribed by the resin supplier.

2.5 Mechanical Behavior of Composite Materials

In introductory strength of materials, the constitutive relationship between stress and strain was established for homogeneous isotropic materials as Hooke's law. A composite material is analyzed in a similar manner, by establishing a constitutive relationship between stress and strain.

Isotropic, homogeneous materials (steel, aluminum, etc.) are assumed to be uniform throughout and to have the same elastic properties in all directions. Upon application of uniaxial tensile load, an isotropic material deforms in a manner similar to that indicated in Figure 2.11 (the dashed lines represent the undeformed specimen). Application of normal stress causes extension in the direction of the stress and contraction in the perpendicular directions, but no shearing deformation. Unlike conventional engineering materials, a composite material is generally

nonhomogeneous and does not behave as an isotropic material. Most composites behave as either *anisotropic* or *orthotropic* materials.
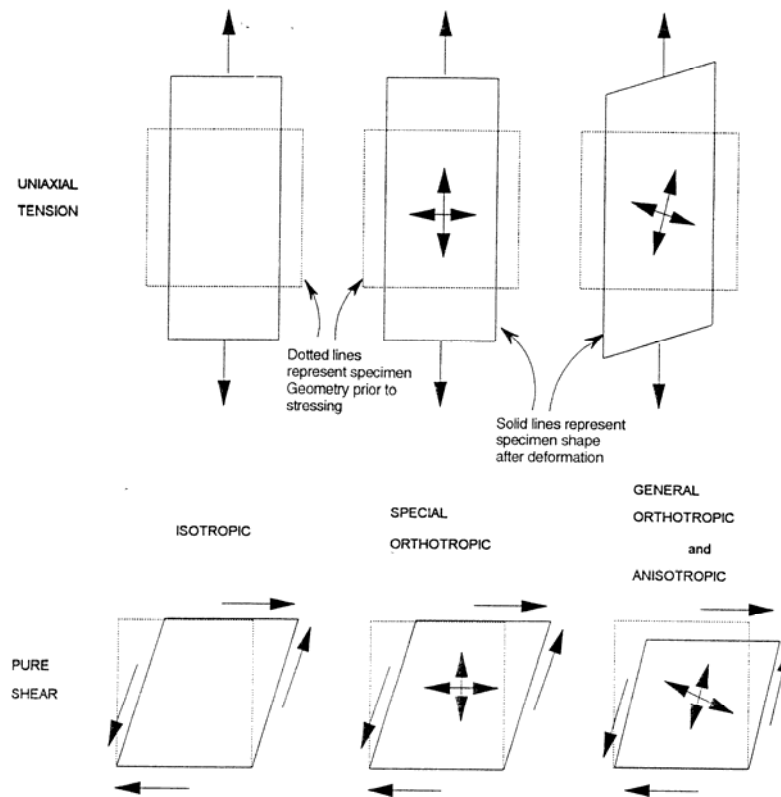
Figure 2.11 Typical material responses for isotropic, anisotropic, and orthotropic materials subjected to axial tension (Jang, 1994, p. 96)

For orthotropic materials, like isotropic materials, application of normal stress in a principal material direction (along one of the intersections of three orthogonal planes of material symmetry) results in extension in the direction of the stress and contraction perpendicular to the stress. The magnitude of the extension in one principal material direction under normal stress in that direction is different from the extension in another principal material direction under the same normal stress in that other direction. Thus different Young's moduli exist in the various principal material directions. In addition, because of different properties in the two principal directions, the contraction can be either more or less than the contraction of a similarly loaded isotropic material with the same elastic modulus in the direction of the load. Thus, different Poisson's ratios are associated with different pairs of principal material

directions (and with the order of the coordinate direction numbers designating the pairs) (Jones, 1999, p. 13).

The material properties of an anisotropic material are different an all directions. Application of a normal stress leads not only to extension in the direction of the stress and contraction perpendicular to it, but to shearing deformation. Conversely, application of shearing stress causes extension and contraction in addition to the distortion of shearing deformation. This coupling between both loading modes and both deformation modes, i.e., shear-extension coupling, is also characteristic of orthotropic materials subjected to normal stress in a non-principal material direction.

2.6 Thermal Characterization of Polymer Composites

2.6.1 Heat Transfer

Heat transfer is energy in transit due to a temperature difference. Whenever there exists a temperature difference in a medium or between media, heat transfer must occur. When a temperature gradient exists in a stationary medium, which may be a solid or a fluid, the term conduction is used to refer to the heat transfer that will occur across the medium. In contrast, the term convection refers to heat transfer that will occur between a surface and a moving fluid when they are at different temperatures. The third mode of heat transfer is radiation in which all surfaces of finite temperature emit energy in the form of electromagnetic waves.

Since this study focuses the measurement of the thermal conductivity, the heat transfer process due to convection and radiation will not be discussed here.

2.6.1.1 Conduction

The word "conduction" at the first view is the transfer of energy from the more energetic to the less energetic particles of a substance due to interactions between the

particles. The physical mechanism of conduction is most explained by considering a solid phases of a substance.

In *solids*, heat conduction is due to two effects: the *lattice vibrational waves* induced by the vibrational motions of the molecules positioned at relatively fixed positions in a periodic manner called a lattice, and the energy transported via the *free flow electrons* in the solid. The thermal conductivity of a solid is obtained by adding the lattice and electronic components. …. The lattice component of thermal conductivity strongly depends on the way the molecules are arranged (Çengel, 1998, p.24).

It is possible to quantify heat transfer processes in terms of appropriate rate equations. These equations may be used to compute the amount of energy being transferred per unit time. For heat conduction, the rate equation is known as *Fourier's law*. The general Fourier's low is:

$$\mathbf{q_i} = -\mathbf{K_{ij}} \frac{\mathbf{dT}}{\mathbf{dX_j}} \tag{2.1}$$

For the one dimensional plane wall having the temperature distribution T(x), the rate equation is expressed as:

$$q = -K \frac{dT}{dX} \tag{2.2}$$

The heat flux q (W/m^2) is the heat transfer rate in the x direction per unit area perpendicular to the direction of transfer, and it is proportional to the temperature gradient in that direction. The proportionality constant K is a transport property known as the thermal conductivity (W/m.°C) and is a characteristic of the material. The minus sign is a consequence of the fact that heat is transferred in the direction of decreasing temperature.

2.6.1.2 Thermal conductivity

Thermal conductivity of fiber reinforced composite laminates is anisotropic in nature. Published literature reveals that fiber reinforced composites have significantly different thermal conductivity values in three directions–strongly anisotropic. The thermal conductivities of anisotropic composites are the highest along the fiber direction, medium in the transverse direction and lowest in through-the-thickness direction.

The thermal conductivity of an anisotropic composite material depends on the resin nature, fiber type and architecture, fiber volume fraction, manufacturing technique, direction of heat flow and operating temperature, leading to a high degree of complexity. Various approaches are used to yield the thermal conductivity of a composite material so that the heat flow in anisotropic composite material in any direction can be estimated.

Analysis of conduction heat transfer for a classical composite walls shows that the assumption of parallel thermal resistance, Figure 2.12(a) gives a lower bound of the thermal resistance and hence an upper bound of the thermal conductivity. The assumption of series thermal resistance, on the other hand, Figure 2.12(b) gives an upper bound of the thermal resistance and consequently a lower bound of the thermal conductivity (Al-Sulaiman, Mokheimer, & Al-Nassar, 2005, p.371).
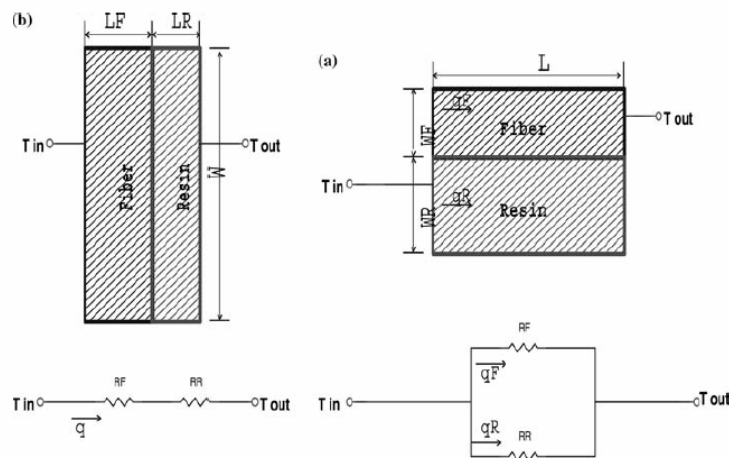

Figure 2.12 Physical problem and the equivalent parallel and series thermal arrangement of a composite wall (Al-Sulaiman, Mokheimer, & Al-Nassar, 2006, p. 371).

2.6.1.3 Heat Capacity

Heat capacity, C_p, is the heat needed to increase the temperature of the system in question by 1 K written as $\partial(H / \partial T) = C_p$, at constant pressure and number of moles (Wunderlich, Pyda, Pak, & Androsch, 2001). The fastest processes are described by fitting quantum-mechanical models to the temperature dependence of the equilibrium heat capacity.

The connection between the macroscopic internal energy and the microscopic molecular motion is most easily established for solids. At sufficiently low temperature only vibrational motion is possible. The classical model of motion in solids to assume that each atom can carry out vibrations in the three dimensions of space. Such motion should contribute a heat capacity at constant volume of $C_v = 3R$ J.K^{-1}.mol^{-1}, where R is the gas constant (8.314 J.K^{-1}.mol^{-1}) and $C_v = (\partial U / \partial T)$ at constant pressure and volume (where U is the internal energy). …. As the temperature increases, some of the vibrations may change to a large-amplitude motion, i.e. to a translation, rotation, or internal rotation. …. Finally, flexible molecules may add internal rotations which are usually called conformational motions. At sufficiently high temperatures, all these changes reduce the heat capacity. At lower temperatures, large amplitude motion causes usually an increase in the observed C_p since it involves positions of higher potential energy (Wunderlich et al., 2001, p.10-13).

It is relatively easily determined for small and homogeneous samples. However, for heterogeneous materials having different phases, it is almost impossible to prepare a small and representative sample, so that the measurement of this property must become particularly troublesome. In this study, heat-flux differential scanning calorimetry was used as a quick and reliable tool for the measurement of an absolute value of heat capacity of fiber reinforced polymer composites.

2.7 NCF Composites and Industrial Use

NCF composites have due to their excellent performance and relatively low cost become an attractive alternative for aerospace, marine and even automotive applications (Mattsson, 2005). In fact, NCF composites are considered to be one of the most promising future concepts for aerospace structural composites (Greenhalgh & Hiley, 2003).

An excellent example of the use of NCF composites in aerospace applications is the rear pressure bulkhead for the Airbus A380 aircraft (Edgren, 2006). The bulkhead is manufactured using NCF and resin film infusion (RFI) technique (Filsinger, Dittmann & Bischoff, 2004), see Figure 2.13.
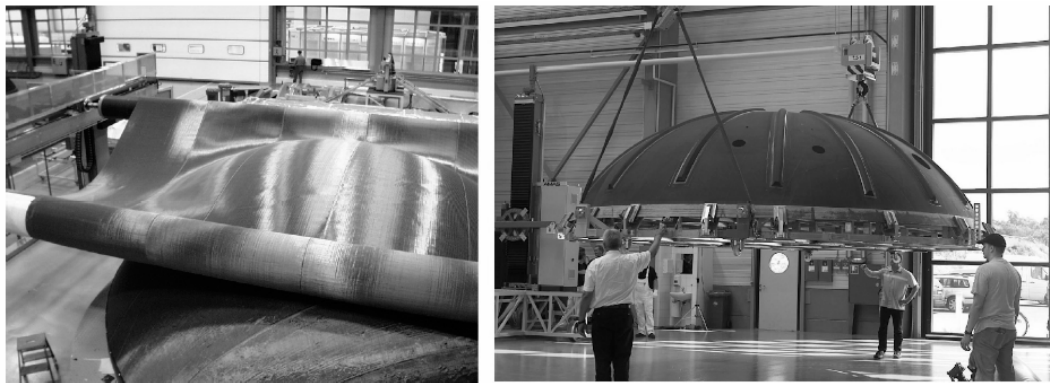

Figure 2.13 Rear pressure bulkhead for the Airbus A380. a) Draping of NCF over mould. b) Finished NCF composite bulkhead (Edgren, 2006).

CHAPTER THREE
EXPERIMENTAL DETAILS

3.1 Materials and Sample Preparation

3.1.1 Materials

Three multiaxial non-crimp glass fabrics were studied in this study (Figure 3.1(a), (b) and (c)). Biaxial fabric (BA), and triaxial fabric (TA) were custom manufactured for this study using a Liba multiaxial warp-knitting machine by Metyx Telateks Tekstil Urunleri San. Tic. A.S. (Turkey). Unidirectional (UD) glass fabric was added for this part of the study. Their parameters, as specified by the manufacturer, are shown in Table 3.1.

Unidirectional (UD) and Biaxial (BA) carbon fabric (Figure 3.2(a) and (b)) provided by Metyx Telateks Tekstil Urunleri San. Tic. A.S. (Turkey) using a Liba multiaxial warp-knitting machine were used for experimental characterization. Figure 3.2 shows a scanned image of both sides of a piece of biaxial carbon fabric and unidirectional carbon fabric which is stabilized by a set of glass fibers on the bottom face. The carbon fabric parameters, as specified by the manufacturer, are shown in Table 3.2.

Polipol polyester 383-T resin system was used as resin in the composite. The resin (specific gravity: 1.11, viscosity brookfield: 950), which is iso-phthalic acid type resin, was mixed before VARTM with the catalyst cobalt octoate (0.35 pph, of a 41% solution in white spirit), the retarder 2.4-pentanedione (0.10 pph), and methylethylketone peroxide (2.2 pph, of a 40% dimethyl phthalate solution). Another resin system used in this study is a two-component epoxy system from Resoltech which consists of R 1040 (unmodified liquid epoxy) and R 1048 (hardener). The composition for the epoxy resin system is specified in the product data sheet from the manufacturer to be (by weight): R1040 (78%) and R 1048 (22%).

Face	**Back**
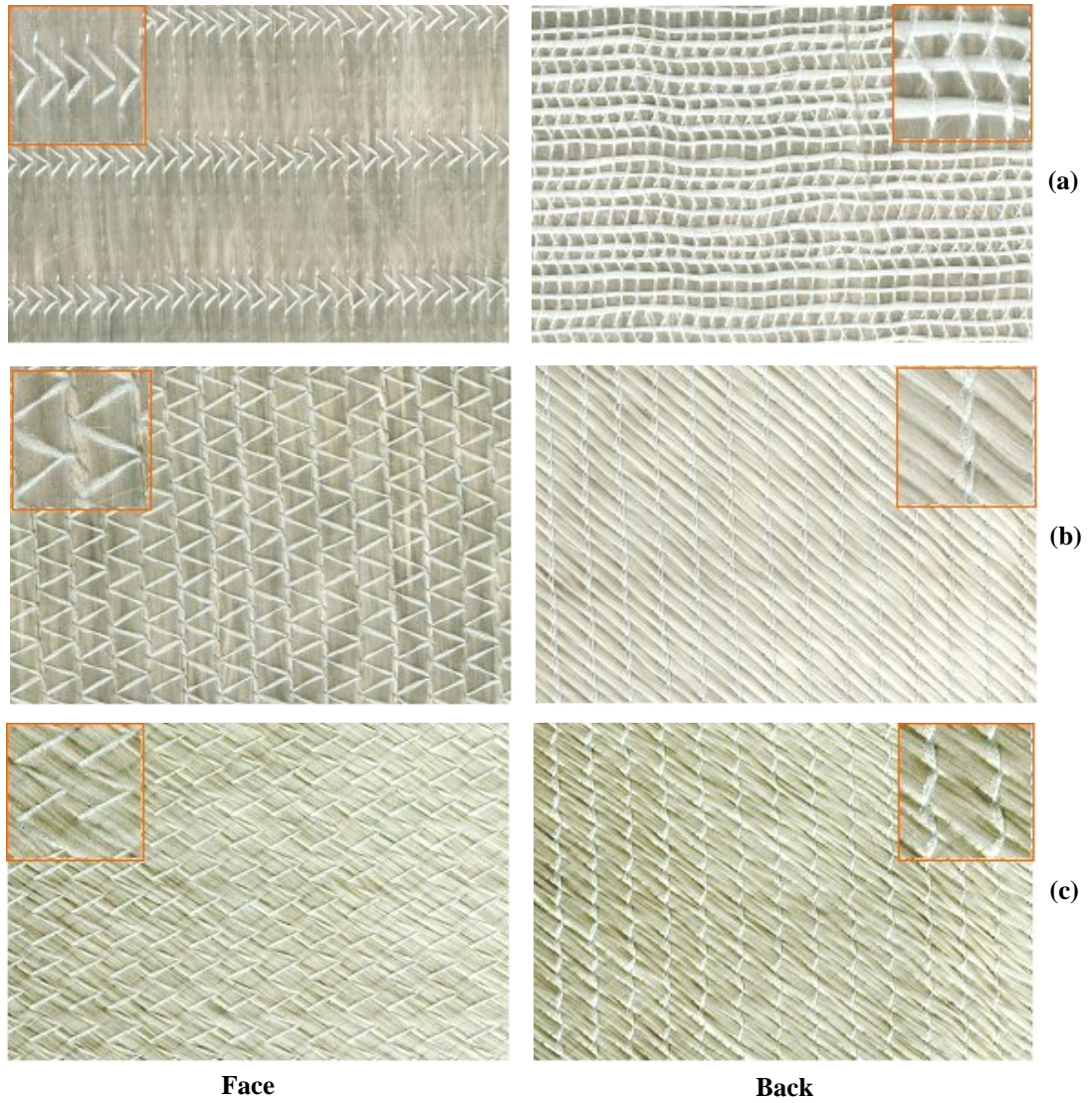
Figure 3.1 Sample of fabrics: (a) unidirectional glass fabric; (b) triaxial 0,+45/-45° glass fabric; and (c) biaxial +45/-45° glass fabric

Face   **Back**
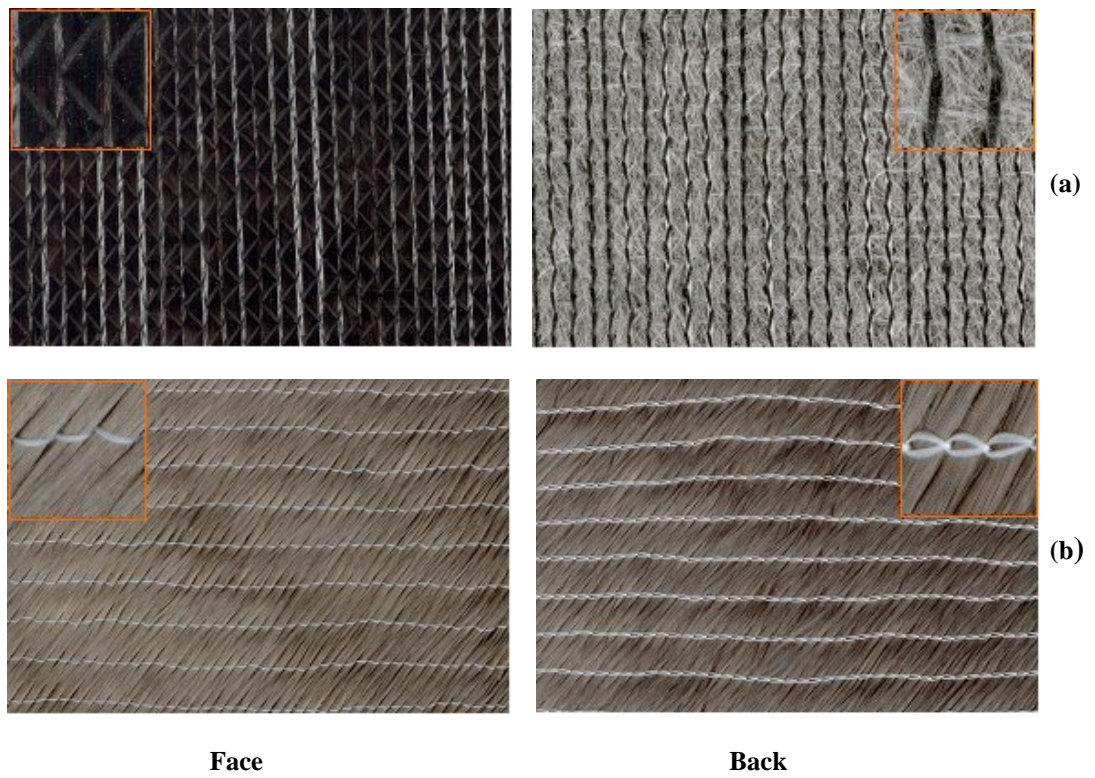
Figure 3.2 Sample of fabrics (a) unidirectional carbon fabric; (b) biaxial +45/-45° carbon fabric

Table 3.1 Specifications of multi-axial multi-ply glass fabrics.

Preform ID	Description	Number of plies	Orientation of plies (deg)	Total weight (g/m^2)	Plies weight (g/m^2)	Stitch pattern
UDGF	Unidirectional glass fabric	1	0	472	472	Tricot
BAGF	Biaxial glass fabric	2	+45;-45	468	234/234	Tricot
TAGF	Triaxial glass fabric	3	0;+45;-45	1408	472/468/468	Tricot

Table 3.2 Specifications of multi-axial multi-ply carbon fabrics.

Preform ID	Description	Fibrous layers				Stitching			
		Areal density [g/m^2]	Fibre	Fibre count in tow	Orientation [°]	Stitch	Linear density [tex]	Knit pattern	Gauge [needles/inch]
UDCF	Unidirectional carbon fabric	200	Toray T700 50E	12K	0	PES	5	Tricot	5
BACF	Biaxial carbon fabric	400	Toray T700 50E	12K	+45;-45	PES	5	Tricot	5

The properties of the constituents from the data sheet provided by the manufacturer are listed in Table 3.3.

Table 3.3 Constituent property data for composite laminate

Properties	Carbon fiber	E-glass fiber	Matrix polyester	Matrix epoxy
Tensile modulus, GPa	390	74	3.15	3.6
Tensile strength, MPa	4410	3448	40	65
Elongation, %	1.20	3.50	2.50	1.70
Density, g/cm^3	1.77	2.40	1.20	1.10

3.1.2 Composite Production

The VARTM equipment at the GOVSA Composites Ltd. was used to manufacture composite plates. Composite plates having different fiber volume fractions shown in Tables 3.4, 3.5 and 3.6 (the data obtained by a resin burn-off method are the reported mean values from the manufacturer) were used for the test specimens. In the VARTM process, the entire fiber reinforced polymer (FRP) composite is produced in one single operation in which resin is injected with the assistance of vacuum (Figure 3.3). A flat glass plate, cleaned and coated with release agent (Freekote), was used as a mold. First, a 44 cm long by 32 cm wide, dry, fibrous preform was laid on top of the tool and was covered by a distribution medium with a high in-plane permeability to accelerate the in-plane flow. A plain weave nylon screen which is a type of plastic wire mesh with high porosity was used as the distribution medium. A sheet of porous peel-ply was draped over the composite to prevent the distribution medium from adhering to the cured panel and to create a clean surface. Thus, a typical VARTM lay-up comprises fiber reinforcements, surface or inter-laminar distribution medium, chemical agents/textiles to minimize defects and facilitate de-molding. After laying up the composite panel, a spiral-wrap, 12-mm-diameter conduit was placed across the width and length of the laminate at points 2.5 cm away from the panel to ensure uniformly applied vacuum. The resin inlet was placed in the middle of the stack and was connected to a resin tank as a resin injection gate. A vacuum bag was next applied and the edges were sealed with a tacky tape. Tacky tape is a 1-in.-wide rubbery material that sticks to both the mold and the bagging material.
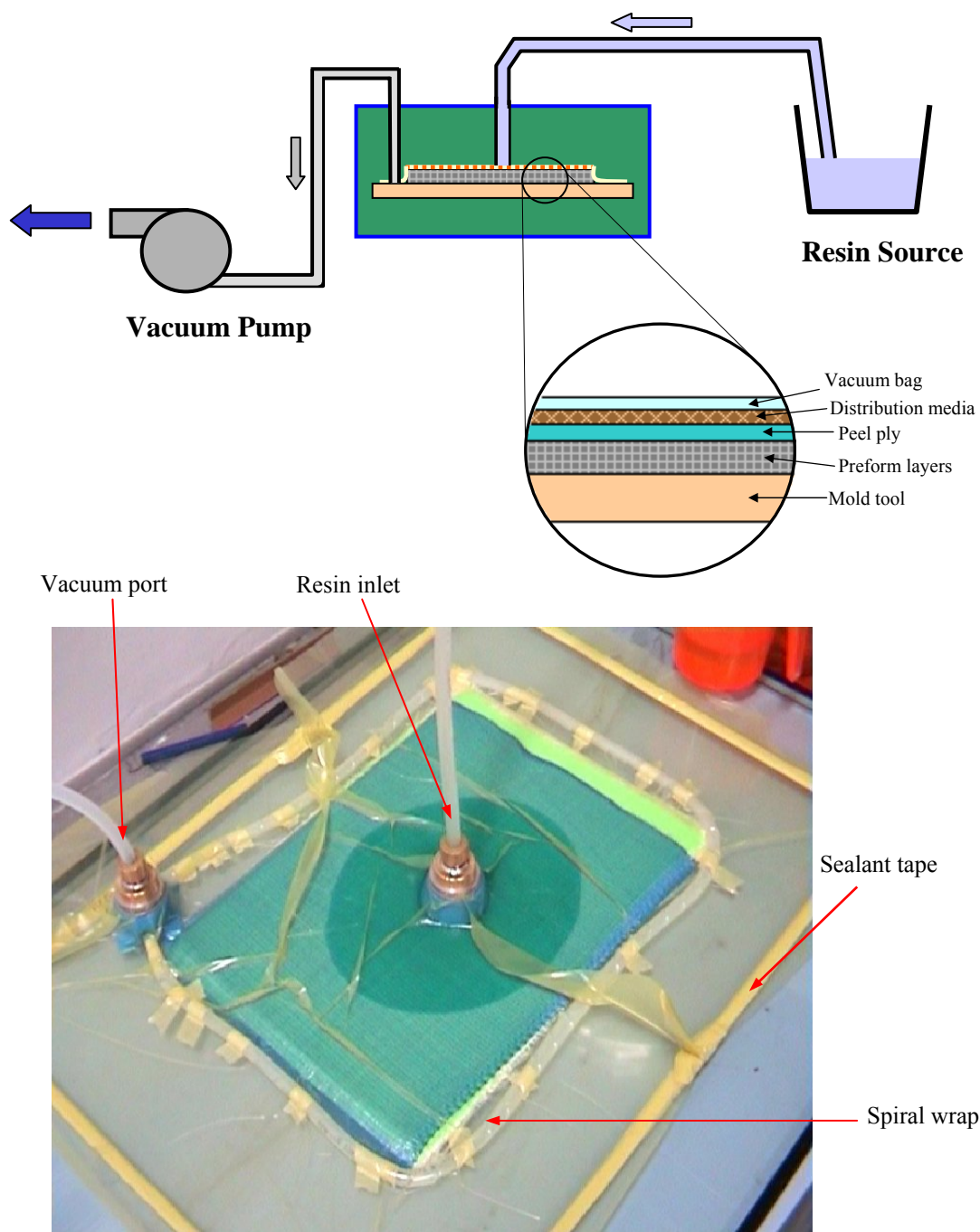
Figure 3.3 Vacuum assisted resin transfer molding process and fabrication setup

A vacuum pump was connected to vacuum port, which was placed on glass plate, using a polyethylene tube, Figure 3.3. With the vacuum bag tightly sealed and the injection gate closed, the vacuum pump was turned on. Vacuum is drawn through the vacuum line to remove air from the mold cavity, induce fiber compaction under atmospheric pressure. Even a small leak in the system may result in voids and poor consolidation of the final composite part. Hence, leaks were detected by using either a listening device or by clamping the vacuum line and using a vacuum gauge. Then, the injection gate was opened to allow resin infusion into the high-permeable distribution medium under the atmospheric pressure.

The flow front of resin through the part can be viewed through the bagging film. Flow in the distribution medium is primarily in-plane. The resin then fills the preform in both the transverse and in-plane directions by "leaking" downward from the high permeable distribution medium.

When the preform was completely infiltrated, the injection tube was clamped and the infused panel was left to cure for 24 h at room temperature and under vacuum. After the solidified laminate was taken out of the mold, a two-hour post-cure at 80°C was done in a hot press. Finally, the edges of the laminates were then removed leaving 42x30 cm rectangular samples from which the testing specimens were cut as illustrated in Figure 3.4. The final dimensions of each test specimen are identified as in Figure 3.5.

The compositions of these laminates, which in this paper will be referred to as the non-crimp stitched fabric composites, are given in Table 3.4 and Table 3.5 for polyester-based and epoxy-based composites, respectively. Table 3.6 provides details of the epoxy composites reinforced with woven roving glass and carbon fabric.

Figure 3.5 illustrates the test directions performed on the composites where machine direction (MD) is the flow direction of fabric in the machine during production, while bias (BD) and cross-direction (CD) are 45° and 90° relative to machine direction, respectively.

Table 3.4 Compositions of polyester composites reinforced with non-crimp stitched fabric.

Composite	V_f (%)	Layup	Number of fabric layers	Laminate thickness (mm)
Unidirectional glass fabric	48.4±0.8	[0]$_{12}$	12	4.8±0.02
Unidirectional carbon fabric	23.1±1.1	[0]$_{12}$	12	5.78±0.02
Biaxial glass fabric	54.7±1.1	[45/-45]$_{12}$	12	5.91±0.01
Triaxial glass fabric	38.7±0.6	[0/45/-45]$_5$	5	5.3±0.015
Quasi-isotropic carbon fabric	44.5±1.8	[45/-45/90 /0]$_6$	12	6.1±0.03

Table 3.5 Compositions of epoxy composites reinforced with non-crimp stitched fabric.

Composite	V_f (%)	Layup	Number of fabric layers	Laminate thickness (mm)
Unidirectional glass fabric	33.7±1.3	[0]$_{12}$	12	7.01±0.04
Unidirectional carbon fabric	24.8±0.6	[0]$_{12}$	12	5.47±0.02
Biaxial glass fabric	36.2±1.3	[45/-45]$_{12}$	12	6.46±0.03
Biaxial carbon fabric	41.5±1.6	[45/-45]$_{12}$	12	6.53±0.031
0/90 glass fabric	32.6±1.2	[0 /90]$_6$	12	7.25±0.041
0/90 carbon fabric	25.6±0.7	[0/90]$_6$	12	5.79±0.043

Table 3.6 Compositions of epoxy composites reinforced with woven roving fabric.

Composite	Areal density [g/m^2]	V_f (%)	Number of fabric layers	Laminate thickness (mm)
Woven roving glass fabric	300	39.2±1.5	12	3.83±0.01
Woven roving carbon fabric	200	38.4±1.4	12	3.53±0.015

T: Tensile specimen

F: Flexure specimen

S: Short Beam Shear
   specimen

MD: Machine Direction

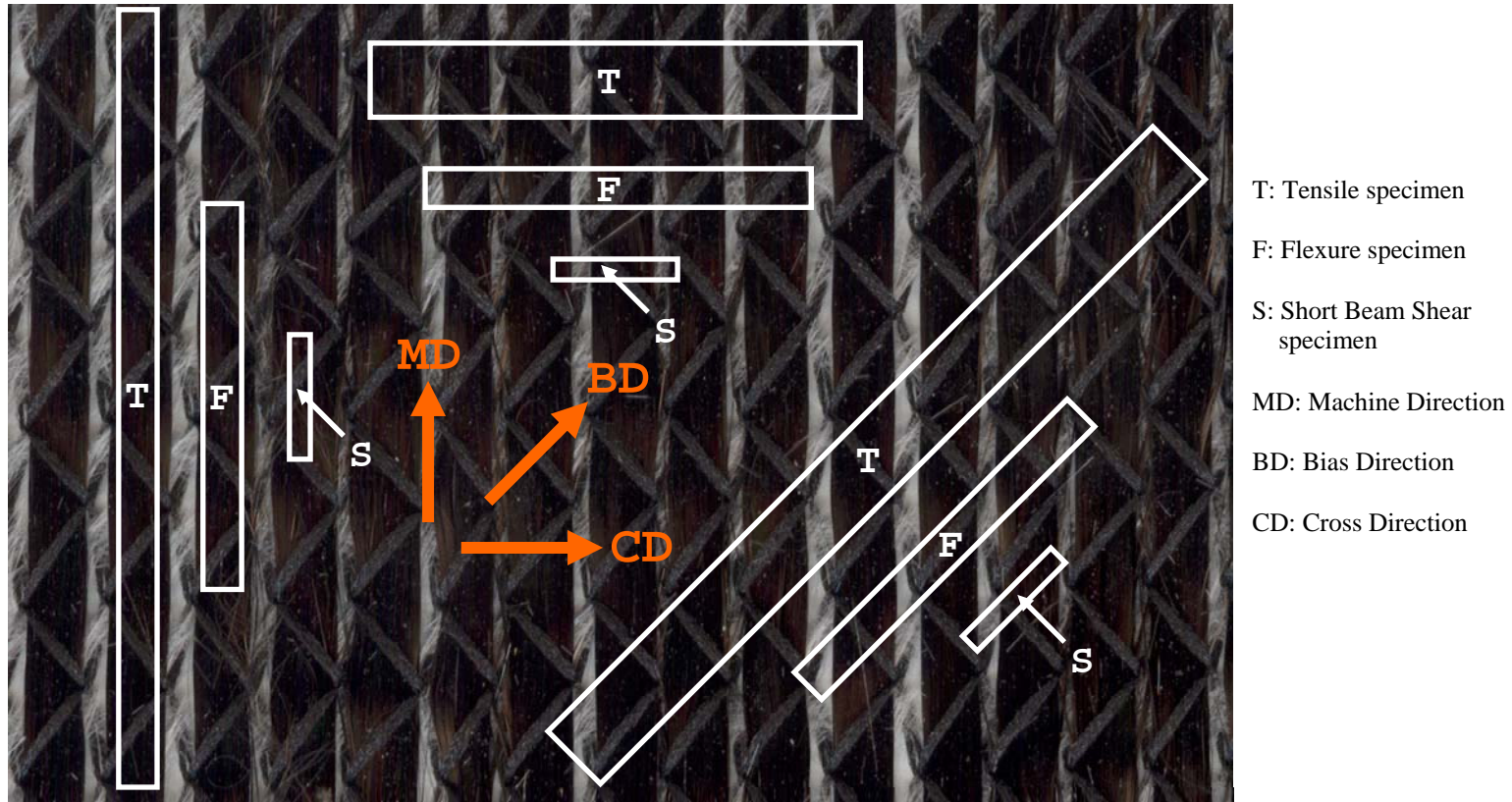BD: Bias Direction

CD: Cross Direction

Figure 3.4 Location of test pieces cut from the laminates used for mechanical testing and directions of measurements.
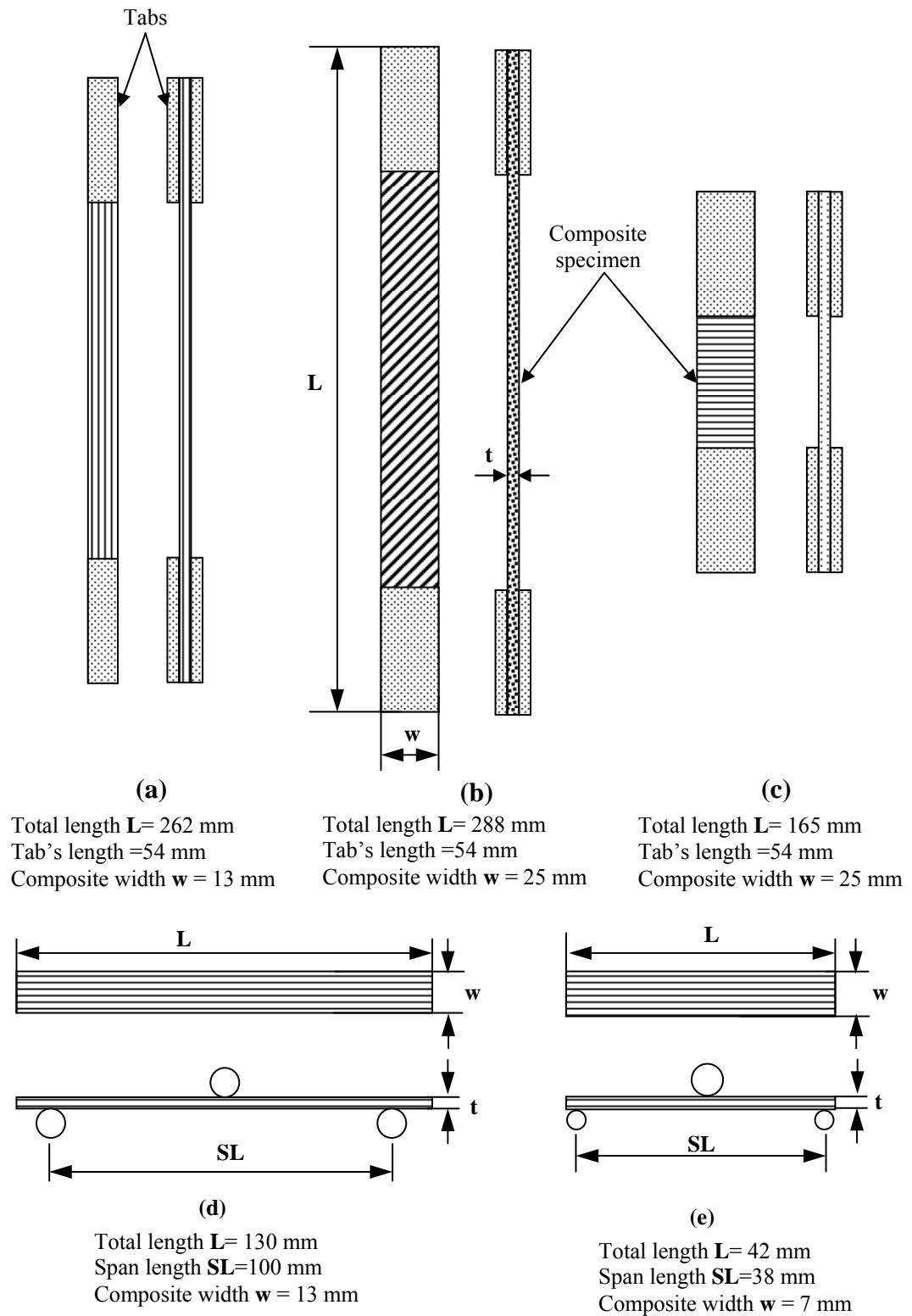
Figure 3.5 Schematic diagrams of the testing geometries: (a) longitudinal, (b) off-axis and (c) transverse tension; (d) flexure; (e) short beam shear.

3.2 Mechanical Properties Test Methods

3.2.1 Tensile Strength Testing

The tensile experiments were conducted by longitudinal (0°), transverse (90°) and balanced crossply (45°) tension (ASTM D-3039) on a Shimadzu AUTOGRAPH AG-G Series universal testing machine, with Trapezium (advanced software for materials testing) for machine control and data acquisition. Four rectangular tabs to be used with the tensile specimens were produced from glass and carbon fiber reinforced epoxy with the lay-up [0/90]$_s$ and were bonded to the griping length of each test specimen using a cold hardening epoxy resin. Tensile tests were performed at a constant cross-head speed of 2 mm/min at room temperature in air. Six tests were made for each material per orientation.

A video extensometer system (SHIMADZU Non-contact Video Extensometer DVE-101/201) was used to measure the elongation of the test specimen (Figure. 3.6). Since clip-on extensometry is difficult to use for these materials owing to damage induced by the clip gauge sharp edges, a video extensometer system is used as principal technique in this study to determine the elastic moduli of such an anisotropic composite. Computer-assisted video-controlled extensometry provides a useful method for the accurate true strain measurements of the composite materials over large plastic strains. The system works by pattern matching a template drawn on to the specimen and following the template as the specimen deforms. Digital readings with a resolution of 5 µm could be achieved with a high-precision CCD camera. The distance between the templates (in pixels on the CCD array) is then used to determine strain. The pattern-matching algorithm uses interpolation to give 1/50th pixel resolution in position in the x direction. Figure 3.7 details a screen shot of a medium specimen under test, and shows the specimen marking for tensile strain. By the use of telephoto lenses, the physical scale of the specimen under test became irrelevant. Providing that the templates were placed as far apart on the screen as possible, the strain resolution was scale-invariant.

Figure 3.6 Photograph of the video-extensometer connected to the tensile testing system (photograph from Biomechanics Laboratory located within Ege University Department of Mechanical Engineering).
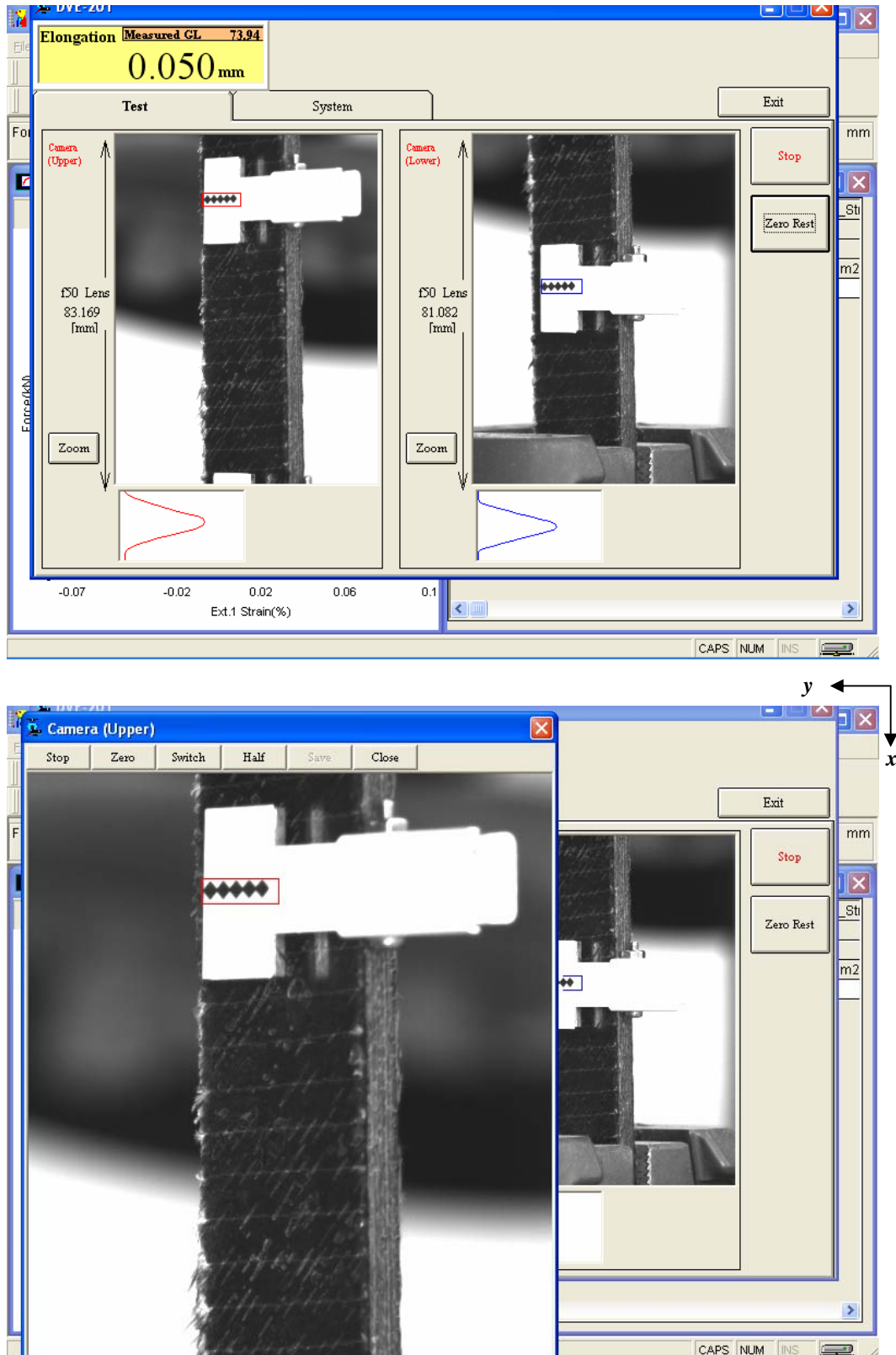
Figure 3.7 Specimen marking for tensile strain.

3.2.2 Flexure Test

One of the most common experiments to characterize materials in flexural conditions is the three-point bending test. Specimens were machined from flat panels with a high-speed diamond saw with a 50/50 mix of water and ethylene glycol coolant. This machining operation resulted in constant width specimens having very smooth cuts. The gauge lengths for the three-point bend test were determined according to ASTM D790 standard. The three-point bend fixture was manufactured by Shimadzu for use in a universal test machine running in compression mode (Figure 3.8(a)). The center loading nose (a cylindrical pin making line contact) moved at a rate of 2 mm/min. Flexural strength is derived from the simple beam theory as follows:

$$\sigma_f = \frac{3PL}{2wt^2} \tag{3.1}$$

where σ_f denotes the flexural strength; P the applied load that leads the specimen to rupture; L the support span; w the specimen width; and t specimen thickness.

For the case where the three-point flexure specimen is not strain-gaged, flexural modulus may be determined from the slope of the initial straight-line part of the load–deflection curve by means of this equation:

$$E_f = \frac{L^3}{4wt^3} \frac{\Delta P}{\Delta \delta} \tag{3.2}$$

where $\Delta P/\Delta \delta$ represents the slope of the force-displacement curve; and E_f the flexural modulus.
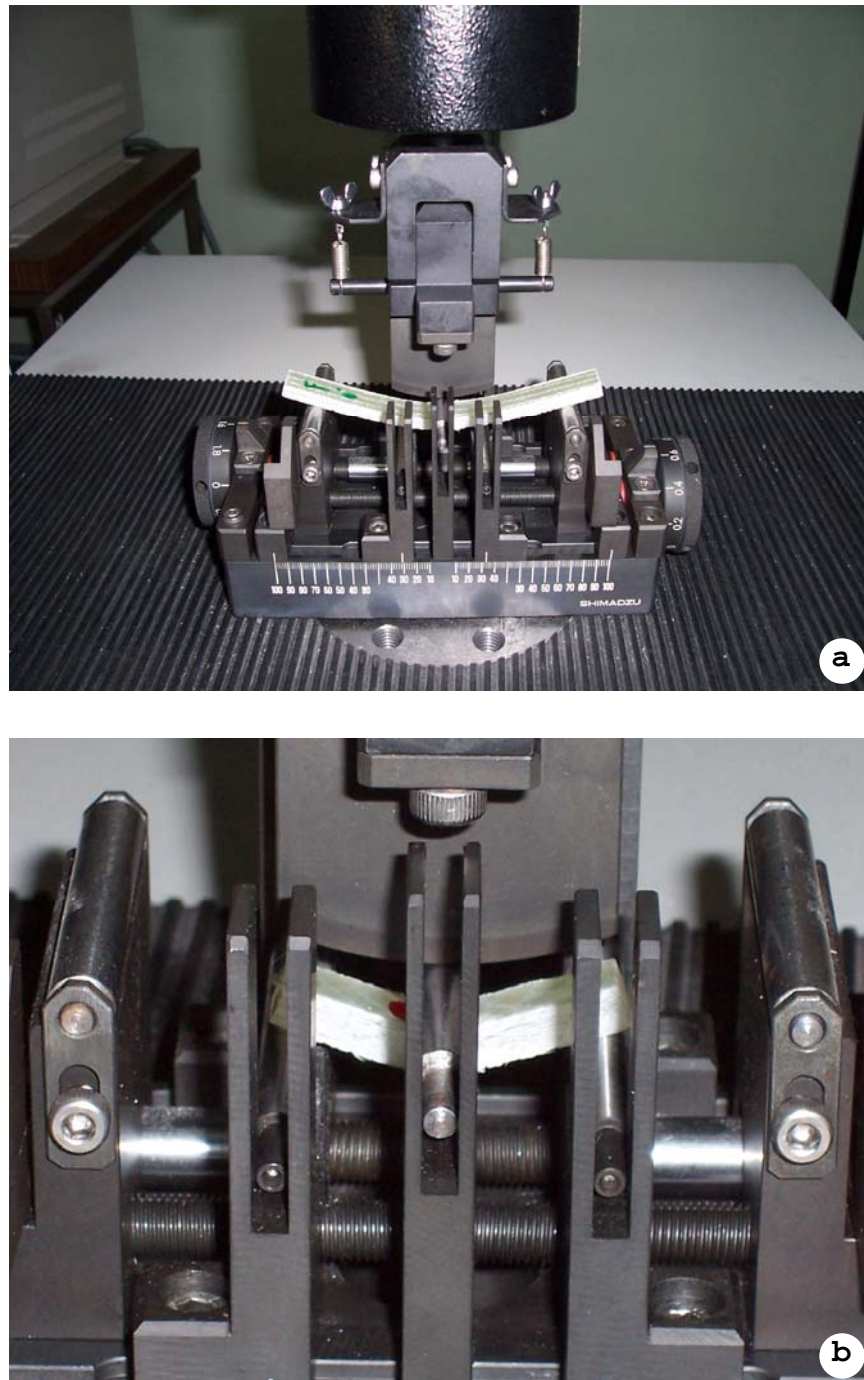
Figure 3.8 (a) Flexure and short beam shear test fixture and (b) laminated beam under load (short beam shear test) (photographs from Biomechanics Laboratory located within Ege University Department of Mechanical Engineering)

3.2.3 Short Beam Shear Test

To determine the interlaminar shear strength of the composites, short beam shear tests were performed following ASTM 2344 'Apparent interlaminar shear strength of parallel fiber composites by short-beam method'. A sliding roller three-point bending fixture, which included a loading pin (diameter 6.4 mm) and two support pins (diameter 3.2 mm), was used for the room temperature short beam shear tests. The test fixture was mounted in a 5-kN capacity, screw-driven load frame. Shimadzu AUTOGRAPH AG-G Series universal testing machine was used, with a crosshead speed of 1.3 mm/min, and at least six specimens were tested for each type of lay-up. The apparent interlaminar shear strength of composites was determined from samples that were tested with a support span/sample thickness ratio of 5:1. The simply supported specimens allow lateral motion and a line load is applied at the mid span of the specimens (Figure 3.8(b)). The apparent shear strength was then calculated as follow:

$$V = 0.75 \left(\frac{P_{max}}{wt} \right) \tag{3.3}$$

where V is the apparent shear strength, P_{max} is the failure load; w and t are the width and thickness of the specimen respectively. Further details of the test procedures are given in the ASTM 2344.

3.3 Studies of the Interface

For fiber-reinforced metals, for instance, the low affinity between the matrix and the reinforcing fiber will result in a decreased interfacial reaction zone and will have some influence on its moldability. On the other hand, a high affinity will cause an increase in the interfacial reaction zone, which will then significantly affect the properties of the composite materials. The same phenomenon is observed in the case of fiber-reinforced plastic (FRP), and it is known that there is along the interface a

special area, which we refer to simply as the "interface", which is different in physical and chemical structures from those of the raw materials themselves.

Along the solid-phase interface, substances of various chemical species will contact and combine; however, the state of the junction will differ in accordance with the type of bond constituting the chemical species: that is primary bonds (ionic bond, covalent bond, metallic bond) or secondary bonds (hydrogen bond, etc.). In other words, the type of interaction along the interface will exert a great influence on the various properties of the composite material. Therefore, to improve the performance of composite material, it is absolutely necessary to clarify the structure of the interface, what is occurring there, and the role to be played by the interface.

Investigators who observed the surface of the composite material can limit the major useful techniques to infrared spectroscopy (IR & FTIR), including reflection adsorption (RA); diffuse reflectance (DRIFT); photoacoustic spectroscopy (PAS); and time resolved spectroscopy (TRS); ion scattering spectrometry (ISS); Raman spectroscopy; Auger Electron Spectroscopy (AES); wide angle x-ray scattering (WAXS); small angle x-ray scattering (SAXS); x-ray photoelectron spectroscopy (XPS), also known as electron spectroscopy for chemical analysis (ESCA); secondary ion mass spectrometry (SIMS); ion scattering photometry (ISS) and Rutherford Backscattering Spectrometry (RBS).

3.3.1 Fourier Transform Infrared (FT-IR) Spectroscopic Measurements

A Fourier transform is a mathematical operation used to translate a complex curve into its component curves. In a Fourier transform infrared instrument, the complex curve is an interferogram, or the sum of the constructive and destructive interferences generated by overlapping light waves, and the component curves are the infrared spectrum. The standard infrared spectrum is calculated from the Fourier-transformed interferogram, giving a spectrum in percent transmittance (%T) vs. light frequency (cm^{-1}).
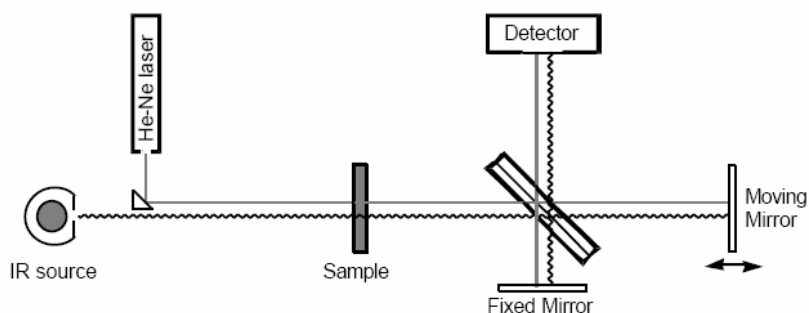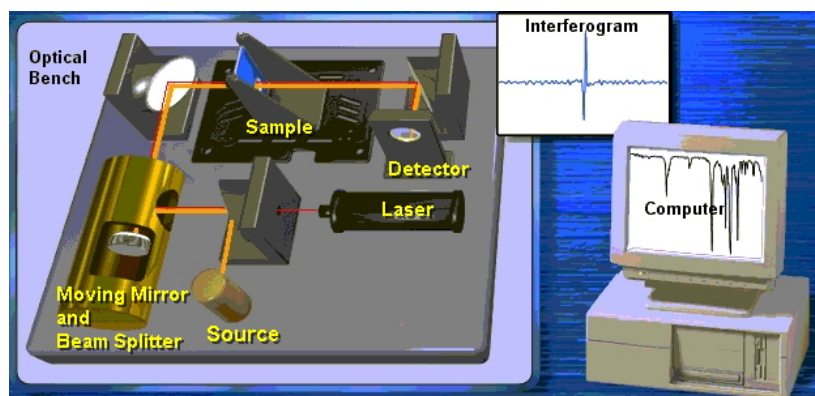
Figure 3.9 Schematic illustration (Levin, 2004) and diagram of the Michelson Interferometer used in an FTIR Spectrophotometer (from Qual instrumentation).

The heart of an FTIR Spectrophotometer is a Michelson Interferometer built around the sample chamber. The key components are a moveable mirror and beam splitter. The moveable mirror is responsible for the quality of the interferogram, and it is very important to move the mirror at constant speed. Radiation from an IR source is directed through the sample cell to a beam splitter. The beam splitter is just a piece of semi-reflective material, usually mylar film sandwiched between two pieces of IR-transparent material. Half of the radiation is reflected from a fixed mirror while the other half is reflected from a mirror which moved continuously over a distance of about 2.5 micrometers. When the two beams are recombined at the detector, an interference pattern is produced. As the movable mirror travels, different frequencies are reflected in different ways. The summation of constructive and destructive interference over time makes an interferogram, from which a Fourier transform is used to calculate a spectrum. A single scan of the entire distance takes about 2 seconds and is stored in the computer. In order that several scans may be

added, they must coincide exactly. Obviously, this would be impossible considering the thermal fluctuations and vibrations in the laboratory. In order to solve this problem, a helium-neon laser is simultaneously directed through the Michelson Interferometer and the interference pattern of the laser is used as a frequency reference.

Figure 3.10 Picture of Perkin-Elmer FT-IR used in this research (photographs from Laboratory located within Dokuz Eylul University Department of Chemistry).

A Fourier transform infrared spectrophotometer (Perkin Elmer BX-II) was employed for the entire study (Figure 3.10). 1 mg of the samples, cured resin, and fiber reinforced composites, were ground into powder with infrared-grade KBr powder (100 mg) and pressed into a pellet for measurement. Long period scanning was utilized so signal-to-noise ratio of the coadded spectrum is sufficient to resolve peaks in which we are interested. Each spectrum was recorded in the range of 400-4000 cm^{-1} with a resolution of 2 cm^{-1}. The background spectrum of KBr pellet was subtracted from the sample spectra.

3.3.2 Scanning Electron Microscopy (SEM) Observation

The SEM uses electrons instead of light to form an image. A beam of electrons is produced at the top of the microscope by heating of a metallic filament. The electron beam follows a vertical path through the column of the microscope. It makes its way

through electromagnetic lenses which focus and direct the beam down towards the sample. Once it hits the sample, other electrons (secondary) are ejected from the sample. Detectors collect the secondary electrons, and convert them to a signal that is sent to a viewing screen similar to the one in an ordinary television, producing an image.

Figure 3.11 Picture of Scanning Electron Microscope (SEM) from Jeol Corp (photograph from Characterization Laboratory located within Dokuz Eylül University Department of Metallurgical and Materials Engineering).

The fracture surfaces of tensile-tested specimens were examined using the scanning electron microscope (JEOL JSM 6060) at excitation voltage equal to 20 KeV in the secondary electron mode (Figure 3.11). In order to reduce the extent of sample arcing, the samples were coated with a thin layer of metallic gold in an automatic sputter coater (Polaran SC7620) prior to examination by SEM. The sputter coater uses argon gas and a small electric field. The sample is placed in a small chamber which is at vacuum. Argon gas is then introduced and an electric field is

used to cause an electron to be removed from the argon atoms to make the atoms ions with a positive charge. The Ar ions are then attracted to a negatively charged piece of gold foil. The Ar ions act like sand in a sandblaster, knocking gold atoms from the surface of the foil. These gold atoms now settle onto the surface of the sample, producing a gold coating.

3.4 Thermal Analysis

3.4.1 Definition

Thermal analysis has been defined by the International Confederation of Thermal Analysis (ICTA) as a general term which covers a variety of techniques that record the physical and chemical changes occurring in a substance as a function of temperature (Mackenzie et al., 1972). This term, therefore, encompasses many classical techniques such as thermogravimetry (TG), evolved gas analysis (EGA), differential thermal analysis (DTA), and differential scanning calorimetry (DSC), and the modern techniques, such as thermomechanical analysis (TMA) as well as dynamic mechanical analysis (DMA), and dilatometry, just to name a few. The application of thermal analysis to the study of construction materials stems from the fact that they undergo physicochemical changes on heating.

3.4.2 Heat-Flux Differential Scanning Calorimetry (DSC)

Essentially, the heat-flux DSC measures the difference in temperature between the sample and reference as a function of time, under controlled temperature, and since the temperature varies linearly with time, as a function of temperature as well. The temperature difference is proportional to the change in the heat flux (energy input per unit time) (Hatakeyama, & Quinn, 1999). The heat-flux is actually derived from a combination of the $\Delta T(t)$ curve and the d $\Delta T(t)/dt$, both of these are transparent to the user since the electronics used yield a direct heat flux value from these terms. If temperature compensation is required, then it is done by Joule heating (for an endothermic process) or by Peltier effect (for an exothermic process). As in the DTA

case, an endothermic signal is in the negative direction, while an exothermic signal is the upward direction.

The structure of a heat-flux DSC system is shown in Figure 3.12. The main assembly of the DSC cell is enclosed in a cylindrical, silver heating block, which dissipates heat to the specimens via a constantan disc which is attached to the silver block. The disc has two raised platforms on which the sample and reference pans are placed. A chromel disc and connecting wire are attached to the underside of each platform, and the resulting chromel-constantan thermocouples are used to determine the differential temperatures of interest. Alumel wires attached to the chromel discs provide the chromel-alumel junctions for independently measuring the sample and reference temperature.

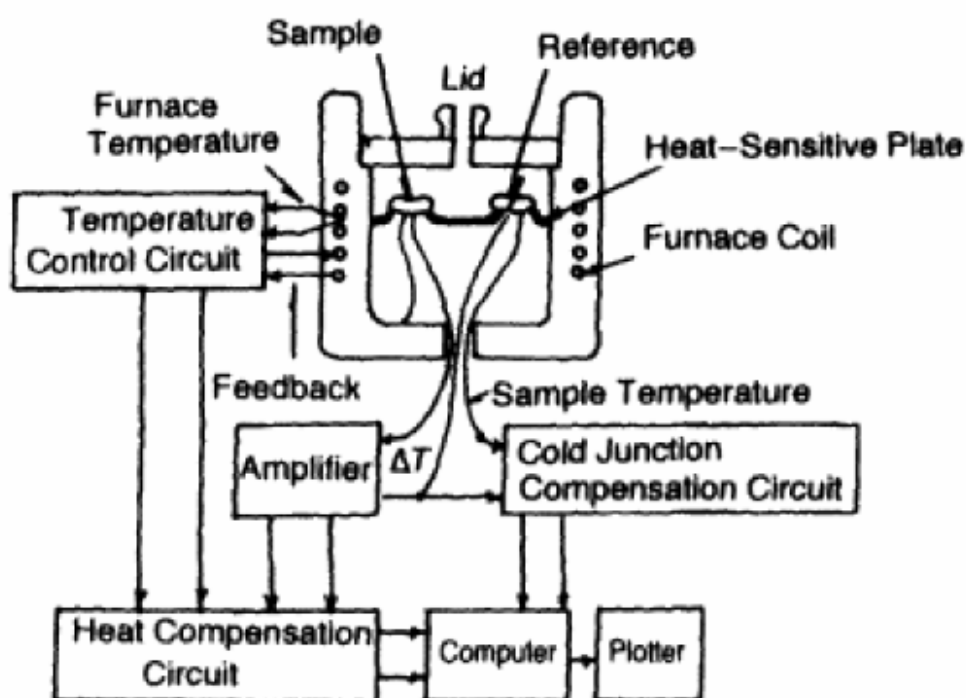Figure 3.12 Schematic diagram of heat-flux DSC apparatus (Hatakeyama et al., 1999, p. 9).

A second series of thermocouples measures the temperature of the furnace and of the heat-sensitive plate. During a phase change heat is absorbed or emitted by the sample, altering the heat flux through the heat-sensitive plate. The variation in heat flux causes an incremental temperature difference to be measured between

the heat-sensitive plate and the furnace. The heat capacity of the heat-sensitive plate as a function of temperature is measured by adiabatic calorimetry during the manufacturing process, allowing an estimate of the enthalpy of transition to be made from the incremental temperature fluctuation (Hatakeyama et al., 1999, p. 8)

In this research, a DSC (Perkin–Elmer Sapphire DSC, equipped with an intracooler and supported by a computer software for data acquisition/analysis) was used for the dynamic and isothermal experiments and data analysis (see Figure 3.13).
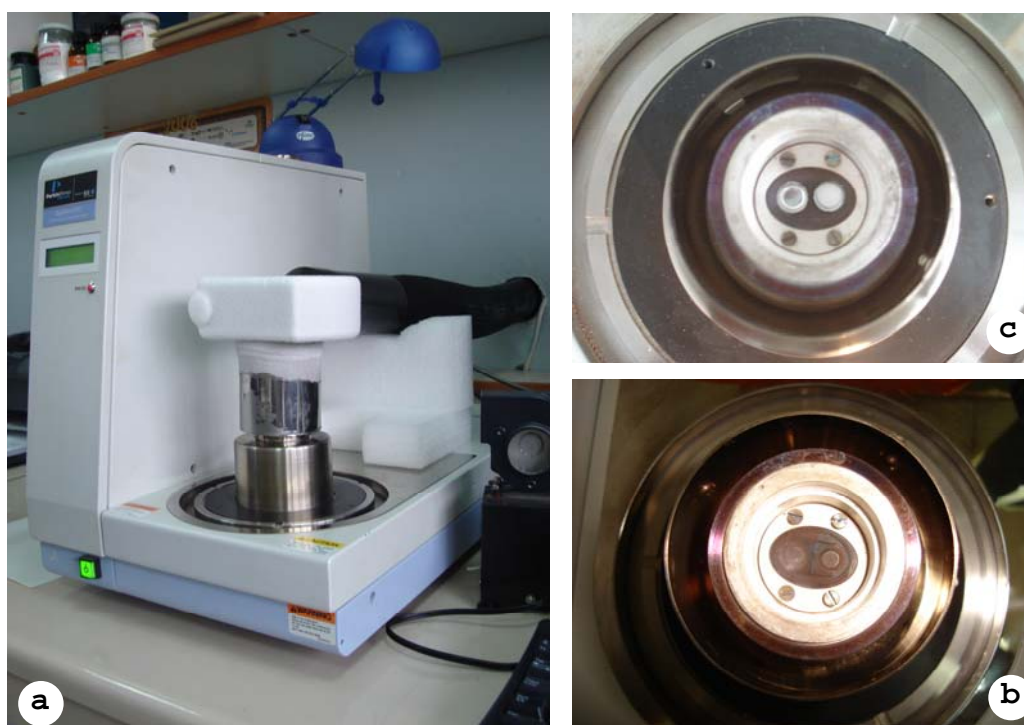

Figure 3.13 (a) Picture of Perkin Elmer Sapphire DSC; (b) the furnace and the sample holder assembly of DSC apparatus; (c) the holder assembly after placement sample and reference material (photographs from the Semiconductor Physics Research Laboratory located within Fırat University Department of Physics).

3.4.3 Differential Thermal Analysis (DTA)

Differential Thermal Analysis (DTA) is an analytical technique in which the temperature difference between a substance and a reference material is measured as a function of temperature whilst the substance and reference material are subjected to the same controlled temperature programme.

A schematic of a classical DTA is shown in Figure 3.14. Thermocouples inserted in each holder measure the temperature difference between the sample and the reference as the temperature of the furnace is controlled by a temperature programmer.
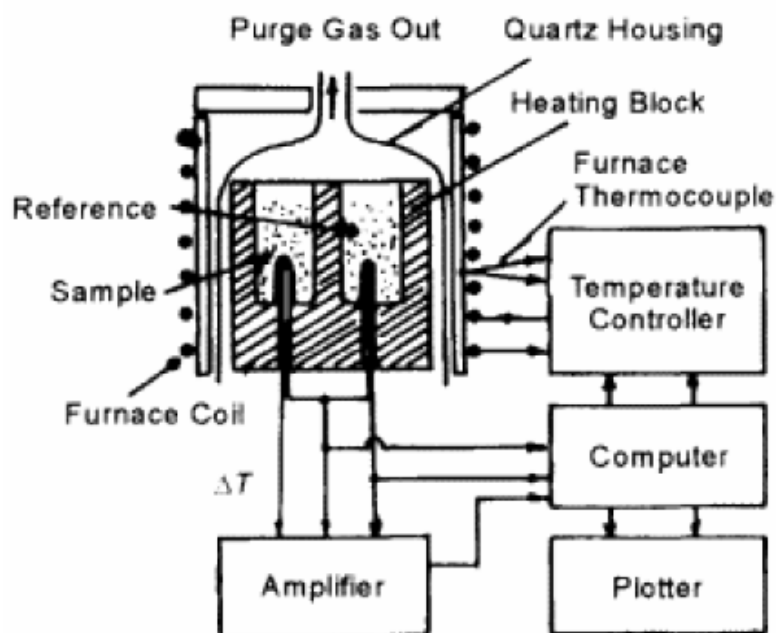

Figure 3.14 Schematic diagram of classical DTA apparatus (Hatakeyama et al., 1999, p. 5)

When the sample holder assembly is heated at a programmed rate, the temperatures of both the sample and the reference material increase uniformly. The furnace temperature is recorded as a function of time. If the sample undergoes a phase change, energy is absorbed or emitted, and a temperature difference between the sample and the reference (ΔT) is detected. The minimum temperature difference which can be measured by DTA is 0.01 K (Hatakeyama et al., 1999, p. 6)

3.4.4 Thermogravimetric Analyzer (TGA)

Thermogravimetry (TG) measures the change in mass of a material as a function of time at a determined temperature (i.e., isothermal mode), or over a temperature range using a predetermined heating rate. Essentially, a TG consists of a

microbalance surrounded by a furnace (Figure 3.15(b)). A computer records any mass gains or losses. Weight is plotted against a function of time for isothermal studies and as a function of temperature for experiments at constant heating rate. Thus, this technique is very useful in monitoring heat stability and loss of components (e.g., oils, plasticizers, or polymers).

Intercomparison of TGA data from different techniques is often required to interpret a result unambiguously. Data collected using simultaneous TGA/DTA apparatuses are preferred, but data from separate measurements can be compared with confidence provided that the experimental conditions are precisely controlled.
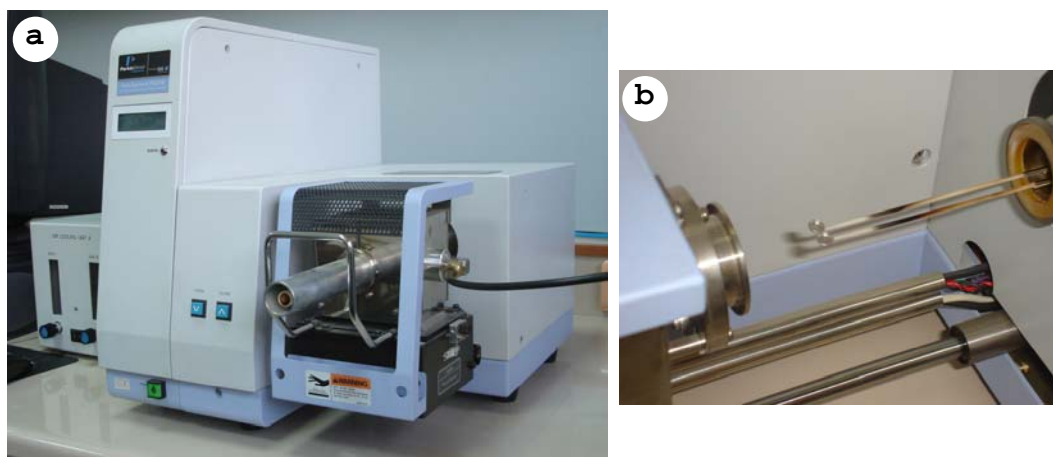
Figure 3.15 (a) Picture of Perkin Elmer TG/DTA used in this research; (b) balance beam mechanism (photographs from the Semiconductor Physiscs Research Laboratory located within Fırat University Department of Physics).

In this study, thermogravimetric analyses were performed by using a Perkin Elmer Pyris Diamond TG/DTA with a temperature increase rate of 20 °C/min in air atmosphere (Figure 3.15). The samples of approximately 5-20 mg were heated from 30 to 550 °C. The instrument was computer controlled and calculations were done using Pyris software.

3.5 Measurement of Thermal Conductivity by DSC

3.5.1 Theory

Several studies of methods for determination of thermal conductivity of solid materials by differential scanning calorimetry have been carried out (G. Hakvoort, van Reijen, & Aartsen, 1985; Khanna, Taylor, & Chomyn, 1988; Flynn & Levin, 1988; Keating & McLaren, 1990; Ladbury, Currell, Horder, Parsonage & Vidgeon, 1990; Camirand, 2000; Merzlyakov & Schick, 2001; Kök, 2006).

Flynn et al., (1988) use this technique and take into account the thermal contact resistance between the sample and furnace, which may not be negligible compared with the thermal resistance of the sample. Flynn and Levin's method for the measurement of thermal conductivity of polymeric and other sheet materials is presented in the following paragraph.

The method used here utilizes the measurement of rate of heat flow into a sensor material during its first order transition to obtain the thermal resistance of a material placed between the sensor material and the heater in the DSC.

If, at constant heating rate, a sensor material (such as indium at its melting point) goes through a "sharp" transition where the temperature over which the transition occurs is much smaller than the temperature change of the heating calorimeter during the interval in which heat must flow into the material to match the transition enthalpy, the neat heat flux from the calorimeter into the specimen will increase linearly, according to Newton's law, until the transition is completed. Therefore, the steady slope of the leading edge of the transition peak of the sensor material will be given by eqn. (3.4)

$$\text{slope (sensor)} = B/R \qquad (3.4)$$

where B is the heating rate, and R is the thermal resistance between the heater in the calorimeter and the sensor specimen. The DSC curve for this case is illustrated by curve (a) in Figure 3.16. If a sheet material is placed between the sensor specimen and the calorimeter, as shown in case (b) in Figure 3.16, then the heat must flow through this increased resistance and the steady slope of the leading edge of the transition peak will be

$$\text{slope (sensor + sheet)} = B/R' \tag{3.5}$$

where R' is the new thermal resistance between the heater and the sensor specimen which now also includes the resistance to heat flow of the sheet material.
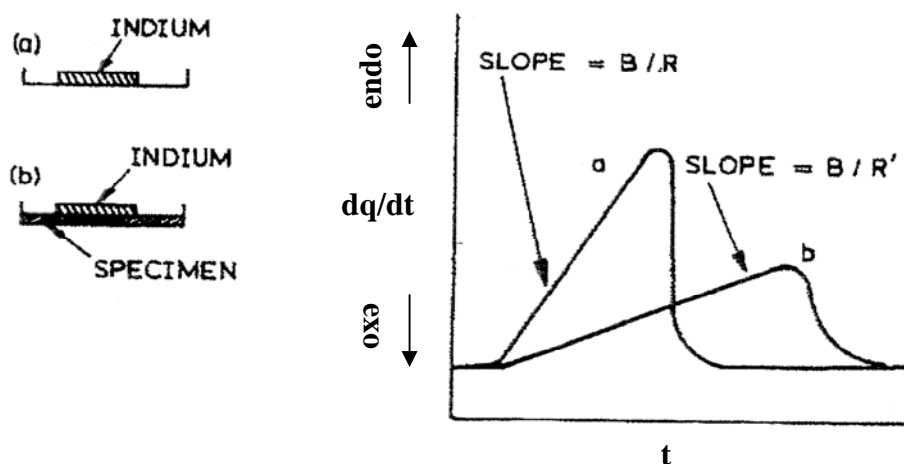

Figure 3.16 DSC curves for melting of (a) indium; (b) indium + specimen sheet (Fleymn et al., 1988, p.94).

Obviously, the thermal resistance of the sheet R_s can be obtained from

$$R_s = R' - R \tag{3.6}$$

…. The thermal conductivity of the sheet k is obtained from

$$k = L/A(R' - R) \tag{3.7}$$

where L is the thickness of the specimen sheet, and A is the contact area between the sensor material and sheet (Flynn et al., 1988, p. 94-95).

3.5.2 Experimental Procedure

In the present work, the thermal conductivity was measured by means of a differential scanning calorimeter (DSC) Perkin-Elmer Sapphire coupled with an intracooler. The intracooler is used to stabilize the system. The instrument was computer controlled and calculations were done using Muse and Pyris software. Nitrogen with a flow rate of 50 ml/min is used as a purge gas to minimize oxidation of the sample during the measurement. Before the experiments, the thermal response and temperature were calibrated with the heat of fusion and the melting point of pure indium. Tests in the DSC were conducted at a dynamic temperature scan rate of 10 °C/min. A series of non isothermal DSC runs provided information about the thermal conductivity of composite materials over a wide temperature range from about 45 to 235 °C. Figure 3.17 shows, as an example, the DSC curves obtained for melting of indium disk and a scan with a carbon/epoxy sample having on its top an indium disk. Thermal conductivity calibration was performed using polyvinyl chloride (PVC) disk. The PVC sample weighed approximately 30 mg, was approximately 0.9 mm thick and had a diameter of approximately 6 mm.

The materials used as samples in this study were polyester based and epoxy based composites. These composite materials with different thicknesses were reinforced with non-crimp stitched glass, carbon and aramid fabric. The main physical characteristics of fiber and matrix materials are given in Table 3.7 and Table 3.8, respectively. A hand lay-up method was employed to fabricate the composite laminates with one layers of stitched fabric reinforcement. The cylindrical specimens of composites with equal diameters (6 mm) were cut using a special cutting tool to measure its thermal conductivity with heat flowing through the thickness direction. A photographic view of the sample is also shown in Figure 3.18.
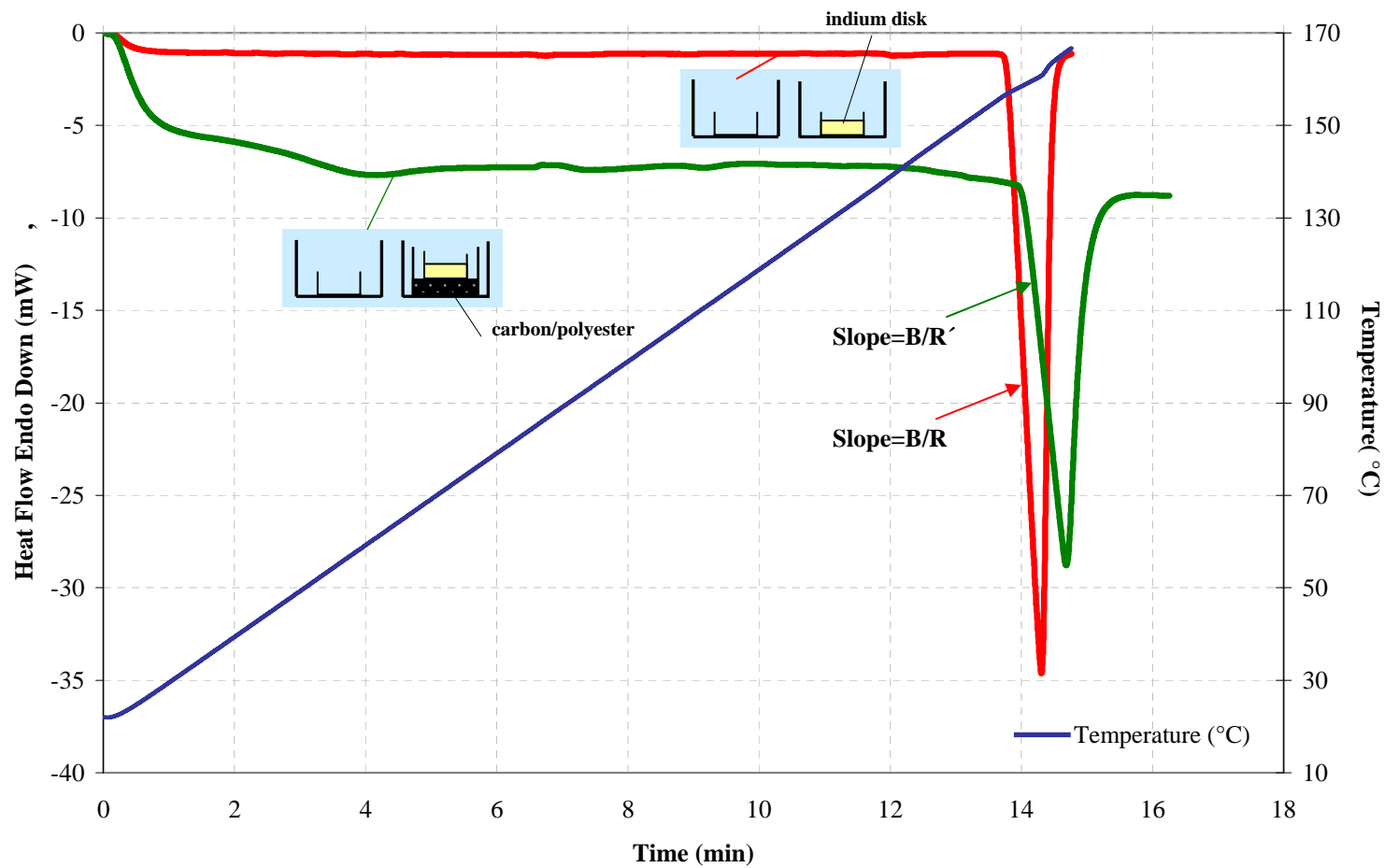
Figure 3.17 The DSC curves obtained for melting of indium disk and a scan with a carbon/polyester sample having on its top an indium disk (carbon/polyester height: 0.90 mm, carbon/polyester diameter: 6.0 mm, indium mass: 33.000 mg, indium diameter: 5.0 mm, scan rate: 10 °C/min).

For each sample, three cylindrical specimens were analysed. The densities of composite materials were measured at room temperature using Archimedes's principle. Pure de-ionized water was used as the immersion liquid. The density of the composites and the content of fibers in the matrix are presented in Table 3.9.
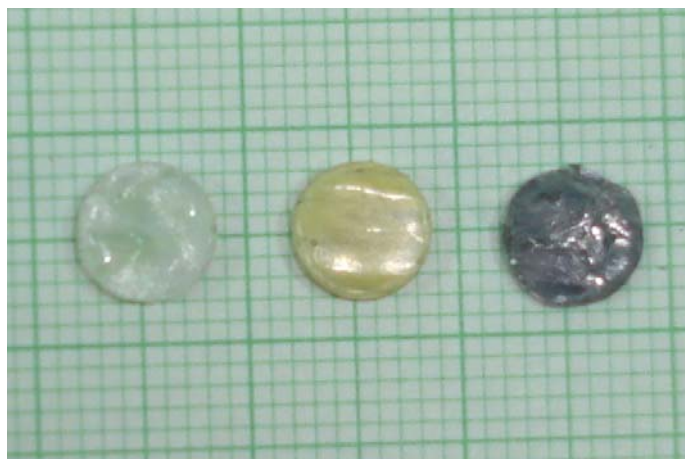

Figure 3.18 Miscellaneous fiber reinforced polyester composite samples tested. Left to right: glass/polyester, aramid/polyester and carbon/polyester composite sample

Table 3.7 Main characteristics of starting fiber materials

Materials	Density [g/m³]	Areal density [g/m²}	Mean fiber diameter [μm]	Thermal conductivity[a] [W/m °C]	Heat capacity [J/g.°C]	Coefficient of thermal expansion [°C⁻¹]
Glass fabric	2.40	472	15	1.03	0.800	0.5×10^{-5}
Carbon fabric	1.77	200	7.5	15	0.800	0.08×10^{-5}
Aramid fabric	1.45	300	12	0.04	1.400	-0.2×10^{-5}

[a]Thermal conductivity values are in the longitudinal direction.

Table 3.8 Main characteristics of starting matrix materials

Materials	Density[a] [g/m³]	Thermal conductivity[a] [W/m °C]	Heat capacity[a] [J/g °C]	Coefficient of thermal expansion [°C⁻¹]
Epoxy	1.2	0.049	0.640	11×10^{-5}
Polyester	1.1	0.091	0.790	8×10^{-5}

[a]Density, thermal conductivity and heat capacity were determined at room temperature.

Table 3.9 Characteristics of polyester based and epoxy based composites for thermal conductivity measurements

Samples	Density (g/cm^3)	Volumetric fiber content (%)
Glass/epoxy	1.168 ± 0.02	15.2 ± 1.1
Carbon/epoxy	1.043 ± 0.03	10.8 ± 1.0
Aramid/epoxy	0,950 ± 0.02	18.8 ± 1.2
Glass/polyester	1.418 ± 0.01	18.7 ± 0.8
Carbon/polyester	0,915 ± 0.02	11.4 ± 1.3
Aramid/polyester	0,984 ± 0.03	18.0 ± 1.8

The sensor materials and their melting points are listed in Table 3.10. All pellet samples were pressed from powder using a cold steel die of approximately 5 mm in diameter. A maximum press pressure of about 500 MPa, was used for all samples. Cylindrical pellets of approximately 30 mg are used to carry out thermal conductivity measurements. Small pieces of indium wire were cut with a scalpel, and then pressed into disks of 5mm diameter. The use of same indium and tin disk whose surface has been exposed to air should be avoided as oxidation of the disk surface alters the melting temperature of this substance. Hence, different indium and tin samples were made in the course of the experiment.

Table 3.10 Sensor materials tested

Sensor material	Melting point (°C)	Flash point (°C)
Benzophenone	48	143
Stearic acid	67	196
Phenantren	99	–
Fluorene	112	151
Benzamid	127	180
Indium	156.6	–
Tin	232	–

It should be noted here that, ideally, the contact area between the sensor material and the composite sample must remain constant after the sensor melting. But, as it is

well known, the geometrical integrity of sensors, even for metallic sensors such as indium, could not be maintained upon recycling through a melting transition. Consequently, the thermal resistance between the sensor material and the composite sample will vary considerably, whereas variation in this thermal resistance must be kept as constant as possible. For this reason, the sensors were encapsulated in aluminum sample pans.

The interfacial resistance between the specimen and the aluminum sample pan should be kept as small as possible with respect to the thermal resistance of the specimen of interest. Therefore, efforts were made to flatten the cylindrical specimens in order to improve surface contacts between them, the calorimeter cup and the base of the encapsulated sensor material. The rough surface of the samples was sanded to arrive at acceptable smooth surface level for thermal conductivity measurements.

3.6 Heat Capacity Measurement by DSC

The principle of heat capacity measurement using DSC has been described elsewhere (O'Neill, 1966; Haines, & Wilburn, 1995). The following procedures describe the operation method used in this study for specific heat capacity measurement.

Operation Method

1. A pair of aluminum sample pans having very similar masses are selected. Empty sample pans are placed on the sample and reference holders in the DSC furnace. It is important to cover the sample pans with the aluminum lids provided. This ensures that the isothermal base line is unaffected by the presence or absence of sample. A front panel control is provided to adjust for the unbalance between the sample pan losses at any temperature; this control was used to make the base lines at 20 °C and 250 °C coincide.

2. By placing empty sample pans in the sample holder and the reference holder at an initial temperature (20 °C) for 6 min the isothermal straight line (curve I) is recorded (Figure 3.19).
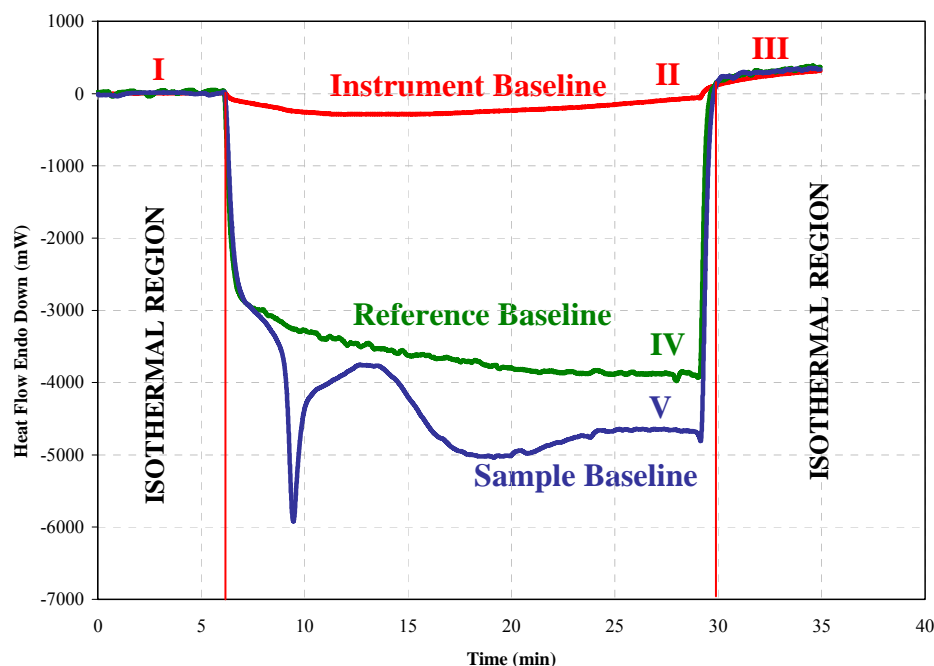

Figure 3.19 Heat capacity measurement using a heat-flux DSC and alumina as a standard reference material.

3. Scanning at a constant rate, the instrument baseline, curve II, is obtained. A scanning rate of 10 °C/min was used and the scan range was from 20 °C to 250°C. It should be noted here that each experiment was carried out under an argon purge (50 ml/min).

4. By maintaining the empty sample pans at a final temperature (250 °C) for 6 min, a straight line (curve III) is recorded. Once the above conditions have been satisfied, the slope, the horizontal and vertical axis sensitivities, the position of the zero point, the purge gas flow rate, and the level of coolant should be kept at those values for the duration of the experiment.

5. An alumina sample (18.1 mg) was used as the heat capacity standard. An alumina standard is now placed in the sample pan with cover and steps 2-4 are repeated. If a standard sample is measured under the same experimental conditions

mentioned above, the DSC curve drops linearly owing to the change in heat capacity of the standard sample as a function of temperature. The linear portion of the DSC trace exhibiting no endothermic or exothermic deviation in the presence of a standard sample is called the reference baseline (curve IV).

6. The alumina sample is removed from the sample pan. Then, the composite sample for which we want to determine the heat capacity is placed into the sample holder and steps 2 to 4 are then repeated to obtain the heat flow curve for the composite sample (curve V).

Finally, it may be necessary to repeat the experimental procedure. The typical thermal program used for the heat capacity measurement was:

- isothermally held at 20 °C for 6 min;
- ramp at 10 °C/min to 250 °C;
- isothermally held at 250 °C for 6 min.

The heat capacity of the material can then be calculated as (O'Neill, 1966; Haines, & Wilburn, 1995),

$$C_{ps} = \frac{m_r y_s}{m_s y_r} C_{pr} \tag{3.8}$$

where C_{ps} and C_{pr} are the heat capacity of the sample and the reference alumina, m_s and m_r are the sample mass and the mass of the reference alumina, and y_s and y_r are the DSC curve difference between baseline and sample and between baseline and reference, respectively. Pyris software is used to measure y_s, y_r and C_{pr} at each sampling point and to calculate C_{ps}. It should be noted here that the reliability of the calorimeter operation was checked by measuring the thermodynamic characteristics of fusion of indium.

CHAPTER FOUR
RESULTS AND DISCUSSION

4.1 Polyester Composites Reinforced with Non-Crimp Stitched Carbon Fabrics

4.1.1 Experimental Results and Discussions on the Mechanical Properties

4.1.1.1 Tensile Properties

Comparisons of the values of tensile strength determined experimentally with the tensile specimen cut different angles from the same unidirectional carbon/polyester laminate were shown in Table 4.1. These results for a $[0]_{12}$ unidirectional carbon/polyester composite, given in Figure 4.1(a) show that the strength falls rapidly when the fiber orientation is not parallel to tensile loading direction. The variation in stiffness in a highly anisotropic unidirectional carbon fabric/polyester and the decrease in stiffness over that of the laminate, even at right angles to the lay of the fibers is shown in Table 4.1.

Laboratory tests have long established that the laminate ply stacking sequence and the ply fiber orientations greatly influence the onset and growth of free edge delamination (Pagano, & Pipes, 1971; Bjeletich, Crossmann, & Warren, 1979). Under tensile loading, the delamination in most laminates, especially those containing 90° plies, is preceded by a number of transverse cracks (Kim, 1989). The stacking sequence of $[0°]_{12}$, where there is no an abrupt change in the various laminating plies, produces an interlaminar normal stress at the free edge under applied uniaxial tension. Because of the absence of transverse cracks in the $[0°]_{12}$ specimen of carbon/polyester under tension in MD, a delamination crack can not propagate in the interface of the laminating plies. Consequently, this specimen did not show any evidence of delamination at an applied axial tension of 641.1 MPa.

Table 4.1 Mechanical properties of carbon fiber/polyester composites in different directions (the data quoted are all average results taken from a minimum of six tests).

Composite	Test direction	Fiber volume fraction V_f (%)	Tensile modulus (GPa)	Tensile strength (MPa)	Elongation at break (%)	Flexure modulus (GPa)	Flexure strength (MPa)	ILSS (MPa)
Unidirectional carbon fabric	Machine		71.345 ± 2.6	641.07 ± 14.1	0.866 ± 0.04	50.445 ± 1.3	542.27 ± 12.8	21.545 ± 0.73
	Bias	23.1 ± 1.1	6.7401 ± 0.4	23.480 ± 0.8	0.387 ± 0.03	6.6410 ± 0.4	57.530 ± 1.5	4.3530 ± 0.24
	Cross		4.5440 ± 0.3	9.8980 ± 0.5	0.203 ± 0.03	4.3770 ± 0.3	22.068 ± 0.76	2.1940 ± 0.1
Quasi-isotropic carbon fabric	Machine		35.248 ± 1.1	353.17 ± 11.5	1.293 ± 0.06	21.674 ± 0.7	200.68 ± 10.5	5.2290 ± 0.34
	Bias	44.5 ± 1.8	38.324 ± 1.2	386.63 ± 13.1	1.039 ± 0.04	21.682 ± 0.7	172.85 ± 8.76	8.4630 ± 0.52
	Cross		39.615 ± 1.1	391.12 ± 13.6	1.032 ± 0.03	22.306 ± 0.7	211.76 ± 10.8	7.4230 ± 0.45

* The values after the ($\pm$) in all the tables refer the standard uncertainty of the measurement.
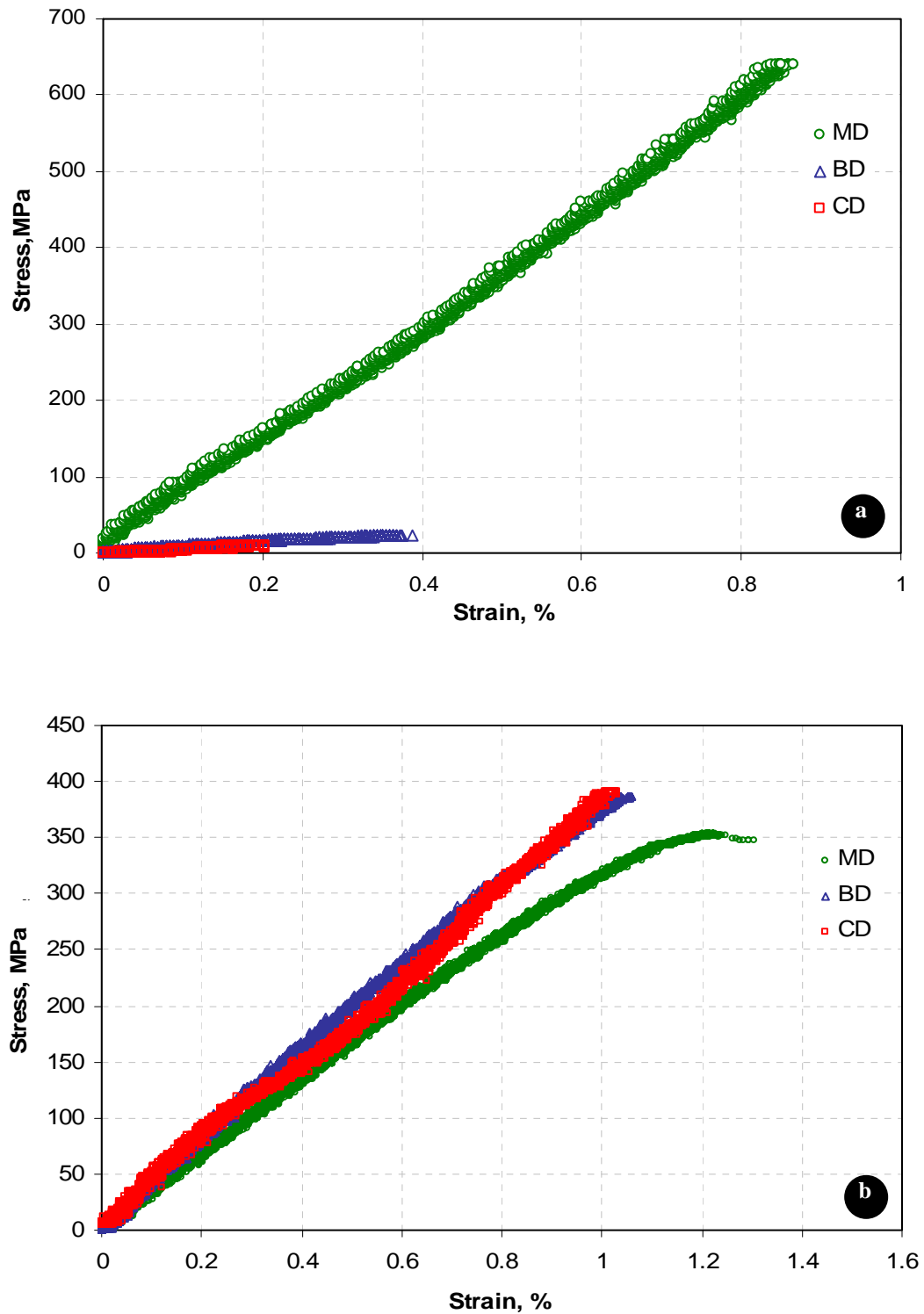
Figure 4.1 Tensile stress–strain curves of laminates in different directions: (a) unidirectional carbon fabric laminate; (b) quasi-isotropic (+45/-45/90/0°) carbon fabric laminate.
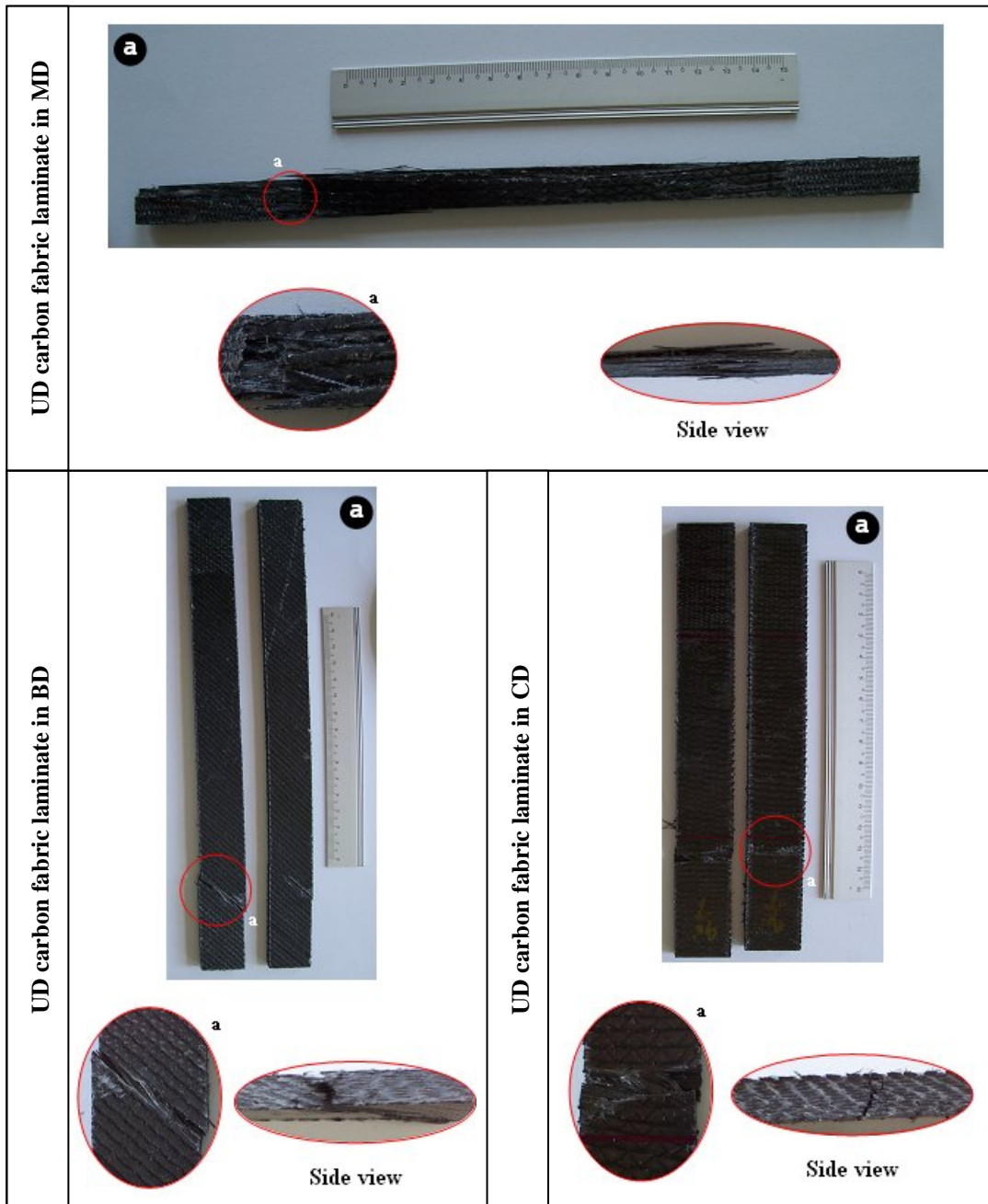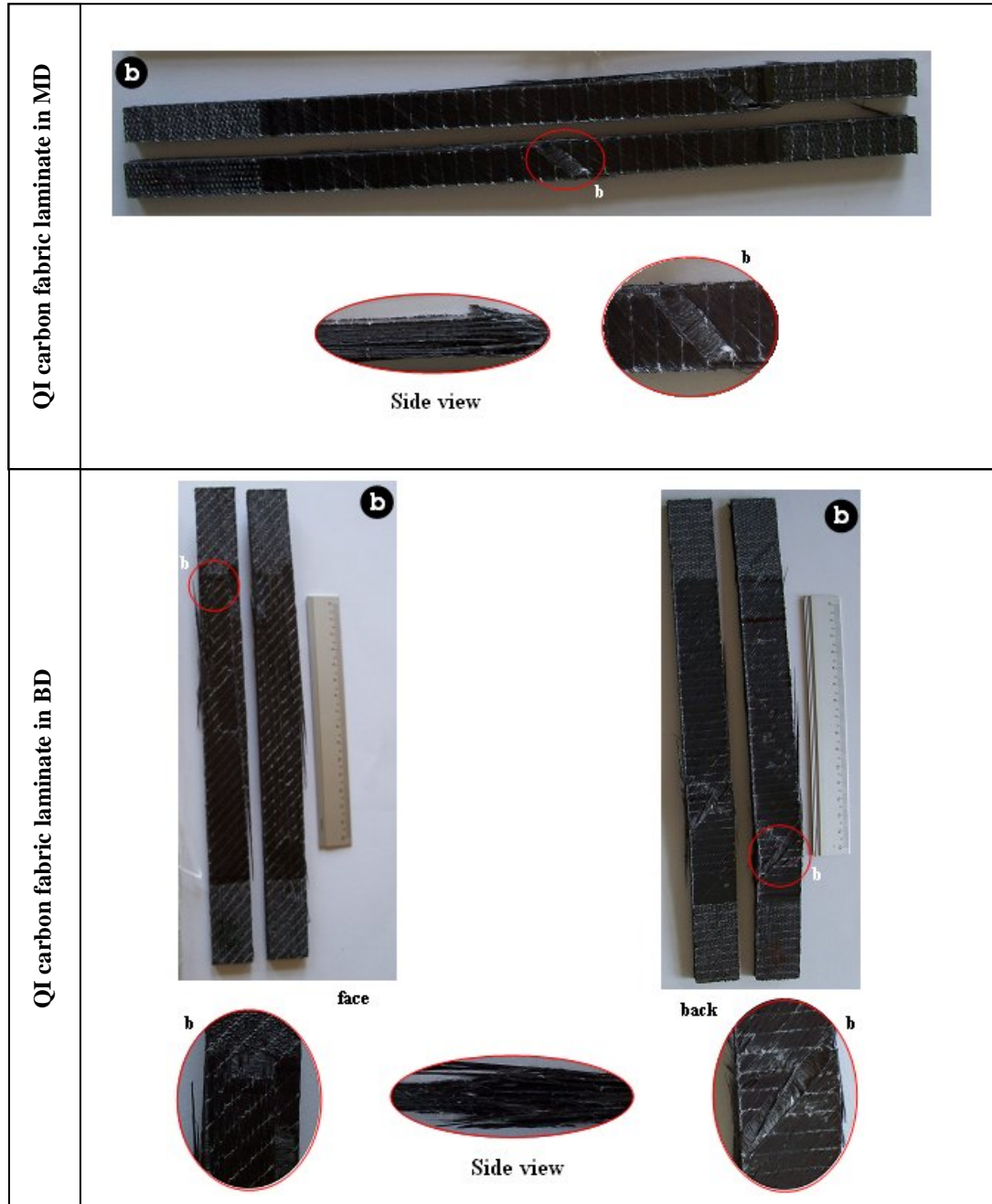
Figure 4.2 to be continued
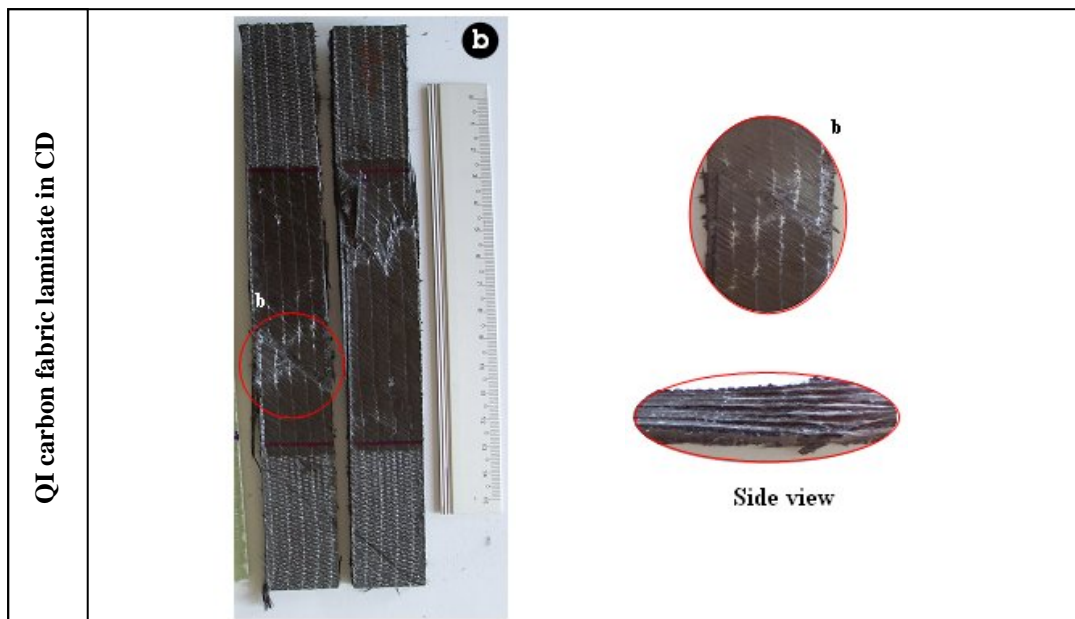
Figure 4.2 to be continued

Figure 4.2 Photographs showing side and front views of representative failures loaded in tension along the MD, BD and CD, for laminates produced from (a) unidirectional carbon fabric; (b) quasi-isotropic carbon fabric.

In the case of unidirectional laminate of carbon/polyester subjected to transverse tensile loading, a number of longitudinal fracture of matrix and debonding of fiber-matrix interface were formed in the laminating plies (Figure 4.2(a)). Note that each of the fracture planes was, macroscopically speaking, parallel to the fibers and normal to the applied tension. Each longitudinal fracture is formed and arrested at the 0°/0° interfaces wherein a series of localized longitudinal cracks can be developed as the applied load advances to higher levels; and consequently, carbon-polyester laminate subjected to transverse tension failed without exhibiting delamination.

It is interesting to note that the strength of quasi-isotropic laminate in test directions performed on the composites are not equal (Figure 4.1(b)). A somewhat surprising feature is that the strength in BD and CD is about 10% higher than that of MD, whereas the stiffness differs merely by a few percent (Table 4.1). It should be noted here that quasi-isotropic carbon-fabric laminates were produced by suitably arranged biaxial carbon fabrics. In the quasi-isotropic (QI) carbon fabric laminates, the fabric layers were separated giving twelve layers, the first layer being (0/90)

orientated (BA fabric turned by 45°), the second (+45/-45), the third (0/90) and the fourth layer being (+45/-45) orientated. This sequence is repeated three more times to make up the twelve layers. The mentioned improvements in the tensile strength in BD and CD cases have been attributed to the combination of fiber orientation and the orientation of the stitch rows, since the tricot knitting pattern runs nearly parallel to these directions as a consequence of the lay up of twelve biaxial carbon fabric with [+45/-45/90/0] orientations (Figure 4.3). It is worth noting that for MD samples there is not stitching in either +45/-45 or 0/90 layers which goes along the loading direction (MD). Experimental data taken from the literature imply that the orientation of the stitch rows with respect to the loading axis greatly influences the tensile properties of non-crimp stitched carbon fabric composites (Harris, Schinske, Krueger, & Swanson, 1991; Herszberg & Bannister, 1993). Both studies report that when the stitch rows were aligned parallel to the direction of tension loading, the strength was improved. Also, the anisotropy of strength for quasi-isotropic laminates is believed to be due to the fact that the nominal 45° direction of the fibers was not controlled during the laminate fabrication by VARTM process.

Another interesting point is demonstrated by the photographs showing side and face views of quasi-isotropic carbon fabric laminates after failure in the test along MD, BD and CD (Figure 4.2(b)). The implication is that matrix cracks form longer cracks oriented both in +45/-45° relative to loading direction. Most of them run from one edge of the specimen to the other. Despite the fact that delaminations were relatively localized at each side of the fracture site in all test directions, the appearance of failed specimens in the side plane tested in the BD is similar to that of the MD and CD tested coupons but with more debris. Comparisons between the actual photographs of fractured tensile specimens show that damage at fracture, in the case of unidirectional fabric laminate, was relatively localised compared with the quasi-isotropic laminate and that the unidirectional fabric laminate retained its through-thickness integrity.
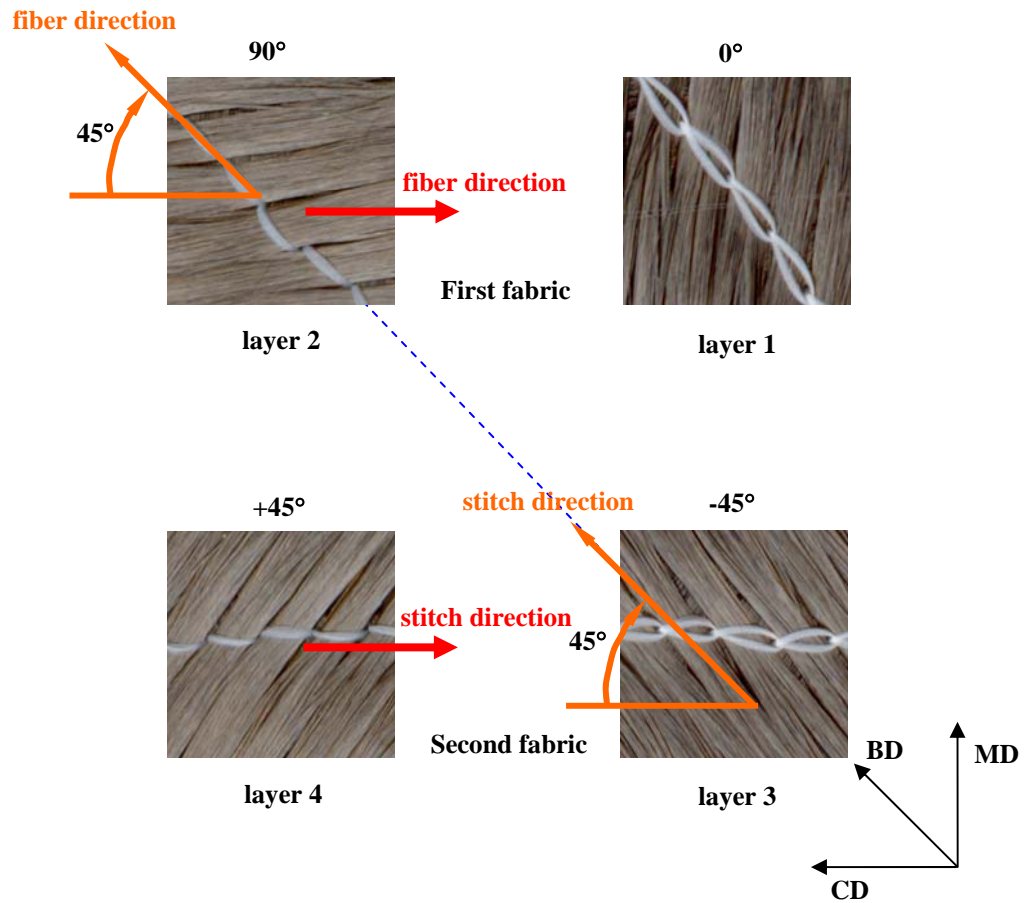
Figure 4.3 The effect of the orientation of stitch rows and fiber orientation on tensile strength behavior with respect to bias/cross directions.

4.1.1.2 Flexural Properties

It is of interest to note here that a catastrophic failure was not observed neither in the unidirectional nor in the quasi-isotropic carbon fabric laminates. From a closer observation on the tested specimens, it can be revealed that there was some visible inter-plane slippage and crack initiation in the mid-plane due to the fact that the through-the-thickness stitching increased delamination resistance of laminates. Hence, delaminations did not grow as readily in the stitched laminate.

It is of interest to note here that the recorded values of the flexural strength of both laminates, except for the unidirectional laminates in the bias and cross directions, were significantly lower than that obtained from tensile tests at all the considered test directions (Table 4.1). When the fractured bent specimens were investigated, it is observed that the upper layers of UD carbon fabric specimens fractured in fiber dominated MD direction as a result of compressive stresses. On the other hand, matrix dominated BD and CD directions had a fracture at the lower layers having tensile stresses. For QI laminate, the layers at the upper side had damaged where the loading in MD, BD and CD directions resulted compressive stresses. It is well known that carbon fibers have higher strength for tensile loading than compressive while polyester shown better strength properties in compressive directions than tensile. The specimens under pure tensile load had higher strength than the specimens subjected to bending which showed compressive failure. The specimens tested for bending and failed in tensile side had higher strength than the specimens tested in pure tension.

In the case of unidirectional carbon fabric laminates, the excitation aspects of the strength-deflection response were confirmed to agree well with the shape of the stress-strain curves in tensile tests (Figure 4.4(a)). Table 4.1 demonstrates that the composite strength falls rapidly with increasing fiber orientation angle (θ).
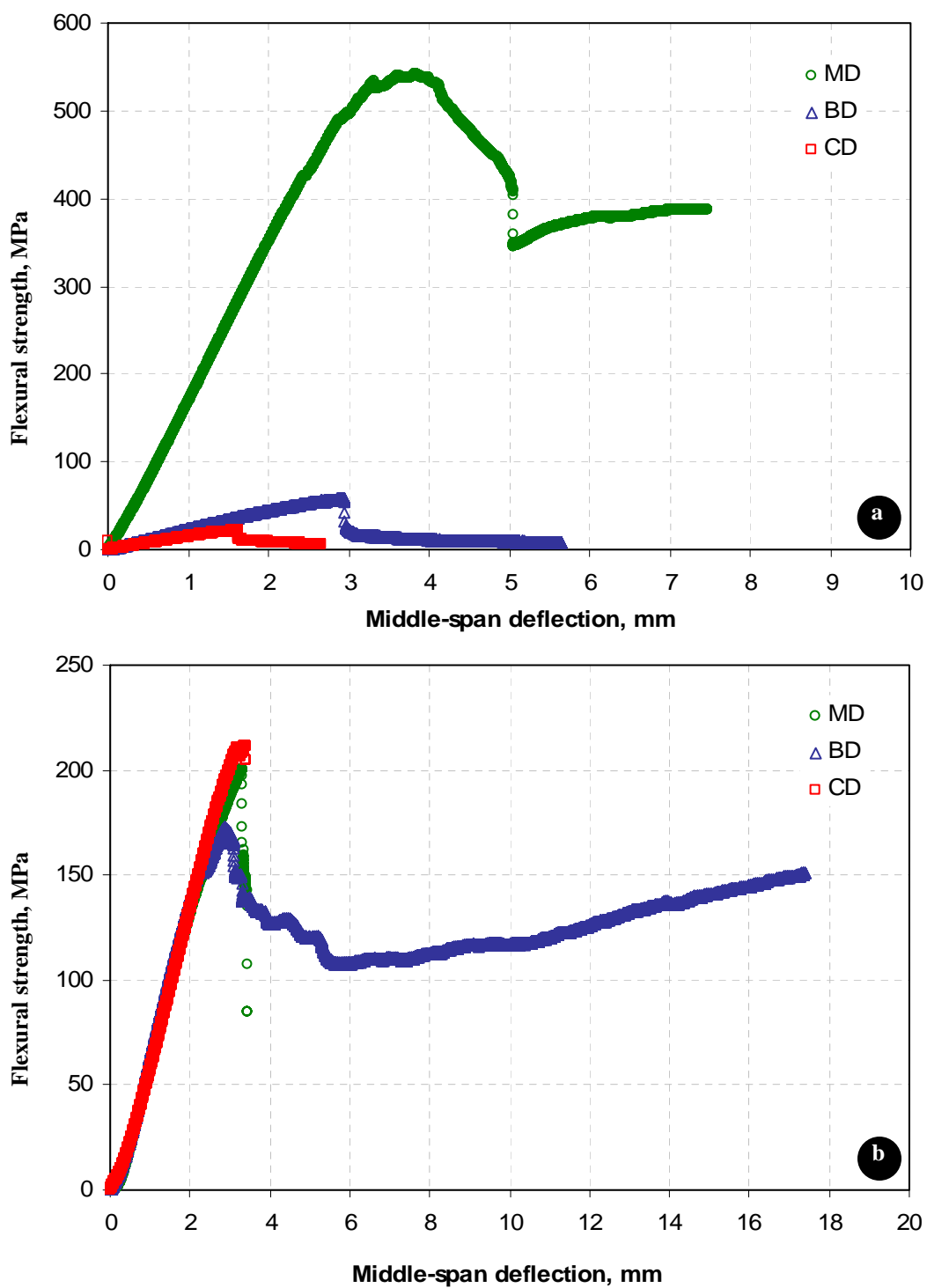
Figure 4.4 Flexural strength-deflection curves of laminates in different directions: (a) unidirectional carbon fabric laminate; (b) quasi-isotropic carbon fabric laminate.

It has already been mentioned in literature that when the angle θ is high, the strength of the composite tends to be matrix- or interface-dominated (Jang, 1994). This statement is true not only of unidirectional composites but also of any lamina in a multidirectional laminate. It can be seen from Figure 4.4(a) that the magnitude of the deflection is quite small for the CD case. This could be due to the fact that when the load is directed toward the laminate the matrix-dominated specimen is a very feeble structure and only local inward deformation cause the specimen to bulge out at the bottom surface layer.

By examining the strength-displacement curves of the quasi-isotropic laminates (Figure 4.4(b)) it is clear that these distributions are quite different. The great improvement in middle-span deflection for the BD case over the MD and CD is seen to occur at a load of about 150 MPa. From an overall point of view, however, we feel that increasing the displacement in BD is not perhaps as important as reducing the strength intensities in BD. The effect of stitching on the flexural properties has been studied by numerous investigators and discussed critically by Mouritz et al. (1997). In a study of the stress concentration effects of modified lock Kevlar® stitches in GFRP composites under four-point bending Mouritz (1996) observed that damage was localised around the stitch loops, which clearly revealed that the bending stresses were highest around the thread. By the same reason the flexural strength was reduced about 15%. It was concluded that not only was the stitch density controlled by selecting the stitch spacing, but the orientation of the stitch rows affected the flexural properties of stitched non-crimp fabric composites.

4.1.1.3 Short Beam Shear Test Results

It is not surprising to find that the interlaminar shear strengths at the time of failure recorded are at least an order of smaller than the flexural strengths of both laminates (Table 4.1).

Comparison of the results with data in Table 4.1 suggests that carbon composites fabricated from unidirectional fabric are more susceptible to interlaminar shear

strength degradation as a function of test directions than composites produced with the fibers in a quasi-isotropic lay-up by using suitably arranged biaxial carbon fabrics. It has been established, both in theory and experiment, that the lamina stacking sequence influences interlaminar stresses and, consequently, delamination in laminates. An approximate elasticity solution has been used by Pipes & Pagano (1974) to study the effect of the stacking sequence on the interlaminar shear stress in +45/-45 laminates. The results of their study indicated that stacking sequence had a significant effect on the interlaminar shear stress and that these stress concentrations (when layers having the [45/45/-45/-45]$_s$ orientation) could be reduced by use of the layers having the opposite [45/-45/45/-45]$_s$ orientation. Experimental results in conjunction with analytical models showed that the distribution and magnitude of interlaminar normal stress and interlaminar shear stress are widely varying due to the stacking sequences and laminate type (Whitney & Browning, 1972; Whitney & Kim, 1977). Multi-ply composites containing cross-ply layers of parallel filaments also experience complex forms of shear failure including delamination between layers, cracking parallel to the fibers of one layer which eventually causes fracture of neighboring crossed layers, and combinations of these two events. Observation of these modes of failure suggests that often crack extension parallel to the fibers in one layer precedes and causes the other modes of failure (Corten, 1968).

It can be observed from Table 4.1 that specimens, made from quasi-isotropic [+45/-45/90/0]$_6$ lay-ups of carbon fiber reinforced polyester, in MD case exhibited the lowest loading capacity with an ultimate strength of 5.2 MPa, which is 61.8% and 42% lower as compared with the 8.5 MPa and 7.4 MPa loading capacity of the specimens in BD and CD cases, respectively. A lay up of twelve biaxial carbon fabrics with [+45/-45/90/0]$_6$ orientation combined with the orientation of the stitch rows and fiber orientation is held responsible for the different behavior with respect to the bias/cross directions (Figure 4.3). The effect of stitching on interlaminar shear strength has been studied by Du, Xue & Gu, (1986) for a prepreg CFRP tape laminate, and improvements in the shear strength due to stitching were recorded to be 14.4% or 25.6% depending on the orientation of the stitch rows.

4.1.2 Fractographic analysis

It is possible to observe clear local differences in the representative images of the breakage region for UD carbon fabric specimens (Figure 4.5(a)). In the upper inset a general view is presented showing ductile deformation of the matrix but a poor matrix-carbon fiber adhesion. In the lower photomicrograph, a higher magnification image clearly shows a clean fiber surface, although a small amount of polymer can be seen between fibers. These observations suggest an adhesive failure in the interface after fiber fracture. Although the UD carbon sample shows adhesive failure (Figure 4.5(a)), its relatively high tensile strength can be explained taking into consideration a highly ordered carbon structure along the fiber axis, while chemical breakage takes place. Pullout effect of fibers was observed from these images.

In Figure 4.5(b) the eleventh and twelfth reinforcement layers are shown, which are (+45/-45) and (0/90) orientated, respectively. Although none of the 45° tows are fully fractured there is evidence of considerable damage to one tow on the right hand side micrographs, corresponding to the side of the coupon that had the visible surface damage. None of the 45°and 90° tows are fractured and there is little or no evidence of individual fiber fracture. It should be noted that on the micrographs the exposed reinforcements are not 'clean'; there are flaky deposits on the reinforcement surface, which are remnants of the resin that was not fully decomposed.
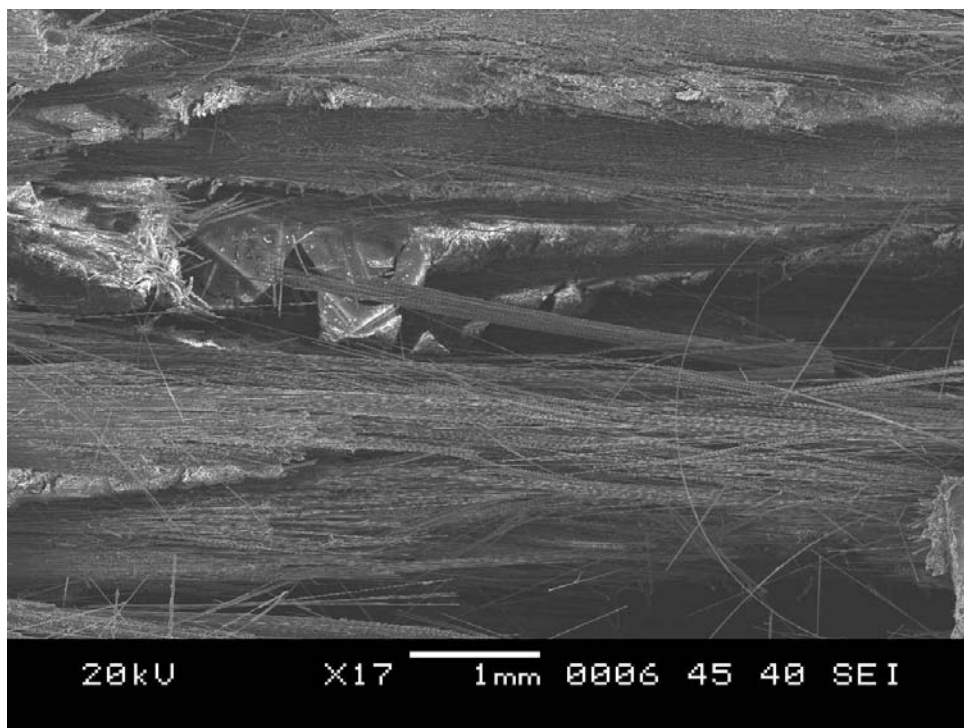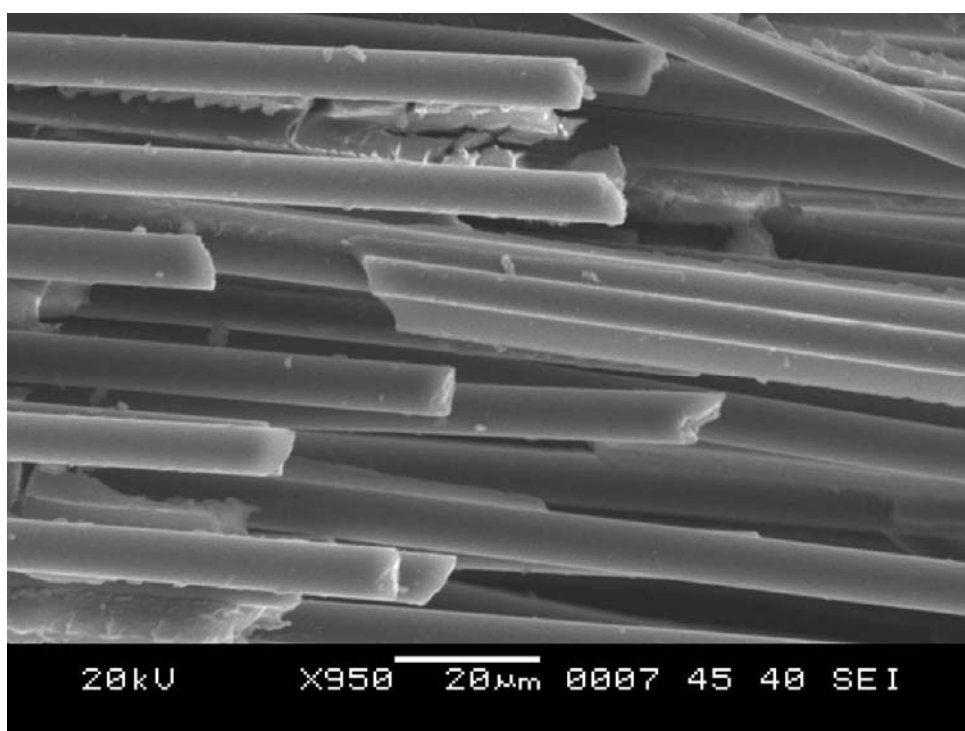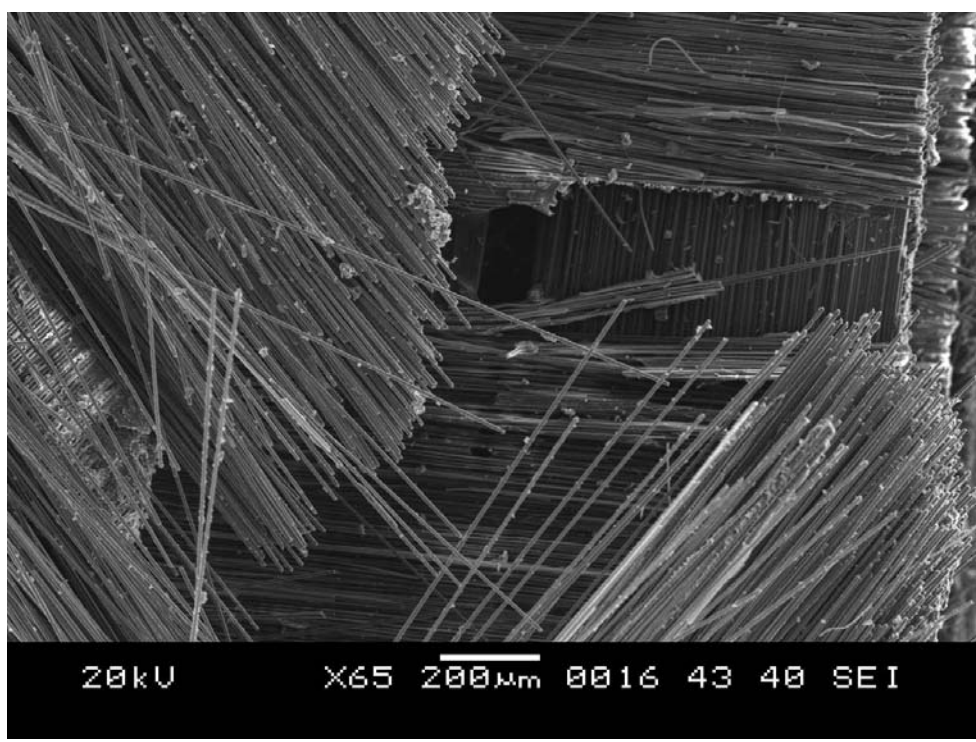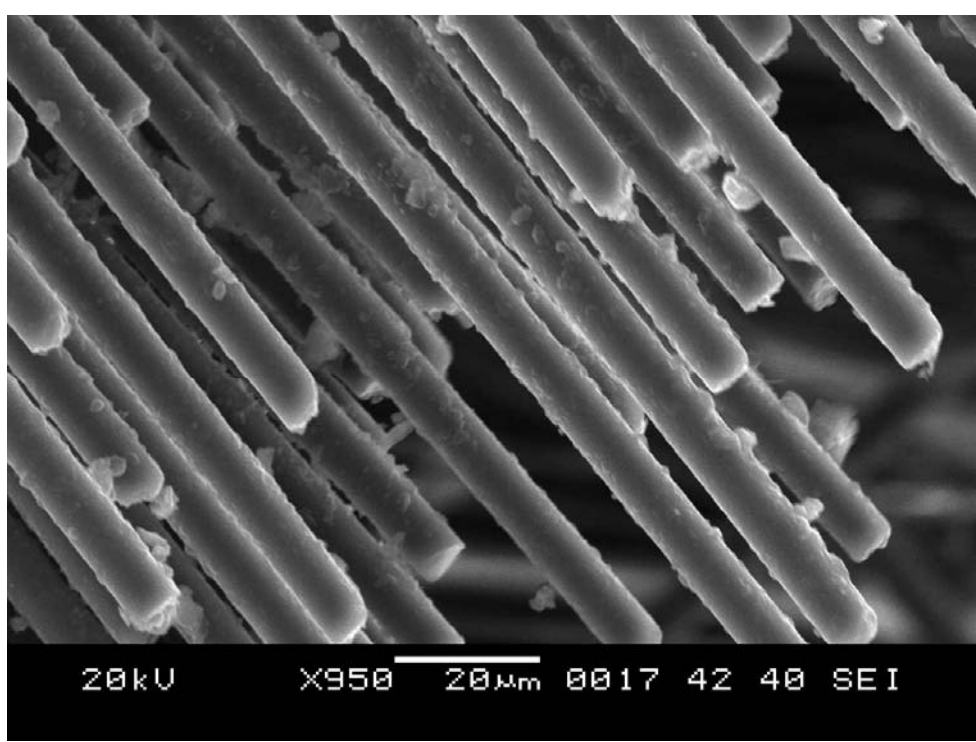
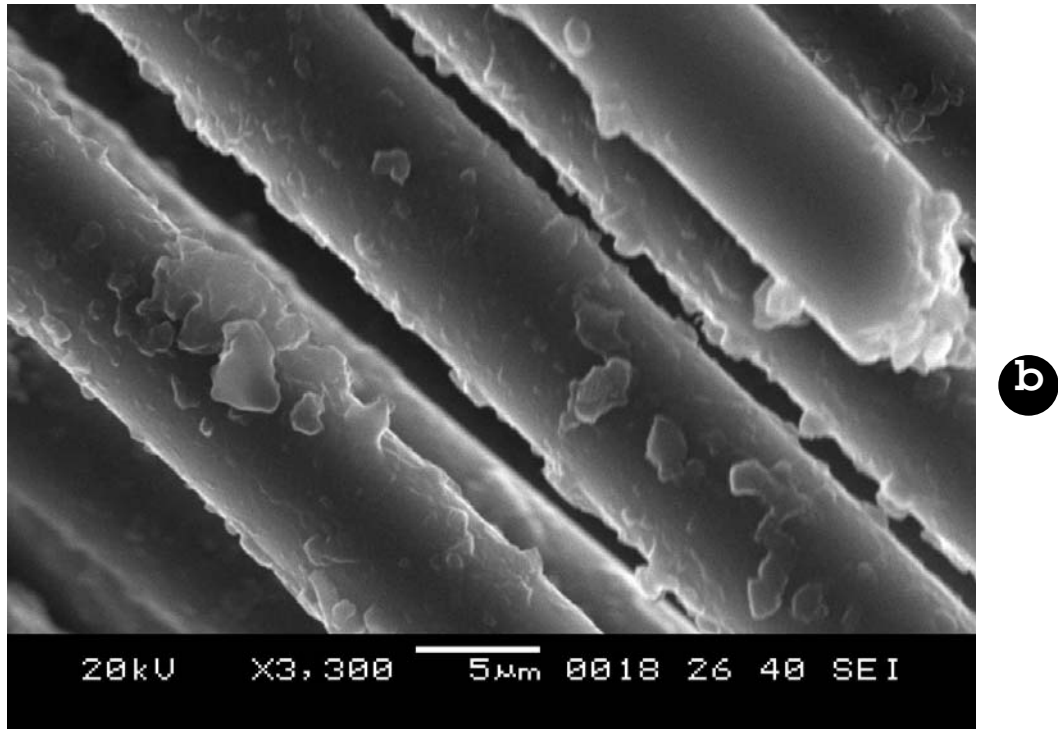Figure 4.5 to be continued

Figure 4.5 to be continued

Figure 4.5 Representative SEM images of the breakage region for (a) unidirectional carbon fabric laminate; (b) quasi-isotropic carbon fabric laminate that were tensile tested in machine direction (at different magnification levels).

4.2 Polyester Composites Reinforced with Non-Crimp Stitched Glass Fabrics

4.2.1 Experimental Results and Discussions on the Mechanical Properties

4.2.1.1 Tensile Properties

Comparisons of the values of tensile strength determined experimentally with the tensile specimen cut different angles from the same unidirectional glass/polyester laminate were shown in Table 4.2.

Experimental results from tensile tests indicated that polyester composites reinforced with unidirectional glass fabrics showed an almost linear relation between stress and strain in the direction of fibers while in the matrix dominated orientations the non-linear stress-strain relation was observed (Figure 4.6(a)). So it has been pointed out that when the fiber orientation angle in unidirectional composites is high, the strength of the composite tends to be matrix- or interface- dominated. Having recognized the nature of this problem, it was noted that a continuous decrease in strength of unidirectional composites can be achieved by deviating the test angles θ from 0°.

Photographs of fracture surfaces of unidirectional composites loaded in tension along the fiber direction exhibits pronounced irregularity and fiber pullout (Figure 4.7(a)). According to these photographs, there was no sign of cumulative damage progression for the CD tested specimens of the unidirectional glass/polyester composites (Figure 4.7(a)). Observations on the cross sections of the fracture plane revealed that for the CD tested specimens fracture modes were the combination of debonding between the fiber bundles and the crack along the fiber/matrix interface. It can be seen that some glass fibers are transversely pulled-out from the matrix when the transverse failure happens.

Table 4.2 Mechanical properties of glass fiber/polyester composites in different directions (the data quoted are all average results taken from a minimum of six tests).

Composite	Test direction	Fiber volume fraction V_f (%)	Tensile modulus (GPa)	Tensile strength (MPa)	Elongation at break (%)	Flexure modulus (GPa)	Flexure strength (MPa)	ILSS (MPa)
Unidirectional glass fabric	Machine		37.827 ± 1.20	610.21 ± 14.1	1.6650 ± 0.06	27.324 ± 0.76	550.36 ± 12.8	31.218± 1.05
	Bias	48.4±0.8	6.6905 ± 0.50	68.962 ± 2.50	5.8110 ± 0.30	5.7330 ± 0.28	81.204 ± 2.95	7.0170± 0.43
	Cross		6.6610 ± 0.50	73.658 ± 2.85	2.2570 ± 0.10	6.6940 ± 0.32	86.477 ± 3.01	6.7510± 0.40
Biaxial glass fabric	Machine		12.365 ± 0.60	150.91 ± 8.56	2.9660 ± 0.12	6.7130 ± 0.33	190.91 ± 10.5	13.232± 0.76
	Bias	54.7±1.1	16.480 ± 0.65	285.21 ± 11.8	2.0340 ± 0.09	14.122 ± 0.62	278.18 ± 11.8	21.965± 0.82
	Cross		8.2630 ± 0.48	133.11 ± 8.16	3.4110 ± 0.16	7.1100 ± 0.46	186.76 ± 10.5	13.787± 0.71
Triaxial glass fabric	Machine		13.821 ± 0.62	352.70 ± 13.1	2.7110 ± 0.11	13.595 ± 0.61	389.90 ± 13.3	19.232± 0.79
	Bias	38.7±0.6	19.294 ± 0.68	259.56 ± 11.5	1.5950 ± 0.05	15.930 ± 0.63	330.58 ± 13.0	16.287± 0.75
	Cross		10.432 ± 0.52	95.347 ± 3.20	2.4310 ± 0.1	7.2290 ±0.47	130.20 ± 8.15	5.957± 0.38

* The values after the (±) in all the tables refer the standard uncertainty of the measurement.
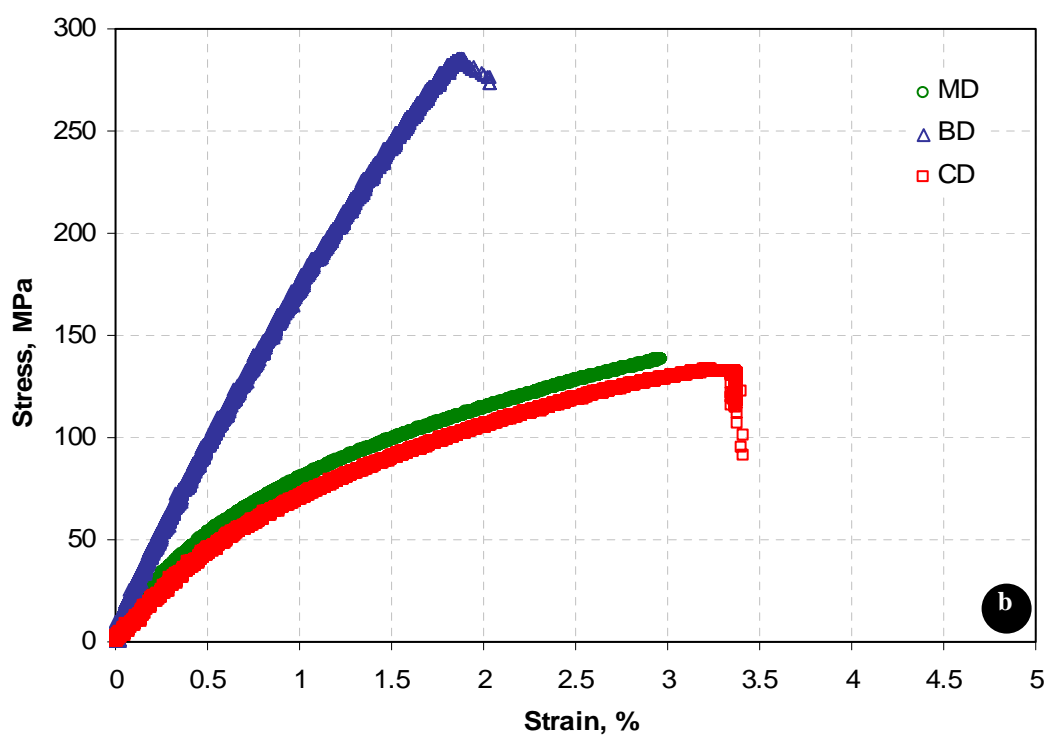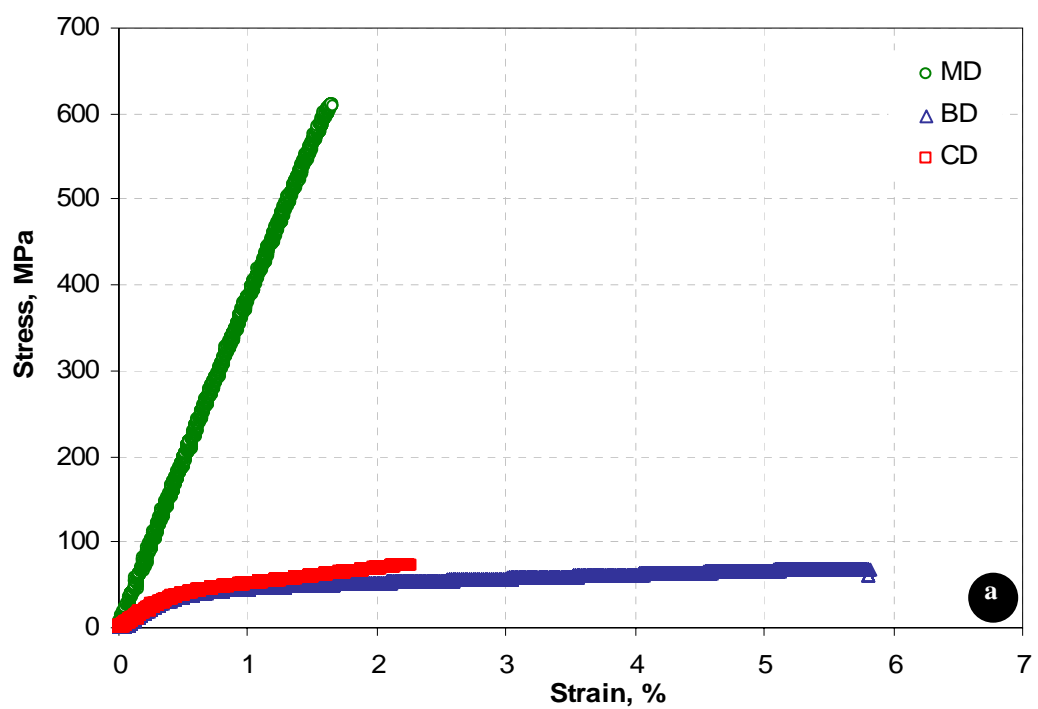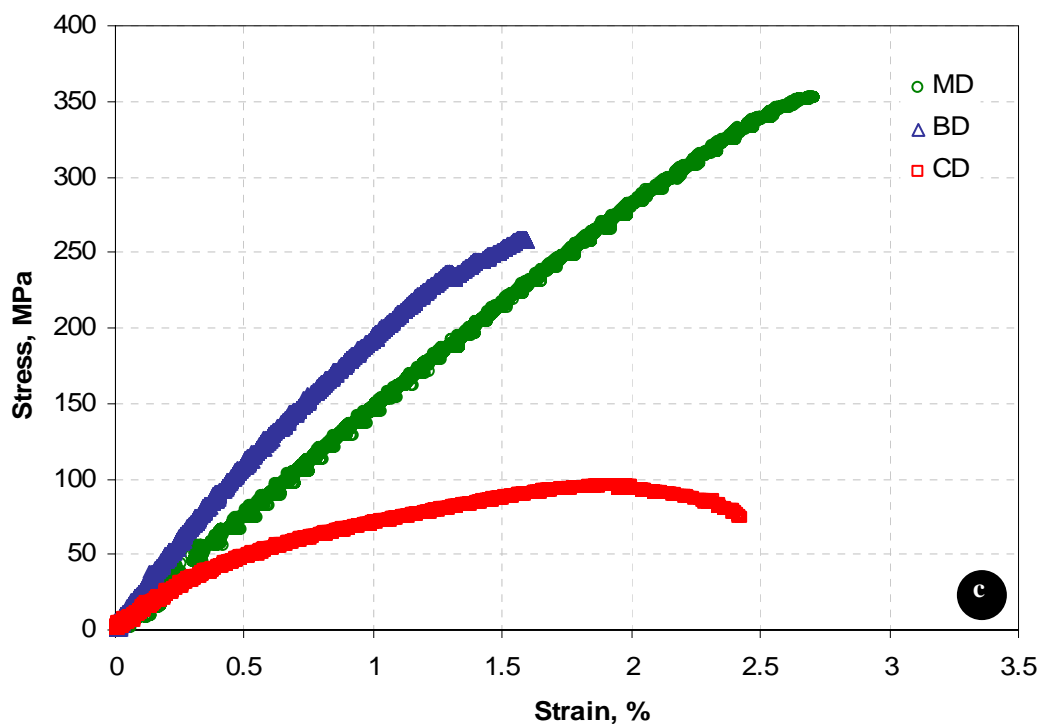
Figure 4.6 to be continued

Figure 4.6 Tensile stress–strain curves of laminates in different directions: (a) unidirectional glass fabric laminate; (b) biaxial +45/-45° glass fabric laminate and (c) triaxial 0,+45/-45° glass fabric laminate.

As would be expected, the biaxial glass fabric laminates were anisotropic materials in which the strength in fiber (BD) directions exceeded those in the other directions by a factor between 1.9 and 2.1 (Table 4.2). These results indicate that the stress–strain curves of the tests in fiber direction were linear, although gradual softening was evident as the load increased (Figure 4.6(b)). Conversely, in the other, a highly non-linear relation due to the matrix-dominated orientations was observed. As a result of a higher nonlinearity in the stress-strain curves of the tests in matrix-dominated orientations, progressive failure due to various interacting micro-failure modes, such as matrix shearing, cracking, fiber debonding, fiber pullout and interply tearing was amplified.

UD glass fabric laminate in MD	
UD glass fabric laminate in BD	

Figure 4.7 to be continued

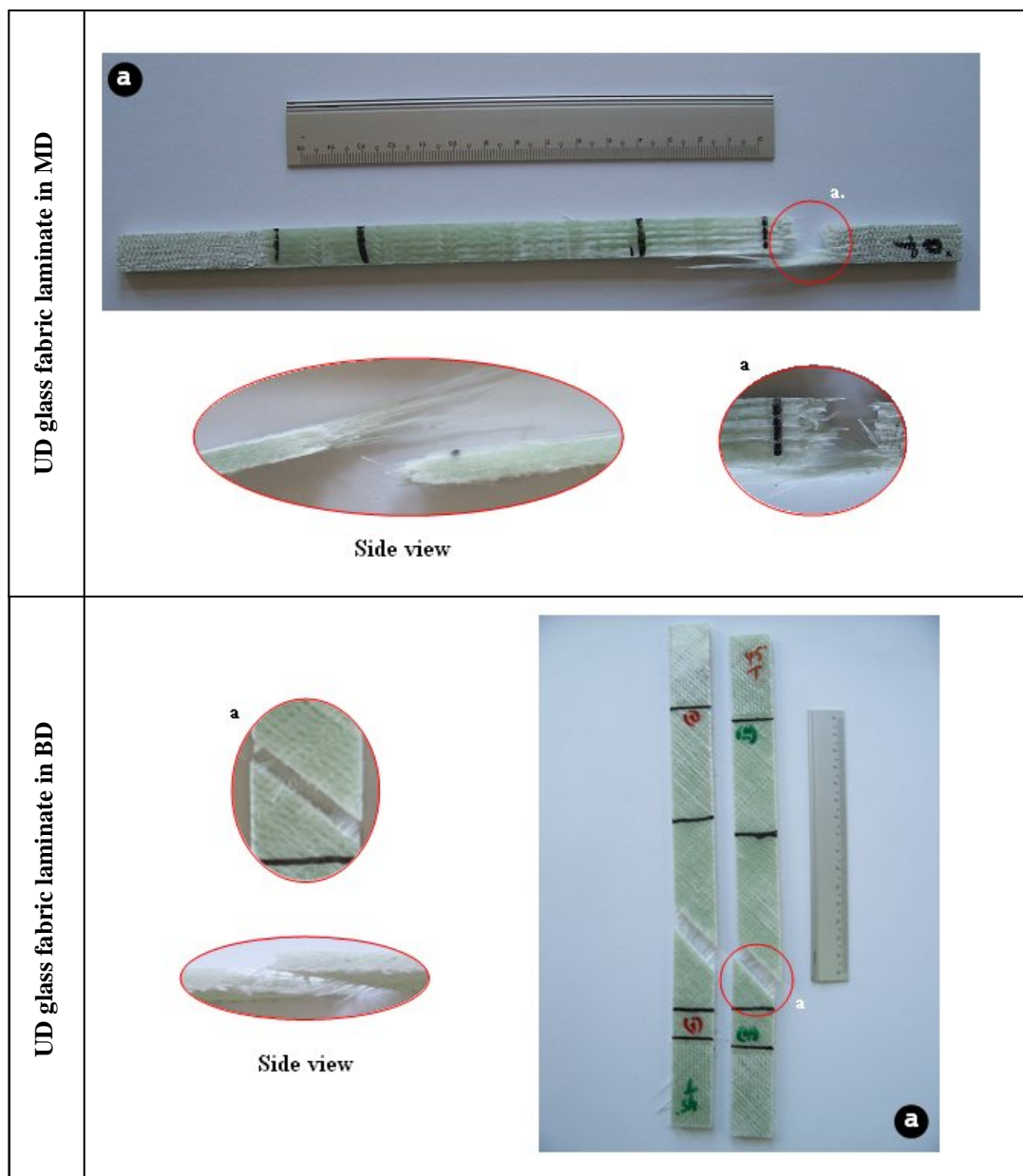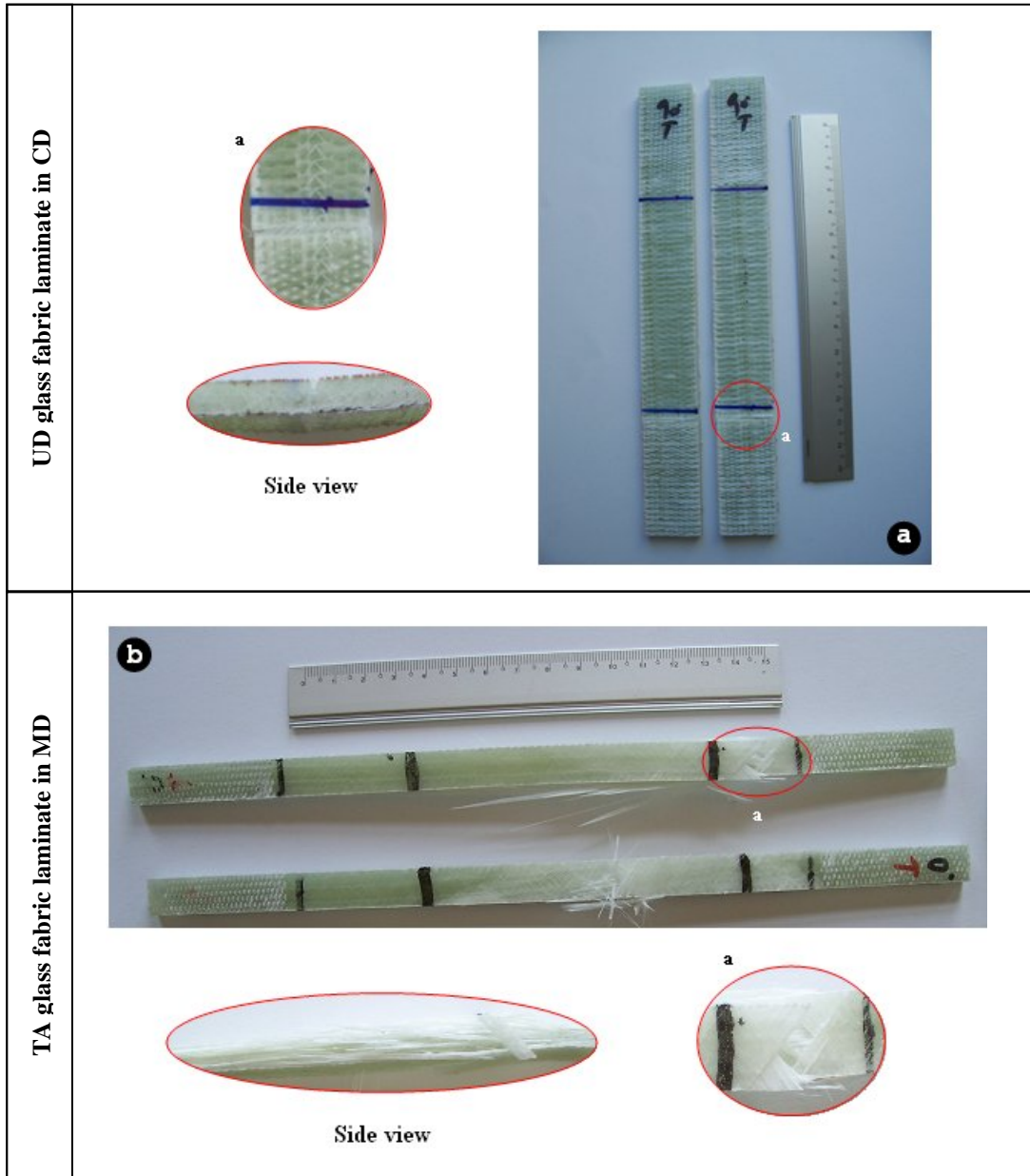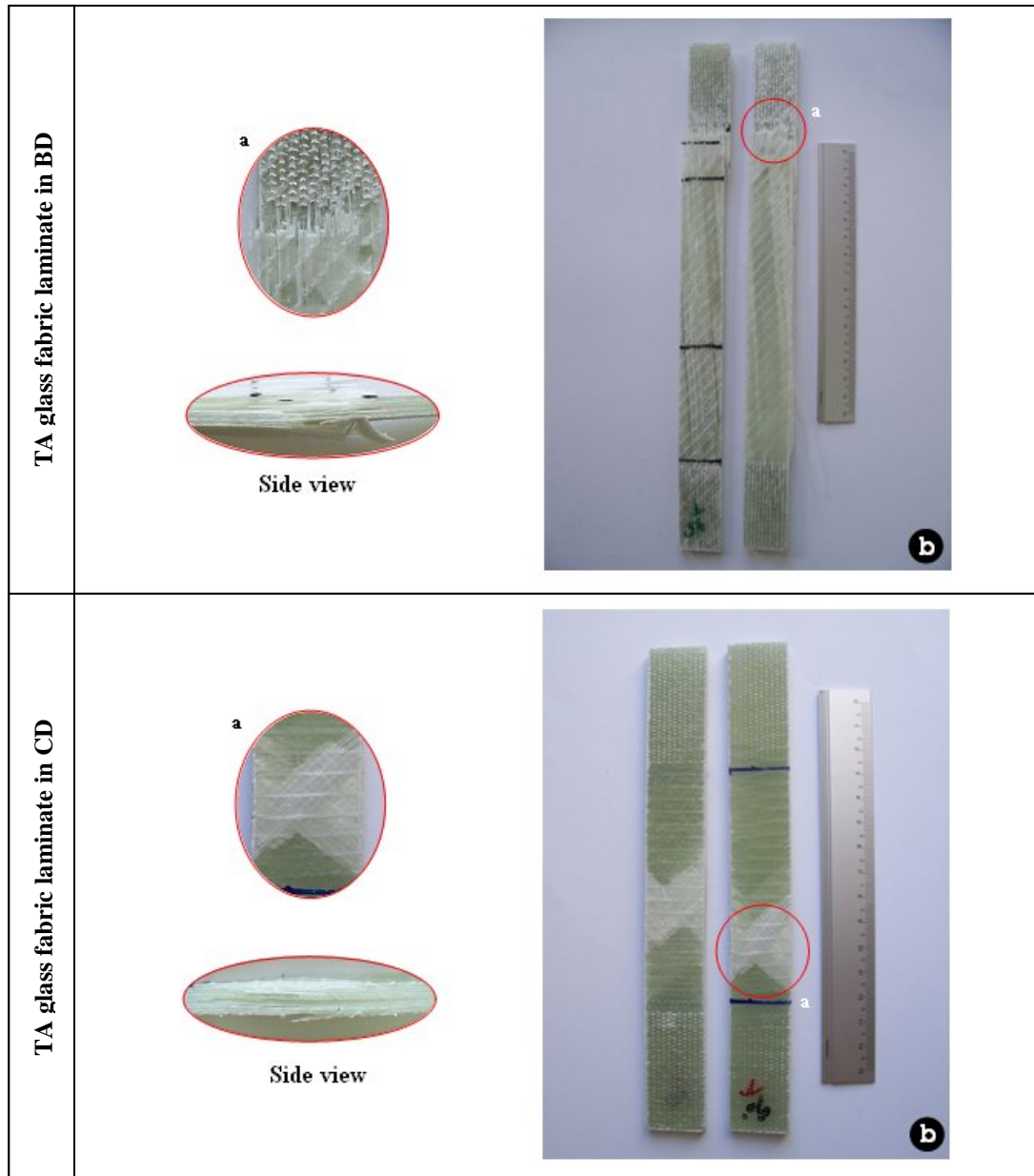|	
UD glass fabric laminate in CD	a Side view a
TA glass fabric laminate in MD	b a Side view a

Figure 4.7 to be continued
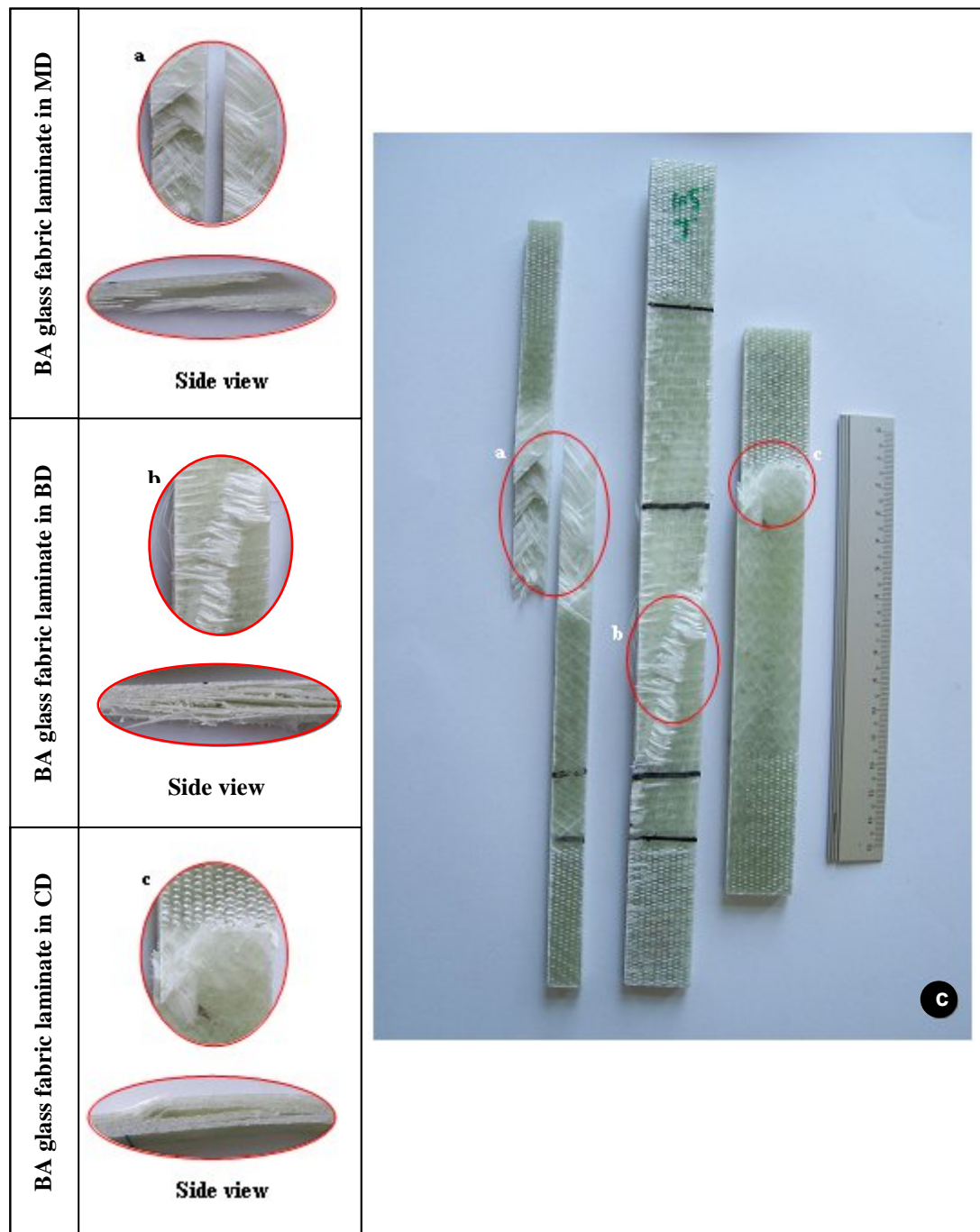
Figure 4.7 to be continued

Figure 4.7 Photographs showing side and front views of representative failures loaded in tension along the MD, BD; and CD, for laminates produced from (a) unidirectional glass fabric; (b) triaxial glass fabric and (c) biaxial glass fabric.

A more visual comparison between the deformations of the fiber direction and matrix-dominated orientations can be seen in Figure 4.7(c) where deformation and delamination of specimens in the front and side plane were photographically illustrated after the tensile tests. The implication is that matrix cracks form longer cracks oriented both in +45°/-45° relative to loading direction. Most of them run from one edge of the specimen to the other. It can also be noted that some delaminations can be seen also from inside the specimen, at crossings of +45°/-45° matrix cracks, as revealed by in Figure 4.7(c). At the end of the test, a dominant delamination reaches the other edge and the specimen fails.

In the bias direction, transversal cracks were dominant over longitudinal cracks, in-spite of some micro-longitudinal cracks in the -45° plies (90° layer positions with respect to an applied load in BD) act to raise the stress in adjacent 45° plies (0° layer positions with respect to an applied load in BD). At failure strain, when the transverse matrix cracks were saturated, longitudinal cracks, due to fiber splitting mechanism, increase and grow together with delaminations.

It can be observed from Table 4.2 that specimens, made from biaxial glass fabric laminates, in MD case have higher ultimate strength, about %13.4, compared to the ultimate strength of the specimens in CD case. Improvements in the tensile strength in MD case have been attributed to the orientation of the stitch rows, since the tricot knitting pattern runs nearly parallel to the machine direction as a consequence of the lay up of twelve biaxial glass fabric with [+45/-45] orientations.

A more significant difference occurred when the triaxial glass-fabric laminates were tested in different directions (Figure 4.6(c)). Here, the measured strength of the non-crimp fabric laminate, tested in the CD, fell on average near 95 MPa compared with about 350 MPa for the MD (Table 4.2). This is so because of the absence of fibers along the CD. In contrast, this condition has no significant effect on the maximum elongation which was reduced by about 11 percent due to the stitching across the plies in the non-crimp fabrics.

As comparison based on the direction of fibers suggests that the ultimate strength reduction appears to be more pronounced in BD specimens. In addition to the 0° layers, BD specimens contain plies with its fiber axis parallel (+45° layers) and perpendicular (-45° layers), to an applied load direction (+45° or BD). As compared to the specimens in MD case, a significant decrease of %36 in the ultimate strength of the specimens in BD case could be attributed to the fact that the effect of the interlaminar normal stress for specimens in BD case is intensified considerably with an interchange of the -45° and +45° layer positions (90° and 0° layer positions with respect to an applied load in BD) and hence this increase of interlaminar normal stress triggers the delamination at a much lower stress level, as indicated in Table 4.2 and Figure 4.6(c).

It may be of interest; however, to examine the effect of ply orientation on the tensile modulus of the triaxial glass fabric laminates (Table 4.2). The difference in tensile moduli for case MD and case BD appears to be significant. The tensile tests showed that bias plies play a larger role on maximum tensile modulus. Furthermore, the strength in BD is greater than the strength of MD at the equivalent strain (Figure 4.6(c) and Table 4.2).

Another interesting point is demonstrated by the photographs showing side and face views of triaxial glass fabric laminates after failure in the test along MD, BD and CD (Figure 4.7(b)). In case BD, at the highest load, the fracture profile is further distorted as a consequence of the machine plies deformation. From Figure 4.7(b) one can see that the specimens failed by splaying of the fibers.

4.2.1.2 Flexural Properties

It is of interest to note here that a catastrophic failure was not observed in the NCF based composites. The specimens exhibited a more localized damage region at the top side of the beam by compression and at the bottom side by tension.

As can be seen from Figure 4.8(a), the unidirectional laminate of glass/polyester exhibit the nonlinear strength-deflection response under off-axis loading (BD case). All the transverse flexure specimens exhibit nonlinear strength-deflection behavior (CD case). It must be pointed out here that the flexural strength-deflection responses showed less nonlinearity than the tensile responses.

No significant differences between properties in MD and CD for the biaxial glass fabric laminate are noted (Figure 4.8(b)). Specimen in BD was the most efficient beam in this group with an ultimate strength of 278.2 MPa (Table 4.2). As illustrated in Figure 4.8(b), more than 46% of the laminate strength was lost in the case of MD and CD due probably to the matrix-controlled failure mode.

To understand how the design modification affects the bending performance of triaxial glass fabric laminates, the strength distribution was examined first. The MD and BD study case helped extend the load carrying region of the specimens after yield (Figure 4.8(c)). It is also of interest to note here that, after yield, the strength-deflection curves were demonstrated the sudden strength drop. This plot demonstrates the improvement obtained in the performance of the composite by suitably changing the compliance of the fiber alignment. The design changes affected the results from 0° to about 90° fiber orientation angle. As observed in Figure 4.8(c), it can be seen that two of the three experimental curves (MD and BD) reached peak strength before failing and have similar initial elastic modulus up to cracking. It can be observed from Table 4.2 that specimens in CD case exhibited the lowest loading capacity with an ultimate strength of 130.2 MPa, which is by a factor of 3.0 and 2.5 lower as compared with the 389.9 MPa and 330.6 MPa loading capacity of the specimens in MD and BD cases, respectively. This seemed to be due to the fact that failure is predominantly controlled by fiber directionality in MD and BD.
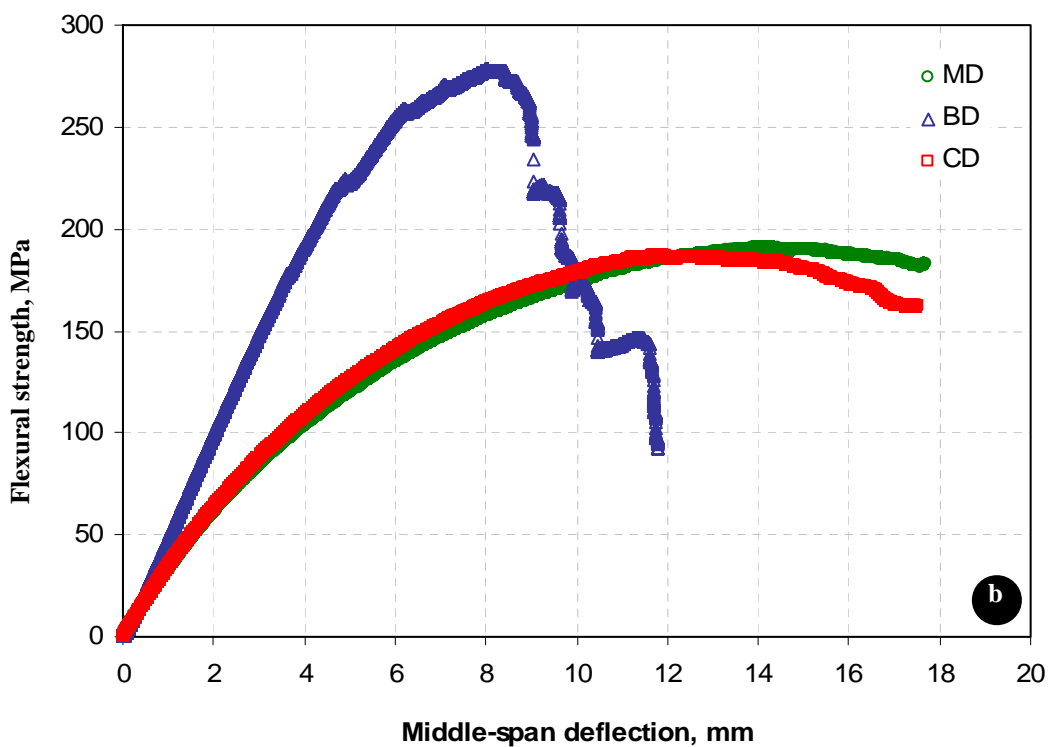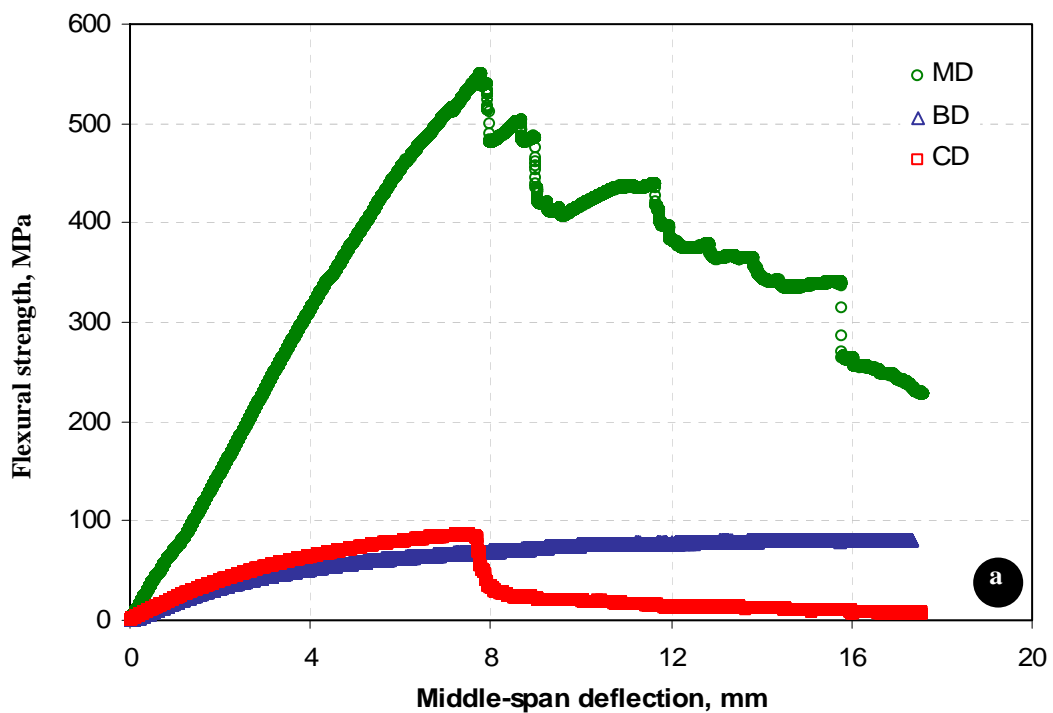
Figure 4.8 to be continued
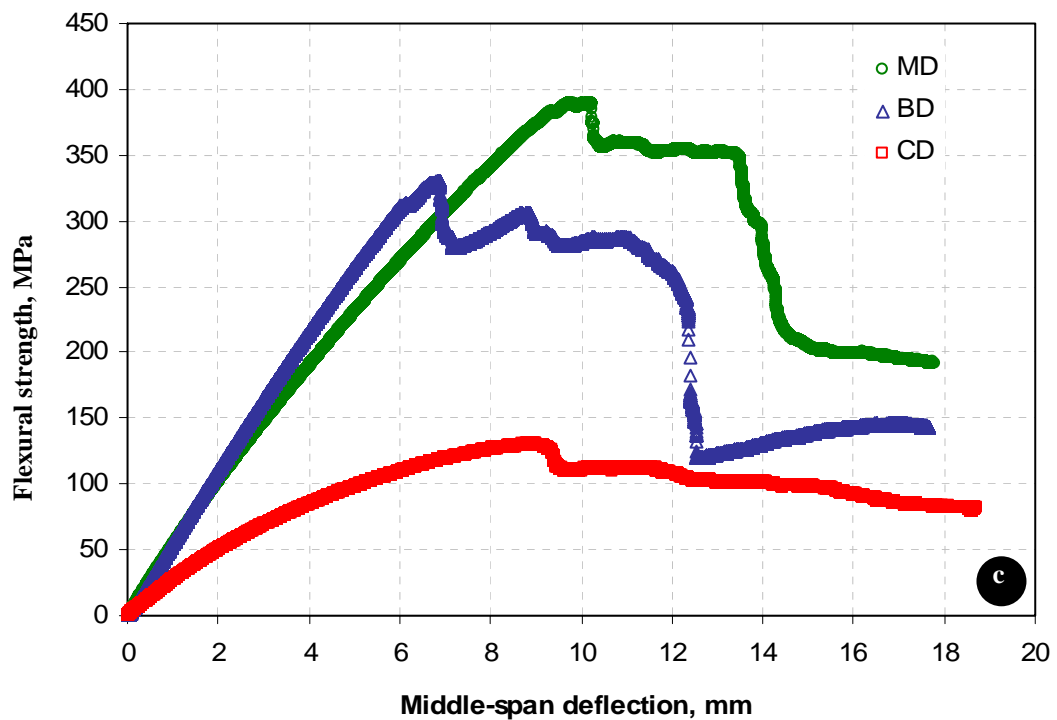
Figure 4.8 Flexural strength-deflection curves of laminates in different directions: (a) unidirectional glass fabric laminate; (b) biaxial glass fabric laminate and (c) triaxial glass fabric laminate.

4.2.1.3 Short Beam Shear Test Results

The experimental results indicate that the magnitude of the interlaminar shear strength was varying due to the stacking sequence, laminate type and fiber orientation angle (Table 4.2).

The measurements seemed to indicate that the unidirectional laminates of glass/polyester are highly susceptible to interlaminar shear strength degradation as a function of test orientation than laminate produced with biaxial and triaxial glass reinforcement fabrics. This finding is directed to comparison based on first inter-ply failure, which is the commonly accepted indication of failure for short beam shear test. However, biaxial and triaxial specimens can continue to sustain significant loads way beyond fracture initiation.

It can be concluded again that the interlaminar shear strengths at the time of failure recorded were considerably lower than that obtained from flexure tests at all the considered test direction (Table 4.2).

4.2.2 Fractographic Analysis

Extensive damage was found in the UD glass fabric laminate specimens which has poor fiber/matrix adhesion (Figure 4.9(a)). The clean fiber surfaces indicate extensive interfacial failure. In addition, there is little matrix material between the fibers on the post-fracture surface, i.e. the fibers are loosely held by the matrix material. Due to the weak fiber/matrix adhesion, the damage evolution occurs at early stages of loading, and the stress transfer from critically stressed fibers to lower-stressed regions cannot be done properly. In triaxial glass fabric laminate specimens (Figure 4.9(c)); fiber surfaces are almost completely devoid of matrix material, designating extensive interfacial failure. In addition, the matrix is no longer holding fibers together. These results may suggest that debonding between fibers and matrix or, in other words, fracture occurring in the interface between fiber and matrix due to poor interfacial adhesion could be the dominant mechanism of failure for this loading mode.

On the other hand, in the case of BA glass fabric laminate specimens (Figure 4.9(b)), where most fibers are covered with the matrix, the failure occurred in both matrix failure and fiber breakage. When tensile stress is continuously applied to the specimens to some stage, fiber breakage will happen progressively at random places, which induces tiny transverse cracks in the matrix as a consequence of a better interfacial adhesion. Some of these cracks will change path when they confront the fibers and then easily propagate along the contact area between fibers to cause longitudinal fiber/matrix splitting through the formation and propagation of longitudinal cracks, resulting in a large deformation of the specimen. Therefore, a progressive failure is expected for such composite systems. However, matrix failure is more apparent in this case, and the broken matrix pieces still adhered to fibers.
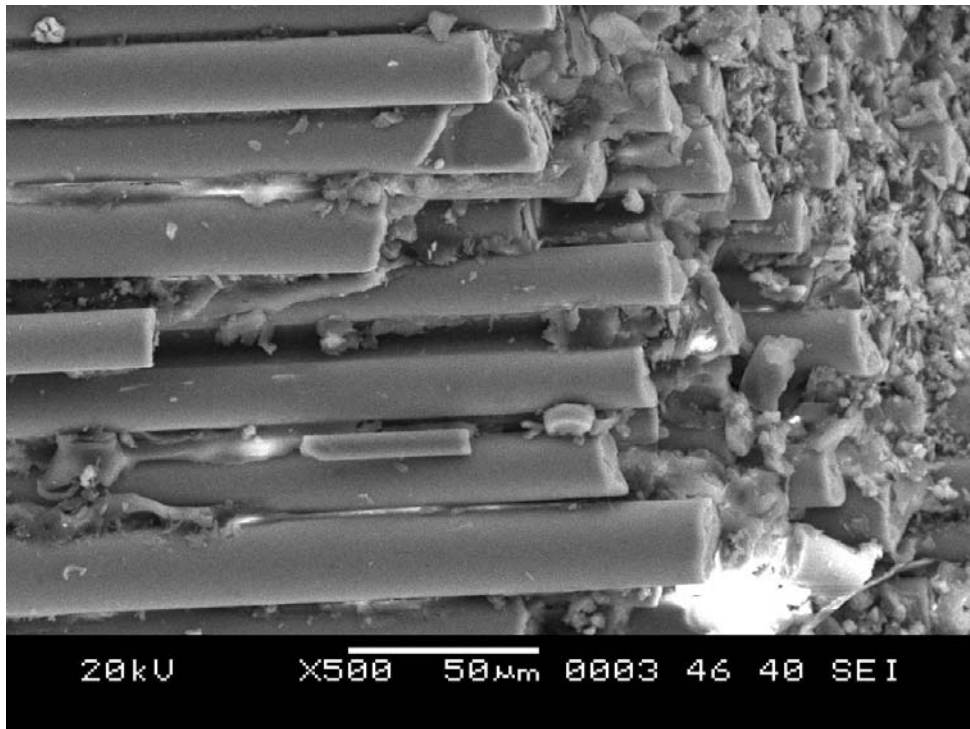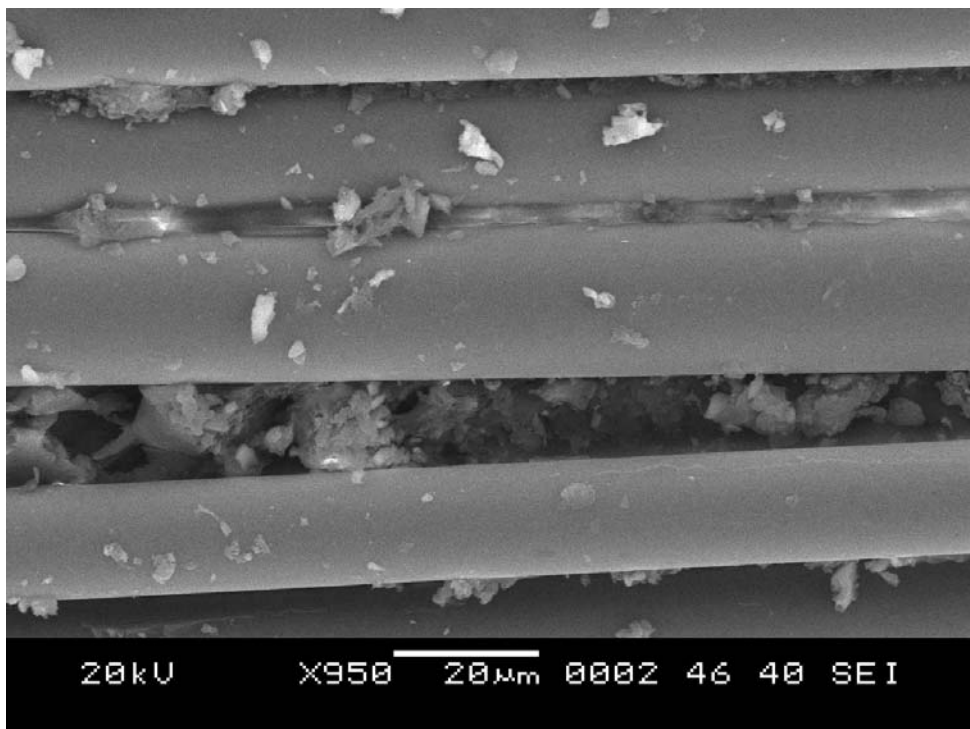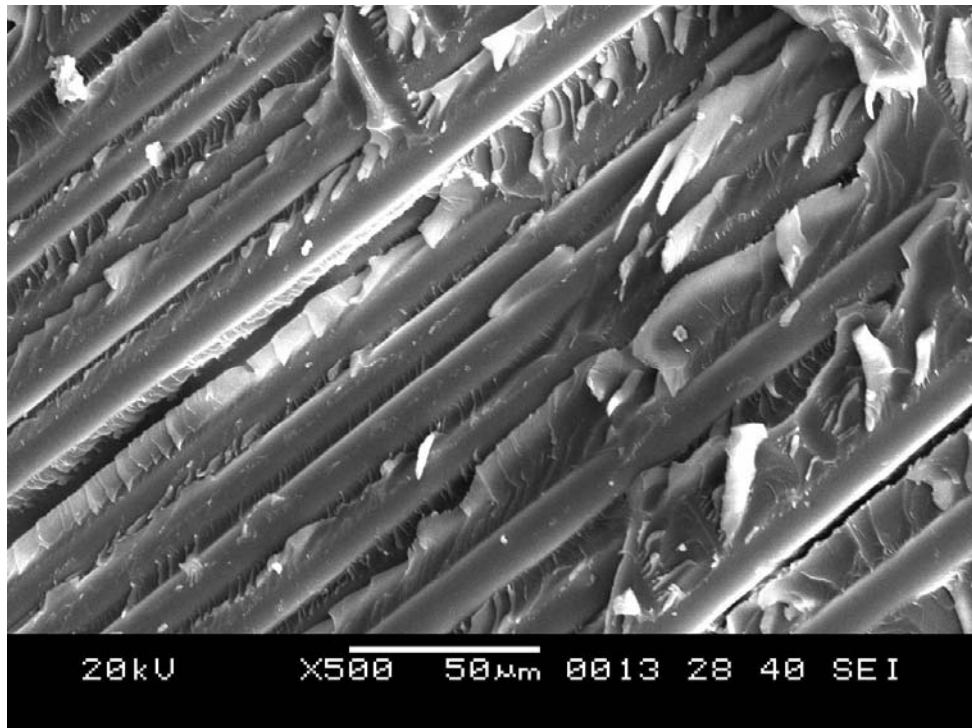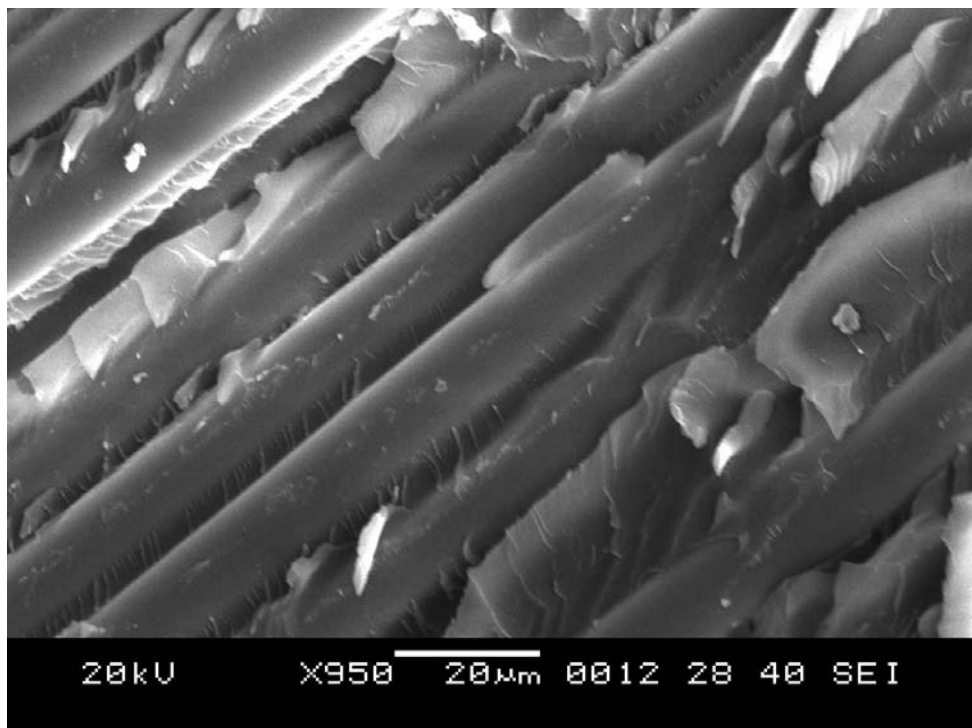
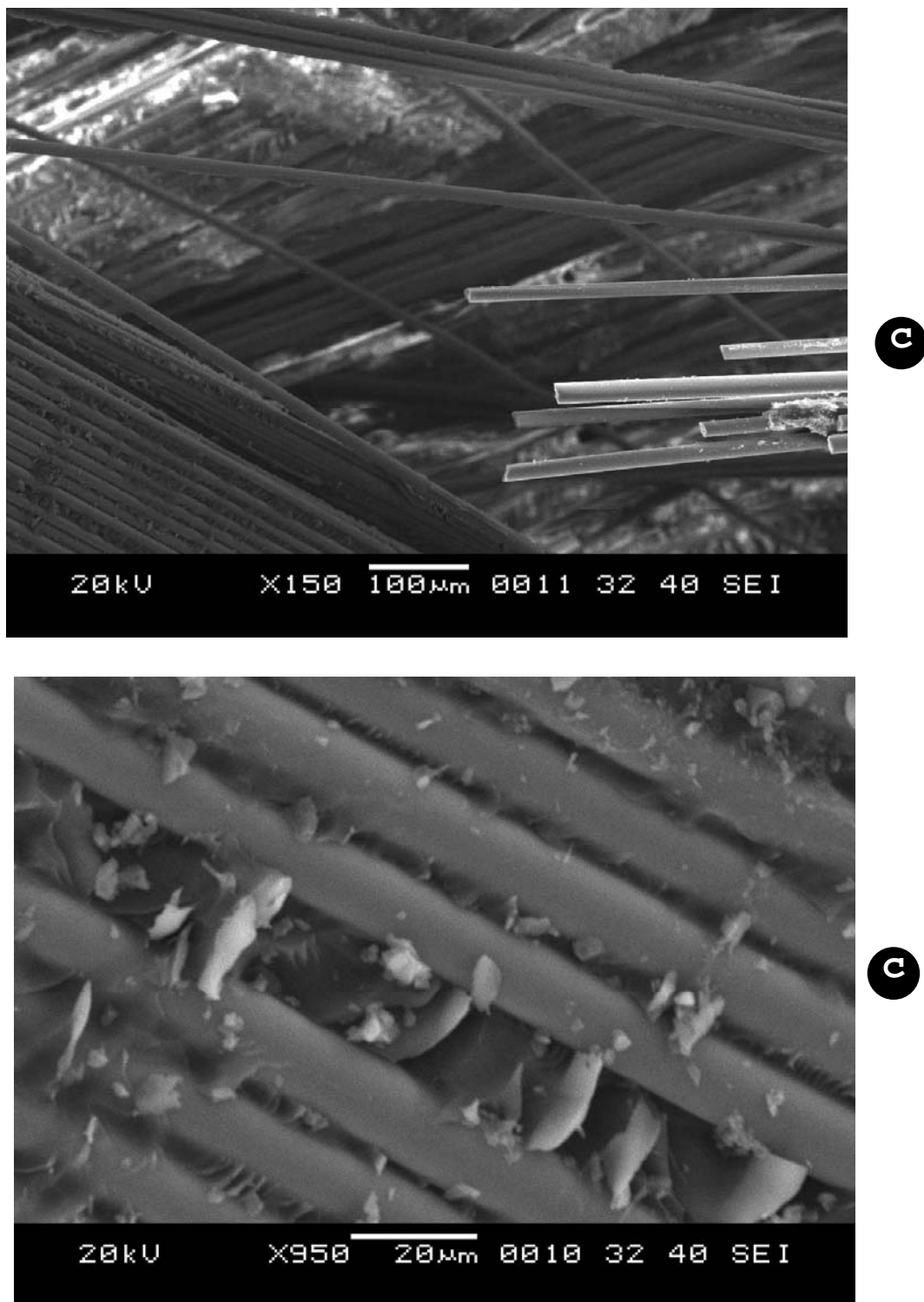Figure 4.9 to be continued

Figure 4.9 to be continued

Figure 4.9 Representative SEM images of the breakage region for (a) unidirectional glass fabric laminate; (b) biaxial glass fabric laminate and (c) triaxial glass fabric laminate that were tensile tested in machine direction (at different magnification levels).

4.2.3 Study of the Interfaces in Polyester Matrix Composites

Figure 4.10 displays the FTIR spectra of cured polyester, carbon fiber/polyester and glass fiber/polyester composites. The frequencies and assignments of FTIR absorption bands were given in Table 4.3. The band at 3448 cm^{-1} is related to stretching vibrations of O-H groups. As can be seen from the spectra of carbon/polyester and glass/polyester, the stretching vibrations of OH group was shifted to 3444 and 3445 cm^{-1} for glass/polyester and carbon/polyester composites, respectively. From this point of view, it is probable that hydrogen bond may occur between polyester and fiber samples. The bands in the range 2900-3100 cm^{-1} correspond to stretching vibrations of C-H groups such as CH_2 and CH_3. It is noticed that the stretching vibrations of C-H groups have approximately the same absorption bands after curing the polyester with glass and carbon fibers.

In the spectrum of cured polyester, a very intensive band was observed at 1728 cm^{-1} due to stretching vibrations of C=O group. Small changes occur leading to the shifts of wavenumber toward higher frequencies in the spectra of glass/polyester and carbon/polyester composites. Weak bands at 1599, 1580 and 1493 cm^{-1} observed in the spectrum of cured polyester can be assigned to aromatic ring. It can be said that these bands attributed to aromatic ring do not change their positions. No interaction occurs between aromatic ring and both fibers. The bands located at 1453 cm^{-1} and 1380 cm^{-1} may correspond to asymmetric and symmetric deformation band of methyl groups, respectively. It is seen from the spectrum of carbon/polyester composite that these bands appear simultaneously. According to Su, Jing, & Liu (2002), the symmetric deformation vibration of methyl groups is composed of two components, which could be assigned to the hydrated state around 1378 cm^{-1} and the other is assigned to the dehydrated state at 1373 cm^{-1}. In the current study the symmetric C-H stretching of methyl groups located at 1380 cm^{-1} could be assigned to the hydrated state. It can be concluded that ethyl groups are surrounded by water. It is probable that the microenvironment around the hydrated methyl group is polar.

Table 4.3 Assignment of the main infrared absorption of the 100%-cured neat polyester resin used in this study

Band (cm^{-1})	Assignment
3448	O-H stretch
3060	
3026	Aliphatic C-H stretch
2982	
1728	C=O stretch
1599	
1580	Aromatic ring stretch
1493	
1453	CH$_3$ asymmetrical bend
1380	CH$_3$ symmetrical bend
1284	CH$_2$ twist
1121	
1065	C-O stretch
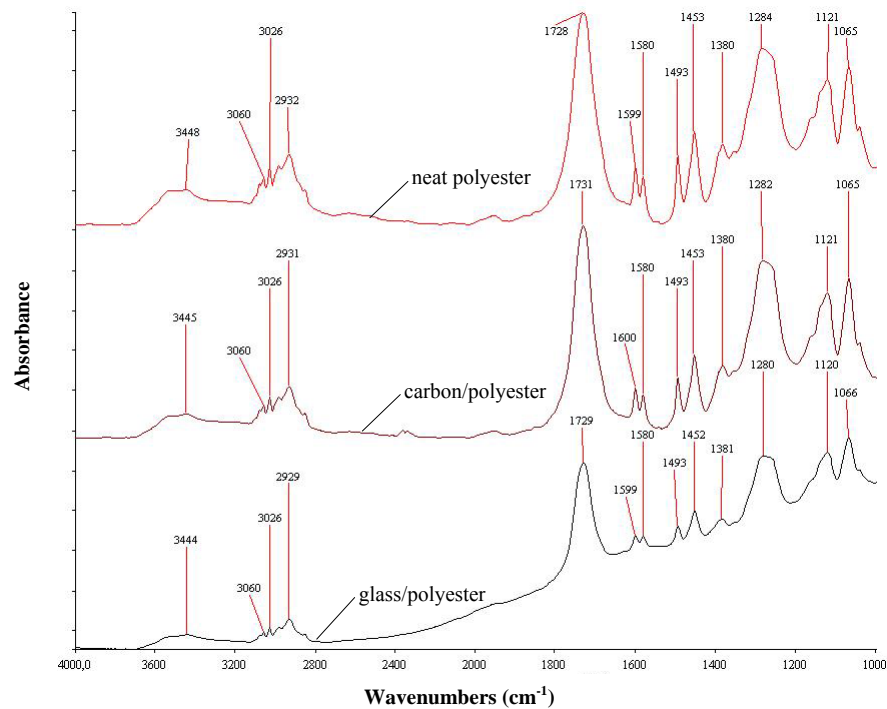
Figure 4.10 FTIR spectra of the neat polyester resin and its glass and carbon fiber composites.

The strong band at 1284 cm^{-1} which appears in the spectrum of polyester is due to twisting vibration of CH$_2$ groups. After the polyester resin is transferred into the fabrics and cured, the band shifted to lower frequencies. The band locations are different in the spectra of glass fiber/polyester and carbon fiber/polyester composite with a value of 1280 and 1282 cm^{-1}, respectively. It can be claimed that C-O weak interactions may occur between CH$_2$ groups and glass fibers. Two intensive bands at 1121 and 1065 cm^{-1} attributed to C-O stretching vibrations do not change their positions in the spectrum of carbon/polyester.

4.3 Epoxy Composites Reinforced with Non-Crimp Glass and Carbon Fabrics

4.3.1 Experimental Results and Discussions on the Mechanical Properties

The mechanical properties of the epoxy laminates in different directions are shown in Table 4.4. To compare the mechanical properties of vacuum infused glass fiber/epoxy and carbon fiber/epoxy composites, the test results were normalized to the average content of fiber in the tested samples (Table 4.5).

4.3.1.1 Tensile Properties

The remark, based on the observations while tensile testing, is that the stress-strain curves of epoxy composites reinforced with non-crimp stitched glass and carbon fabrics were linear in the direction of fibers. However, in the matrix dominated orientations non-linear relation between the stress and the strain was observed. The ultimate strength of laminates was lost in the matrix dominated orientations owing to the matrix controlled failure mode.

Even the thinner carbon laminates have better tensile performance than the thicker and considerably heavier glass laminates under loading conditions where the strength is mainly fiber dominated (Table 4.5). If it is assumed that the maximum failure strain of epoxy matrices is approximately 0.3 percent then the composite will fail at that strain. Also, if it is assumed, for simplicity, that the matrix carries no load, the strength of an epoxy matrix reinforced with 30 volume percent of 390 GPa high modulus carbon fibers, as calculated by means of Figure 4.11(b), would be about 363 MPa. Conversely, the strength of the same matrix reinforced with 30 volume percent of 74 GPa low modulus glass fibers, as calculated by means of Figure 4.11(a), would be about 98 MPa. Since higher modulus fibers are usually weaker, the curious result discussed by Fitzer, & Hüttner (1981) to note at this stage is that for composites that fail at the matrix failure strain, the strengths can be larger when stiffer; usually weaker fibers are used as the reinforcement.

Table 4.4 Mechanical properties of glass and carbon fiber/epoxy composites in different directions (the data quoted are all average results taken from a minimum of six tests).

Composite	Test direction	Tensile modulus (GPa)	Tensile strength (MPa)	Elongation at break (%)	Flexure modulus (GPa)	Flexure strength (MPa)	ILSS (MPa)	V_f (%)
Unidirectional glass fabric	Machine	24.170±3.87	399.96±13.6	1.6642±0.038	19.406±0.36	449.75±13.8	26.068±0.79	
	Bias	3.7057±0.04	51.121±2.34	7.7537±0.19	4.6779±0.08	98.675±6.96	8.1325±0.12	33.7±1.3
	Cross	7.2940±0.16	56.636±2.93	0.7655±0.021	5.0025±0.10	92.575±6.88	10.003±0.14	
Unidirectional carbon fabric	Machine	85.706±8.62	488.53±14.1	0.6293±0.026	25.822±0.72	310.63±12.54	33.765±0.26	
	Bias	7.8488±0.15	21.852±0.52	0.3151±0.014	2.8612±0.027	42.049±1.65	4.3646±0.05	24.8±0.6
	Cross	5.5478±0.10	12.527±0.163	0.2047±0.011	2.1810±0.023	28.251±0.96	6.3288±0.04	
Biaxial glass fabric	Machine	0.8817±0.008	53.755±1.36	16.615±0.17	3.7843±0.05	123.79±8.07	6.1519±0.11	
	Bias	11.524±0.153	175.42±11.02	2.6710±0.02	11.445±0.15	306.95±12.46	19.702±0.39	36.2±1.3
	Cross	1.2110±0.018	42.593±3.27	14.846±0.62	6.6606±0.14	134.31±8.39	10.918±0.14	
Biaxial carbon fabric	Machine	4.9972±0.07	75.019±4.39	12.171±0.163	3.4960±0.40	102.47±7.02	8.6345±0.13	
	Bias	130.76±8.16	467.35±13.88	0.3832±0.014	20.937±0.50	209.88±11.57	18.851±0.30	41.5±1.6
	Cross	5.7299±0.09	86.200±6.59	12.422±0.16	5.2590±0.11	112.34±7.36	9.1213±0.13	
0/90 glass fabric	Machine	12.856±0.158	193.27±11.34	1.4924±0.014	8.8862±0.13	199.95±11.31	12.572±0.16	
	Bias	4.1259±0.05	51.857±2.53	8.0834±0.12	2.3488±0.03	56.385±2.87	6.0403±0.10	32.6±1.2
	Cross	12.697±0.164	203.95±11.43	1.7791±0.015	8.8878±0.13	189.89±11.26	8.6141±0.128	
0/90 carbon fabric	Machine	65.161±3.37	362.98±13.06	0.5427±0.017	16.936±0.20	305.01±12.4	10.777±0.143	
	Bias	3.9698±0.08	45.102±1.95	16.989±0.21	3.7424±0.06	72.873±4.28	6.2971±0.15	25.6±0.7
	Cross	64.968±3.34	356.43±12.9	0.6333±0.013	19.149±0.31	305.01±12.41	14.255±0.18	
Woven roving glass fabric	Machine	15.072±0.18	257.91±11.89	1.5340±0.013	11.896±0.15	358.89±12.92	18.621±0.28	
	Bias	7.6719±0.15	66.245±3.42	7.5460±0.16	5.2539±0.10	172.91±10.96	16.372±0.18	39.2±1.5
	Cross	14.641±0.17	275.55±12.03	1.8270±0.018	12.862±0.161	394.01±13.48	22.933±0.64	
Woven roving carbon fabric	Machine	43.489±1.72	332.07±12.84	0.7385±0.013	27.557±0.83	440.86±13.82	32.379±1.36	
	Bias	14.559±0.17	89.755±6.72	4.3937±0.08	8.6024±0.128	233.08±10.6	20.804±0.47	38.4±1.4
	Cross	41.575±1.41	375.87±13.26	0.8908±0.012	29.824±1.04	478.83±13.97	30.695±1.18	

* The values after the (±) in all the tables refer the standard uncertainty of the measurement.

Table 4.5 Normalized mechanical properties of glass and carbon fiber/epoxy composites in different directions.

Composite	Test direction	Normalized tensile modulus (GPa)	Normalized tensile strength (MPa)	Normalized flexure modulus (GPa)	Normalized flexure strength (MPa)	Average fiber content V_f (%)
Unidirectional glass fabric	Machine	21.516	356.41	17.292	400.78	
	Bias	3.3022	45.554	4.1685	87.929	30
	Cross	6.4930	50.468	4.4578	82.494	
Unidirectional carbon fabric	Machine	103.68	591.23	31.250	375.93	
	Bias	9.4990	26.446	3.4627	50.890	30
	Cross	6.7142	15.161	2.6396	34.190	
Biaxial glass fabric	Machine	0.9492	57.913	4.0744	133.28	
	Bias	12.407	188.87	12.323	330.49	39
	Cross	1.3038	45.887	7.1712	144.60	
Biaxial carbon fabric	Machine	4.6929	70.451	3.2830	96.229	
	Bias	122.79	438.89	19.662	197.09	39
	Cross	5.3809	80.950	4.9387	105.49	
0/90 glass fabric	Machine	11.453	172.18	7.9166	178.14	
	Bias	3.6757	46.199	2.0926	50.233	29
	Cross	11.312	181.69	7.9180	169.17	
0/90 carbon fabric	Machine	73.723	410.67	19.161	345.09	
	Bias	4.4915	51.028	4.2340	82.448	29
	Cross	73.504	403.26	21.665	345.08	
Woven roving glass fabric	Machine	15.009	256.82	11.845	357.38	
	Bias	7.6397	65.967	5.2318	172.18	39
	Cross	14.579	274.39	12.808	392.36	
Woven roving carbon fabric	Machine	44.155	337.16	27.979	447.61	
	Bias	14.783	91.130	8.7341	236.65	39
	Cross	42.212	381.63	30.280	486.16	

In the case of tension transverse to the fibers (Figure 4.12), failure initiates by cracking in matrix or along the fiber/matrix interface. The failure of a carbon/epoxy composite whose failure is matrix-dominated can occur at lower strains. It is possible to relate this striking result to the fact that when differences in thermal expansion between the carbon fiber and epoxy matrix cause the epoxy matrix to be prestressed in tension on cooling from the cure temperature of 80 °C reached in a hot press during composite production. Since the epoxy matrix and carbon fiber must be bonded together in order to prestress the matrix, very low strengths might be expected from well-bonded materials (Table 4.5). It is reasonable to conclude from the discussed data that the modulus of carbon fiber is very large in the direction of the fibers, but very small in the direction perpendicular to the fiber axis; thus, any contribution to the modulus of the composite will depend on the alignment of the fiber direction. In other words, the transverse tensile modulus is normally insensitive to the fiber/matrix adhesion if good interfacial bonding is achieved.

In the case of biaxial glass fabric laminates, improvements in tensile strength in MD case as compared to that in CD case (Table 4.5 and Figure 4.13) is believed to be due to the fact that the stitch rows run nearly parallel to machine directions as a consequence of the lay up of biaxial glass non-crimp fabric (NCF) blankets with [+45/-45] orientations. For the biaxial carbon fabric laminate, the tensile strength in CD is larger than in MD (Table 4.5). The observed difference may be attributed to the difference in influence of stitching and friction between plies. By examining actual photographs of fractured tensile specimens resulting from a variety of uniaxial loading conditions it is clear that the fracture surface of the composite having plies ±45° with fibers exhibit both longitudinal type and transverse type fracture characteristics (Figure 4.14).

Tensile tests conducted in the machine and bias direction resulted in significant delamination of the bidirectional (0/90°) specimen (Figure 4.16). It is well known from a phenomenological manner that, the 90° layer with its fiber axis perpendicular to an applied load direction suffers transverse cracks at the lower load levels.
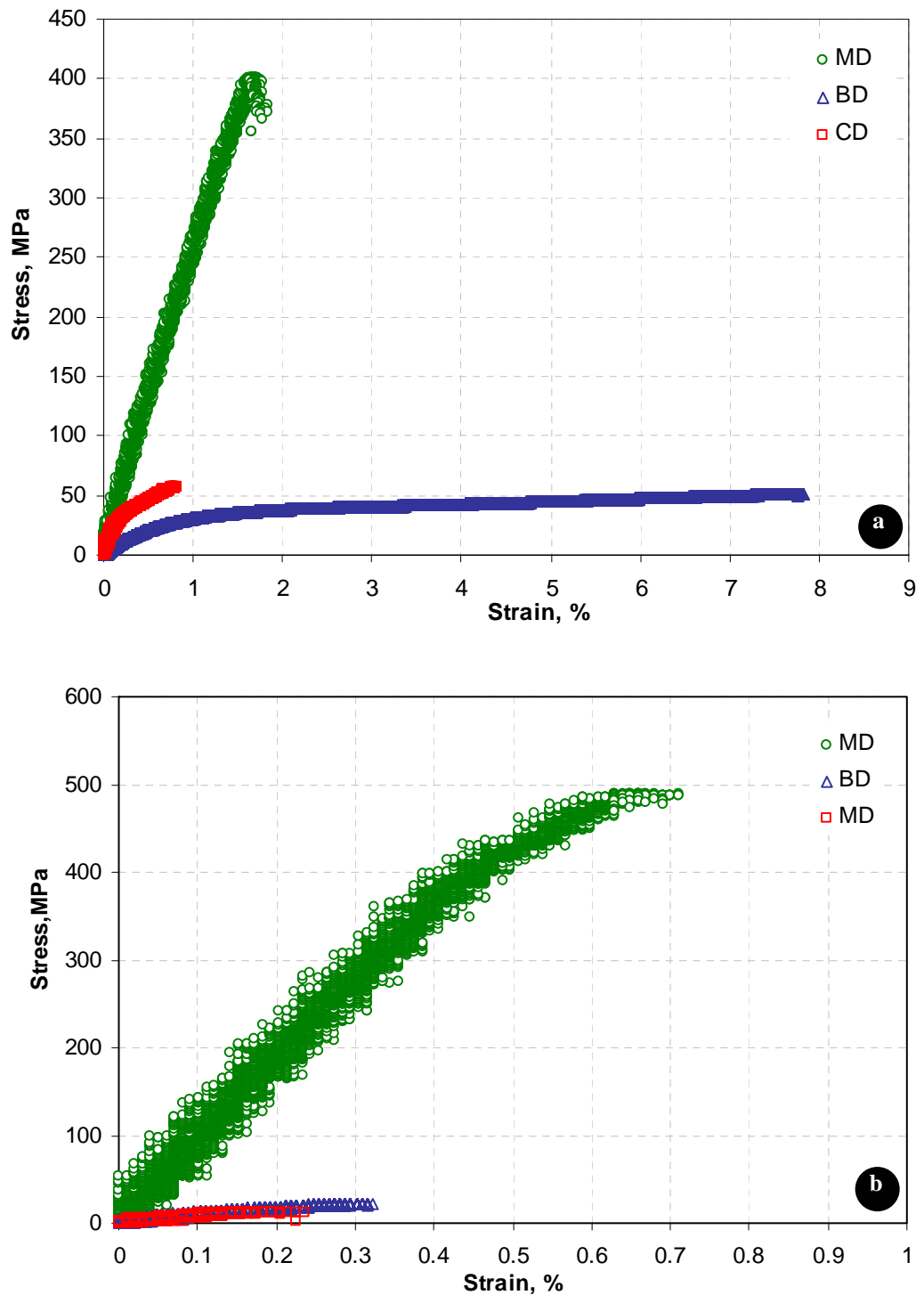
Figure 4.11 Tensile stress–strain curves of laminates in different directions: (a) unidirectional glass fabric laminate (V_f = 33.7 %); (b) unidirectional carbon fabric laminate (V_f = 24.8 %).

UD glass and carbon fabric laminate in MD	UD glass and carbon fabric laminate in BD	UD glass and carbon fabric laminate in CD

Figure 4.12 Photographs showing side and front views of representative failures loaded in tension along the MD, BD; and CD, for laminates produced from unidirectional glass and carbon fabric.

Figure 4.13 Tensile stress–strain curves of laminates in different directions: (a) biaxial +45/-45° glass fabric laminate (V_f = 36.2 %); (b) biaxial +45/-45° carbon fabric laminate (V_f = 41.5 %).

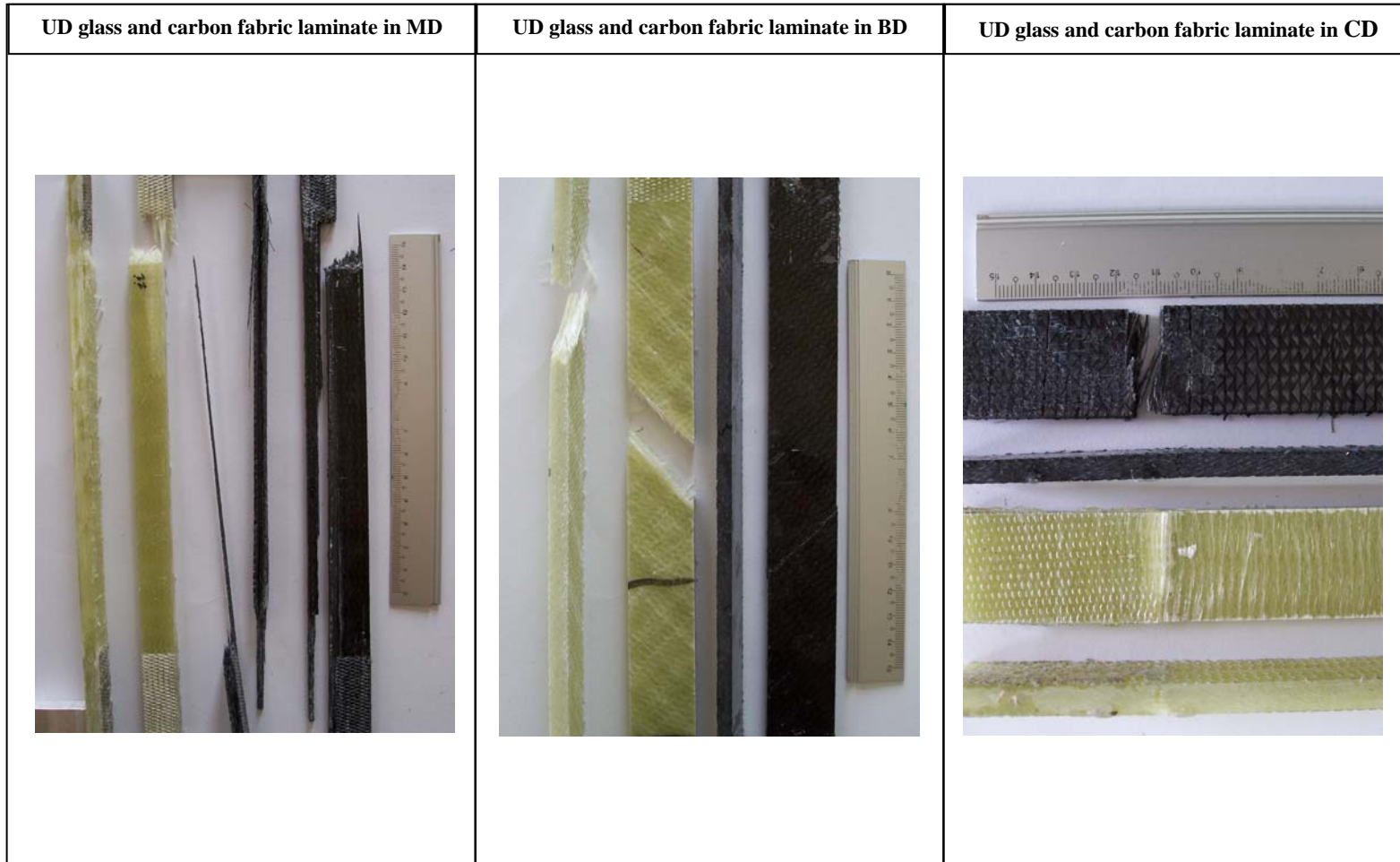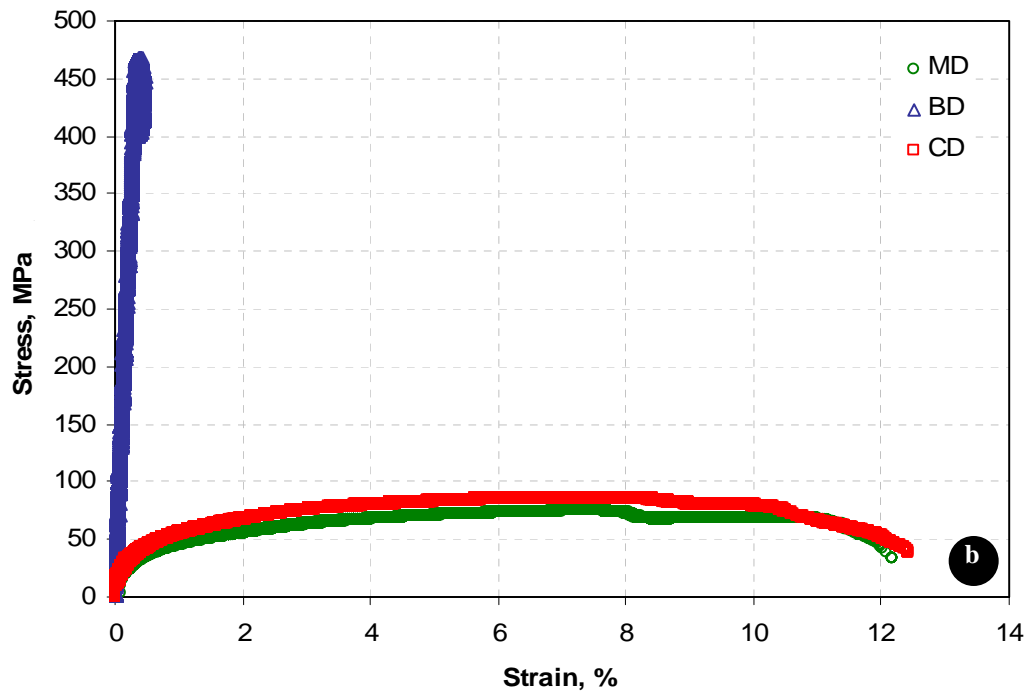| BA glass and carbon fabric laminate in MD	BA glass and carbon fabric laminate in BD	BA glass and carbon fabric laminate in CD

Figure 4.14 Photographs showing side and front views of representative failures loaded in tension along the MD, BD, and CD, for laminates produced from biaxial glass and carbon fabric.
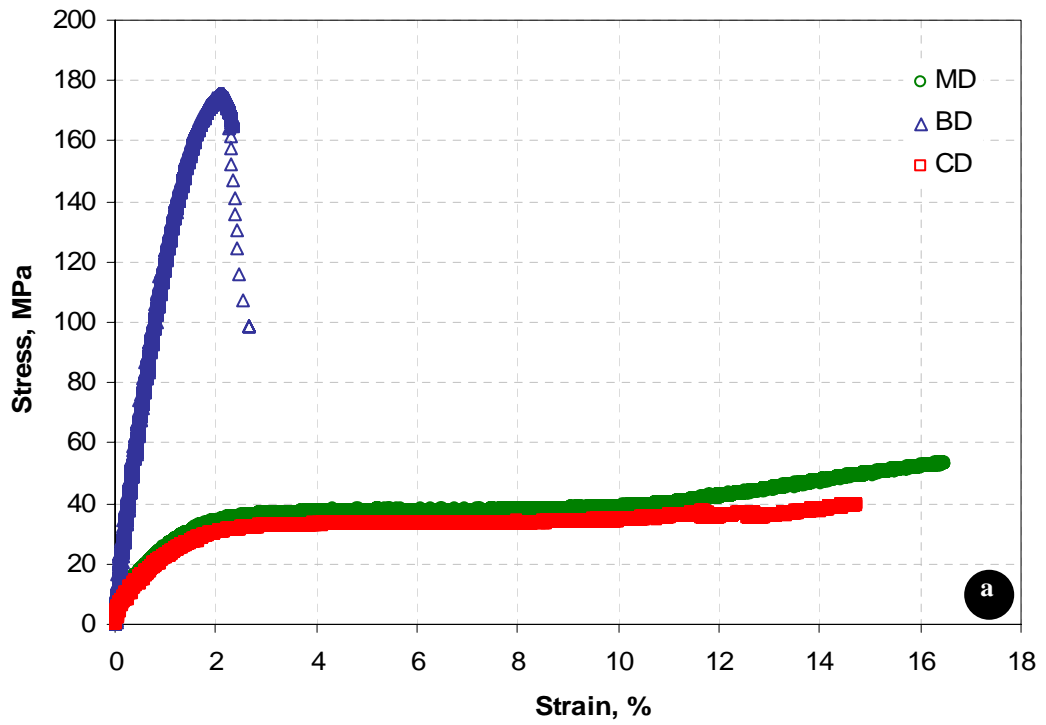
Figure 4.15 Tensile stress–strain curves of cross-ply laminates produced from: (a) unidirectional glass fabric (V_f= 32.6 %); (b) unidirectional carbon fabric (V_f= 25.6 %).

0/90 glass and carbon fabric laminate in MD	0/90 glass and carbon fabric laminate in BD	0/90 glass and carbon fabric laminate in CD

Figure 4.16 Photographs showing side and front views of representative failures loaded in tension along the MD, BD, and CD, for cross-ply laminates produced from unidirectional glass and carbon fabric.
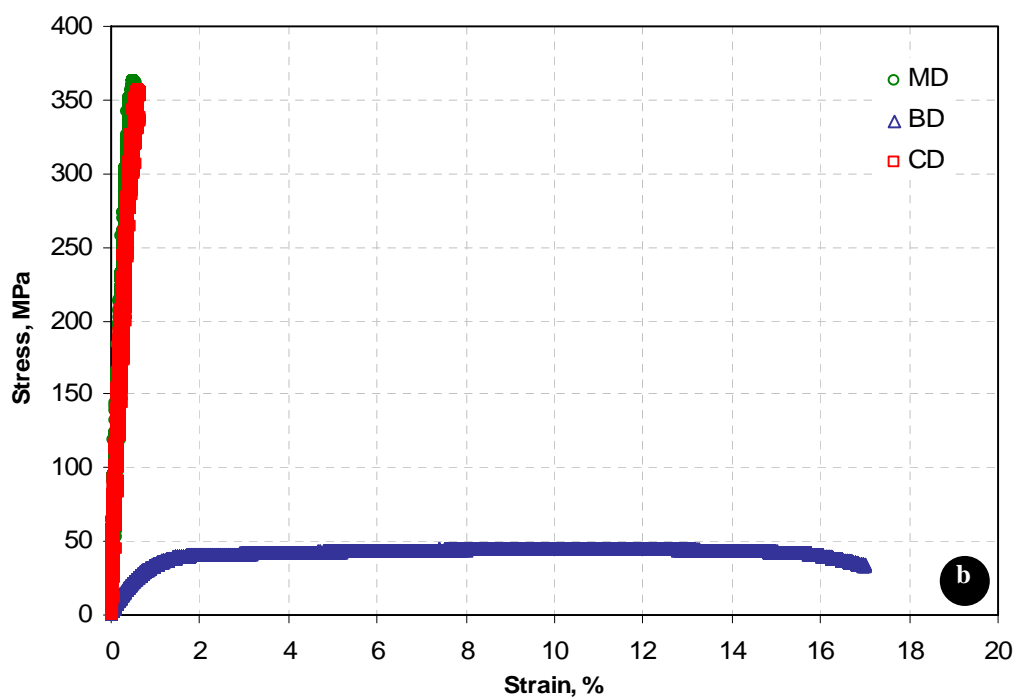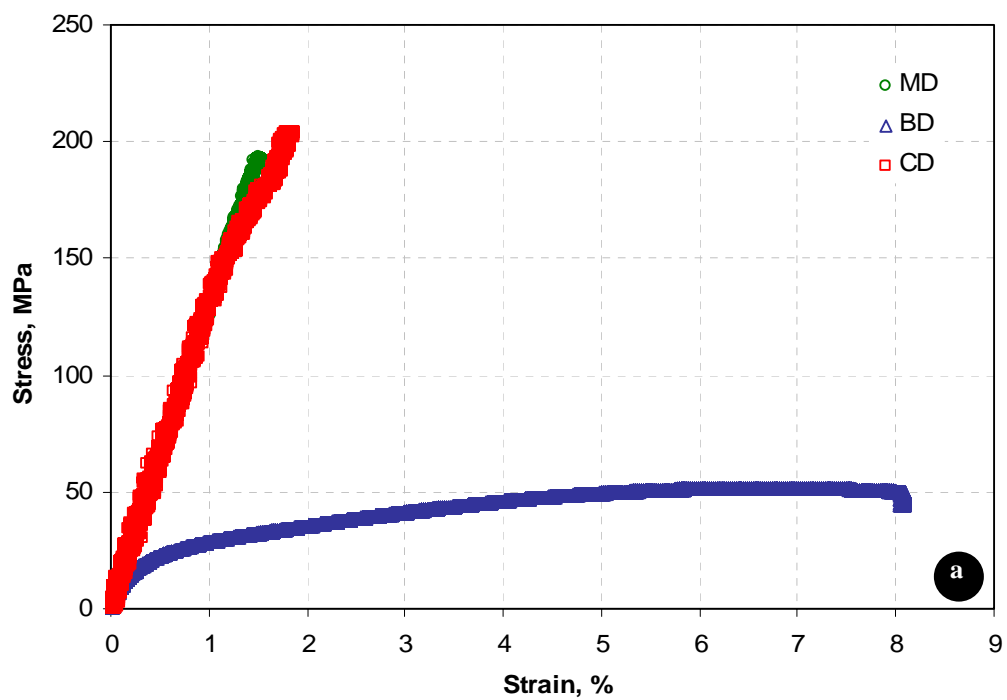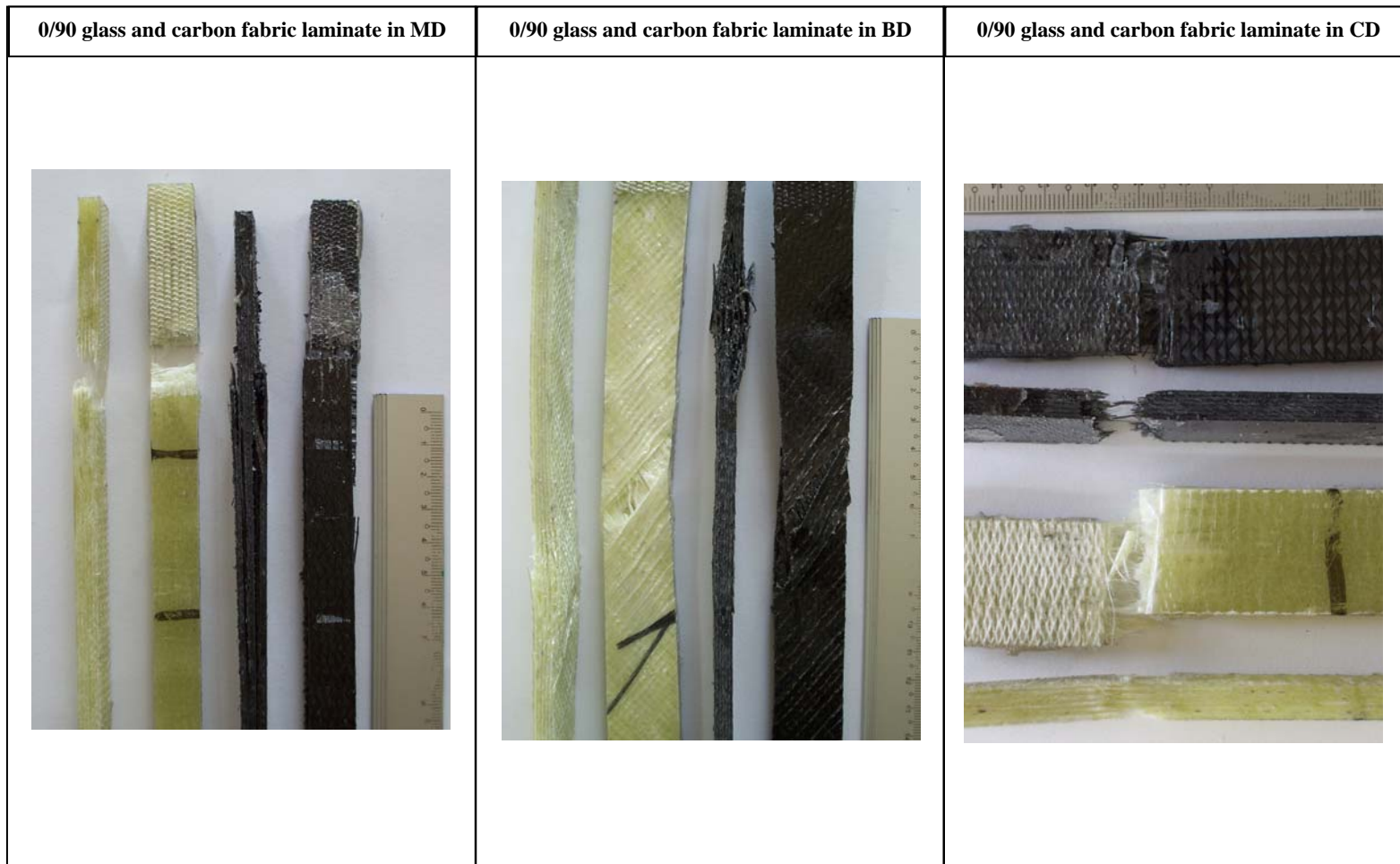
As each transverse crack is formed and arrested at the 0°/90° interfaces, the crack impinges upon the outer 0° layers and causes a pair of local stress concentration zones. Consequently, a series of localized delaminations may eventually separate the 0°/90° interface totally, causing fiber breakage in the 0° plies. One of the most notable features of the cross ply laminates, [0/90], is the first ply failure point where the nonlinearity starts in the stress-strain curve for BD case. The cracks or damage which causes a reduction in the stiffness of the cross-ply laminate results in local stress concentration. It is believed that this stress concentration may lead to immediate fracture in neighboring plies or laminates (Figure 4.16).

The anisotropy may be a consequence of the orthogonal arrangement of the fibers in the woven plain weave fabrics that are made by interlacing two yarn systems at a 90° angle. From the stress–strain curves shown in Figure 4.17, it is seen that the strength of woven fabric composite was greater in the two orthogonal directions (in this particular instance, MD and CD) in which each warp and weft yarn lay than in any other direction. A somewhat surprising feature is that the strengths and stiffness in MD and CD are not equal to each other (Table 4.5). In other words, the experimental data do not allow for an adequate description of the orthogonal model. The reason maybe attributed to the fact that the nominal warp and weft directions of the fibers were not controlled during the laminate fabrication by VARTM process.

The experimental results show that the delamination does not occur at the mid-plane, except for the carbon/epoxy laminates in the machine direction, in the case of MD and CD, as shown in Figure 4.18, whereas extensive delamination occurred in the glass/epoxy specimen subjected to tension in BD. The large increase in elongation-at-break of woven fabric composites tested in BD suggested that the effect of knee in the stress-strain curve on break strain may be much more significant in matrix controlled failure mode (in the case of BD) than in fiber-controlled failure modes (in MD and CD cases) (Figure 4.17). Figure 4.17 clearly indicates that once the knee point is passed the composite may be capable of significant further extension, although it is permanently damaged.

Table 4.6 Normalized tensile strength of woven carbon fabric and cross-ply laminates in different directions.

Composite	Test direction	Tensile modulus (GPa)	Tensile strength (MPa)	Average fiber content V_f (%)
0/90 carbon fabric	Machine	81.451	453.73	
	Bias	4.9623	56.378	32
	Cross	81.210	445.54	
Woven roving carbon fabric	Machine	36.241	276.73	
	Bias	12.133	74.796	32
	Cross	34.646	313.23	
0/90 glass fabric	Machine	14.197	213.43	
	Bias	4.5560	57.265	36
	Cross	14.021	225.22	
Woven roving glass fabric	Machine	13.842	236.86	
	Bias	7.0460	60.837	36
	Cross	13.446	253.06	

If the test results are normalized to the average fiber volume fraction (Table 4.6) it is apparent that the tensile strength and modulus of composite plates made from woven carbon fabric is lower than those of its equivalent cross-ply laminate. This decrease in tensile strength and modulus of woven carbon fabric reinforcement laminate may be attributed to the presence of fiber undulation in woven fabrics where the fiber yarns in one direction crisscross the yarn in the other direction. In the course of tensile loading, these crimped fibers straighten out more and more, creating high stresses in the matrix and thus microcracks are formed in the matrix at relatively low loads. On the other hand, the tensile strengths of a plain woven glass fabric reinforcement laminate are higher than those of its equivalent cross-ply laminate made from unidirectional glass fabric. It is possible to relate this result to the fact that the stresses necessary for matrix microcracking is higher in composites made with woven roving glass fabric compared to its equivalent cross-ply laminate. The mentioned difference in the stresses may be attributed to the weaker interaction between woven glass fabric and epoxy resin. It is believed that this weaker interaction may not be able to create high enough stresses in the matrix necessary for matrix microcracking.
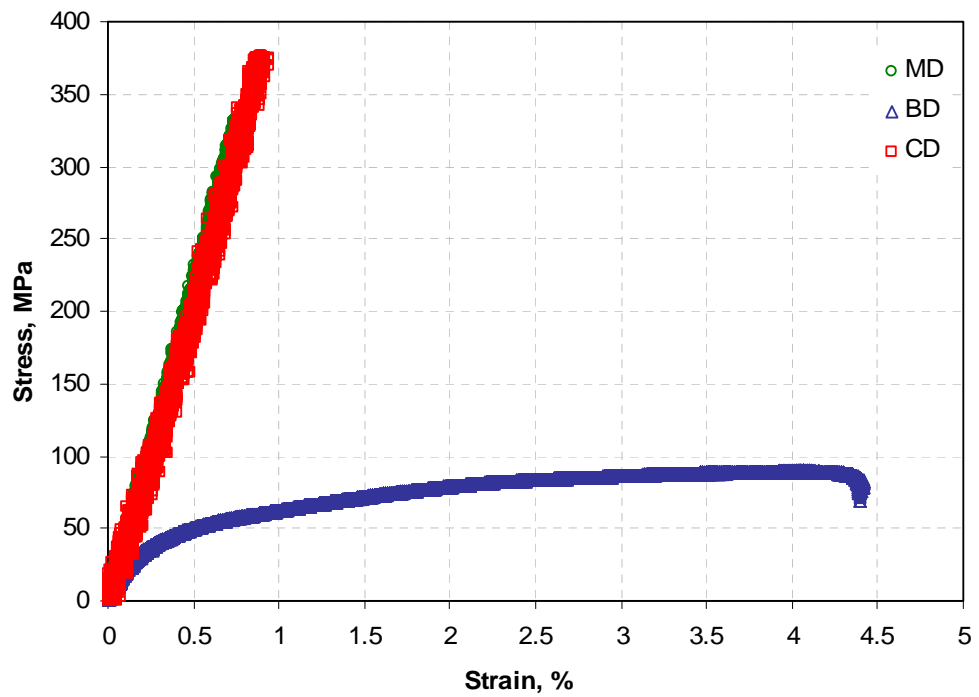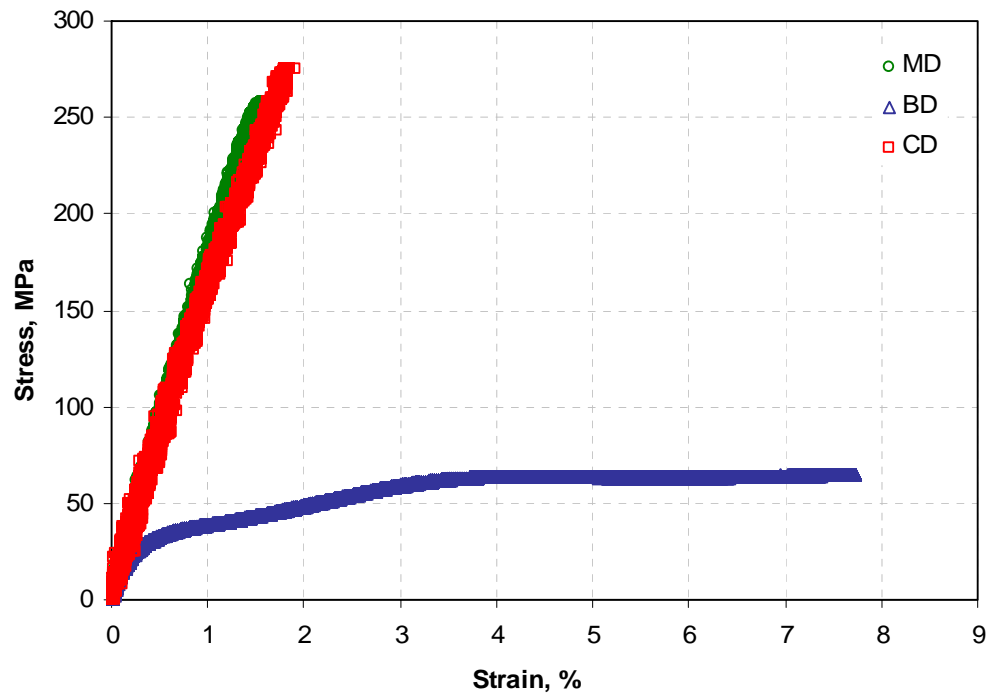
Figure 4.17 Tensile stress–strain curves of laminates in different directions: (a) woven roving glass fabric laminate (V_f = 39.2 %); (b) woven roving carbon fabric laminate (V_f = 38.4 %).

Woven roving glass and carbon fabric laminate in MD	Woven roving glass and carbon fabric laminate in BD	Woven roving glass and carbon fabric laminate in CD

Figure 4.18 Photographs showing side and front views of representative failures loaded in tension along the MD, BD; and CD, for laminates produced from woven roving glass and carbon fabric.

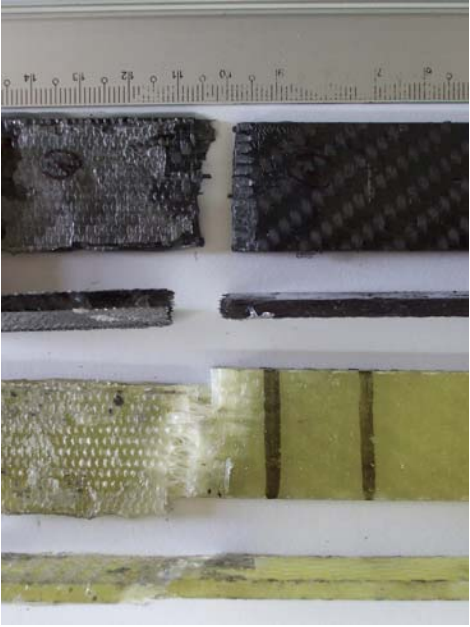Comparison of experimental data on tensile modulus with prediction of classical laminate theory (CLT) is presented in Table 4.7. A rule of mixture calculation based on the fraction and properties of the constituents was used. The constituent property data for composite laminate were obtained from data sheet provided by the manufacturer (Table 3.3). It is seen that experimentally determined modulus data in fiber direction are up to 26% lower than the theoretically expected modulus values. It is well known that tensile modulus measured parallel to the direction of the fibers depend mostly on the properties of the fiber. In this direction the composites are highly sensitive to variations in the direction of the reinforcement and the effect of the matrix is less pronounced.

Table 4.7 Comparison of experimental results and CLT computed results on tensile stiffness of unidirectional laminates

Material	V_f (%)	Test direction	Tensile modulus (GPa)		
			Computed	Experiment	Difference (%)
UD glass fabric/polyester	48.4	Machine	37.867	37.827	+0.11
		Cross	5.9340	6.6610	-10.91
UD glass fabric/epoxy	33.7	Machine	27.325	24.170	+13.05
		Cross	5.2988	7.2940	-27.35
UD carbon fabric/polyester	23.1	Machine	89.804	71.345	+25.87
		Cross	3.5250	4.5440	-22.43
UD carbon fabric/epoxy	24.8	Machine	96.203	85.706	+12.25
		Cross	3.9964	5.5478	-27.96

Note: Difference = (computed data – experimental data)/(experimental data)×100.

On the other hand, when the results are examined, it is seen that the modulus data in the transverse direction to the fiber axis (CD case) are rather interesting. Based on the obtained data, a significant discrepancy was reported between theoretical and experimental values.

The potential explanation for the difference between the experimental and predicted values could be that laying up of the fabric in composite production are not truly aligned in the desirable direction since the nominal direction of the fibers was

not controlled during the laminate fabrication by VARTM process. Another point should be made here is that deviation from perfect alignment of fibers accumulates from precision in cutting the laminates for specimens with desired directions.

Table 4.8 Influence of matrix on composite properties

Material	Test direction	Normalized tensile strength (MPa)	Normalized ILSS (MPa)	Average fiber content V_f (%)
UD glass fabric/polyester	Machine	504.31	25.800	40
	Cross	60.874		
UD glass fabric/epoxy	Machine	474.73	30.941	40
	Cross	67.224		
UD carbon fabric/polyester	Machine	666.05	22.384	24
	Cross	10.285		
UD carbon fabric/epoxy	Machine	472.77	32.666	24
	Cross	12.123		

The higher dependence of the experimental tensile strength of composites on the type of the matrix can be easily inferred (Table 4.8). The results on the strength of unidirectional carbon fabric reinforced composites in fiber direction show that the strength value for polyester based laminates was about %40 higher than that of epoxy based ones. Further confirmation of the strength contribution of the polyester resin was provided by tensile tests in a unidirectionally reinforced sample of glass fabric. Polyester composite sample, containing unidirectional glass fabric, in fiber direction exhibited a loading capacity with a ultimate strength of 504 MPa, which is about 6% higher as compared with the 474.73 MPa loading capacity of the epoxy based ones.

The values of transverse tensile strength and interlaminar shear strength (Table 4.8) are reasonable in light of experimental work indicating that the above-mentioned properties of well-bonded epoxy based composites were superior to those exhibited by less well-bonded polyester based composites. Such findings are not very surprising. However, an interesting but surprising observation was recorded in the longitudinal strength values of the well-bonded epoxy based composites. For these epoxy based composites, considerably poor performance was shown in longitudinal strengths. Contrary to epoxy based composites, although the matrix-dominated properties were poor the longitudinal strength of polyester based composites was

much better. What has been observed, when Table 4.8 is once more examined within the light of these findings, is: the variation percent in interlaminar shear strength values, which are the criteria for the degree of adhesion of the layers, directly influences the variation percent of the tensile strength values along the fiber direction. For example, while a 46% decrease in interlaminar shear strength values of carbon fabric reinforced composites causes a 40% increase in tensile strength; a 20% decrease in glass fabric reinforced composites induces a 6% increase.

It may be concluded based on these findings that, perfect adhesion of a polymer through stable bonds to fiber reinforcement would result in poor mechanical performance of a practical composite in fiber direction if polymer and fiber had a wide mistmatch in coefficients of thermal expansion (thermal expansion coefficients of starting fiber and matrix materials were given in Table 3.7 and Table 3.8, respectively). A reasonable conclusion appears to be that, effectiveness of the bond between resin and fiber will not produce a high-strength composite when measured parallel to the direction of the fibers.

4.3.1.2 Flexural Properties

Similar comments can be said about the flexural strength/middle-span deflection responses in the test directions performed on the specimens as in the results on tensile stress/strain response (Figure 4.19-Figure 4.22). The lamina stacking sequence has a significant effect on the recorded values of the flexural strengths.

The failure of the glass/epoxy and carbon/epoxy flexural specimens in the direction of fibers also undergoes a process of cumulative damage progression. The linear relationship between the flexural strength and middle-span deflection is maintained until the peak stress is reached, followed by a sudden drop in the flexural strength, as shown in Figure 4.19. However, for the matrix dominated orientations, before attaining the maximum value, the flexural strength/middle-span deflection relation becomes non-linear, and then the flexural strength decreases gradually to the low value.

The failure of epoxy composites reinforced with non-crimp stitched fabrics generally results from the failure of its matrix material As the compressive strength of the epoxy matrix used is higher than its tensile counterpart, the failure of the non-crimp stitched fabric laminated beams under the three-point bending must be initiated from the bottom surface. Matrix crazing has also been found to occur on the top surface of the specimens after the bending test, although no fabric fracture was observed. This means that the matrix material in the top surface also failed after the test, being caused by an excessive compressive stress. No apparent laminate delamination was found in any of the beams tested during this study.

In the case of unidirectional and biaxial laminates, the experimental results from flexure tests suggest that the glass fabric laminate would outperform the carbon fabric laminate (Table 4.5). The compressive strength for this type of material is approximately 50-60% of that in tension. In a flexural test this means that the strength is governed by the compressive strength and not the tensile. If we recognize the fact that the compressive strength of the glass fiber used is higher than that of the carbon fiber, we can easily understand this experimental finding mentioned above.

In the case of 0/90° laminates, the flexural strength of carbon fabric laminates is greater than that of glass fabric laminates at all the considered test directions (Table 4.5). The important drawback of the experiment is non-symmetry of the layout of the samples, which makes the results difficult to interpret. Notwithstanding this, the first possible explanation for the higher flexural strength of carbon fabric laminate could arise from the fact that any change in the lamina stacking sequence affects the effectiveness of the tensile strength with respect to the compressive strength. Another possible explanation for this result may lie in the difficulties associated with achieving good wetting out of the glass fabric laminates at the higher volume fractions.

It can be observed from Table 4.5 that specimens, made from woven-roving glass and carbon fiber-reinforced epoxy, in CD case exhibited the highest loading capacity with a ultimate strength of 392.4 and 486.2 MPa, which is about 9.8% and 8.6% higher as compared with the 357.4 and 447.6 MPa loading capacity of the glass/epoxy and carbon/epoxy specimens, respectively, in MD case. Similar comments can be said about the discrepancies between the flexural strength/middle-span deflection responses in machine and cross directions as in the results on tensile properties of the woven fabric composite laminates in the same directions.
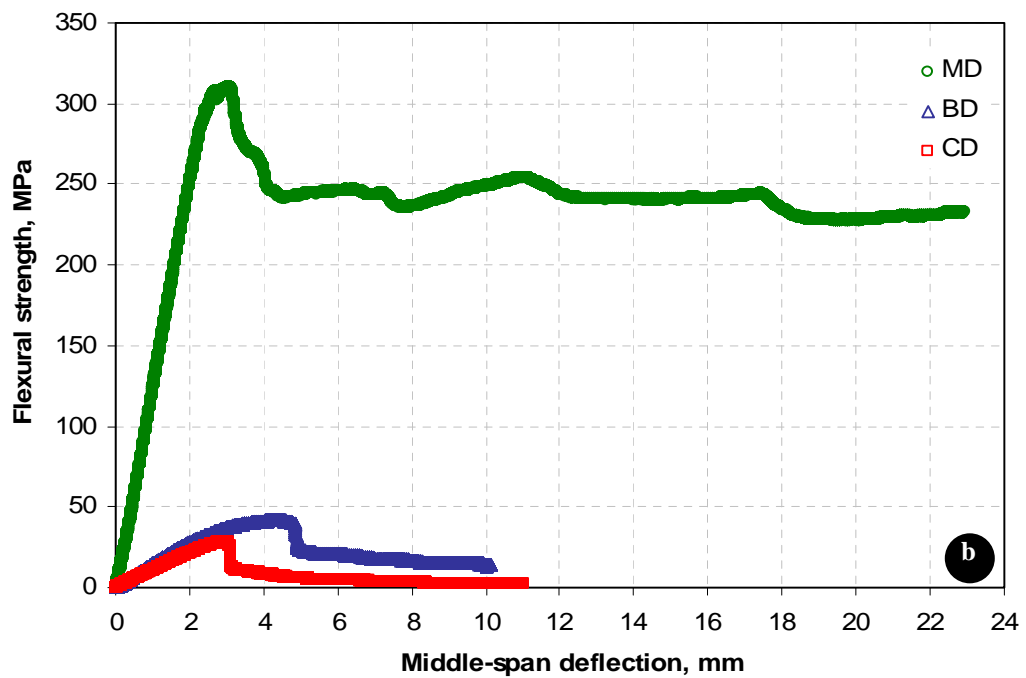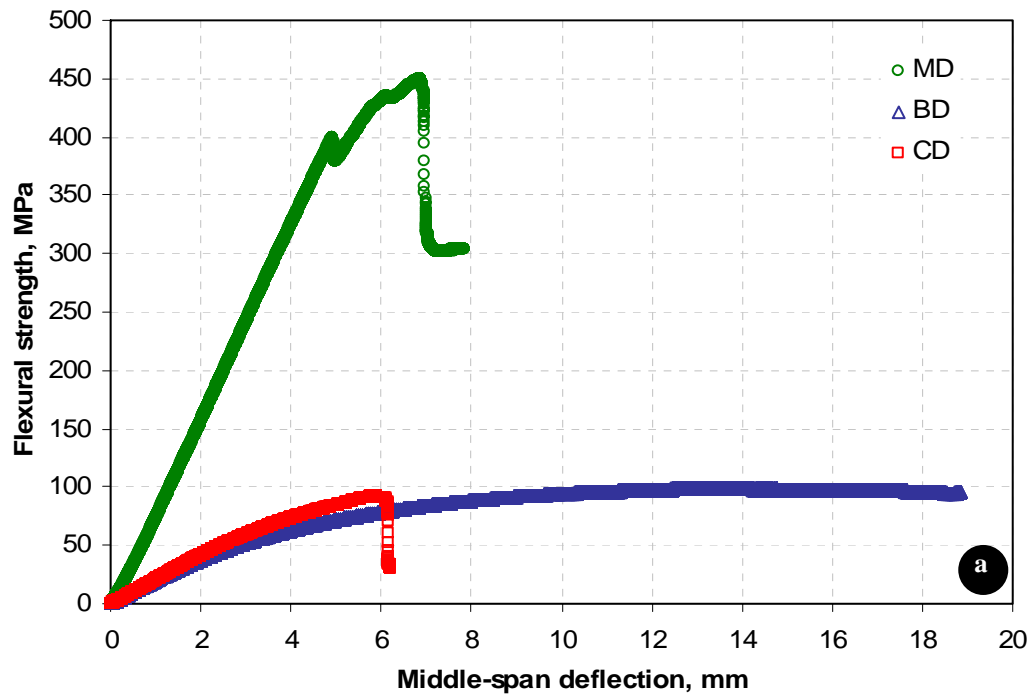
Figure 4.19 Flexural strength-deflection curves of laminates in different directions: (a) unidirectional glass fabric laminate (V_f = 33.7 %); (b) unidirectional carbon fabric laminate (V_f= 24.8 %).
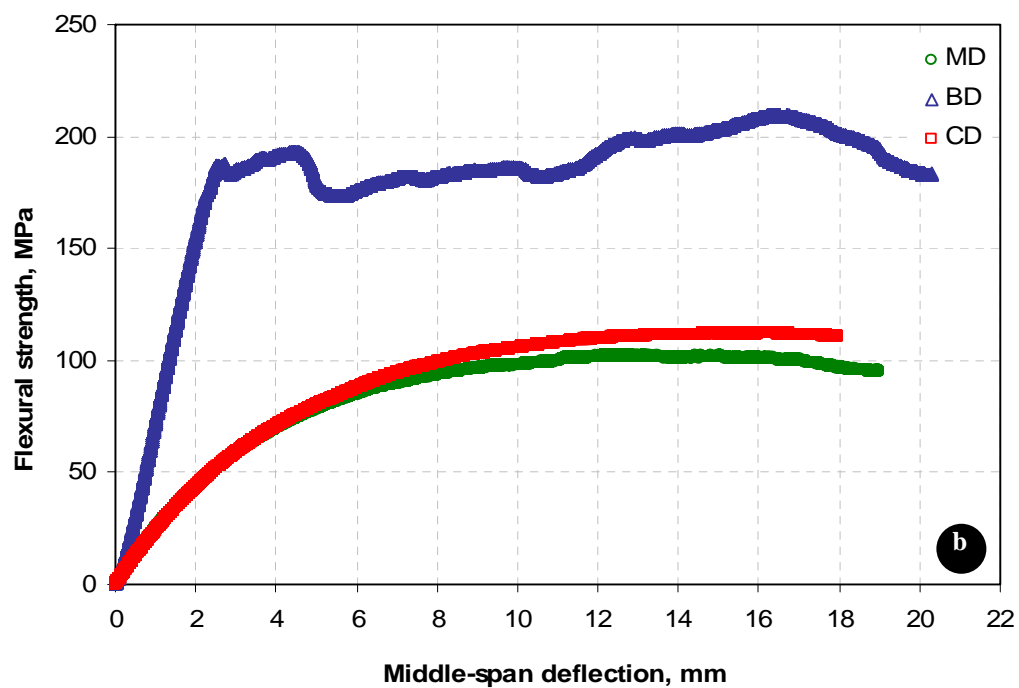
Figure 4.20 Flexural strength-deflection curves of laminates in different directions: (a) biaxial +45/-45° glass fabric laminate (V_f = 36.2 %); (b) biaxial +45/-45° carbon fabric laminate (V_f = 41.5 %).

Figure 4.21 Flexural strength-deflection curves of cross-ply laminates produced from: (a) unidirectional glass fabric (V_f= 32.6 %); (b) unidirectional carbon fabric (V_f= 25.6 %).
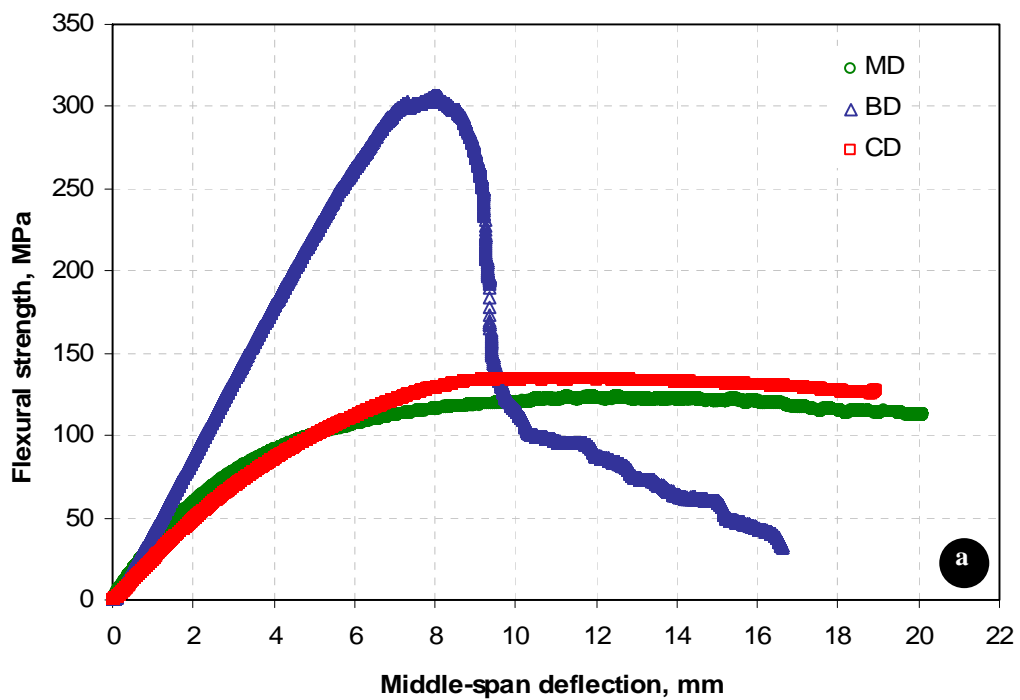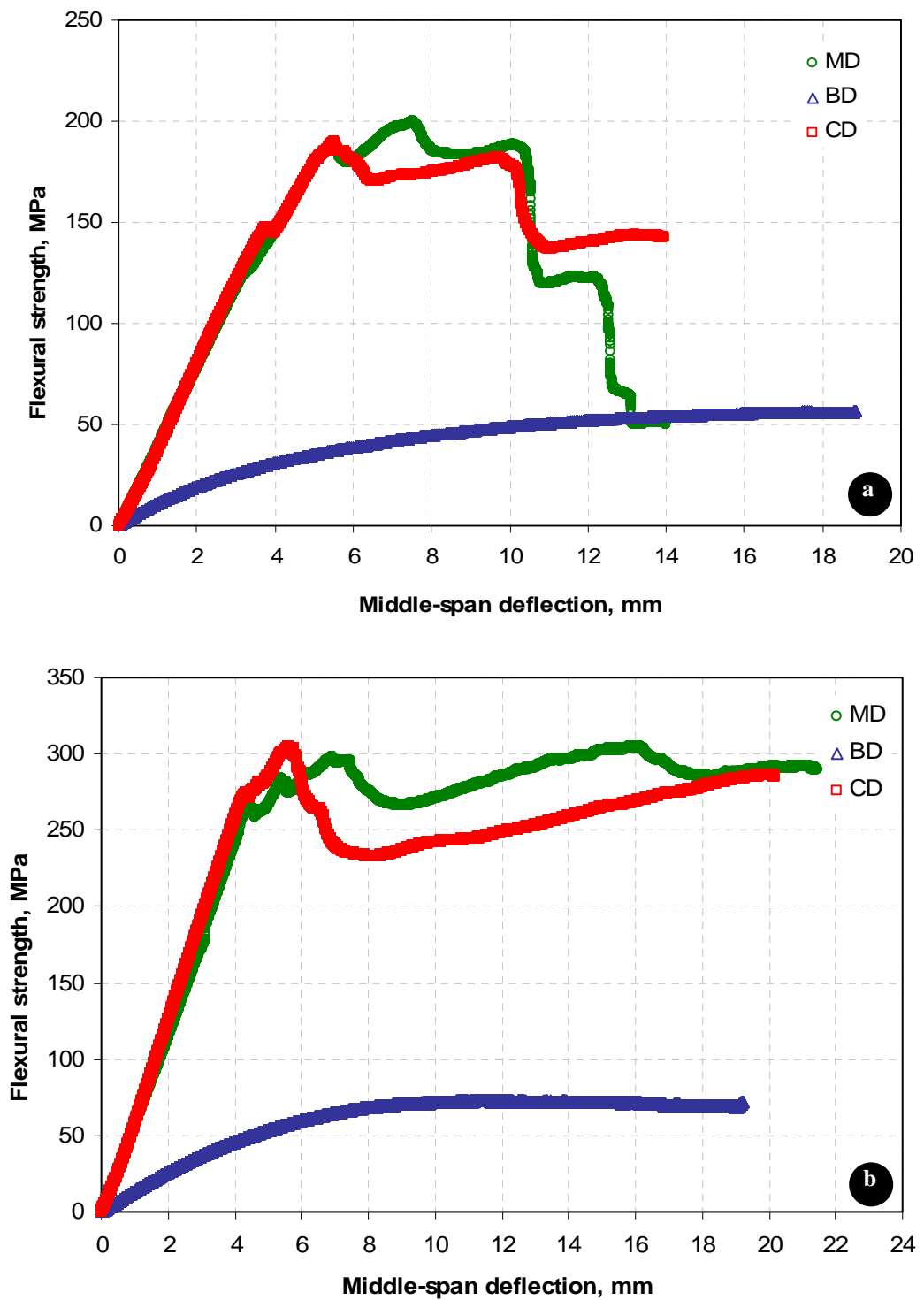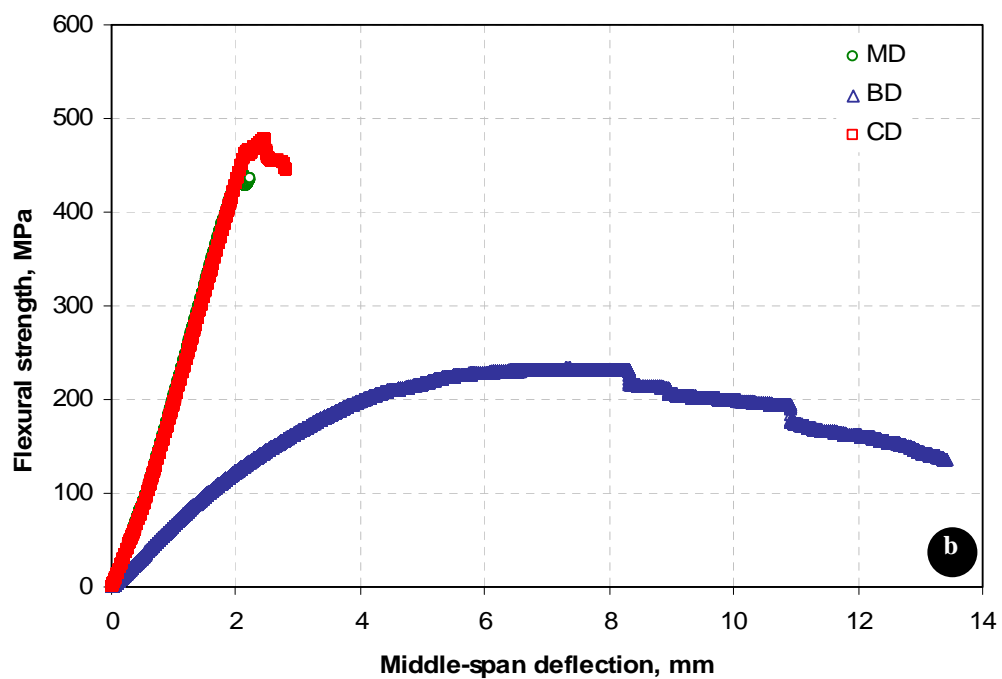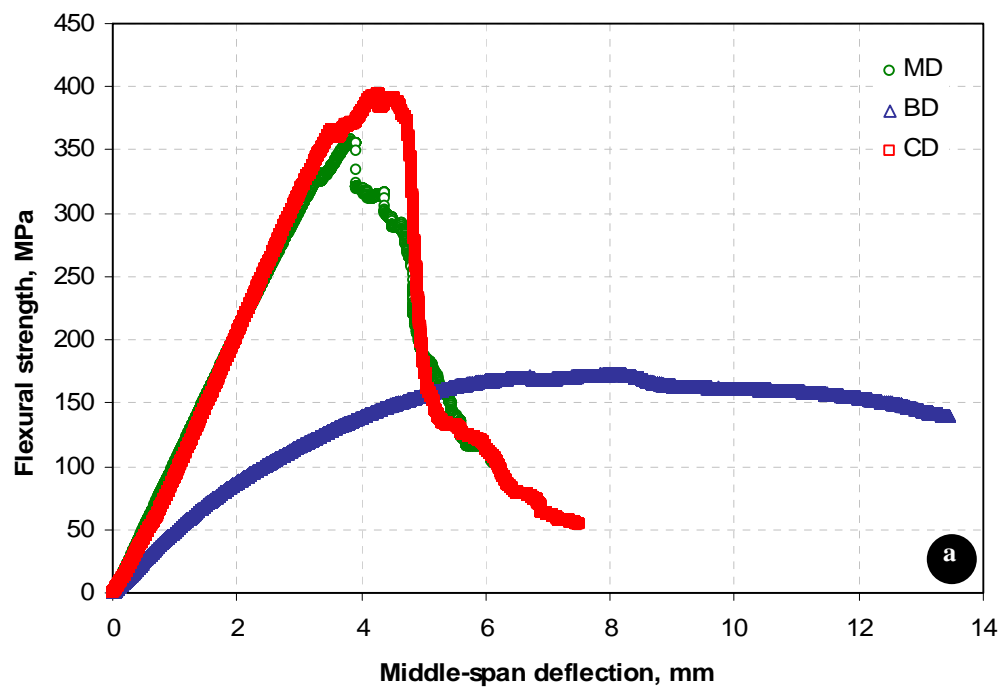
Figure 4.22 Flexural strength-deflection curves of laminates in different directions: (a) woven roving glass fabric laminate (V_f = 39.2 %); (b) woven roving carbon fabric laminate (V_f = 38.4 %).

4.3.1.3 Short Beam Shear Test Results

Failure occurs suddenly in a macroscopically brittle mode by crack initiation and propagation. A sharp drop in the load–displacement curves and an audible cracking sound accompany catastrophic delamination. In few tests failure was not visible at the time of the load drop, but upon removing the specimen or with slightly higher displacement it would manifest visibly.

The result of this investigation demonstrates that, contrary to the general belief that the matrix-dominated property of the ILSS was confirmed by its independence of fiber orientation and laminate lay-up, the lamina stacking sequence and laminate type have a significant effect on the recorded values of the interlaminar shear strengths (Table 4.4).

Observed results from the experiment suggest again that the strengths in the three-point flexure test are much higher than those in the short beam shear test at all the considered direction.

4.3.2 Fractographic Analysis

It is well known in the fiber composite technology community that the fiber-matrix interface gives fiber composites their structural integrity. The interface consists of the bond between fiber and matrix and the immediate region adjacent to this bond. Epoxy composites broken in tension along the machine direction and observed under different moderate magnification levels showed obvious differences between good bonding and poor bonding at the interface (Figure 4.23). A mechanically coupled composite showed excellent retention of epoxy on broken fiber ends, while a noncoupled composite showed clean holes in the matrix and uncoated fiber ends pulled from the polymer. The fracture surface of a unidirectional composite with intermediate bond strength is shown in Figures 4.23(a) and 4.23(b). Note the considerable amount of fiber pull-out and the irregular fracture surfaces. The clean fiber surfaces on debonding cracks indicate extensive interfacial failure.

Despite this fact, the fiber show traces of matrix still into and around the fiber. The fibers are loosely held by the matrix material after failure.

The fracture surfaces of multiaxial composites are illustrated in Figures 4.23(c) and 4.23(d). The fracture surface of these composites exhibits both longitudinal type and transverse type fracture characteristics. Photomicrographs at high magnification clearly illustrate that the bond quality at the interface plays a predominant role as to the type of fracture surface that a composite will exhibit when it is loaded in the matrix dominated orientation. When the composite is loaded in the matrix-dominated direction the matrix-dominant fracture surface is predominantly brittle and the fracture surface traverses matrix and interface as well as some fibers.

From Figure 4.23(e) it could be clearly seen that the fracture surface of plies shows fibers coated with the matrix, and there are no indications of fibers pull-out. The fibers are held together by the matrix material, unlike those in cross-ply carbon fabric laminate (Figure 4.23(f)), confirming the strong fiber-matrix adhesion. The fracture mostly occurred in the matrix phase rather than in the interface between the reinforcing fiber and the matrix, but still such interaction is by friction and mechanical interlocking. In the fracture surfaces of cross-ply carbon fabric laminate (Figure 4.23(f)), fiber surfaces are almost completely devoid of matrix material, indicating fiber-matrix interfacial failure followed by extensive fiber pull-out from the matrix.

In plies of woven roving fabric laminate (Figures 4.23(g) and 4.23(h)), failure occurred by both cohesive fracture of the matrix and fiber breakage. However, composite showed considerable matrix failure together with the fibers being tightly held by the matrix material. Considerable amount of matrix tearing propagated along the resin rich region could be observed, together with cavities left by the pull-out fibers (Figure 4.23(h)). In this case the broken matrix pieces still adhered to fibers. It can be inferred that mechanical interlocking and friction are responsible for the failure mode observed on the matrix.
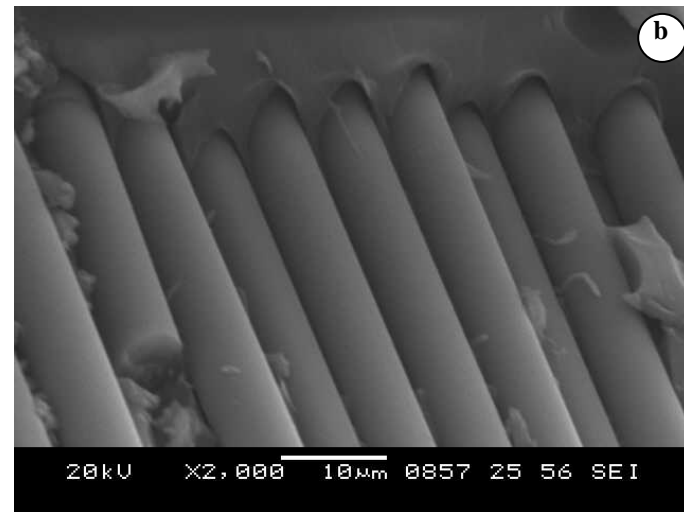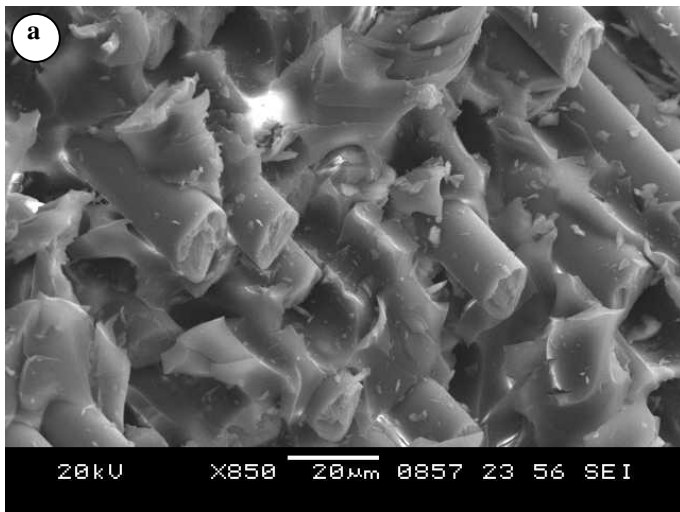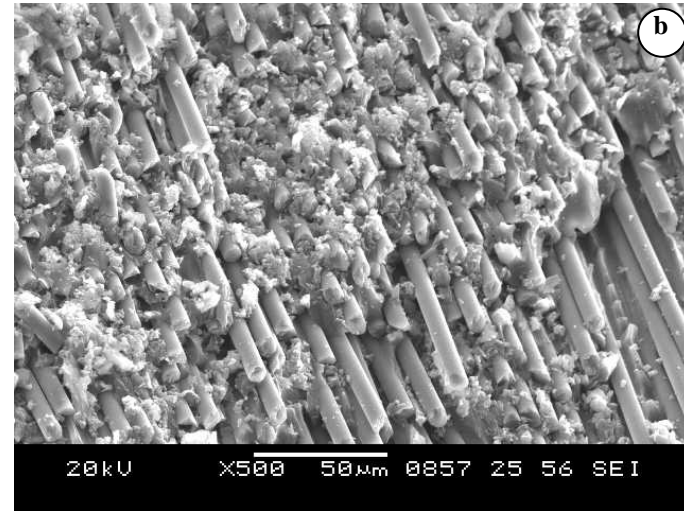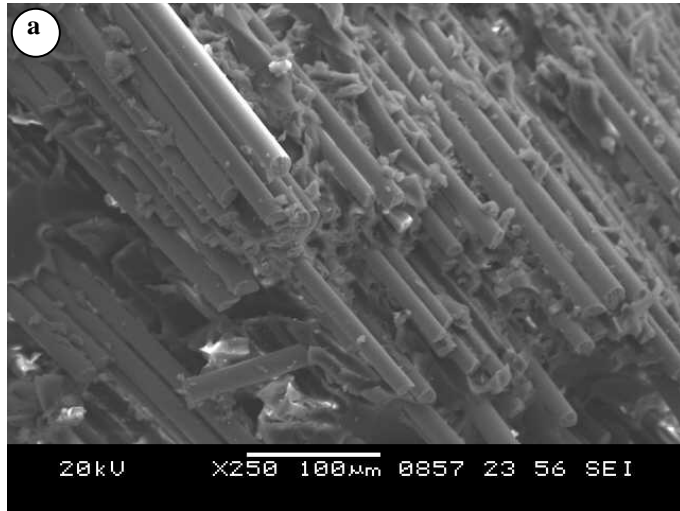
Figure 4.23 to be continued
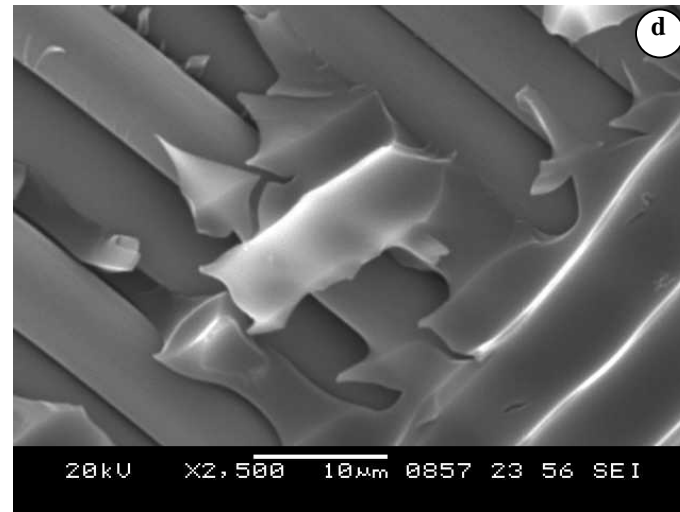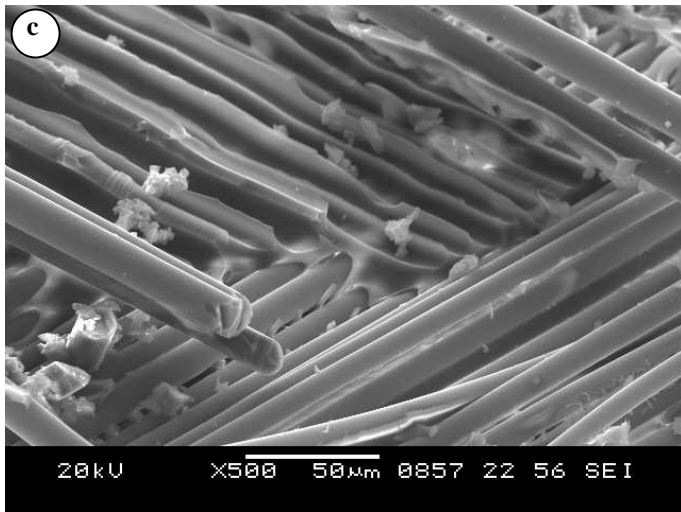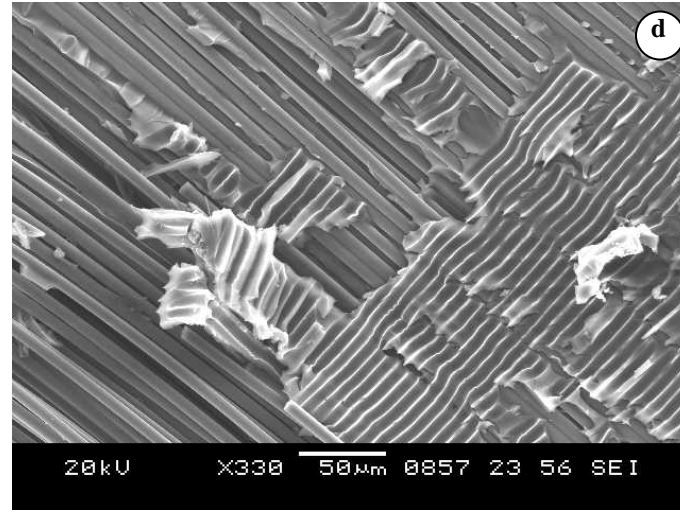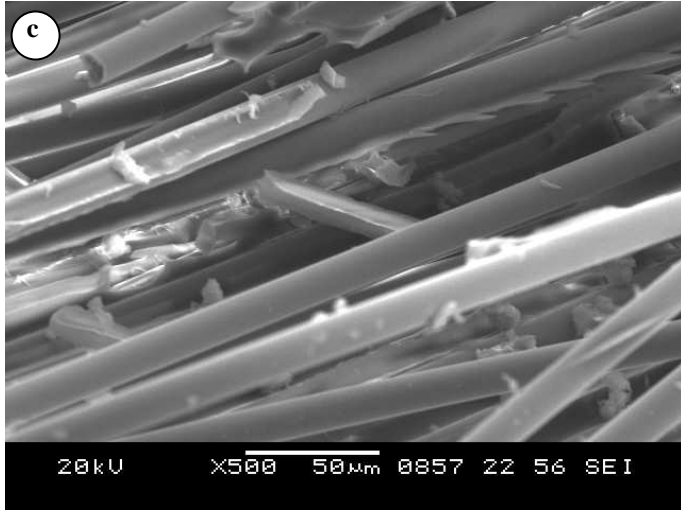
Figure 4.23 to be continued
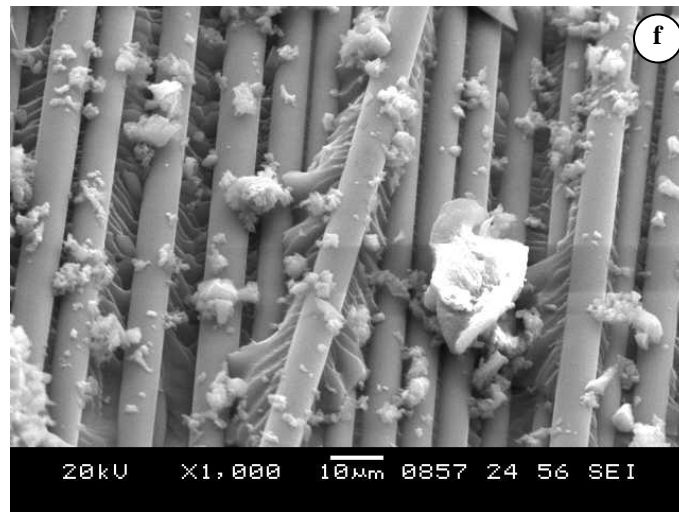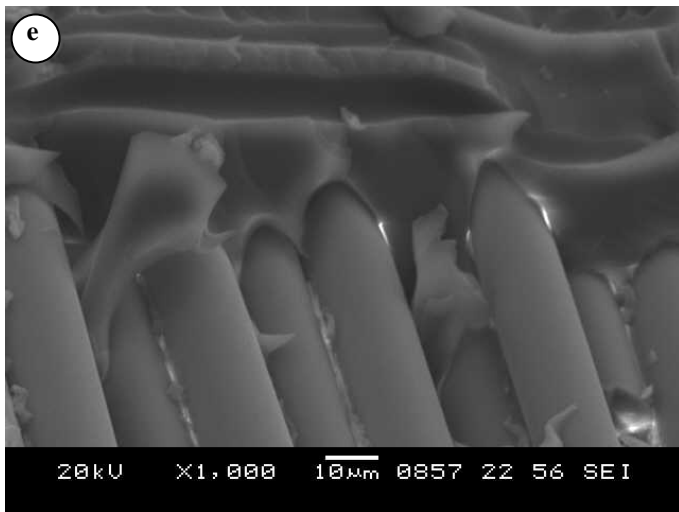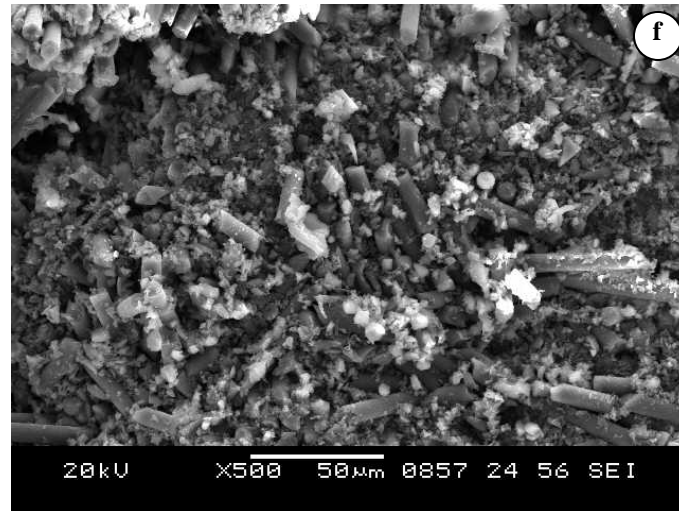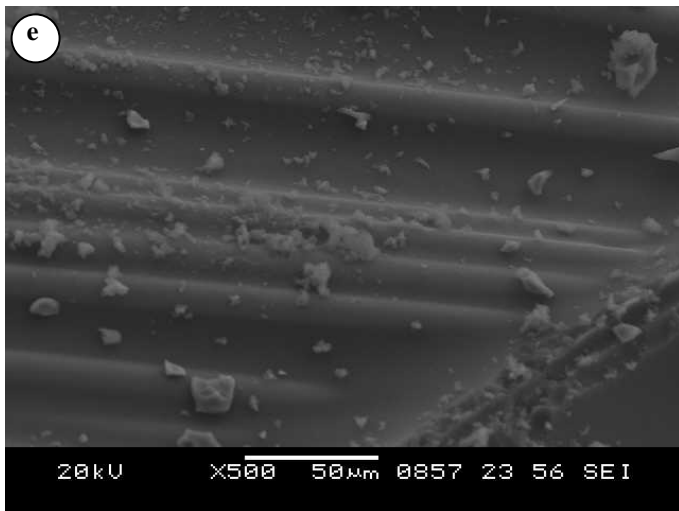
Figure 4.23 to be continued
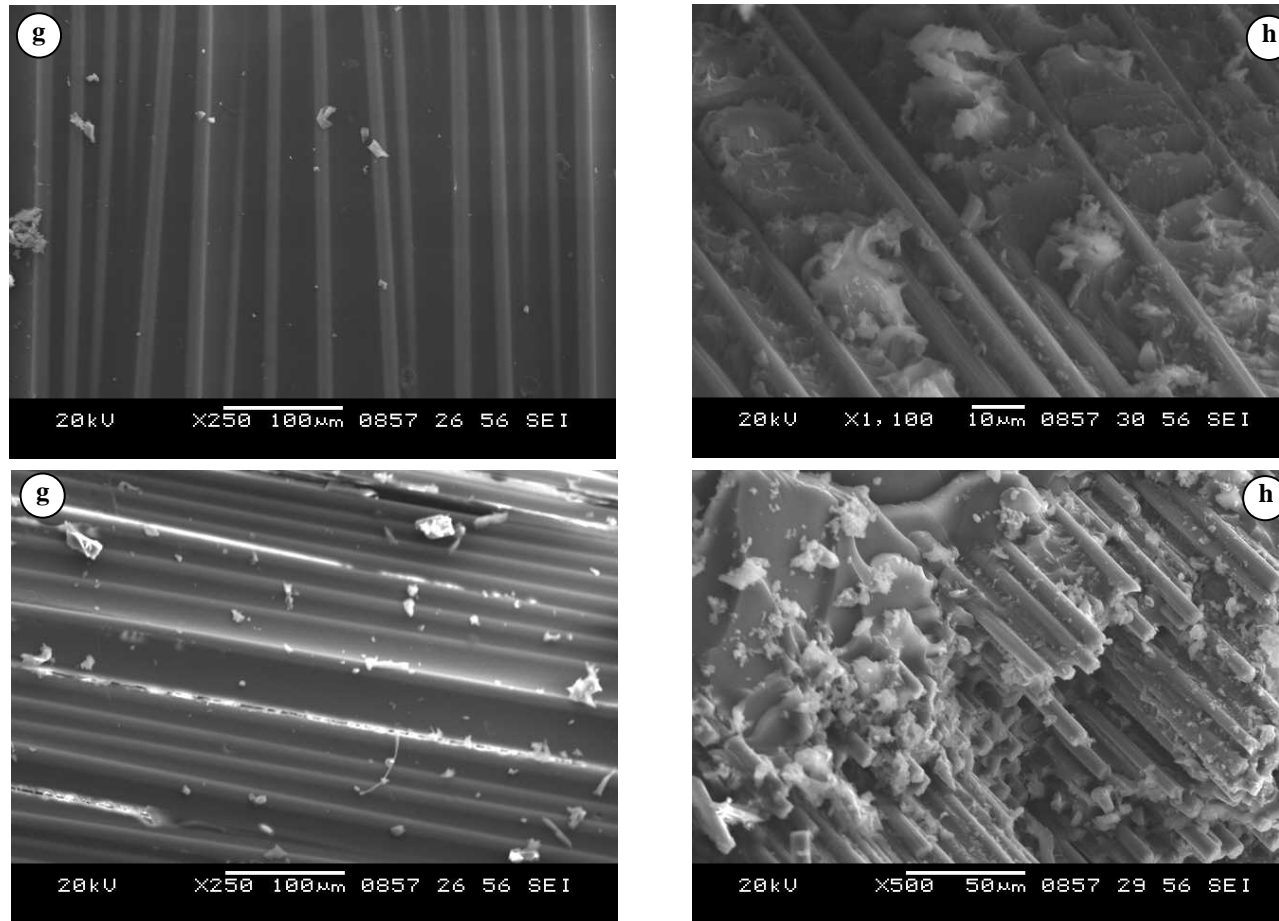
Figure 4.23 Representative SEM images of the breakage region for (a) unidirectional glass fabric and (b) unidirectional carbon fabric laminate; (c) biaxial glass fabric and (d) biaxial carbon fabric laminate; (e) cross-ply laminate made from glass fabric and (f) cross-ply laminate made from carbon fabric; (g) woven roving glass fabric and (h) woven roving carbon fabric laminate.

4.3.3 Study of the Interfaces in Epoxy Matrix Composites

Figure 4.24 shows the FTIR spectra of the 100%-cured neat epoxy resin, and its carbon and glass fiber composites. Table 4.9 shows the assignment of the main infrared absorption of the neat epoxy used in this work. OH stretching vibrations of epoxy give a typical broad band at 3364 cm^{-1}. As can be seen from the spectra of the neat epoxy and its carbon and glass fiber composites, the stretching vibrations of OH groups of the epoxy resin was shifted to 3397 and 3419 cm^{-1} for glass and carbon fiber reinforced epoxy, respectively. The change in carbon/epoxy composite is higher than that of glass/epoxy composite. There is an interaction between OH groups of the epoxy resin and carbon fiber. Aliphatic C-H stretching vibrations can be seen in the range of 3000-2800 cm^{-1}. There are not so much variations for these bands.

The band at 2360 cm^{-1} in the spectrum of carbon/epoxy composite can not be seen properly in the spectra of the neat epoxy resin and glass fiber reinforced epoxy. A new absorbing peak at 2360 cm^{-1} which is observed in the spectrum of carbon/epoxy composite shows a bond formation between carbon fiber and epoxy resin. It indicates that epoxy resin has reacted with carbon fiber. It is probable that a strong interaction between carbon fiber and epoxy resin occurs in comparison with epoxy resin and glass fiber. Considering epoxide and hydroxyl group are the only two reaction groups in epoxy molecule, the 2360 cm^{-1} band may be a conclusion of bond formed by the interaction OH groups and carbon fiber.

According to these mentioned results, among these fibers and matrix materials used in this study, carbon fiber and epoxy resin can be considered much more compatible one than the others for the production of polymer composites.

Table 4.9 Assignment of the main infrared absorption of the 100%-cured neat epoxy resin used in this study

Band (cm^{-1})	Assignment
3364	O-H stretch
2925	Aliphatic C-H stretch
2862	
1608	Aromatic ring stretch
1510s	
1453	CH$_3$ asymmetrical bend
1376	CH$_3$ symmetrical bend
1296m	Epoxy ring mode: the C-C, C-O
1243s	
1176	Ar-O-R asymmetrical bend
1108	
1036	Ar-O-R symmetrical bend
828	Aromatic ring bend out of plane
753	Monosubstituted aromatic ring stretch
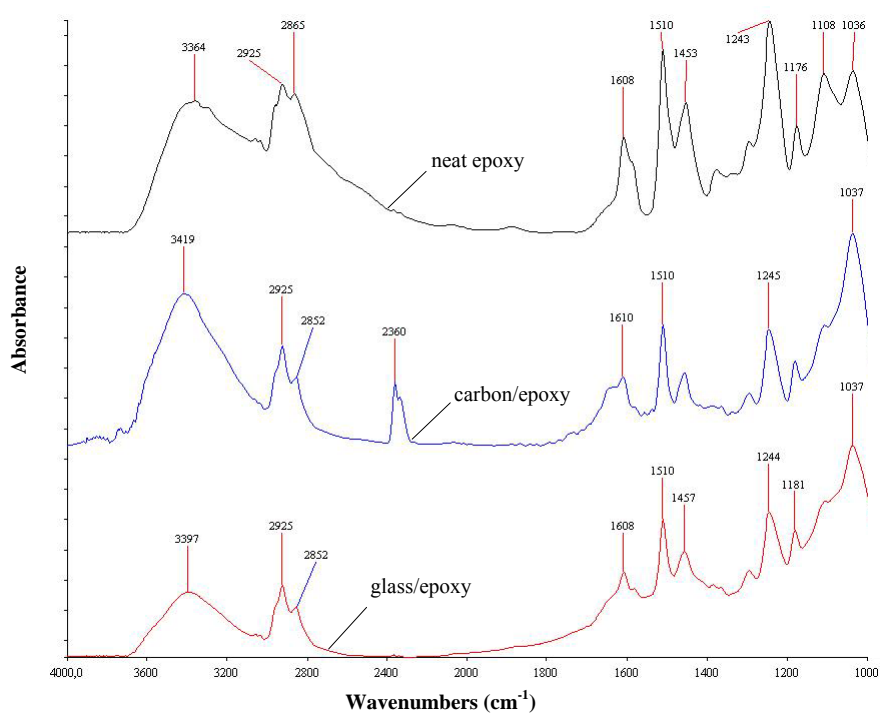
Figure 4.24 FTIR spectra of the neat epoxy resin and its glass and carbon fiber composites.

4.4 Thermal Characterization of Polyester- and Epoxy-Based Composites

4.4.1 Heat Capacity

The heat capacity of the epoxy based composites in a glassy state shows no peculiarities: it smoothly increases with rising temperature. Besides, as for many polymers in the low temperature region below the devitrification temperature their heat capacity obeys $C_p \sim T^{-1}$-law. Such character of the dependence remains till the temperature of the subsequent transformation onset (B point, Figure 4.26). And further the relationship $C_p = f(T)$ deviates from a linear one and a relatively rapid increase in the heat capacity takes place that is, probably, due to approaching of C_p the devitrification region. This non-isothermal transformation of the glassy state to a liquid or rubbery state, called devitrification, is a phenomenon that cannot occur in isothermal experiments (unless degradation of the polymer network occurs). Considering the high reactivity of the resins used and the results for a heating rate of 10 °C/min, one can conclude that before a complete devitrification can occur, the glass transition temperature of the vitrified resin starts increasing due to the residual cure reaction while in the glassy state.

It should be noted here that the devitrification of the polymeric matrix can be observed by DSC as a stepped increase in the heat capacity of the sample during heating due to an enhancement of molecular motion in the polymer. But in densely cross-linked polymers, i.e. unsaturated polyester and epoxy resin, it is hard to observe the devitrification region due to restriction of main-chain motion and the sample baseline step occurs over a broad temperature interval introducing a large error in the determination of devitrification temperature (Figure 4.25). Owing to widespread intramolecular and intermolecular hydrogen bonding it is difficult to measure devitrification temperature of many polymers in the dry state. In the light of the information mentioned, it has been concluded that the devitrification region is around the starting point of the endothermic peak observed in DSC curves.

The heat capacity of epoxy based composites in the glassy state rather sharply grows with rising temperature (section BCD, Figure 4.26), undergoing a visible jump at the temperature of the devitrification transformation beginning, and afterwards the C_p values increase still more rapidly.

It is worth of note here that after completing the calorimetric experiment and unloading the samples of epoxy based and polyester based composites from the pan they were not transparent, dark-yellow colored unlike the starting samples and their masses differed slightly according to the masses prior to the beginning of measurements. This corroborates, certainly, the onset of their thermal decomposition under conditions of the calorimetric apparatus.

An endothermic transition for a glassy state which corresponds to an increase in enthalpy, is indicated as a peak in the downward direction (Figure 4.25). It is possible to arrive this conclusion by a careful examination: The sudden increase in heat capacity starting at the devitrification region, has continued at the temperature interval where the mentioned endothermic transition has been detected and has reached its maximum value at this interval. The increase in heat capacity during the endothermic transition, and also on the devitrification region, is caused by the beginning of large-amplitude motion that is characteristic of the liquid or rubbery state. Three major types of large-amplitude motion are possible: translation of the molecule as a whole (also called positional motion), orientational motion (also based on motion of the whole molecule), and conformational motion (the internal rotation of the various segments of flexible molecules). On the other hand, the decrease in thermal conductivity at the above mentioned temperature interval is to be of concern (Figures 4.27, 4.30 and 4.33). It is remarkable, that the thermal conductivity was complex and was phase transition dependent similar to the strong phase transition dependence of the complex heat capacity related to latent heat. At this point, it is necessary to emphasize that a change of the composite's thermal conductivity in the range of temperature involving a phase change is not dominated mainly by the increase of its heat capacity in the above-mentioned phase transition region.

Figure 4.25 DSC heat flow curves for the empty pan baseline, alumina standard and the glass/epoxy composite. The sample weight for the alumina and glass/epoxy were 18.1 and 15.0 mg, respectively. The heating rate was 10 °C/min.

Figure 4.26 Heat capacity of glass/epoxy composite material obtained from DSC experiments.

Figure 4.27 Thermal conductivity as a function of temperature for glass/epoxy composite material.

Thermoset polymers can be polycrystalline or amorphous in nature and may belong to inorganic, organic, or combinations of inorganic and organic classes of materials. In the vicinity of the devitrification temperature of the fully cured epoxy resin in the non-isothermal DSC curve of epoxy based composites, structure scattering, which is independent of temperature, plays an important role in the thermal resistance. So in the range of temperature involving a phase change, the slight decrease of the thermal conductivity in all investigated samples can be explained on the basis of temperature independent various phonon scattering mechanisms (Dhami & Dey, 2000), namely, structural scattering, stray scattering, and chain defect scattering. It is reasonable to interpret these processes as being associated with the presence of intergranular boundaries. Moreover, the thermal conductivity resulted from phonon lattice contribution can be explained as; by increasing temperature the number of phonon–phonon collisions (Kotkata, El-Fouly, Fayek, & El-Hakim, 1986) increases which leads to a decrease in the mean free path of phonons. This leads to the slight decrease in thermal conductivity according to the relation:

$$\lambda = 1/3 C_p v l \qquad (4.1)$$

where C_p is the heat capacity per unit volume, v is the average phonon velocity and l is the phonon mean free path. Also this decrease of thermal conductivity with temperature may be attributed to the fact that in the process of heating, the composites were subjected to some composition changes. As the test temperature goes up, the phonon vibration frequency will be quickened to make the collision possibility increase, so the mean free path decreases rapidly, which leads to the rapid decrease of its thermal diffusivity. Because its heat capacity ascends slowly, the thermal conductivity is dominated mainly by the phonon mean free path, and thermal conductivity decreases with increasing temperature. From a scientific and practical point of view, the mean free path decreases and thus the contributions to the corresponding thermal resistance increase linearly with the rise of temperature, resulting in the decrease of thermal conductivity in this temperature range.
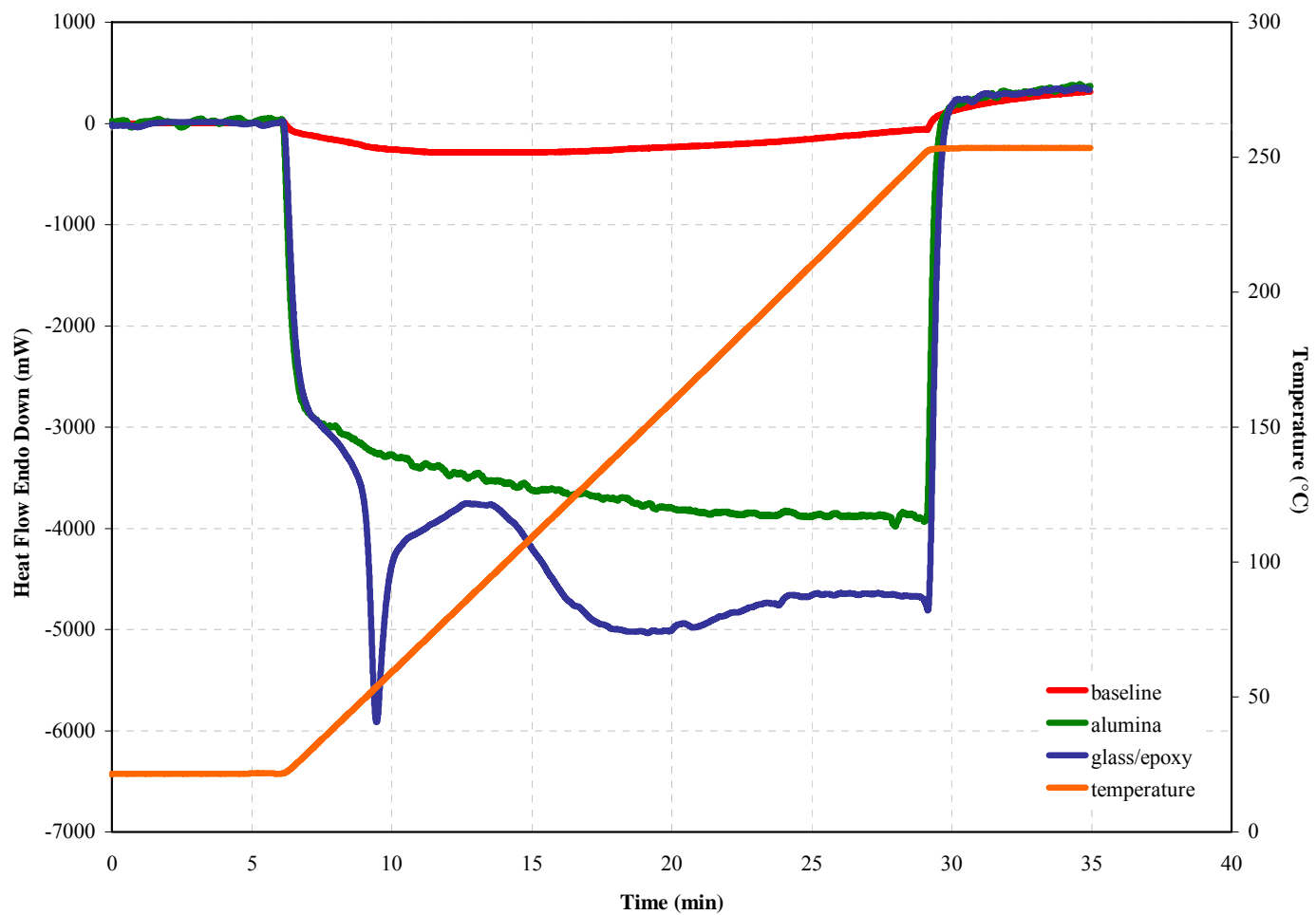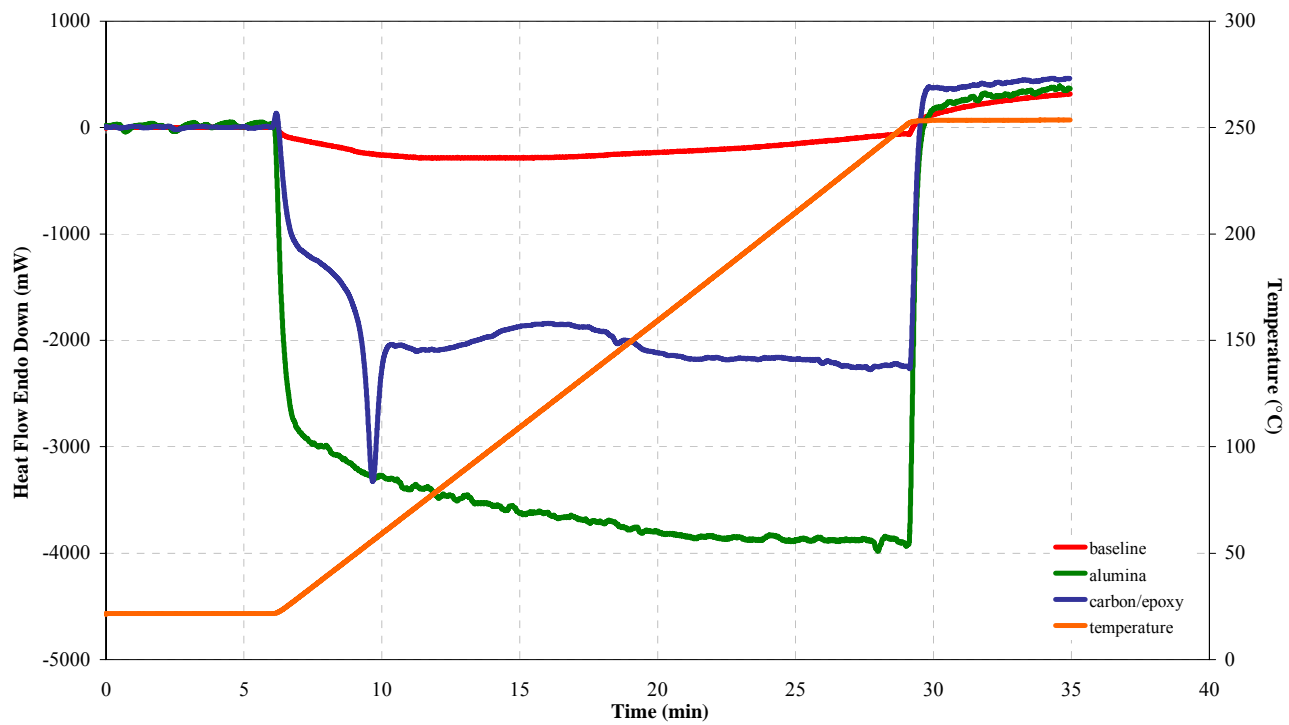
Figure 4.28 DSC heat flow curves for the empty pan baseline, alumina standard and the carbon/epoxy composite. The sample weight for the alumina and carbon/epoxy were 18.1 and 7.9 mg, respectively. The heating rate was 10°C/min.
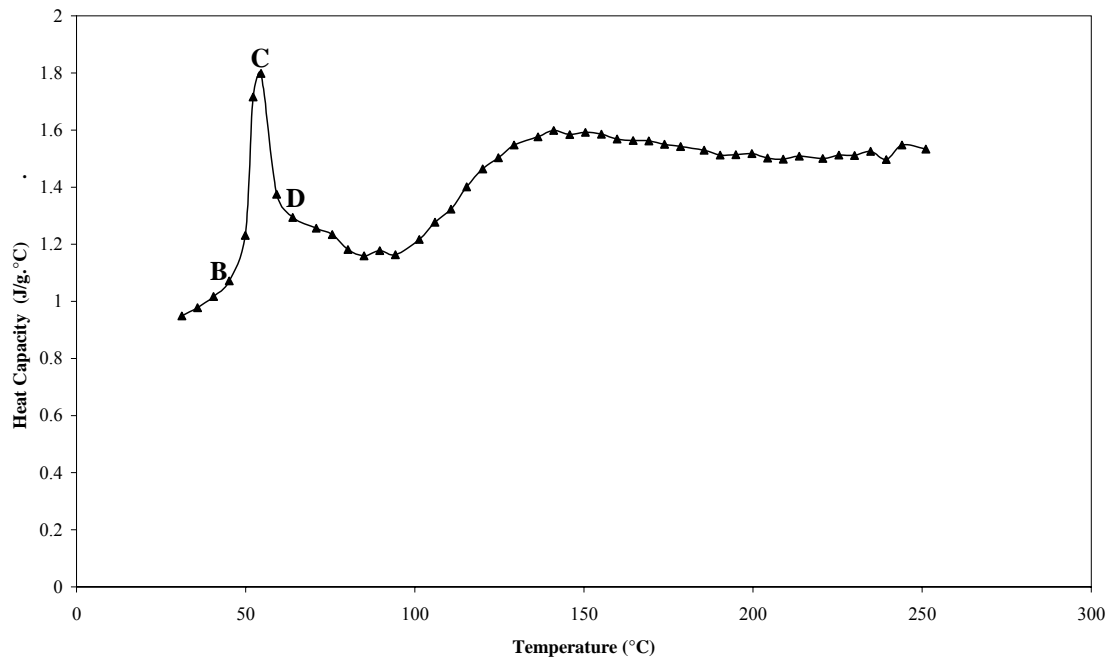
Figure 4.29 Heat capacity of carbon/epoxy composite material obtained from DSC experiments.

Figure 4.30 Thermal conductivity as a function of temperature for carbon/epoxy composite material.

Figure 4.31 DSC heat flow curves for the empty pan baseline, alumina standard and the aramid/epoxy composite. The sample weight for the alumina and aramid/epoxy were 18.1 and 8.4 mg, respectively. The heating rate was 10 °C/min.

Figure 4.32 Heat capacity of aramid/epoxy composite material obtained from DSC experiments.
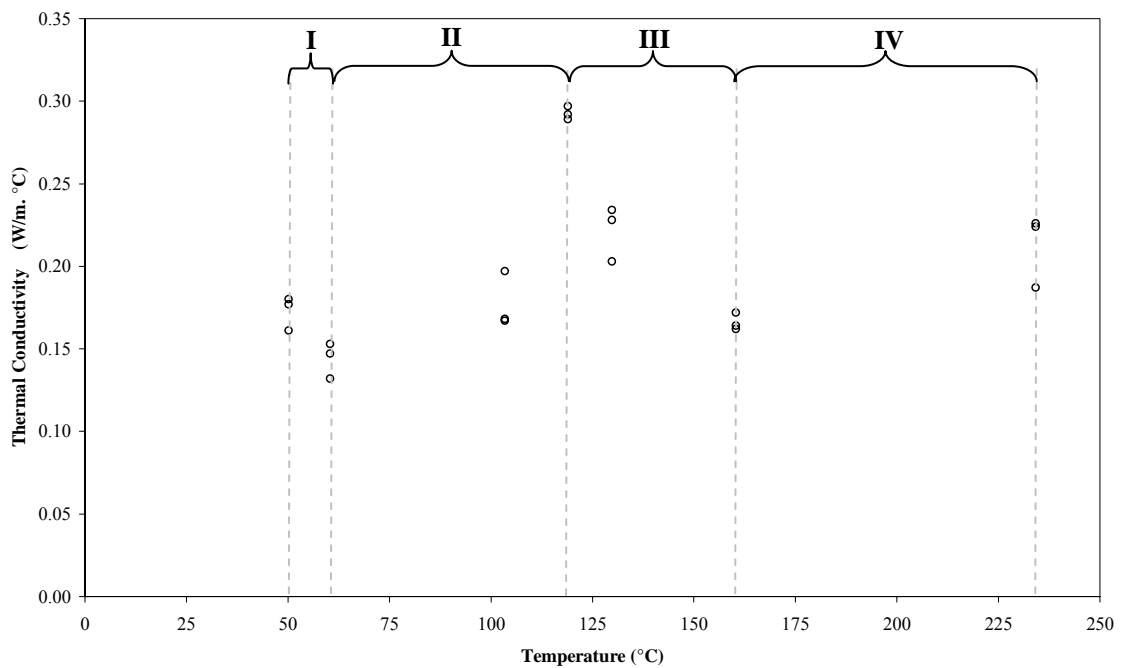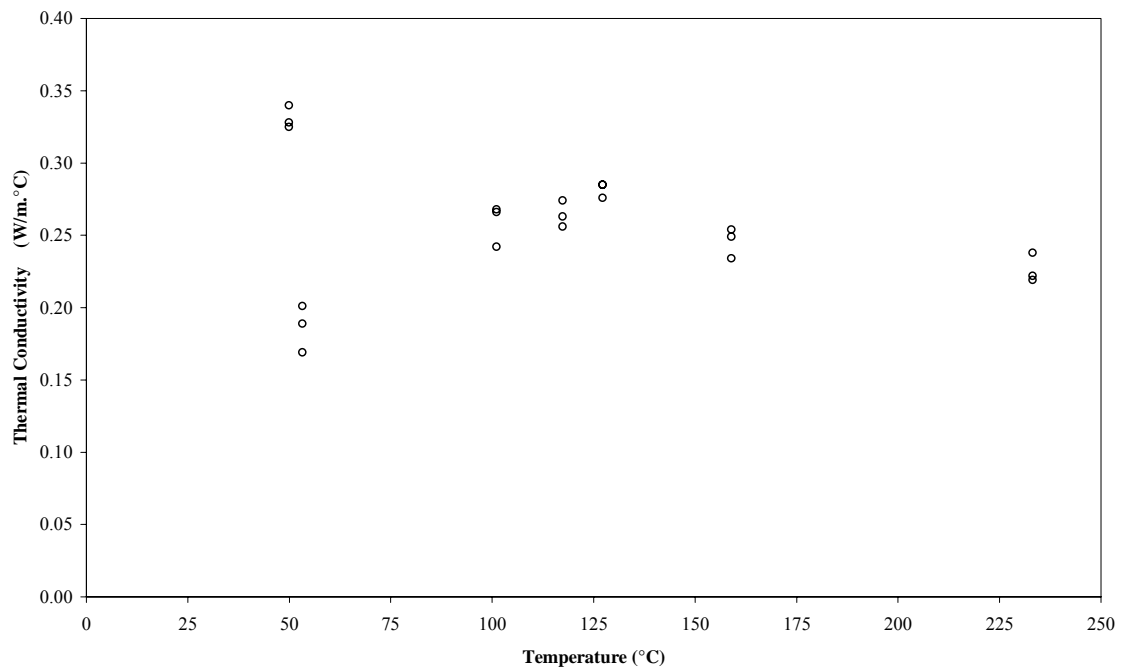

Figure 4.33 Thermal conductivity as a function of temperature for aramid/epoxy composite material.

The most noticeable feature in the curves for the epoxy based composites sample is the disappearance of the exothermic crystallization peak before the endothermic peak (Figures 4.25, 4.28 and 4.31). Experiments are performed with fully cured composites to investigate the relationship between temperature and thermal properties. Composites cured at a particular temperature until the cure reaction stops due to vitrification. Thus, it is important to emphasize here that, when dynamic scans are carried out on the fully cured samples, no exothermic energy is released until the endothermal peak temperature is reached. Therefore, excess heat capacity can not be detected at crystallization. This disappearance of the exothermic crystallization peak could be attributed to the fact that fiber reinforcement would prevent the epoxy from releasing heat energy at this temperature range before the endothermic transition of epoxy resin.

It must be pointed out here that in thermograms obtained for the polyester based composites one can not observe crystallization exothermic process over the experimental time scale used (Figures 4.34, 4.37 and 4.40).

Even in the absence of a transition at elevated temperatures after the endothermic transition, the instrument measures the effect of the heat capacity of the sample, which may vary with temperature. This variation is usually nearly linear, but the curvature becomes noticeable over wide temperature ranges (Figures 4.26, 4.29 and 4.32). The greater C_p values of the composites at elevated temperature are normally due to the greater degrees of molecular vibrations at higher temperature.

It must also be pointed out that the exothermic transition occurred over a broad temperature interval, as shown in Figure 4.25, and the weak exothermic plateau at high temperature side (Figures 4.28 and 4.31), which corresponded to the reaction in the unpolymerized portion in the resin, cause a jump of the thermal conductivity (Figures 4.27, 4.30 and 4.33). In these samples this unpolymerized part in the epoxy resin polymerizes in a temperature range around 100 °C. A step increase in the curve of the heat capacity is also due to the above-mentioned polymerization.

The result based on an observation of different specific heat capacities of epoxy based composites indicating that the formation of different degrees of network due to differences in fiber type affect the heat capacity of the composites as shown in Figures 4.26, 4.29 and 4.32. Besides, it is possible to relate the higher heat capacity for the composites containing aramid fiber to the fact that the liquid epoxy resin may adequately wet the surfaces of the aramid fiber, as compared to the glass and carbon fiber. It must be pointed out here that good wetting of the fiber by liquid resin was of prime importance since poor wetting would produce voids at the interface which would hinder percolation network of fibers in composites and hence limit the thermal conductivity, as well as the heat capacity of composite materials.

The principal conclusion to note at this stage is that good wetting of the fiber by liquid resin is the determining factor that contributes to the high heat capacity of fiber reinforced epoxy composite. Accordingly, the other two grades, glass fiber and carbon fiber, did not show the percolation-like behavior in the studied epoxy composites, which may be due to their poor wettability resulting in a greater difficulty in formation of filler networks.

The plots of the temperature-dependent heat capacity of polyester based composites are shown in the temperature range where it is thermostable being in the glassy state (Figures 4.35, 4.38 and 4.41). The observed behavior of the temperature dependence of the heat capacity of polyester based composites in the glassy state is similar to that of the epoxy based composites, according to the calorimetric data. However, it is seen that the character of the change in C_p of polyester based composites in the glassy state with rising temperature slightly differs from that of epoxy based composites, i.e. the C_p values of polyester based composites increase more gradually. This manner is likely to be explained by the influence of unsaturated polyester available in the composite composition. It is interesting to note here that, in the DSC endotherm region, the peaks of the temperature dependences of the heat capacity of polyester composites were small as compared to that of epoxy

Figure 4.34 DSC heat flow curves for the empty pan baseline, alumina standard and the glass/polyester composite. The sample weight for the alumina and glass/polyester were 18.1 and 18.4 mg, respectively. The heating rate was 10 °C/min.
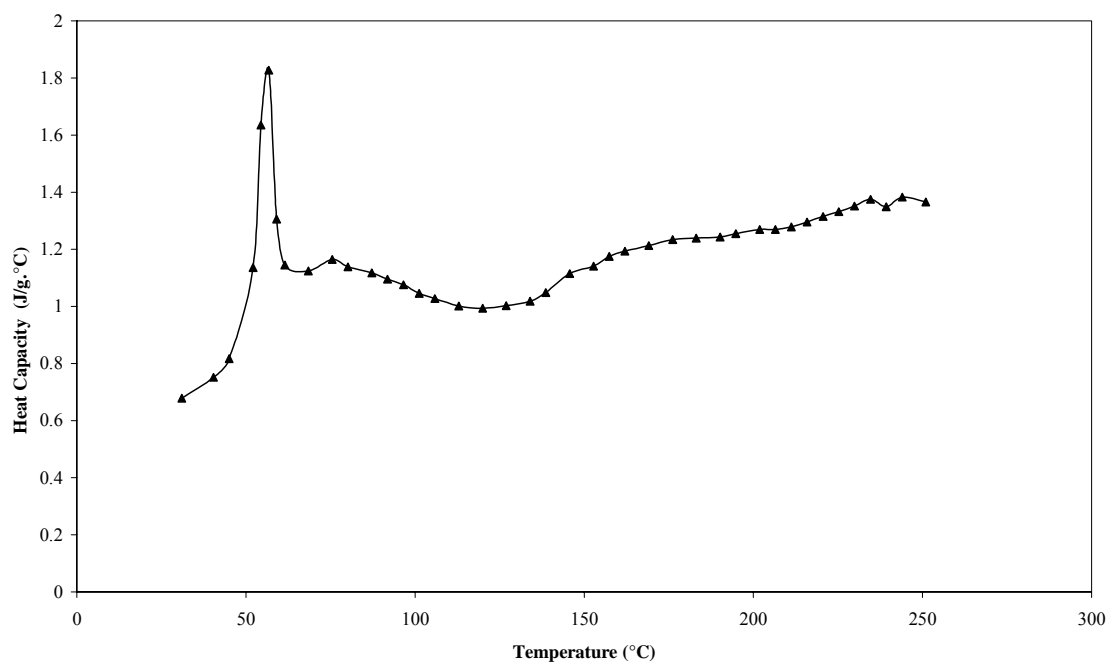
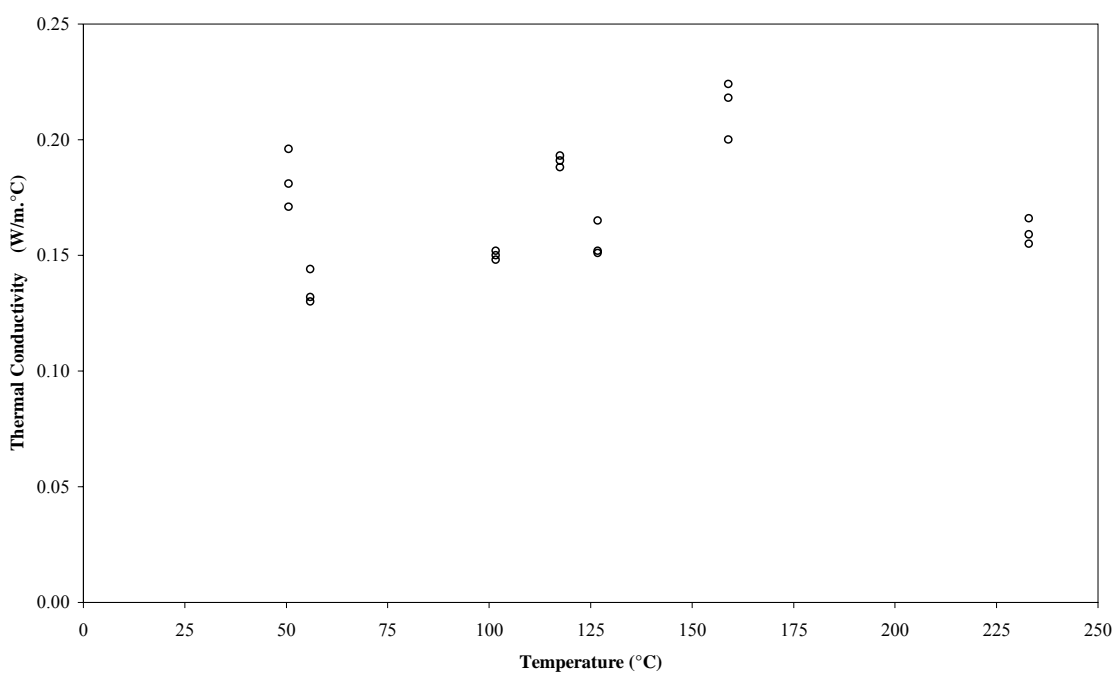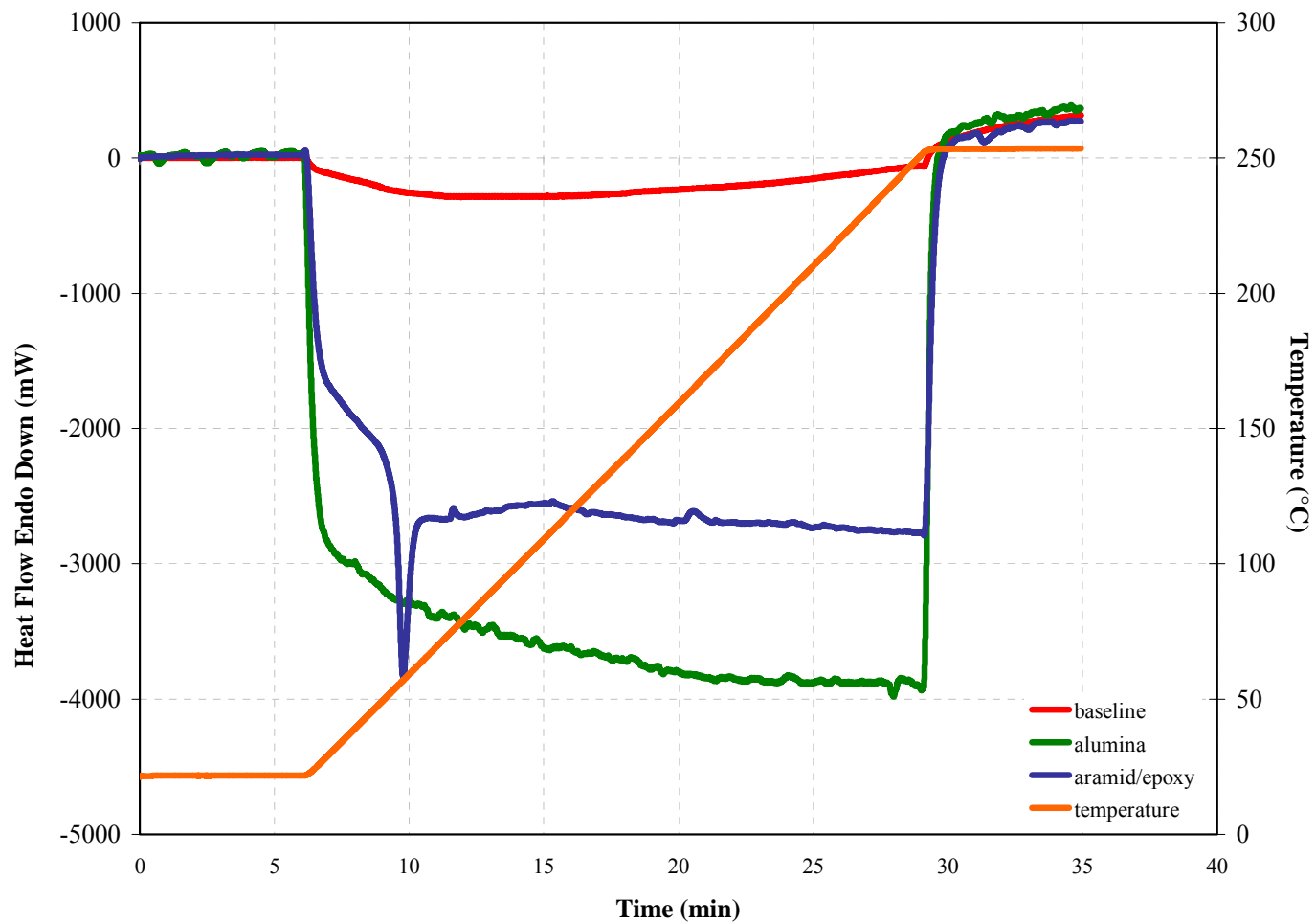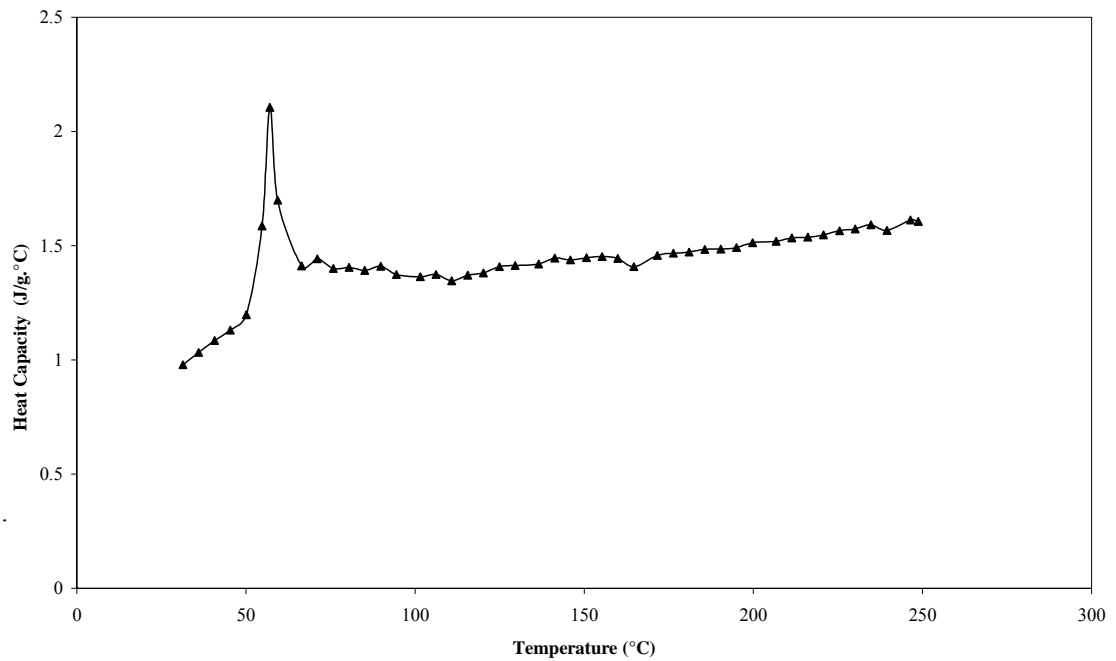Figure 4.35 Heat capacity of glass/polyester composite material obtained from DSC experiments.

Figure 4.36 Thermal conductivity as a function of temperature for glass/polyester composite material.

composites. The almost considerable increase in the specific heat capacity with time during the initial interval of the endothermic transformation reflects the increase in configurational and/or vibrational contributions in the rubbery state originated by the network growth. A relative reduction of the intensity of peaks in polyester composites is believed to be due to the fact that the increase in the mentioned contributions for polyester based composites were lower than those of epoxy based ones. In Figures 4.34, 4.37 and 4.40, it is seen that no evidence of an exothermic crystallization reaction is observed in the DSC trace as in the case of polyester composites. This fact can be interpreted in at least two different ways: either the enthalpy of the reaction is too weak to be detected, or there is no reaction during the experimental time.

Increments of the thermal conductivity after the DSC endotherm for polyester composites have been attributed to the weak exothermic plateau at high temperature side, which corresponded to the reaction in the unpolymerized portion in the resin (Figures 4.36, 4.39 and 4.42).

It should be noted that the numerical magnitudes of C_p for polyester based composites, are almost always lower than those of epoxy based composites. This also brings out that these varying microstructure of resin matrix is found to be influencing the amount of heat absorbed by the composites and hence heat capacity of the composites. Suitable wetting of the fibers by the liquid polymeric matrix should occur when the nature of the fiber surface is compatible with that of the liquid polymeric surface from the viewpoint of the hydrophilic–hydrophobic properties or the specific (or polar) London dispersive components of the surface free energy. As we know, fibers used in this study are highly hydrophilic in nature and are not highly compatible with the hydrophobic polyester resin, as compared to epoxy resin. The poor wettability of fibers with polyester resin can be held responsible for the decrease of filler network formation in the composite system. As a result, reduced percolation network of fibers in polyester based composites would have a negative impact on heat capacity of the composites.
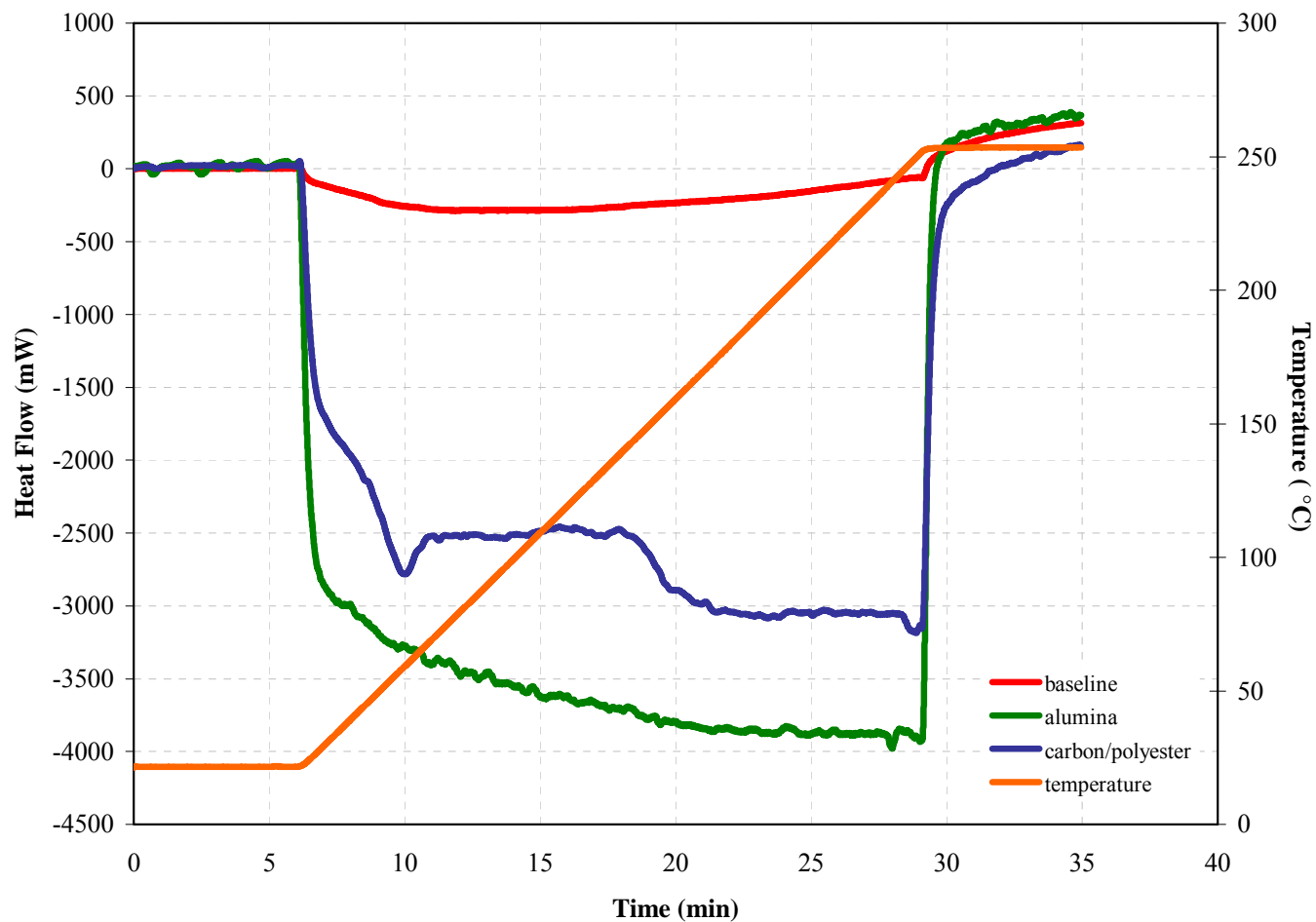
Figure 4.37 DSC heat flow curves for the empty pan baseline, alumina standard and the carbon/polyester composite. The sample weight for the alumina and carbon/polyester were 18.1 and 9.3 mg, respectively. The heating rate was 10 °C/min.
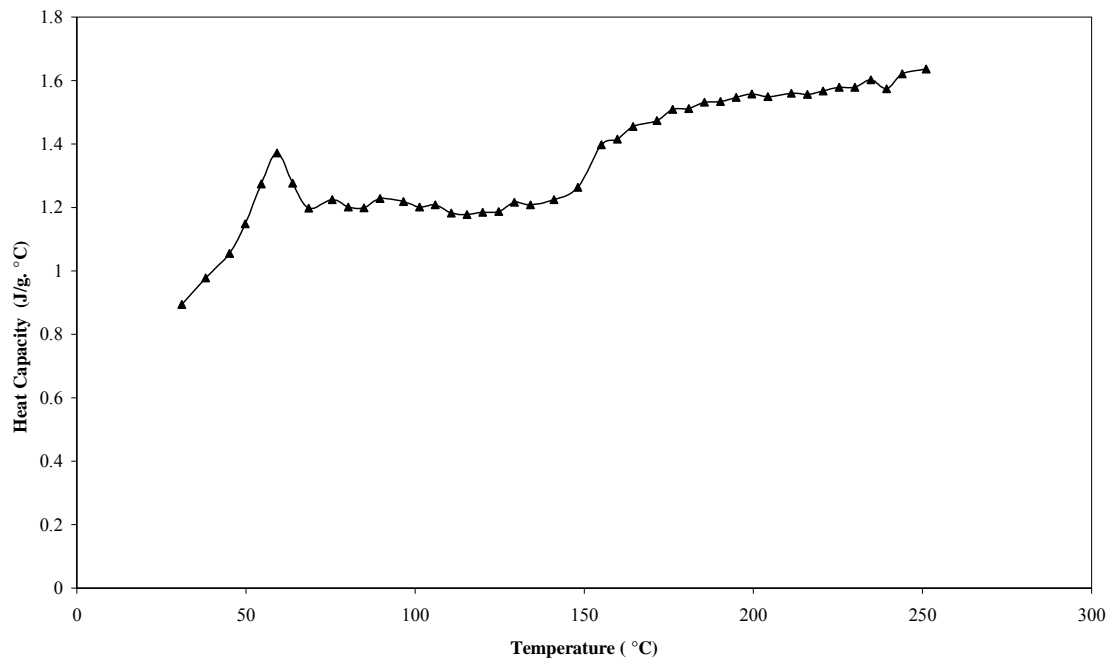
Figure 4.38 Heat capacity of carbon/polyester composite material obtained from DSC experiments.
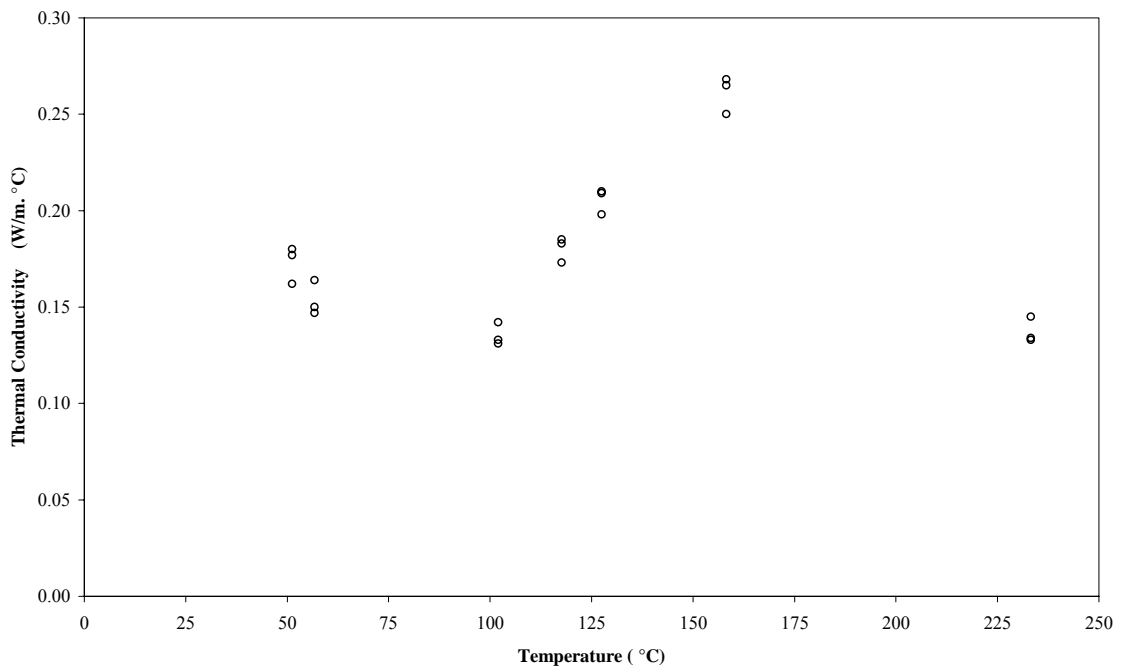
Figure 4.39 Thermal conductivity as a function of temperature for carbon/polyester composite material.
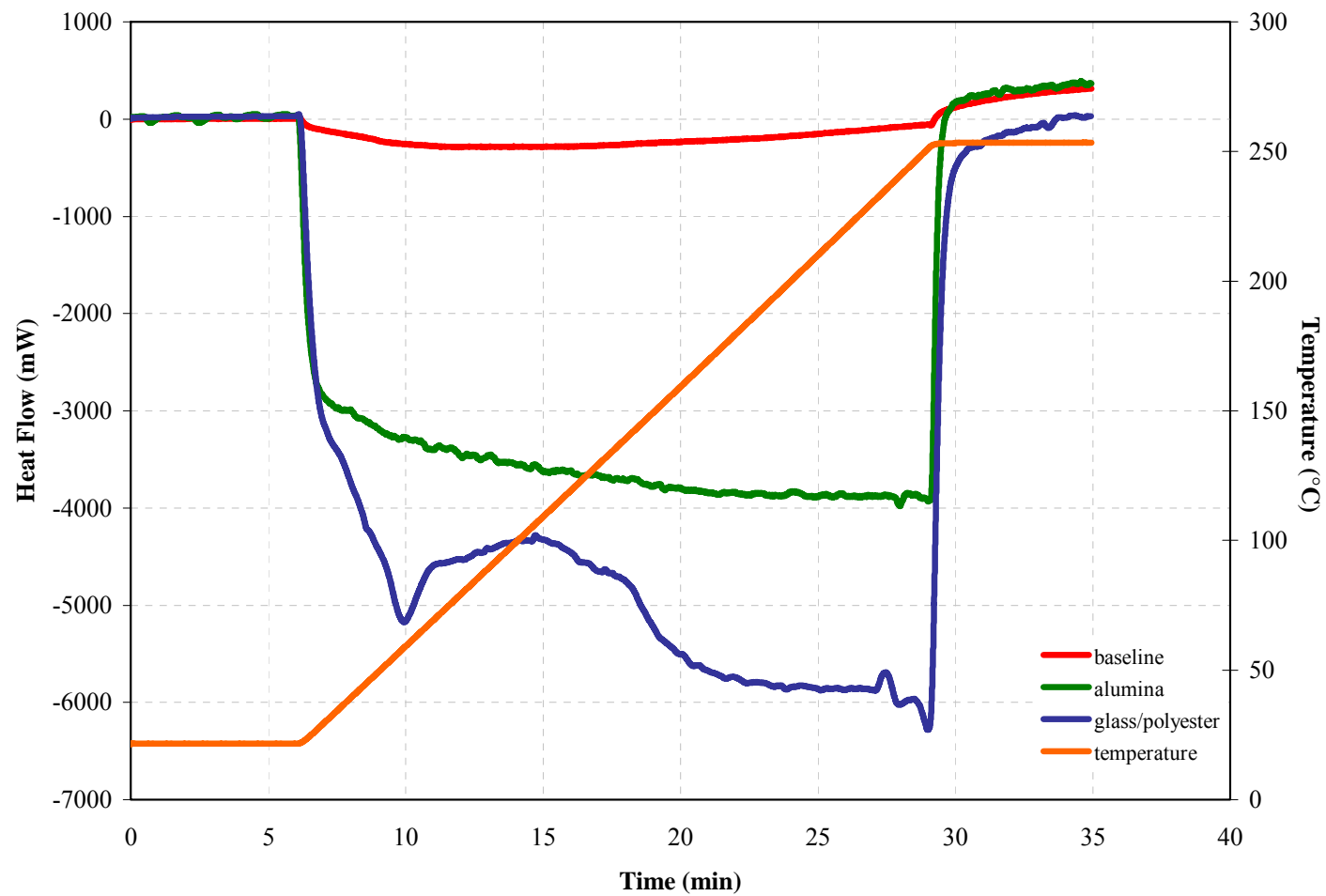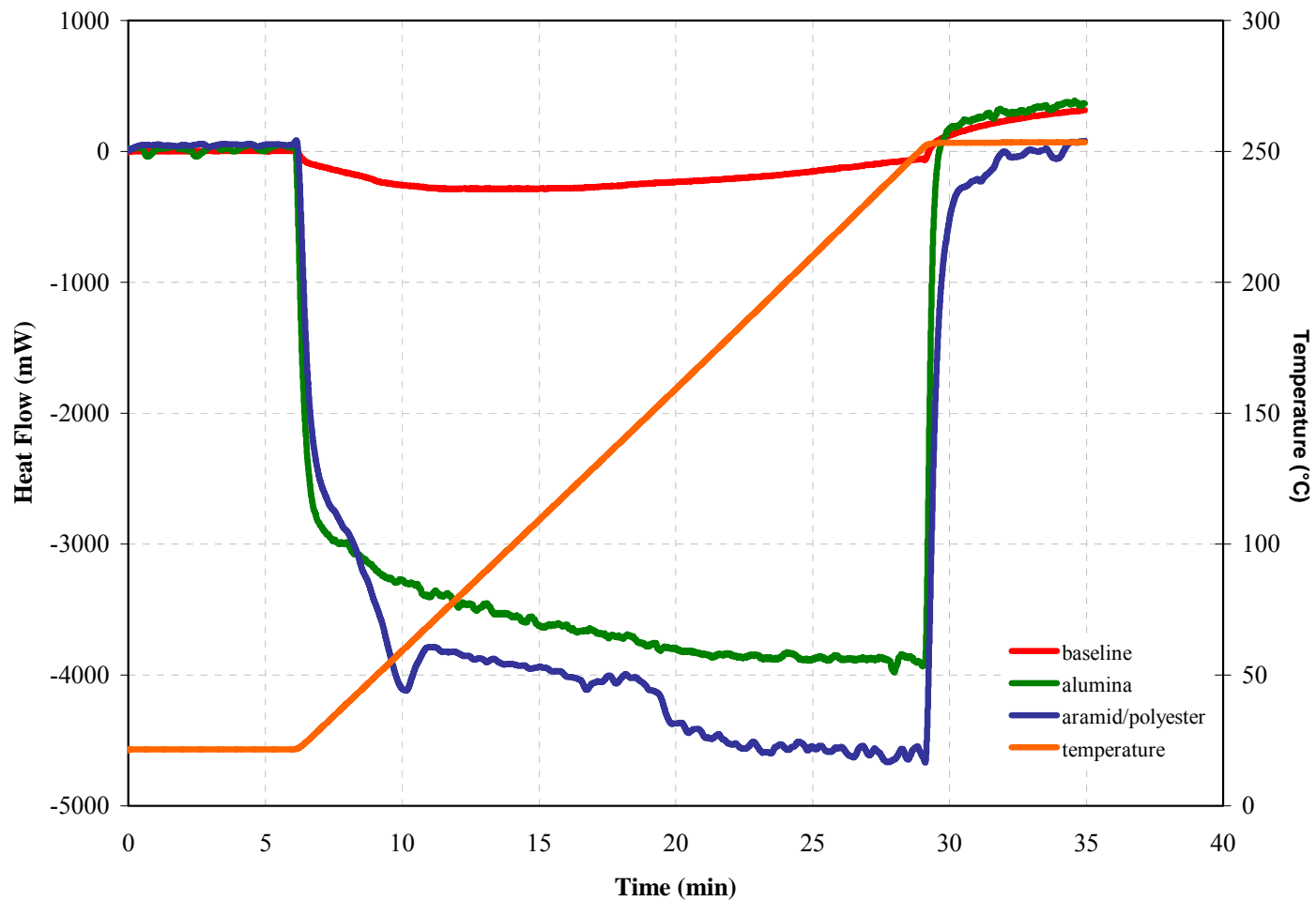
Figure 4.40 DSC heat flow curves for the empty pan baseline, alumina standard and the aramid/polyester composite. The sample weight for the alumina and aramid/polyester were 18.1 and 13.8 mg, respectively. The heating rate was 10 °C/min.
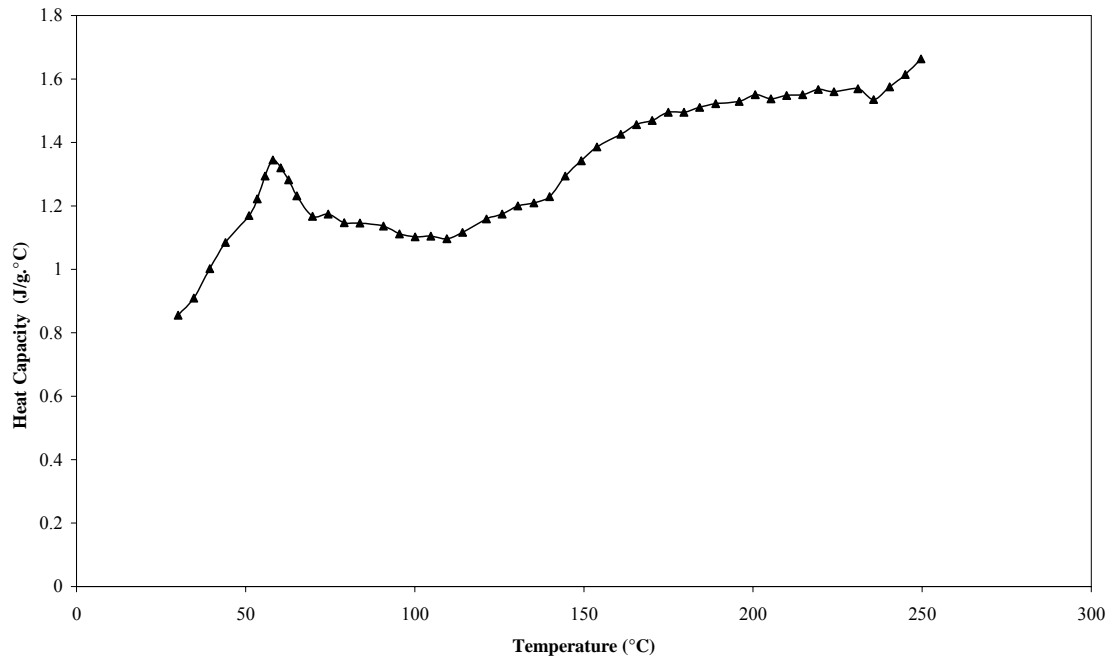
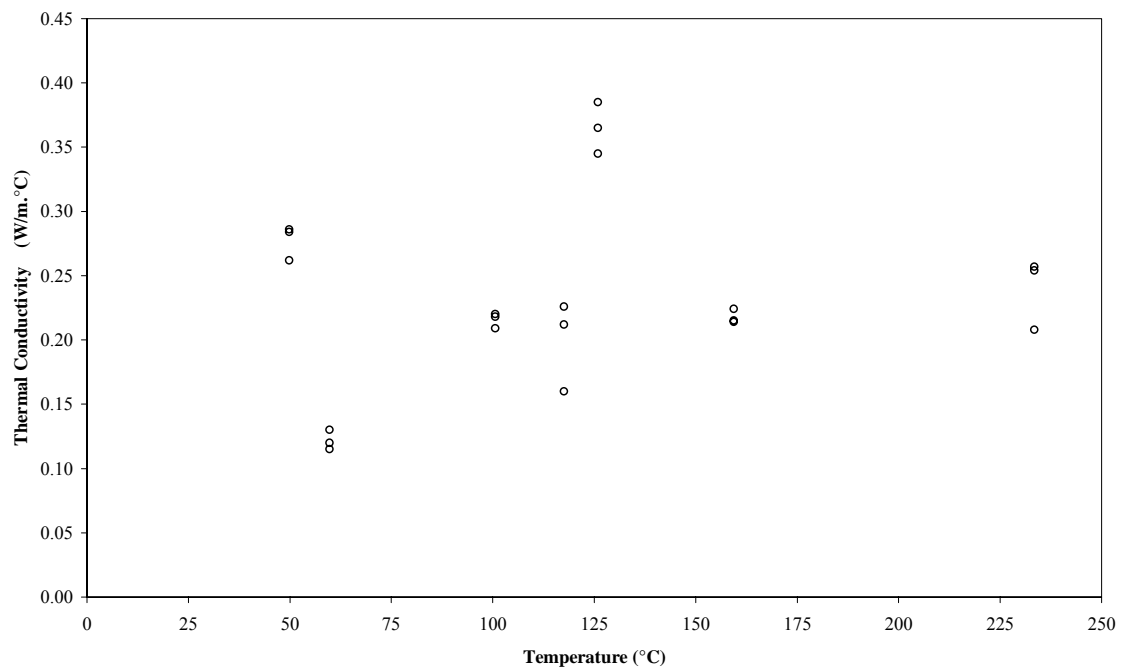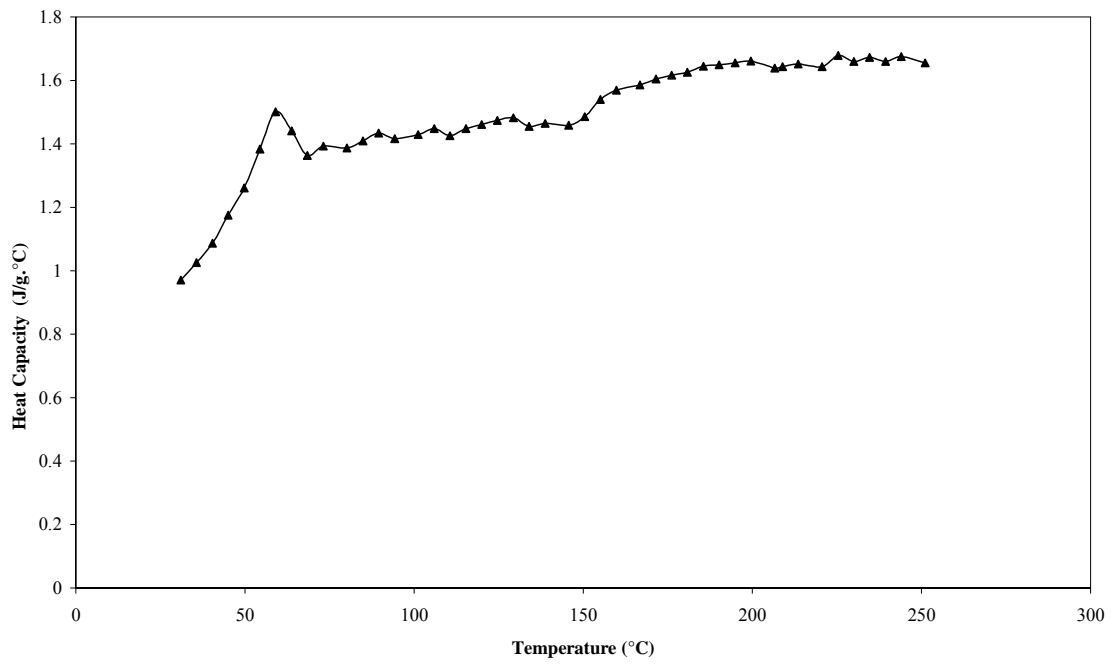Figure 4.41 Heat capacity of aramid/polyester composite material obtained from DSC experiments.
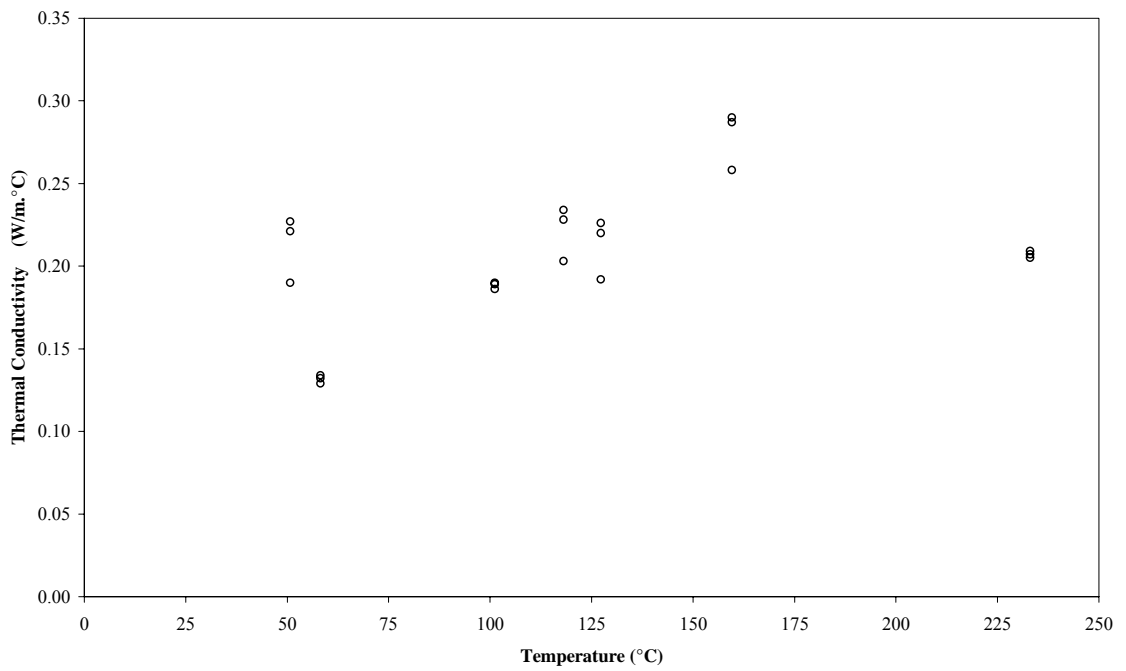
Figure 4.42 Thermal conductivity as a function of temperature for aramid/polyester composite material.

The differences in the C_p values of the tested polyester composites and epoxy composites are noticeable especially in the vicinity of the endothermal peak temperatures of composites and at elevated temperatures. Nevertheless, the heat capacity values of them change, as temperature rises, in a similar manner. In the vicinity of the devitrification temperature and in the solid state far below a devitrification temperature, differences in C_p of the polyester based and epoxy based composites are small. These small deviations are quite explicable and could be attributed to the fact that in the solid state well below the devitrification temperature the heat capacity of the material is mostly due to molecular vibrations as other contributions, i.e. free volume, are normally negligible. It should be noted here that the heat-flux DSC apparatus allows the measurements of C_p of composites with an uncertainty of ±3.5% in the whole temperature interval.

4.4.2 Thermal conductivity

The variations of thermal conductivity with temperature for epoxy based composites are shown in Figures 4.27, 4.30 and 4.33. The plots of the thermal conductivity versus temperature for polyester based composites are presented in Figures 4.36, 4.39 and 4.42. The data observed in these figures appear to be composed of four regions that vary in position as the type of resin used is altered.

In the first region, it is seen that the thermal conductivity of all the composites shows a similar trend of decreasing almost linearly with temperature to a minimum value (Figure 4.27). In these cases, the minimum value of the range of interest is the end of the endothermic process. A dramatic decrement of the thermal conductivity within the designated temperature range most probably is due to the destruction of crystallites in the solid-glass transition range and results in an increase in free volume. The increase in free volume is known to cause a dramatic increase in the distance between the polymer chains and thus an increase the resistance to energy transfer between the polymer molecules. The increment of the thermal resistance would probably result in the decrease of thermal conductivity in this temperature range.

On the other hand, a close look at the values of the thermal conductivity in the first region would provide interesting information about the contributions of various scattering mechanisms at play in determining the thermal resistance of the composites. At temperatures in the vicinity of devitrification region, near the beginning of the endothermic transition, scattering by microvoids (vacant-site scattering) becomes predominant besides structure scattering. As temperature increases and the polymer passes to rubbery through leathery state, gradually individual units, atomic groups and small chain segments undergo intensive thermal motion and large torsional rotations, and the sliding of chain segments starts to play a dominant role in governing the variation of properties with temperature. This has a two-fold effect on the structure of the polymer composites; initially the dominant chain moments create some vacant sites or microvoids which scatter phonons in the similar way to the point defects (Lee, & Millens, 1977). With the rise of temperature, the number and size of these microvoids increases and consequently, the contribution of vacant-site scattering to thermal resistance would increase linearly with temperature. Thus structure scattering and vacant-site scattering become the predominant scattering processes over certain range of devitrification temperature of the fully cured resin resulting in a decrease in the thermal conductivity with a rise of temperature (Figure 4.27).

Even though the temperature rises beyond the endothermic transition initiation region, there is a dramatic decrease (first region) in the thermal conductivity of carbon/polyester composites (Figure 4.39). It is possible to explain this fact as follows: it is believed that, by the effect of the carbon fiber, which is an additional material, in the devitrification region of the some amount of the crystal structure within the resin, has transformed into the endothermic transition centered at around 60 °C, even destroying partially. It is thought that these crystals are primarily destroyed in this endothermic transition. It is explained in details in the prior paragraph, how this destruction causes decrease in thermal conductivity (first region in thermal conductivity-temperature graphic).

The thermal conductivity values for both epoxy based and polyester based composites progressively increases in the second region as the temperature increases (Figure 4.27). The main source of this variation can be directly attributed to the increasing segmental mobility of the polymer molecules. It is believed that the mobility of chain segments is more dominant than the density effect in this region.

For further increase of temperature over the characteristic temperature T_0 where the composite sample started to significantly degrade the effective thermal conductivity showed a decreasing trend for all samples (the third region in Figure 4.27).

Even in amorphous polymers there exists some local order which is termed as intermediate range order (IRO) (Kroschwitz, 1985). In the low temperature region below the characteristic temperature T_0, the temperature dependence of the thermal conductivity is controlled by variation of phonon mean free path. Below T_0 structure scattering and chain-defect scattering are the main phonon scattering mechanisms. In the former case lattice wave propagate uniformly inside each small domain with dimensions equal to the size of the IRO region and then are abruptly scattered by a sudden change of refractive index at the boundary. The dimensions of IRO at T_0 depend mainly on the processing conditions and degree of polymerization; hence it does not vary with temperature. Therefore the contribution to thermal resistance corresponding to these processes is temperature-independent.

As for the chain defect scattering (Perpechoko, 1981), defects introduced by bends and relatively smaller lengths of chain segments also scatter phonons, i.e. the elastic wave propagating along the chain finds itself at a point beyond which it can no longer proceed in the same direction with the same velocity. Therefore it is reflected along the same chain or is refracted along some other permitted direction. In the temperature region below T_0, with a rise in temperature the polymeric chains straighten out more and more, increasing the corresponding mean-free path and thus the contributions to the corresponding thermal resistance decreases linearly with the rise of temperature. This increased the effective thermal conductivity of the polymer

composite, and it became maximum in the vicinity of the characteristic temperature T_0 (the second region in Figure 4.27).

As in aramid fiber/polyester composite graphic (Figure 4.42), in some graphics various ups and downs are observed in the second region by the increase of temperature. It is known that, when the temperature of the composite increases, air voids are created between the fiber material and the matrix material due to the separation of these components. It is thought that, these ups and downs in thermal conductivity may have occurred because of the air voids.

In the third region, it has been found that the thermal conductivity of the composites falls dramatically as the temperature increases up to the characteristic temperature T_0 (Figure 4.27). This fall in thermal conductivity may be attributed to possible crosslinking and degradation effects which are indicated by the DSC curve as shown in Figures 4.25, 4.28, 4.31 for epoxy based composites and Figures 4.34, 4.37, 4.40 for polyester based composites. Based on the mentioned non-isothermal thermogram of composites, no exotherm peak was observed at high temperatures; however, it is also noticed that DSC trace has a small exothermic plateau appearing at the higher temperature side. In other words, a local overheating was observed for the composites when the temperature exceeded considerably the maximum endothermal peak temperature. It must be emphasized that in this work, this exothermic plateau is associated with the reaction in the unpolymerized portion in the resin, this transition indicating the crosslinking and degradation of the polymer.

The crosslinking of thermosetting materials generally involves the transformation of low molecular weight liquids to amorphous networks with infinite molecular weight by means of exothermic chemical reactions. Besides, when thermosets are being used, the degradation can be highly exothermic. The exothermic heat released during the crosslinking and degradation process can possibly cause excessive temperatures in the interior of composites. Thus the recorded temperature gradient in the composite produced by an imposed heat flow will be reduced to some extent. This thermal behavior exhibited by such composites depends strongly on the rate of

degradation and crosslinking process. Consequently, the reduced temperature gradient found in the composites during the crosslinking and degradation of thermosetting materials, produced a reduction in the rate of heat conduction through the polymer and thus an apparent reduction in the corresponding value of the thermal conductivity (the third region in Figure 4.27).

From a closer observation on the fourth region (refer to Figure 4.27), it can be revealed that the char/fiber material was measured to have the next highest thermal conductivity and was measured to increase steadily with temperature. The decomposed char/glass fiber sample was observed to have air voids along the sample cross-section and some cracks between plies; however, after completing the calorimetric experiment the thickness of the sample differed significantly from the initial sample thickness prior to the beginning of measurements. In the char/glass fiber material, since the presence of high conductive media, which has a much higher thermal conductivity than that of polymers, the increase in thermal conductivity may be expected for these char/fiber materials as they degrade. The rate of increase of the char/glass material conductivity with temperature in the fourth region was slower than that of the virgin composite material in the second region.

In some graphics (Figures 4.30, 4.33, 4.39 and 4.42), the fourth region, where the thermal conductivity increases depending on temperature, is not detected. This observation points out that, at the temperature region mentioned, the degradation process of the matrix material still continues. It is believed that, the material is not in the char/fiber condition which is necessary for the thermal conductivity to increase by temperature beyond the third region. It is possible to comment this as a result of the interaction between the matrix and the fiber or the effect of fiber on the matrix material.

From the analysis of the results it can be said that though the volume content of different types of fibers in the matrix varies in the epoxy based composites, the influence of changing the fiber type on the temperature dependency of thermal conductivity would be much less important. Composites made with unsaturated

polyester resin present very similar behavior as in the case of epoxy based composites. Consequently, it can be concluded that a continuously-reinforced composite's through-the-thickness thermal conductivity is strongly affected by and perhaps dominated by the conductivity of the polymer matrix. It is evident that phase transition with temperature in the polymer matrix becomes important when analyzing the through-the-thickness thermal conductivity data in fiber reinforced composite materials.

At higher test temperature all phonon scattering mechanisms take place. Therefore, it is much more difficult to understand the actual nature of diffusion of heat in relation to structure of fibers and matrix, voids and fiber-matrix interfaces. However, the mentioned complexity becomes much easier to understand in lower temperature region where the sample needs to be as close to room temperature as possible since the thermal conductivity would be comparatively very structure sensitive of fiber reinforced composites. Regarding the argument in this paragraph, from a closer observation on the experimental data relating to lower temperature region, it can be revealed that polyester based composites made with glass and carbon fabrics exhibit high through-the-thickness thermal conductivity as compared to epoxy based ones. The reason may lie with the microstructures of polyester matrix that may help in diffusion of heat in the thickness direction in which thermal conductivity was measured.

An interesting thing is that, at temperatures in the vicinity of glass transition region, although the heat capacity is more in case of epoxy based composites made with glass and carbon fabrics the through-the-thickness thermal conductivity is higher for polyester based composites having same reinforcements. It must be emphasized here that, epoxy based composites made with glass and carbon fabrics exhibit high heat capacity does not point out that they showed highest through-the-thickness thermal conductivity as compared to polyester based ones having same reinforcements. So again, it is clear that aramid fiber accelerates the diffusion of thermal energy in the direction perpendicular to the fibers in case of epoxy based composites compared to polyester based ones.

Thermal properties data published for composites made with same matrix and having same reinforcements used in this study were reviewed and collated (Sweeting, & Liu, 2004; Pilling et al., 1979; Gowayed, & Jhy-Cherng, 1995; Ott, 1979; Kalogiannakis et al., 2003). The values for thermal conductivity and heat capacity obtained in this work are generally lower than those found in the literature. A large number of literature values vary drastically. This makes a direct comparison difficult, as no data can be found for fiber content range of interests. In the published works, different type of commercially available epoxy resins, as well as polyester resins were selected for composite manufacturing. The mentioned selection is such an important factor that the evaluations on the properties of composites cannot be made unless a common type of epoxy resin is used in composite production. This selection may provide an explanation as to the variance in the density and consequently in the thermal properties of the composites.

The measurement method used in this study, necessiates round specimens as thin as possible, as mentioned earlier. Extraction of specimens from composite plates is an arduous and sensitive process. If the fabric layer number is greater than one, it has been observed that during this process, specimens have been deformed along the fabric interfaces. Therefore, the number of fabric layers used for the production of the composite material has been limited to one and, in accordence, measurements have been carried out over a single fiber volume fraction. This makes it difficult to compare the data directly with the ones in literature. It is a known fact that the variation of thermal properties is related to fiber volume fraction. Despite these complications mentioned above, when comparison has been made by considering the variation of volume fraction, it has been determined that data in this study shows similarity to literature from time to time. For example, Sweeting et al., (2004) measured experimentally the thorough-the-thickness thermal conductivity of carbon/epoxy laminates. The fiber volume fraction of the laminates was 49% and measurements were performed from room temperature to 180 °C. Within the temperature range, they reported that the through-the-thickness thermal conductivity changes from approximately 0.5 to 0.7 W/m.K. At this point, it is necessary to emphasize that a large number of measurements have been performed on epoxy

based composites in the literature, while no data related to thermal conductivity, as well as heat capacity was found for polyester based composites, particularly made with carbon fiber. This case, unfortunately, makes difficult to evaluate the experimental results on the basis of published data.

Due to difficulties in controlling the test conditions such as changes in degree of contact between the base of aluminum sensor container and the composite sample, the behaviors of the experimental thermal conductivity values show a wide scatter of as much as ±41%. The contact area between the composite sample and the calorimeter cup potentially maximize severe effects of the scatter in thermal conductivity data due to composite sample often tend to warp and buckle upon heating.

4.4.3 Thermal Stability

The TGA scan in the form of weight loss versus temperature for epoxy based composites is plotted in Figure 4.43 for decomposition in an air atmosphere. There is a small change in the decomposition curve at the beginning. TGA decomposition curve of glass/epoxy composite shows an initial weight loss of about 1.9% below 295 °C. It is well known that at a slower heating rate, decomposition may be more evident. Hence, the composite is run in a TGA at a heating rate of 20°C/min. In thermogravimetry analyzers, the drift of baseline due to air buoyancy effects of the sample container and convection cannot be ignored. Considering all these factors, this small weight loss in the beginning is believed to be the vaporization of water absorbed in a composite during the storage period. That the loss occurred in a wide temperature range up to 295 °C means that the sample contains not only absorbed water, but also water of highly bonded. In DTA curve, the loss of water of crystallization is shown by a broad endotherm. It should be noted here that the apparatus used in this measurement was of suspension type, and it excels in vibration resistance, and the macrocell can be used. It is therefore possible to sample a large amount and it is particularly suited to determine of trace elements. Brennen & Cassel (1978) used a TGA to measure moisture content in an epoxy for PC board and observed a similar change. They found that moisture vaporized slightly above the glass transition temperature of the epoxy.

Between 295 and 347 °C, there is a gradual weight loss of about 6.5% due to volatilization of unreacted small molecules such as accelerator/hardener etc. which continues for some period at a very slow rate. As the actual decomposition of the cured composite materials begins at elevated temperatures, the weight loss occurs at a faster rate. As seen in the Figure 4.43, the majority of the sample decomposition occurs over a relatively wide temperature range (347–458 °C). The intersection point between the starting mass line (during the unreacted hardener elimination) and the maximum gradient tangent to the TGA curve basically provide primary onset of decomposition temperature. This temperature was directly computed by the TGA instrument.
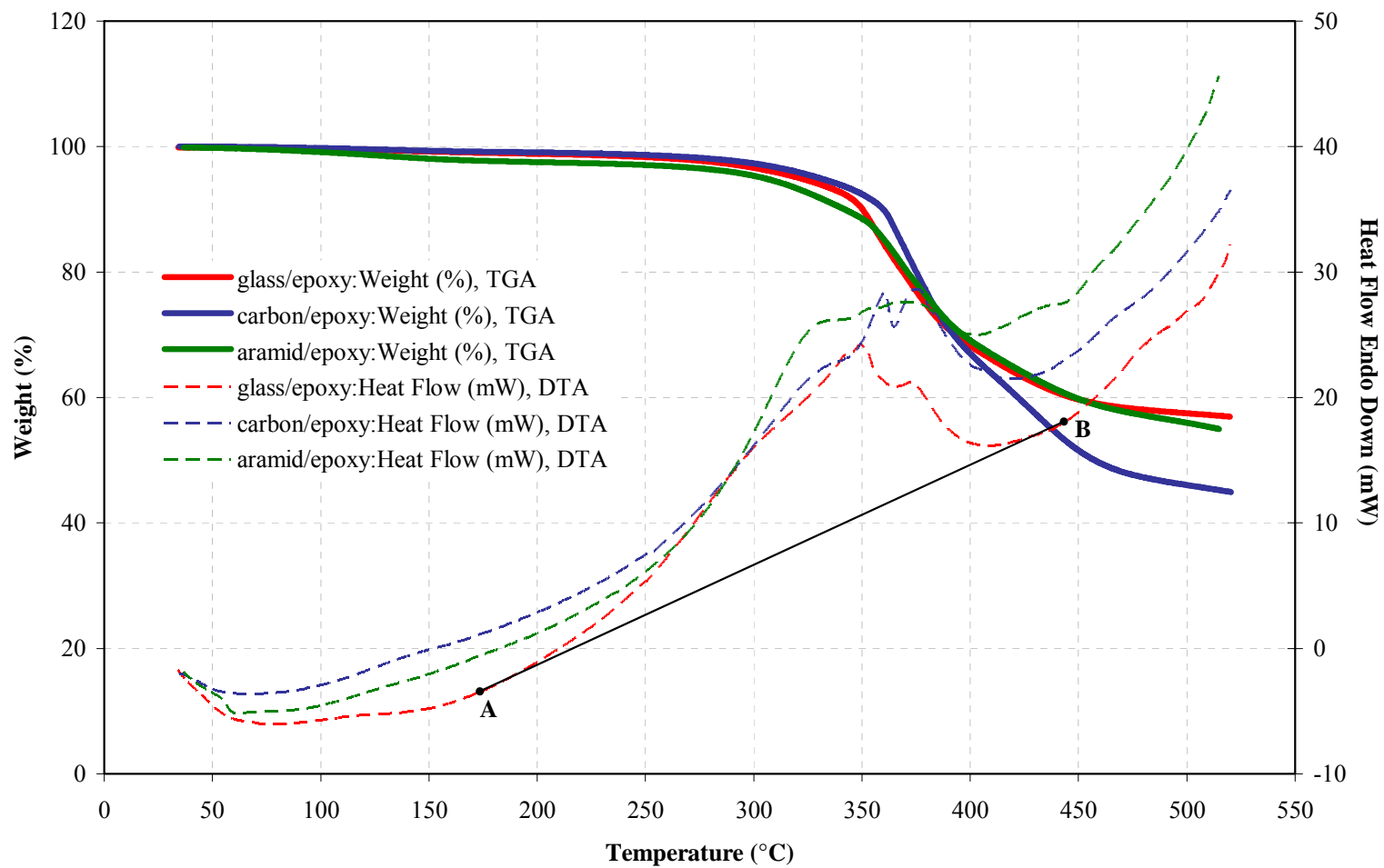
Figure 4.43 TGA thermogram of epoxy based composites in air atmosphere at a heating rate of 20 °C/min with the corresponding DTA plot.

The polymer decomposition begins at 347 °C and gets completed at 458 °C with a total weight loss of 42.9%. The weight loss of composites in this step may be attributed to the decomposition of the cross-linked polymer backbone structure. This degradation step is accompanied by an exothermic effect in the simultaneous differential thermal analysis (DTA) curve composed of two peaks centered at 347 and 378 °C. Almost no decomposition occurs below 295 °C, while above 458 °C the decomposition continues to slowly occur until it stops at approximately 550 °C.

It should be noted here that it was, of course, not possible to directly compare the TGA and DTA spectra for the composites, as the composites under consideration have different volume fraction of the fiber content. The examination of the corresponding TGA and DTA curves does not show any significant differences between the two composites made with glass and carbon fiber. The DTA curve of carbon fiber/epoxy composite is made up two peaks, similar to the glass fiber/epoxy composite. However, the peak shifts towards high temperature are more marked. Based on the results of the TGA/DTA experiments for carbon fiber/epoxy composite it can be clearly seen that the second DTA peak is now larger than the first one. It indicates that a prominent weight loss is observed in the second exothermic peak zone at around 375 °C.

The TGA and corresponding DTA data obtained for aramid/epoxy composite in air atmosphere is also given in Figure 4.43. Two major stages of weight loss can be observed in TGA curve as in the case of glass fiber/epoxy composite mentioned above. The thermogram of aramid/epoxy composite show a steady weight loss up to 353 °C (12% weight loss) and thereafter the polymer decomposition occurs. Since a close correspondence is seen between the measured mass fractions of glass and aramid fiber, the comparison of TGA/DTA curves of glass/epoxy composite with those obtained for the aramid/epoxy composite could be possible. A closer observation on the TGA curve indicated that the temperature at which the rate of mass loss is a maximum is increased by 6 °C, as compared to that in glass /epoxy composite. The major decompositions as revealed from the TGA inflections that occur at 353 °C in the case of aramid/epoxy composite, while it is 347 °C for

glass/epoxy composite. This indicates that the aramid/epoxy composite is thermally more stable than the glass/epoxy composite, although the difference is not remarkable. Simultaneous DTA measurements, presented in Figure 4.43, reveal a broad exotherm in the region of 329 °C for the aramid fiber/epoxy sample, whereas two exothermic peaks are observed on DTA curves of glass fiber/epoxy and carbon fiber/epoxy composites.

The total enthalpy of reaction can be determined by integrating (with respect to time) the area between the exothermic energy rate and the straight line between two chosen points A and B in Figure 4.43. The measured enthalpies of reaction for the aramid/epoxy and glass/epoxy composite are found to be 172.90 and 155.17 J/g, respectively (Table 4.10). As compared to the glass/epoxy composite, a significant increase of %11 in the enthalpy of reaction of the aramid/epoxy composite could be attributed to the effectiveness of the interface that consists of the bond between aramid fiber and epoxy resin and the immediate region adjacent to this bond. DTA results also revealed that aramid/epoxy composite is thermally more stable than is glass/epoxy composite.

Figure 4.44 shows TGA thermograms of the polyester based composites investigated in this study. The weight loss behavior of these polyester based composites containing different type of fiber reinforcements was found to follow the patterns as in the case of epoxy based composites discussed above. However, it is especially noteworthy that the percentage weight loss due to loss of moisture in the case of glass/epoxy, carbon/epoxy and aramid/epoxy composite are observed at temperatures of 295, 297 and 294 °C, respectively, while the corresponding values are 182, 170 and 132 °C for glass/polyester, carbon/polyester and aramid/polyester composite, respectively. It is possible to relate this result to the fact that the polyester based composites contain only absorbed water. But contrary to epoxy based composites, polyester composites may not contain water of highly bonded.

Table 4.10 TGA/DTA analysis

Sample Specimen	Peak Temperature	Enthalpy change (mJ)	ΔH (J/g)	Nature of the peaks
Glass/epoxy composite	348.94	3091.45	155.17	Exothermic
Carbon epoxy composite	360.21	2699.45	302.32	Exothermic
Aramid/epoxy composite	329.07	1908.00	172.90	Exothermic
Glass/polyester composite	405.62	417.58	33.17	Exothermic
Carbon/polyester composite	418.13	1510.77	263.26	Exothermic
Aramid/polyester composite	414.51	295.48	28.84	Exothermic
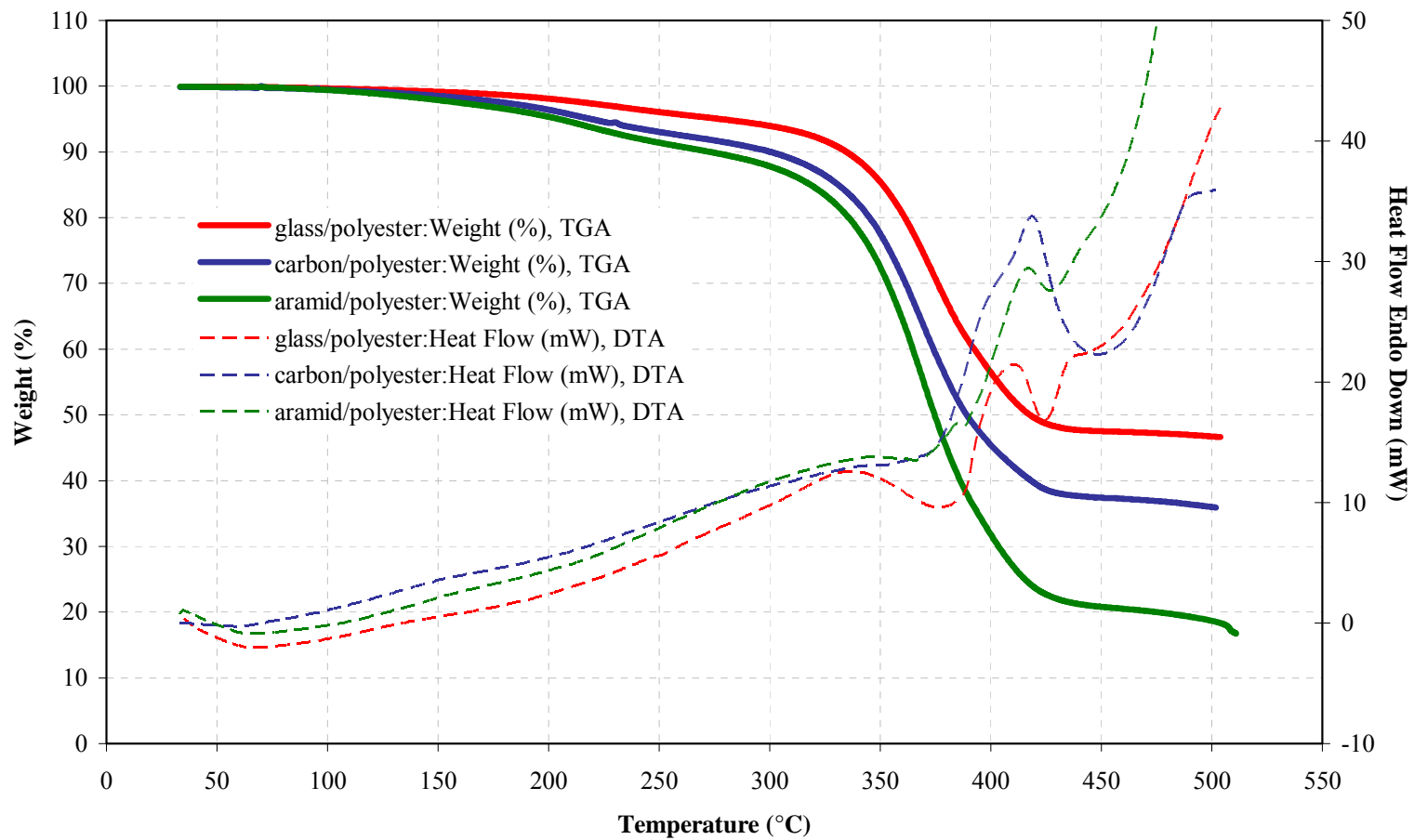
Figure 4.44 TGA thermogram of polyester based composites in air atmosphere at a heating rate of 20 °C/min with the corresponding DTA plot.

The difference in degradation behaviour of the polyester based composites containing various fiber reinforcements could be clearly read from the DTA thermograms. The corresponding results are presented in Table 4.10. Based on the numbers of peaks in the DTA curve, the weight loss processes of the glass/polyester and aramid/polyester composites was considered as several stages (Figure 4.44). The DTA plot of polyester based composite having glass fiber shows one weak endothermic transition centred at around 70 °C followed by an endothermic peak centred at around 383 °C and an exothermic peak centred at around 406 °C. It is believed that, the weak endothermic transition in the low temperature range may correspond to an evaporation of moisture and excessive curing agents (the catalyst/retarder systems) from the polymeric matrix. When the DTA curves have been discussed in the light of this information mentioned, the weak endothermic transition occurred in a wide temperature range indicates that there was large quantity of curing agents confined in the polymeric precursor even though the resin was charred. Similar comments can be said about the weak endothermic transition in the low temperature range observed in DTA curve of aramid/polyester composite.

The endothermic peak centred at around 383 °C in the DTA curve of glass/polyester composite may be attributed to the melting of the polymeric matrix. It is possible to arrive this conclusion by a careful examination of the DTA curves; the endothermic transition around 375 °C is much weaker in aramid/polyester composite compared to glass/polyester composite. The type of fiber used may be thought to be responsible for the variation of intensities of endothermic peak observed in DTA curves.

The pronounced exothermic peak appearing in the DTA curves above 350 °C correspond to the degradation of the polymeric material. It should be noted here that different degradation behavior in the DTA curves of polyester based composites made with glass and aramid fibers may be due to the chemical reaction between the mentioned fiber reinforcement and the polyester resin. These stages of weight loss, however, were not observed in DTA curves for the glass/epoxy and aramid/epoxy composites (Figure 4.43).

There was also very little difference in the fiber volume fraction of both composites reinforced with same type of fibers. Nevertheless, in one of the ordinates of graphics, presenting weight loss as a percentage depending on temperature, and in the other presenting the energy required for this weight loss makes an indirect comparison possible. The measured enthalpy of reaction for the major decomposition peak of glass/polyester composite is found to be less than that of glass/epoxy composite. From a closer observation on the DTA test data (refer to Table 4.10) it can be revealed that the values of the measured decomposition enthalpies of the carbon/polyester and aramid/polyester composites are lower than those observed in epoxy based ones.

Contrary to epoxy based composites, the decrease in enthalpy may be directly attributed to the weak interaction between fiber and polyester resin. Although it is seen from the TGA curve that the degradation process continues, at the simultaneous DTA curve, it is of interest to observe that for the same region, no exothermic peak, indicating degradation, has been detected (Figure 4.44). When the DTA curve has been examined, it has been determined that exothermic peaks have shifted towards high temperature values. It might be possible to explain this striking result as; polyester resin undergoes serious degradation during this process (TGA curve). However, this degradation has a quantitative characteristic during the process towards high temperature values, in which the exothermic peaks are formed. In DTA curve, quantitative degradation has transformed into a qualitative characteristic in the temperature region, where the exothermic peaks are observed. Degradation, which has gradually progressed so far, has suddenly exposed itself at regions near the completion of the process. Contrary to epoxy based composites, it is possible to explain this process met in polyester based composites, by the properties of polyester resin and its interaction with the fiber material. It must be emphasized here that, shifting of the exothermic peaks in polyester based composites towards to high temperature region does not point out that they are more stable than epoxy based composites. What is of importance is the energy required for degradation to occur. As mentioned earlier, the enthalpy difference necessary for degradation is much greater in epoxy based composites compared to polyester based composites.

It must be emphasized that, although weight loss ratios are greater in polyester based composites compared to epoxy based composites, the energy required for this weight loss is less when again compared to epoxy based ones. It has been concluded based on the findings that, polyester based composites are thermally less stable than epoxy based ones.

CHAPTER FIVE
CONCLUSION

The remark, based on the observations while tensile testing, is that the stress-strain curves of polyester based and epoxy based composites reinforced with non-crimp stitched glass and carbon fabrics were linear in the direction of fibers. However, in the matrix dominated orientations non-linear relation between the stress and the strain was observed. The ultimate strength of laminates was lost in the matrix dominated orientations owing to the matrix-controlled failure mode.

As might be hoped, this work has not just quantified the qualitative measurements; it has also produced a number of quite unexpected results as well. In particular, the quasi-isotropic carbon fabric laminates behaves as an anisotropic materials in which the experimental data do not allow for an adequate description of the quasi-isotropic model. It has been shown that the complex combination of fiber orientation, loading direction and stitch rows run nearly parallel to these directions as a consequence of the lay up of NCF blankets plays a major role in the tensile strength of composites.

Similar comments can be said about the flexural strength/middle-span deflection responses in the test directions performed on the specimens as in the results on tensile stress/strain response. The lamina stacking sequence has a significant effect on the recorded values of the flexural strengths. It is observed that the specimens in the direction of fibers offer substantially greater load capacity than that obtained with the specimens in the matrix dominated orientations, indicating that failure controlled by fiber directionality can have beneficial effect on load carrying performance.

Perhaps the most significant result of this investigation is the strong correlation between the changes in interlaminar shear strength values and fiber orientation angle. In addition, the lamina stacking sequence and laminate type have a significant effect on the recorded values of the interlaminar shear strengths. It has been observed that the recorded values of the flexural strength of laminates were at least an order of

greater than that obtained from short beam shear tests at all the considered test directions.

It has been concluded based on the discussed data that, matrix-fiber interactions that promote strong bonds will not produce a high strength composite when measured parallel to the direction of the fibers.

In this study, a more detailed description, including actual photographs of fractured tensile specimens resulting from a variety of uniaxial loading conditions, of the dependence of the fracture surface on the geometric variables of the fibers is provided. Photographs of fracture surfaces of multiaxial composites loaded in tension along the fiber direction exhibits pronounced irregularity and fiber pullout. By examining actual photographs it is clear that the fracture surface of the composite having plies ±45° with fibers exhibits both longitudinal type and transverse type fracture characteristics.

The fracture surface of composites was examined using the scanning electron microscopy after measuring the tensile tests in machine direction and documented in representative photomicrographs. Composites observed under different moderate magnification levels show obvious differences between good bonding rarely and poor bonding commonly at the interface. A chemically non-coupled composite showed uncoated clean fiber ends pulled from the polymer. Even the highest magnification could not show the presence of a monolayer of polyester resin on fiber.

A comparison of the infrared curves shows evidence for the inability of carbon and glass fiber to alter the absorption band of the cured neat polyester resin used in this study. From this comparison, it may be concluded that a strong interaction does not occur between polyester resin and both types of fibers. On the basis of FTIR results, it is probable that a strong interaction between carbon fiber and epoxy resin occurs in comparison with epoxy resin and glass fiber.

It is found that the type of fibers and matrix present in the composites influences the heat capacity (absorption) and thermal conductivity (transmission) of thermal energy. Polyester based composites having same reinforcements showed lowest heat capacity as compared to composites made with epoxy as matrix. This brings out that the microstructure of the resin matrix within the composites is found to be influencing the amount of thermal energy absorbed by the composites and consequently heat capacity of the composites.

It is worth noting that the outstanding thermophysical properties of composites result from the chemical or physical processes taking place at the interfaces between the fibers and the surrounding matrix. Consequently, thermophysical properties, i.e., thermal conductivity and heat capacity, are the most structural dependent properties, depending both on macrostructure i.e. voids, cracks, defects as well as microstructure i.e. perfection and orientation of crystallites. Composites being a two phase material with boundaries between them, and the degrees of percolation network in the composite system due to differences in fiber and resin type used may vary a lot in both macrostructure and microstructure and hence in thermal properties.

Composites display a characteristic jump in heat capacity around the devitrification temperature. The rapid increase in the heat capacity on the devitrification is caused by the beginning of large-amplitude motion that is characteristic of the liquid. As temperature increases and the polymer passes to rubbery through leathery state, small chain segments undergo intensive thermal motion and the sliding of chain segments play a crucial role in governing the characteristic changes of heat capacity in the vicinity of devitrification region. It was concluded from this study that, in the endothermic transition region, the peaks of the temperature dependences of the heat capacity of polyester composites were small as compared to that of epoxy composites. A relative reduction of the intensity of peaks seemed to indicate that, during the initial interval of the endothermic transformation, the increase in configurational and/or vibrational contributions in the liquid state originated by the network growth for polyester based composites were lower than those of epoxy based composites.

Differential scanning calorimeter apparatus was found to be a reliable and accurate technique for the determination of the thermal conductivity of various composite materials. The data can be observed to be composed of four regions over the range of temperature tested. A dramatic decrement of the thermal conductivity within the first region can be probably attributed to the destruction of crystallites in the solid-molten transition range and results in an increase in free volume. As it is well known, the increase in free volume can possibly cause an increase in the distance between the polymer chains and thus an increase the resistance to energy transfer between the polymer molecules. Therefore, the increment of the thermal resistance could probably result in the decrease of thermal conductivity in the first temperature range.

The results, which indicate that the thermal conductivity in the second temperature region shows an increasing trend, are interpreted in the light of various phonon scattering mechanisms, namely, structural scattering, stray scattering and chain defect scattering. In this region, with a rise in temperature the polymeric chains straighten out more and more, increasing the corresponding phonon mean-free path. Depending on the mentioned physical state, the contributions to the corresponding thermal resistance decreases linearly with the rise of temperature. It may be that this reduction in the thermal resistance results in the increase in thermal conductivity in the second temperature range.

The heat transfer mechanism is a complex phenomenon because it is primarily governed by atomic level structure in the composites. There are, also other events that increase the complexity of the heat transfer mechanism, such as the elevated test temperatures and the phase transition phenomena. In the third region, the fall in thermal conductivity may be attributed to the reduced temperature gradient found in the composites during the crosslinking and degradation of thermosetting materials. It is believed that the mentioned reduced temperature gradient produced a reduction in the rate of heat conduction through the resin matrix and thus an apparent reduction in the corresponding value of the thermal conductivity.

From a closer observation on the fourth region, it can be revealed that the thermal conductivity of the char/fiber material steadily increases with temperature. Because of the presence of high conductive media, which has a much higher thermal conductivity than that of resin matrix, the observed increase in thermal conductivity may be expected for these char/fiber materials as they degrade.

It can be concluded from the analysis of the results that through-the-thickness thermal conductivity of continuously-reinforced composites is strongly affected by and perhaps dominated by the conductivity of the resin matrix. At this point, it is necessary to emphasize that phase transition with temperature in the polymer matrix play a crucial role when analyzing the through-the-thickness thermal conductivity data in continuously fiber reinforced composites.

It is interesting to observe that, around the devitrification temperature, though the heat capacity is more in case of epoxy based composites made with glass and carbon fabrics the through-the-thickness thermal conductivity is higher for polyester based composites having same reinforcements. It should be strongly emphasized here that, the mentioned epoxy based composites exhibit high heat capacity does not mean that they showed highest through-the-thickness thermal conductivity as compared to polyester based ones. In addition, it is concluded again that aramid fiber accelerate the diffusion of thermal energy in the direction perpendicular to the fibers in case of epoxy based composites compared to polyester based ones.

A careful observation on the TGA thermograms of the composites revealed that the weight loss behavior of polyester based composites containing different types of fiber reinforcements was found to follow the pattern as in the case of epoxy based ones. However, the difference in degradation behavior of the polyester based composites could be clearly read from the DTA thermograms. From a closer observation on the DTA test data revealed that the values of the measured decomposition enthalpies of the polyester based composites are lower than those in epoxy based ones, both having same fiber reinforcements. As compared to epoxy

based composites, the reduction of enthalpy may be directly attributed to the weak interaction between the fiber and polyester resin.

A careful comparison between the DTA thermograms of composites made with epoxy and polyester as matrix revealed that, in case of polyester based composites, degradation, which has gradually progressed so far, has suddenly exposed itself at region near the completion of the process. It should be emphasized here that, shifting of the exothermic peaks in polyester based composites towards to region near the completion of the process does not mean that they are thermally more stable than epoxy based ones. The enthalpy difference required for degradation to occur is much greater in epoxy based composites compared to polyester based ones. It can be concluded based on the findings that, epoxy based composites are thermally more stable than polyester based ones.

REFERENCES

Agari, Y., & Uno, T. (1986). Estimation on thermal conductivities of filled polymers. *Journal of Applied Polymer Science,* 32 (7), 5705-5712.

Agari, Y., Ueda, S., & Nagai, S. (1993). Thermal conductivity of polymer composite. *Journal of Applied Polymer Science*, 49 (9), 1625-1634.

Al-Sulaiman, F. A., Mokheimer, E. M. A., & Al-Nassar, Y. N. (2006). Prediction of the thermal conductivity of the constituents of fiber reinforced composite laminates. *Heat Mass Transfer*, 42, 370-377.

Bibo, G. A., Hogg, P. J., & Kemp, M. (1997). Mechanical characterisation of glass and carbon fibre reinforced composites made with non-crimp fabrics. *Composites Science and Technology*, 57, 1221–41.

Bischoff, T., Wulfhorst, B., Franzke, G., Offermann, P., Bartl, A. M, Fuchs, H., Hempel, R., Curbach, M., Pachow, U., & Weiser, W. (1998). Textile reinforced concrete facade elements—an investigation to optimize concrete composite technologies. In *Proceedings of the International SAMPE Symposium*, 43 (2), 1790-1802.

Bjeletich, J. G., Crossman, F. W., & Warren, W. J. (1979). The Influence of Stacking Sequence on Failure Modes in Quasi-isotropic Graphite-Epoxy Laminates. In J. R. Cornie, & F. W. Crossman, (Eds.), *Failure Modes in Composites-IV* (118). New York: Metallurgical Society of AIME.

Boller, A., Jin, Y., & Wunderlich, B. (1994). Heat capacity measurement by modulated DSC at constant temperature. *Journal of Thermal Analysis*, 42 (2-3), 307-330.

Brennan, W. P., & Cassel, R. B. (1978). Applications of thermal analysis in the electrical and electronic industries. *Thermal Analysis Application Study*, *25*, 1-13. Retrieved October 11, 2005, from Sage Journal Online.

Brown, R. (Ed.). (1999). *Handbook of Polymer Testing*. New York: Marcel Dekker.

Bujard, P., Kuhnlein, G., Ino, S., & Shiobara, T. (1994). Thermal conductivity of molding compounds for plastic packaging. *IETT Transactions on Components, Packaging, and Manufacturing Tecnology Part A*, 17 (4), 527-532.

Camirand, C. (2000). Étude de la chaleur spécifique et de la conductivité thermique des hydrures métalliques par calorimétrie différen tielle, *Master's Thesis*, Université du Québec à Trois-Rivières, Trois-Rivières.

Chamis, C. C. (1984). Simplified composite micromechanics equations for hygral thermal and mechanical properties. *SAMPE Quarterly*, 15 (3), 14-23.

Corten, H. T. (1968). Influence of fracture toughness and flaws on the interlaminar shear strength of fibrous composites. In R. T. Schwartz, & H. S. Schwartz, (Eds.), *Fundamental aspect of fiber reinforced plastic composites* (89-107). New York: John Wiley & Sons.

Crookston, J. J., Long, A. C., & Jones, I. A. (2005). A summary review of mechanical properties prediction methods for textile reinforced polymer composites. *Proceeding of the Institution of Mechanical Engineers, Part L: Journal of Materials: Design and Applications*, 219 (2), 91-109.

Çengel, Y. A. (1998). *Heat transfer: a practical approach*. USA: McGraw-Hill.

De Araujo, F. F. T., & Rosenberg, H. M. (1976). The thermal conductivity of epoxy-resin/metal-powder composite materials from 1.7 to 300 K. *Journal of Physics D: Applied Physics*, 9, 665-675.

Demain, A., & Issi, J. P. (1993). The effect of fiber concentration on the thermal conductivity of a polycarbonate/pitch-based carbon fiber composite. *Journal of Composite Materials*, 27 (7), 668-683.

Dexter, H. B., & Hasko, G. H. (1996). Mechanical properties and damage tolerance of multiaxial warp-knit composites. *Composites Science and Technology*, 56 (3), 367.

Dexter, H. B. (1996). Innovative textile reinforced composite materials for aircraft structures. In *Proceedings of the 28th International SAMPE Technical Conference*, 28, 404-416.

Dhami, A. K., & Dey, T. K. (2000). Temperature dependence of thermal conductivity of vanadium substituted BPSCCO system between 10 and 150 K. *Bulletin of Materials Science,* 23 (5), 439-445.

Drapier, S., & Wisnom, R. M. (1999). Finite-element investigation of the compressive strength of non-crimp-fabric-based composites. *Composites Science and Technology*, 59, 1287–1297.

Drapier, S., & Wisnom, R. M. (1999). A finite-element investigation of the interlaminar shear behaviour of non-crimp-fabric-based composites. *Composites Science and Technology*, 59, 2351-2362.

Du, X., Xue, F., & Gu, Z. (1986). Experimental study of the effect of stitching on strength of a composite laminate. In *Proceedings of the International Symposium on Composite Materials and Structures*, 912-918.

Edgren, F. (2006). Physically based engineering models for NCF composites. Ph.D. dissertation, Department of Aeronautical and Vehicle Engineering, School of Engineering Sciences, Stockholm, Sweden.

Edgren, F., Matsson, D., Asp, L., & Varna, J. (2004). Formation of damage and its effect on non-crimp fabric reinforced composites loaded in tension. *Composites Science and Technology*, 64, 675–692.

Filsinger J., Dittmann R. P, & Bischoff T. (2004). Textile preforming technologies for fuselage applications. In *Proceedings of the 25th Jubilee International SAMPE Europe Conference*, Paris, 450-455.

Fitzer, E., & Huttner, W. (1981). Structure and strength of carbon/carbon composites. *Journal of Physics D: Applied Physics*, 14 (3), 347-371.

Flynn, J. H., & Levin, D. M. (1988). A method for the determination of thermal conductivity of sheet materials by differential scanning calorimetry (DSC). *Thermochimica Acta*, 126, 93-100.

Franzke, G., Offermann, P., Bischoff, T., Wulfhorst, B. (1997). Multi-axial warp knitted layers—a textile for reinforcing concrete. In *Proceedings of the 11th International Conference on Composite Materials Gold Coast*, Australia.

Fricke, H. (1924). A mathematical treatment of the electric conductivity and capacity of disperse systems I. The electric conductivity of a suspension of homogeneous spheroids. *Physical Review*, 24 (5), 575-587.

Gill, P. S., Sauerbrunn, S. R., & Reading, M. (1993). Modulated differential scanning calorimetry. *Journal of Thermal Analysis*, 40 (3), 931-939.

Gowayed, Y., & Jhy-Cherng, H. (1995). Thermal conductivity of cpmposite materials made from plain weaves and 3-D weaves. *Composite Engineering*, 5 (9), 1177-1186.

Greenhalgh E., & Hiley M. (2003). The assessment of novel materials and processes for the impact tolerant design of stiffened composite aerospace structures. *Composites Part A: Applied Science and Manufacturing*, 34, 151-161.

Grove, S. M. (1990). Model of transverse thermal conductivity in unidirectional fibre-reinforced composites. *Composites Science and Technology*, 39 (3), 199-209.

Haines, P. J., & Wilburn, F. W. (1995). In P.J. Haines, (Ed.), *Thermal methods of analysis: principles, applications and problems* (chapter 3). London: Blackie Academic and Professional.

Hakvoort, G., van Reijen, L. L., & Aartsen, A. J. (1985). Measurement of the thermal conductivity of solid substances by DSC. *Thermochimica Acta*, 93, 317-320.

Harris, H., Schinske, N., Krueger, R., & Swanson, B. (1991). Multiaxial stitched preform reinforcements for RTM fabrication. In *Proceedings of the 36th International SAMPE Symposium*, San Diego, 36 (1), 521-535.

Hasko, G., Dexter, H. B., Loos, A & Kranbuehl, D. (1994). Science based RTM for fabrication primary aircraft structures. In *Proceedings of the 39th International SAMPE Symposium*, San Diego.

Hasselman, D. P. H., Donaldson, K. Y., & Thomas, J. R. (1993). Effective thermal conductivity of uniaxial composite with cylindrically orthotropic carbon fibers and interfacial thermal barrier. *Journal of Composite Materials*, 27 (6), 637-644.

Hatakeyama, T., & Quinn, F. X. (1999). *Thermal analysis: fundamentals and applications to polymer science* (2nd ed.). Chichester: John Wiley & Sons.

Herszberg, I., & Bannister, M. K. (1993). Tensile properties of thin stitched carbon/epoxy composites. In *Proceedings of the 5th Australian Aeronautical Conference Part 1*, Melbourne, 213-218.

Hörsting, K., Wulfhorst, B., Kaldenhoff, R., Offermann, P., Franzke, G., Diestel, O., & Engelmann, U. (1993). Properties of components made of reinforcing layers. In *Proceedings of the5th Internationales Techtextil-Symposium*, Frankfurt, 1-21.

Huang, Y., & Young, R. J. (1995). Effect of fibre microstructure upon the modulus of PAN- and pitch-based carbon fibres. *Carbon*, 33 (2), 97–107.

Ishida, H., & Rimdusit, S. (1998). Very high thermal conductivity obtained by boron nitride-filled polybenzoxazine. *Thermochimica Acta*, 320, 177-186.

Ishida, H., & Rimdusit, S. (1999). Heat capacity measurement of boron nitride-filled polybenzoxazine. *Journal of Thermal Analysis and Calorimetry*, 58, 497-807.

Jang, B. Z. (1994). Advanced polymer composites. New York: ASM International.

Johansson, G., Joelsson, M., & Bastos, M. (1992). Some physical measurements in the one-phase region of a water-dextran-poly(ethylene glycol) system. *Polymer*, 33 (1), 152-155.

Jones, R. M. (1999). *Mechanics of composite materials* (2nd ed.). USA: Taylor & Francis, Inc.

Kalogiannakis, G., van Hemelrijck, D., & van Assche, G. (2004). Measurements of thermal properties of carbon/epoxy and glass/epoxy using modulated temperature differential scanning calorimetry. *Journal of Composite Materials*, 38 (2), 163-175.

Katz, S.H., & Milewak, J.V. (1978). *Handbook of fillers and reinforcements*. New York: Van Nostrand, Reinhold.

Keating, M. Y., & Mclaren, C. S. (1990). Thermal conductivity of polymer melts. *Thermochimica Acta,* 166, 69-76.

Khanna, Y. P., Taylor, T. J., & Chomyn, G. (1988). New differential scanning calorimetry based approach for the estimation of thermal conductivity of polymer solids and melts. *Polymer Engineering and Science,* 28 (16), 1034-1041.

Kim, R. Y. (1989). Experimental observations of free-edge delamination. In N. J. Pagano, (Ed.). *Interlaminar response of composite materials,* (111-160). Amsterdam: Elsevier Science Publishers B.V.

Krielaart, G. P., Brakman, C. M., & van der Zwaag, S. (1996). Analysis of phase transformation in Fe-C alloys using differential scanning calorimetry. *Journal of Materials Science*, 31 (6), 1501-1508.

Kroschwitz, J. I. (Ed.). (1985). *Encylopedia of polymer science and engineering* (2nd ed.). New York: Wiley.

Kuriger, R. J., & Alam, M. K. (2002). Thermal conductivity of thermoplastic composites with submicrometer carbon fibers. *Experimental Heat Transfer*, 15, 19-30.

Ko, F. K. (1989). Three-dimensional fabrics for composites. In T. W. Chou, & F. K. Ko, (Eds.). *Textile structural composites* (129-171). Amsterdam: Elsevier Science Publishers B.V.

Ko, F. K. (1993). Textile preforms for carbon-carbon composites. In J. D. Buckley, & D. D. Edie, (Eds.). *Carbon-carbon materials and composites* (71-104). New Jersey: Noyes Publications.

Ko, F. K., & Du, G. W. (1992). Processing of textile preforms. In *Proceedings of the Science and Innovation in Polymer Composites Processing*, MIT, USA.

Kong, H., Mouritz, A. P., & Paton, R. 2004). Tensile extension properties and deformation mechanisms of multiaxial non-crimp fabrics. *Composite Structures, 66*, 249-259.

Kotkata, M. F., El-Fouly, M. H., Fayek, S. A., & El-Hakim, S. A. (1986). The effect of TI addition on the electrical and thermal transport properties of amorphous As_2Se_3. *Semiconductor Science and Technology*, 1 (5), 313-319.

Kök, M. (2006). The measurement of thermal conductivity by DSC and its applications. M.Sc. dissertation, Graduate School of Natural and Applied Sciences, Fırat University, Elazığ, Turkey.

Ladbury, J. E. S. D., Currell, B. R., Horder, J. R., Parsonage, J. R., & Vidgeon, E. A. (1990). Application of DSC for the measurement of the thermal conductivity of elastomeric materials. *Thermochimica Acta*, 169, 39-45.

Lazarus, P. (1996). Resin infusion of marine composites. In *Proceedings of the 41st International SAMPE SymposiumPart 2*, Anaheim, CA, 1447-1458.

Lee, T. C. P., & Millens, W. (1977). US Patent 834, 4046.

Leong, K. H., Ramakrishna, S., Huang, Z. M., & Bibo, G. A. (2000). The potential of knitting for engineering composites—a review. *Composites Part A: Applied Science and Manufacturing*, 31, 197-220.

Levin, S. (2004). *Fourier transform Infrared (FTIR)*. Retrieved April 13, 2006, from http://www.forumsci.co.il/HPLC/FTIR_page.html

Lewis, S. M., & Jakubowski, J. C. (1997). Low cost VARTM process for commercial and military applications. In *Proceedings of the 42nd International SAMPE Symposium Part 2*, Anaheim, CA, 1173-1187.

Liba Maschinenfabric GmbH. (April 27, 2005). *Warp knitting machine with multiaxial weft insertion*. Retrieved September 16, 2005, from http://www.liba.de/tricot/cop_max_allg.html

Mackenzie, R. C., Keattch, C. J., Dollimore, D., Forrester, J. A., Hodgson, A. A., & Redfern, J. P. (1972). Nomenclature in thermal analysis-II. *Talanta*, 19 (9), 1079-1081.

Maewal, A., Gurtman, G. A., & Hegemier, G. A. (1978). Mixture theory for quasi-one-dimensional diffusion in fiber-reinforced composites. *Journal of Heat Transfer, Transaction ASME*, 100 (1), 128-133.

Mallick, P. K. (1993). *Fiber reinforced composites* (2nd ed.). New York: Marcel Dekker.

Mallick, P. K. (1997). Introduction: definitions, classifications, and applications. In P. K. Mallick, (Ed.), *Composites engineering handbook* (1-50). New York: Marcel Dekker.

Mark, H. F. (Ed.). (1989). *Encyclopaedia of Polymer Science and Engineering*. New York: Wiley and Sons.

Mattsson, D. (2005). Mechanical performance of NCF composites. Ph.D. dissertation, Department of Applied Physics and Mechanical Engineering, Luleå University of Technology, Luleå, Sweden.

Mazumdar, S. K. (2001). *Composite manufacturing: materials, product, and process engineering*. New York: CRC Press.

Merzlyakov, M., & Schick, C. (2001). Thermal conductivity from dynamic response of DSC. *Thermochimica Acta*, 377, 183-191.

Mikael, J., & Peter, G. (2000). Broad-band transient recording and characterization of acoustic emission events in composite laminates. *Composites Sciences and Technology*, 60, 2803–2818.

Mouritz, A. P. (1996). Flexural properties of stitched GRP laminates. *Composites Part A: Applied Science and Manufacturing*, 27 (7), 525-530.

Mouritz, A. P., Leong, K. H., & Herszberg, I. (1997). A review of the effect of stitching on the in-plane mechanical properties of fibre-reinforced polymer composites. *Composites Part A: Applied Science and Manufacturing*, 28A, 979-991.

Nquyen, L. B., Juska, T., & Mayes, S. J. (1997). Evaluation of low cost manufacturing technologies for large scale composite ship structures. In *Proceeding of the 38th ATAA/ASME/ASCE/AHS/ASC Structures, Structural Dynamics, and Materials Conference, V.2, AIAA*, New York, 992-1001.

O'neill, M. J. (1966). Measurement of specific heat functions by differential scanning calorimetry. *Analytical Chemistry*, 38 (10), 1331-1336.

Ott, H. J. (1981). Thermal conductivity of composite materials. *Plastics and Rubber Processing and Applications*, 1 (1), 9-24.

Pagano, N. J., & Pipes, R. B. (1971). The Influence of Stacking Sequence on Laminate Strength. *Journal of Composite Materials*, 5, 50-57.

Palmer, R. J., Dow, M. B., & Smith, D. L. (1991). Development of stitching reinforcement for transport wing panels.In *Proceedings of the 1st NASA Adv. Comp. Tech. Conference*, Part 2, 621-646.

Perpechoko, I. I. (1981). *An introduction to polymer physics*. Moscow: Mir.

Pike, T., MacArthur, M., & Schade, D. (1996). Vacuum assisted resin transfer molding of a layered structural laminate for application on ground combat vehicles. In *Proceedings of the 28th International SAMPE Technical Conference*, Seattle, 374-380.

Pilling, M. W., Yates, B., Black, M. A., & Tattersall, P. (1979). The thermal conductivity of carbon fiber-reinforced composites. *Journal of Materials Science*, 14, 1326.

Pipes, R. B., & Pagano, N. J. (1974). Interlaminar stresses in composite laminates-an approximate elasticity solution. *Journal of Applied Mechanics*, 41 (3), 668-672.

Progelhof, R. C., Throne, J. L., & Ruetsch, R. R. (1976). Methods for predicting thermal conductivity of composite systems: a review. *Polymer Engineering and Science*, 16 (9), 615-625.

Qual instrumentation. (n.d.). *FTIR spectrophotometer*. Retrieved April 13, 2006, from http://ocw.mit.edu/NR/rdonlyres/Chemistry/5-32Intermediate-Chemical-ExperimentationSpring2003/CA6722BA-7333-4A99-B4AB-1F7B880080C6/0/

Roth, Y., & Himmel, N. (2002). Theoretical model and experimental investigation on the effect of stitching on the in-plane stiffness of CFRP. In *Proceedings of the 10th European Conference on Composite Materials*, Brugge, Belgium.

Seemann, W. H. (1990). U.S. Patent 4, 902, 215.

Seemann, W. H. (1994). U.S. Patent 5, 316, 462.

Šimáček, P., & Advani, S. G. (2004). Desirable features in mold filling simulations for liquid composite molding processes. *Polymer Composites*, 25 (4), 355-367.

Sjogren, A., Edgren, F., & Aps, L.E. (2004). Effects of stitching pattern on the mechanical properties of non-crimp fabric composites. *In Proceedings of the 11th European Conference on Composite Materials (ECCM 11)*, Rhodos, Greece.

Springer, G. S., & Tsai, S. W. (1967). Thermal conductivities of unidirectional materials. *Journal of Composite Materials*, 1, 166.

Stumpf, H., Mader, E., Baeten, S., Pisanikovski, T., Zah, W., Eng, K., Anderson C.-H., Verpoest, I., & Schulte K. (1998). New thermoplastic composite preforms based on split-film warp-knitting. *Composites Part A: Applied Science and Manufacturing*, 29A, 1511-1523.

Su, Y., Jing, W., & Liu, H. (2002). FTIR spectroscopic study on effects of temperature and polymer composition on the structural properties of PEO-PPO-PEO block copolymer micelles, *Langmuir*, 18, 5370-5374.

Sweeting, R. D., & Liu, X. L. (2004). Measurement of thermal conductivity for fiber reinforced composites. *Composites Part A: Applied Science and Manufacturing*, 35, 933-938.

Truong, T. C., Vettori, M., Lomov, S., & Verpoest, I. (2005). Carbon composites based on multi-axial multi-ply stitched preforms. Part 4. Mechanical properties of composites and damage observation. *Composites Part A: Applied Science and Manufacturing*, 36 (9), 1207–1221.

Wang, Y. (2002). Mechanical Properties of Stitched Multiaxial Fabric Reinforced Composites from Mannual Layup Process. *Applied Composite Materials*, 9, 81-97.

Wang, Y., Li, J., & Do, B. P. (1995). Properties of composite laminates reinforced with E-glass multiaxial non-crimp fabrics. *Journal of Composite Materials*, 29 (17), 2317–2333.

Whitney, J. M., & Browning, C. E. (1972). Free-edge delamination of tensile coupons. *Journal of Composite Materials*,6 (2), 300-303.

Whitney, J. M., & Kim, R. Y. (1977). Effect of stacking sequence on the notched strength of laminated composites. In *Proceedings of the 4th Composite Materials: Testing and Design Conference*, Philadelphia, 229-242.

Wunderlich, B., Pyda, M., Pak, J., & Androsch, R. (2001). Measurement of heat capacity to gain information about time scales of molecular motion from pico to megaseconds. *Thermochimica Acta, 377*, 9-33.

Xu, M. X., Liu, W. G., Gao, Z. X., Fang, L. P., & Yao, K. D. (1996). Correlation of change in electrical resistance with strain of carbon fiber-reinforced plastic in tension. *Journal of Applied Polymer Science*, 60 (10), 1595-1599.

Yu, J. L., Liu, Y. M., & Jang, B. Z. (1994). Mechanical properties of carbon fiber reinforced polyester/urethane hybrid network composites. *Polymer Composites*, 15 (6), 488–495.